PATHOLOGICAL HYPERACTIVITY AND HYPEREXCITABILITY IN THE CENTRAL NERVOUS SYSTEM

EDITED BY: Michael Telias, Menahem Segal and Alexander Galazyuk
PUBLISHED IN: Frontiers in Molecular Neuroscience and
Frontiers in Synaptic Neuroscience

frontiers Research Topics

frontiers

ISSN 1664-8714
ISBN 978-2-88976-728-1
DOI 10.3389/978-2-88976-728-1

About Frontiers

Frontiers is more than just an open-access publisher of scholarly articles: it is a pioneering approach to the world of academia, radically improving the way scholarly research is managed. The grand vision of Frontiers is a world where all people have an equal opportunity to seek, share and generate knowledge. Frontiers provides immediate and permanent online open access to all its publications, but this alone is not enough to realize our grand goals.

Frontiers Journal Series

The Frontiers Journal Series is a multi-tier and interdisciplinary set of open-access, online journals, promising a paradigm shift from the current review, selection and dissemination processes in academic publishing. All Frontiers journals are driven by researchers for researchers; therefore, they constitute a service to the scholarly community. At the same time, the Frontiers Journal Series operates on a revolutionary invention, the tiered publishing system, initially addressing specific communities of scholars, and gradually climbing up to broader public understanding, thus serving the interests of the lay society, too.

Dedication to Quality

Each Frontiers article is a landmark of the highest quality, thanks to genuinely collaborative interactions between authors and review editors, who include some of the world's best academicians. Research must be certified by peers before entering a stream of knowledge that may eventually reach the public - and shape society; therefore, Frontiers only applies the most rigorous and unbiased reviews.
Frontiers revolutionizes research publishing by freely delivering the most outstanding research, evaluated with no bias from both the academic and social point of view. By applying the most advanced information technologies, Frontiers is catapulting scholarly publishing into a new generation.

What are Frontiers Research Topics?

Frontiers Research Topics are very popular trademarks of the Frontiers Journals Series: they are collections of at least ten articles, all centered on a particular subject. With their unique mix of varied contributions from Original Research to Review Articles, Frontiers Research Topics unify the most influential researchers, the latest key findings and historical advances in a hot research area! Find out more on how to host your own Frontiers Research Topic or contribute to one as an author by contacting the Frontiers Editorial Office: frontiersin.org/about/contact

PATHOLOGICAL HYPERACTIVITY AND HYPEREXCITABILITY IN THE CENTRAL NERVOUS SYSTEM

Topic Editors:
Michael Telias, University of Rochester, United States
Menahem Segal, Weizmann Institute of Science, Israel
Alexander Galazyuk, Northeast Ohio Medical University, United States

Citation: Telias, M., Segal, M., Galazyuk, A., eds. (2022). Pathological Hyperactivity and Hyperexcitability in the Central Nervous System. Lausanne: Frontiers Media SA. doi: 10.3389/978-2-88976-728-1

Table of Contents

frontiers | Frontiers in Molecular Neuroscience

TYPE Editorial
PUBLISHED 12 July 2022
DOI 10.3389/fnmol.2022.955542

OPEN ACCESS

EDITED AND REVIEWED BY
Clive R. Bramham,
University of Bergen, Norway

*CORRESPONDENCE
Michael Telias
michael_telias@urmc.rochester.edu
Menahem Segal
menahem.segal@weizmann.ac.il

SPECIALTY SECTION
This article was submitted to Neuroplasticity and Development, a section of the journal Frontiers in Molecular Neuroscience

RECEIVED 28 May 2022
ACCEPTED 30 May 2022
PUBLISHED 12 July 2022

CITATION
Telias M and Segal M (2022) Editorial: Pathological hyperactivity and hyperexcitability in the central nervous system.
Front. Mol. Neurosci. 15:955542.
doi: 10.3389/fnmol.2022.955542

Editorial: Pathological hyperactivity and hyperexcitability in the central nervous system

Michael Telias [1]* and Menahem Segal [2]*

[1]Flaum Eye Institute, University of Rochester, Rochester, NY, United States, [2]Department of Neurobiology, The Weizmann Institute of Science, Rehovot, Israel

KEYWORDS

hyperexcitability, hyperactivity, fragile X syndrome, Alzheimer's disease, neuron, brain, epilepsy

Editorial on the Research Topic
Pathological hyperactivity and hyperexcitability in the central nervous system

The brain contains a delicate and precise balance between excitatory and inhibitory neurons, which have different roles in the formation, development, and homeostasis of brain circuits. The balance between these populations is maintained by a number of local control mechanisms, regulating presynaptic efficacy as well as postsynaptic excitability. In pathology, an abnormal excitation-to-inhibition (E/I) ratio leads to neuronal hyperexcitability and network hyperactivity, constituting the basis for epilepsy and subsequent cognitive dysfunction, and is associated with many neurodevelopmental, neurodegenerative, and psychiatric diseases. Epileptic seizures can be induced by blocking GABAergic inhibition and repressed by enhancing inhibition, illustrating the role of E/I-ratio imbalance in neuronal pathology (Smolarz et al., 2021; Vlachou, 2022). In this Topic, the contributing studies showcase the centrality of hyperexcitability and hyperactivity in five different pathologies with diverse etiologies and symptoms.

Fragile X syndrome

In recent years, much attention has been focused on neurodevelopmental disorders including autism spectrum disorders, Rett syndrome, and Angelman syndrome which are accompanied by epileptic seizures, sensory hypersensitivity, repetitive behavior, and attention deficits; each symptom potentially caused by independent mechanisms (Antoine). These diseases all share phenotypic traits with the archetype of developmental disorders, fragile X syndrome (FXS) (Telias, 2019), a monogenic X-linked disorder. For example, neuronal hyperexcitability can explain sensory hypersensitivity in FXS patients. Here, Deng et al. propose that reduced expression and activation of HCN

channels contributes to hyperexcitability of dorsal root ganglia in the *fmr1*$^{-/-}$ mouse; while the study by Avraham et al. shows a role in FXS-hypersensitivity for altered neuron-glia interactions, in which *fmr1*$^{-/-}$ satellite glial cells fail to properly contact and cover the dorsal root ganglia. Beyond sensory processing, other cognitive functions are affected by hyperactivity in FXS. The in-depth review by Liu et al. provides an excellent analysis of the latest research on the subject, with an emphasis on molecular and physiological mechanisms, overall suggesting that excitability and homeostatic plasticity are both impaired in FXS, in a region-selective manner.

Hearing loss

In hearing loss, as the hair cells in the cochlea die, the auditory nerve becomes hyperactive, giving rise to tinnitus (Shore et al., 2016). This increase in firing has repercussions in the downstream brain nuclei that receive cochlear inputs, and understanding them is essential to improve hearing restoration strategies. Downstream to the cochlea, circuits cross into the contralateral hemisphere, forming the main auditory pathway. Interneurons in the brain stem carry signals from the terminals of spiral ganglion cells to the contralateral superior olive nucleus, and from there the fibers ascend to the inferior colliculus. Yet, evidence for the existence of ipsilateral pathways and their roles is emerging. Hsiao and Galazyuk demonstrate that the pathological hyperactivity that results from unilateral sound exposure affects both the ipsi- and the contralateral pathways, but the largest effect was measured in the ipsilateral inferior colliculus, an unexpected result that challenges existing paradigms, as most studies using unilateral acoustic damage focus almost exclusively on the nuclei of the contralateral side. Further downstream effects of cochlear damage and subsequent hyperactivity can affect sensory gating in the auditory system. De Vis et al. show that acoustic damage to the cochlea in guinea pigs affects signal transmission between the pre-frontal cortex and the medial geniculate nucleus, essential for gating of sensory input, providing a physical substrate for tinnitus. Since the prefrontal cortex is involved in sensory gating for many different pathways other than audition, their results could have far-reaching consequences.

Alzheimer's disease

Neuronal hyperexcitability and network hyperactivity are intrinsically related to Alzheimer's Disease (AD) progression, in both sporadic and familial AD (Palop and Mucke, 2016; Kazim et al., 2021). Hypersynchrony in the brains of AD patients can be observed long before clinical symptom manifestations, increasing the risk for epilepsy and faster cognitive decline, while hyperexcitability has been linked to activation and accumulation of β-amyloid and tau. The source of the hyperactivity in AD remains unknown, as animal models show defects in both inhibition and excitation. In an age-dependent rat model of AD, enhanced excitability is partially caused by increased activity of β-adrenergic receptors (Goodman et al., 2021). Now, Smith et al. show that hippocampal neurons in AD become hyperexcitable due to intrinsic changes in membrane properties, independent of changes in pre-synaptic input. The study shows that affected neurons have increased input resistance, deceased rheobase, and lower firing thresholds, together with a decrease in sag associated with functional upregulation of HCN channels, providing new insights into the mechanisms of hyperexcitability in AD.

Hyperexcitability and hyperactivity in pain and psychomotor behavior

The study by Kearns et al. demonstrates that hypersensitivity to pain (hyperalgesia), induced by chronic exposure to opioids, is mediated by specific alternations in excitatory and inhibitory spinal neurons. Chronic treatment with morphine was associated with both enhanced excitation of excitatory neurons, as well as with reduced excitation of inhibitory neurons. The effect seems to be mediated by changes in neurotransmitter-dependent mechanisms, as treatment with morphine did not alter most passive membrane properties in any of the tested cell populations. The study by Zhang et al. discusses hyperactivity in the context of locomotion and psychomotor behavior. Inhibition of 14-3-3 protein in the hippocampus induces locomotor hyperactivity that is mitigated by pharmacological blockade of dopamine and by inhibition of firing of dopamine neurons in the ventral tegmental area. This work also identifies the lateral septum as a relay station between the ventral tegmental area and the hippocampus.

Afterword

This Frontiers Topic highlights the versatility of hyperactivity and hyperexcitability in neurological disease, observed in neurodevelopmental and neurodegenerative disorders; as a consequence of intrinsic changes in neuronal properties or due to circuit-wide changes affecting excitation and/or inhibition. The mechanisms underlying each case might differ, but the phenotypic outcome remains the same. Most importantly, for each individual case, it is still unclear whether hyperactivity is just a consequence of an imbalanced system, or

is in itself the source of further dysfunctionality by amplifying the defects associated with the disease.

Author contributions

MT and MS contributed equally to the writing and editing of this manuscript. Both authors contributed to the article and approved the submitted version.

Funding

MT was supported by an unrestricted gift from the Research for Preventing Blindness Foundation to the Flaum Eye Institute.

Conflict of interest

The authors declare that the research was conducted in the absence of any commercial or financial relationships that could be construed as a potential conflict of interest.

Publisher's note

References

Goodman, A. M., Langner, B. M., Jackson, N., Alex, C., and Mcmahon, L. L. (2021). Heightened hippocampal beta-adrenergic receptor function drives synaptic potentiation and supports learning and memory in the TgF344-AD rat model during prodromal alzheimer's disease. *J. Neurosci.* 41, 5747–5761. doi: 10.1523/JNEUROSCI.0119-21.2021

Kazim, S. F., Seo, J. H., Bianchi, R., Larson, C. S., Sharma, A., Wong, R. K. S., et al. (2021). Neuronal network excitability in Alzheimer's disease: the puzzle of similar versus divergent roles of amyloid beta and tau. *eNeuro* 8, ENEURO.0418-20.2020. doi: 10.1523/ENEURO.0418-20.2020

Palop, J. J., and Mucke, L. (2016). Network abnormalities and interneuron dysfunction in Alzheimer disease. *Nat. Rev. Neurosci.* 17, 777–792. doi: 10.1038/nrn.2016.141

Shore, S. E., Roberts, L. E., and Langguth, B. (2016). Maladaptive plasticity in tinnitus—triggers, mechanisms and treatment. *Nat. Rev. Neurol.* 12, 150–160. doi: 10.1038/nrneurol.2016.12

Smolarz, B., Makowska, M., and Romanowicz, H. (2021). Pharmacogenetics of drug-resistant epilepsy (review of literature). *Int. J. Mol. Sci.* 22, 11696. doi: 10.3390/ijms222111696

Telias, M. (2019). Molecular mechanisms of synaptic dysregulation in fragile x syndrome and autism spectrum disorders. *Front. Mol. Neurosci.* 12, 51. doi: 10.3389/fnmol.2019.00051

Vlachou, S. (2022). GABAB receptors and cognitive processing in health and disease. *Curr. Top. Behav. Neurosci.* 52, 291–329. doi: 10.1007/7854_2021_231

frontiers in Synaptic Neuroscience

ORIGINAL RESEARCH
published: 22 June 2021
doi: 10.3389/fnsyn.2021.684141

Effect of Unilateral Acoustic Trauma on Neuronal Firing Activity in the Inferior Colliculus of Mice

*Chun-Jen Hsiao and Alexander V. Galazyuk**

Department of Anatomy and Neurobiology, Northeast Ohio Medical University, Rootstown, OH, United States

Neural hyperactivity induced by sound exposure often correlates with the development of hyperacusis and/or tinnitus. In laboratory animals, hyperactivity is typically induced by unilateral sound exposure to preserve one ear for further testing of hearing performance. Most ascending fibers in the auditory system cross into the superior olivary complex and then ascend contralaterally. Therefore, unilateral exposure should be expected to mostly affect the contralateral side above the auditory brain stem. On the other hand, it is well known that a significant number of neurons have crossing fibers at every level of the auditory pathway, which may spread the effect of unilateral exposure onto the ipsilateral side. Here we demonstrate that unilateral sound exposure causes development of hyperactivity in both the contra and ipsilateral inferior colliculus in mice. We found that both the spontaneous firing rate and bursting activity were increased significantly compared to unexposed mice. The neurons with characteristic frequencies at or above the center frequency of exposure showed the greatest increase. Surprisingly, this increase was more pronounced in the ipsilateral inferior colliculus. *This study* highlights the importance of considering both ipsi- and contralateral effects in future studies utilizing unilateral sound exposure.

Keywords: hyperactivity, bursting, sound exposure, binaural effect, unanesthetized mice

OPEN ACCESS

Edited by:
Manuel A. Castro-Alamancos, Drexel University, United States

Reviewed by:
Wei Sun, University at Buffalo, United States
Shaowen Bao, University of Arizona, United States

***Correspondence:**
Alexander V. Galazyuk
agalaz@neomed.edu

Received: *22 March 2021*
Accepted: *18 May 2021*
Published: *22 June 2021*

Citation:
Hsiao C-J and Galazyuk AV (2021) Effect of Unilateral Acoustic Trauma on Neuronal Firing Activity in the Inferior Colliculus of Mice. Front. Synaptic Neurosci. 13:684141. doi: 10.3389/fnsyn.2021.684141

INTRODUCTION

Neuronal hyperactivity is present in many brain diseases. In the auditory system it is believed that hyperactivity may underlie both hyperacusis (exaggerated sensitivity to sound) and tinnitus (a phantom sound without an external stimulus) (Gerken, 1996; Salvi et al., 2000; Eggermont and Roberts, 2004; Roberts et al., 2010; Galazyuk et al., 2012; Salloum et al., 2016; Shore et al., 2016). One of the most common causes for the development of hyperactivity in the auditory system is acoustic trauma after sound exposure. It has been shown that sound exposure leads to cochlear damage and subsequent threshold shifts (Liberman and Kiang, 1978; Kujawa and Liberman, 2009). In response to this damage, the central auditory system increases its gain to compensate for the reduced sensorineural input from the cochlea (Salvi et al., 2000; Schaette and McAlpine, 2011; Galazyuk et al., 2012; Auerbach et al., 2014). As a result of this change in gain, hyperactivity develops in the auditory system as well as in non-auditory brain structures. Noise-induced hyperactivity has been described for the cochlear nucleus (Kaltenbach and Afman, 2000; Brozoski and Bauer, 2005), inferior colliculus (Ma et al., 2006; Bauer et al., 2008; Mulders and Robertson, 2013; Ropp et al., 2014),

medial geniculate nucleus (Kalappa et al., 2014), and auditory cortex (Syka and Rybalko, 2000), but not necessarily in auditory nerve fibers (Eggermont and Roberts, 2004).

Hyperactivity in the auditory system has been defined as elevated spontaneous firing, increased bursting, and synchronous firing of auditory neurons. These maladaptive changes have been observed at most levels of the central auditory system (for review see Shore et al., 2016). In the dorsal cochlear nucleus (DCN), sound exposure leads to elevated spontaneous activity, increased neural synchrony, and bursting in fusiform neurons (Wu et al., 2016). Similarly, in addition to increased spontaneous firing, abnormally high neural synchrony and bursting were also reported for non-lemniscal regions of the inferior colliculus (Bauer et al., 2008; Mulders and Robertson, 2013) and elevated bursting was reported for the auditory thalamus (Kalappa et al., 2014). Increased spontaneous firing and synchrony were also found in the auditory cortex following sound overexposure (Robertson and Irvine, 1989; Noreña and Eggermont, 2003). Since hyperactivity often links to hyperacusis and tinnitus, deep knowledge about its development is vital to uncover brain mechanisms underlying these disorders.

Development of hyperactivity in the auditory system in general and in particular in the IC following sound exposure is a complex, long lasting, and dynamic process (for review see Zhao et al., 2016). Immediately after exposure, spontaneous firing rates are elevated in DCN and VCN, whereas IC activity remains unchanged. Two weeks later, increased IC activity begins to be detected, along with continuous hyperexcitation in the DCN (Gröschel et al., 2014). At this stage, ablation of the DCN results in major reductions of IC hyperactivity (Manzoor et al., 2012). However, approximately 8 weeks after exposure the hyperactivity in the IC becomes more prominent, stable, and does not change much after cochlear ablation (Mulders and Robertson, 2009, 2011; Robertson et al., 2013). Nevertheless, this does not mean that the hyperactivity in the IC is intrinsic and completely independent of ascending inputs. Even after the 2-month period the cochlear nucleus has been found to continue to convey hyperexcitation to the IC (Manzoor et al., 2012, 2013).

The vast majority of animals' studies utilize unilateral sound exposure to induce tinnitus in order to preserve one ear for further behavioral hearing and/or tinnitus assessments (for review see Galazyuk and Hébert, 2015). In the auditory system, the majority of ascending fibers cross into the superior olivary complex and then ascend via the contralateral side of the brainstem to the auditory cortex. Therefore, unilateral exposure is expected to induce hyperactivity predominantly on the contralateral side of the auditory neuroaxis above the level of the auditory brainstem. On the other hand, it is well known that a significant number of neurons within the auditory system have crossing fibers at every level of the auditory pathway (Schofield and Cant, 1996a,b). Therefore, all levels of the central auditory system receive and process information from both the ipsilateral and contralateral sides. Indeed, it has been clearly demonstrated that after ablation of the unilateral auditory nerve, such changes are evident not only in the ipsilateral cochlear nucleus where the auditory nerve fibers are terminated, but also in the contralateral cochlear nucleus, which receives normal input from the cochlea (Rubio, 2006; Whiting et al., 2009). These findings challenge the expectation that the most profound changes in neuronal activity should occur in the contralateral side after unilateral exposure. Our recent work provided some evidence that auditory neurons in the ipsilateral IC show a dramatic increase in bursting after a unilateral sound exposure (Longenecker and Galazyuk, 2016). Therefore, it is important to determine and compare the changes in neural firing of contra- and ipsilateral auditory pathways after unilateral sound exposure.

In the present study we exposed mice unilaterally and recorded changes in the spontaneous firing rate and bursting in neurons of the inferior colliculus in unanesthetized mice. These changes were assessed and compared in contralateral and ipsilateral ICs. We found that all exposed mice developed hyperactivity in the IC and this hyperactivity was the most pronounced in the IC region linked to the frequency range of the sound exposure. Although the hyperactivity was present at both the contra- and ipsilateral IC, the most robust changes were observed in the ipsilateral IC. Our findings strongly suggest that future studies on hyperactivity should pay close attention to the side of recording.

MATERIALS AND METHODS

Subjects

A total of 12 CBA/CAJ mice were used in this study (5 mice in the control group and 7 mice in the sound exposed (SE) group). All animals were between 6 and 12 months of age. Mice were housed in pairs within a colony room, with a 12 h light-dark cycle, at 25°C. Animal procedures in this study were approved by the Institutional Animal Care and Use Committee at Northeast Ohio Medical University.

Sound Exposure

Animals were at least 5 months old at the time of sound exposure. The procedure of exposure was performed under general anesthesia with intraperitoneal injection of a ketamine/xylazine mixture (100/10 mg/kg). Additional injections (50% of the initial dose) were given to mice intramuscularly 30 min after the initial injection to maintain an appropriate level of anesthesia. One octave narrowband noise centered at 12.5 kHz (8–17 kHz) was presented to mice unilaterally for 1 h. The noise was generated by a wave form generator (Wavetek model 395), amplified (Sherwood RX-4109) to 116 dB Sound Pressure Level (SPL), and then played through an open field loudspeaker (Fostex FT17H) in a soundproof camber. The open field loudspeaker was calibrated with a 0.25 inch microphone (Brüel and Kjaer,4135). Before exposure, the left external ear canal of exposed mice was blocked with a foam earplug (3M classic earplugs, 3M company) followed by a Kwik-Sil silicone elastomer plug (World Precision Instruments). This manipulation typically reduces sound level by 30–50 dB SPL (Turner et al., 2006; Ropp et al., 2014).

Auditory Brainstem Responses (ABR)

Mice were anesthetized with ketamine/xylazine (100 and 10 mg/kg, respectively). ABRs were recorded in response to

5 ms tone bursts (0.5 ms rise/fall time) presented at frequencies of 4, 12.5, 20, 30, and 40 kHz with the sound level ranged from 80 to 10 dB SPL in 10 dB steps using an RZ6 multi-I/O processor (Tucker-Davis Technologies). Tone bursts were delivered at the rate of 50/s through a speaker (LCY K-100 Ribbon Tweeter, Madisound), which was placed 10 cm in front of the animal's head. ABR thresholds were measured before, directly following, and 1 month after sound exposure. Stainless-steel electrodes (disposable subdermal needle electrode, LifeSync Neuro) were placed subdermally at the vertex (active), the ipsilateral and contralateral mastoids (references), and at the base of animal's tail (ground). The evoked potentials were amplified (RA4PA MEDUSA Preamp, Tucker-Davis Technologies), filtered (100–3,000 Hz bandpass), and averaged across 300 repetitions. Thresholds were determined by visual examination of the averaged ABR waveforms in response to each frequency and sound level combination.

Surgery

A total of 8 mice were used for extracellular recordings. Each mouse was anesthetized during surgery by using 1.5–2.0% isoflurane. A midline incision of the scalp was made and the tissue overlying the cranium was removed. Then a small metal rod was glued to the cranium using dental cement (C&B Metabond, Japan). Following at least 2 days recovery, each animal was trained to stay in a holding device in a single-walled sound attenuating room. The holding device consisted of a custom-made small plastic tube and a small metal holder. During electrophysiological recordings, animals' ears were unobstructed for free-field acoustic stimulation.

Extracellular Recordings

Recordings were made from both the ipsi- and contra-lateral inferior colliculus relative to the side of exposure in awake mice inside a single-walled sound attenuating chamber (Industrial Acoustics Company, Inc.). Throughout the recording session (3–4 h), the animal was offered water periodically and monitored for signs of discomfort. After a recording session, the exposed skull was covered with a Kwik-Sil silicone elastomer plug (World Precision Instruments) and the animal was returned to its holding cage. Experiments were conducted at least 2 months post exposure in the SE group and recordings were performed every other day for up to 2 weeks, after which the animal was sacrificed with an IP injection of Fatal-Plus. No sedative drugs were used during recording sessions. If the animal showed any signs of discomfort, the recording session was terminated, and the mouse was returned to its cage.

Recording electrodes were inserted through a small hole drilled in the skull and dura overlying the IC. Extracellular single-unit recordings were made with quartz glass micropipettes (10–20 MΩ impedance, 2–3 μm tip) filled with 0.5 M sodium chloride. Electrodes were fabricated using a P2000 horizontal micropipette puller (Sutter Instrument). The electrode was positioned into the drilled hole by means of a precision (1 μm) digital micromanipulator MP285 (Sutter Instrument) using a surgical microscope (Leica MZ9.5). The relative position of each electrode was monitored from the readouts of digital micrometers using a common reference point on the brain surface.

Extracellular recordings were limited to the central nucleus of the IC based on the depth of recordings. Vertical advancement of the electrode was made by a precision piezoelectric microdrive (Model 660, KOPF Instr.) from outside the sound-attenuating chamber. Recorded action potentials were amplified (Dagan 2400A preamplifier), monitored audio-visually on a digital oscilloscope (DL3024, YOKOGAWA), digitized and then stored on a computer hard drive using EPC-10 digital interface and PULSE software from HEKA Elektronik at a bandwidth of 100 kHz.

The search stimulus consisted of a frequency modulated 3–60 kHz sweep (150 ms duration, 65 dB SPL) presented once per second. This train was repeated while the recording electrode was advanced in 2–4 μm steps. The characteristic frequency of recorded neurons was assessed manually by presenting tone pips 100 ms in duration using a wide range of sound frequencies (3-53 kHz, 2 kHz step) and sound levels (20, 30, 40, and 55 dB SPL). The spontaneous firing rate (SFR) was assessed during a 30 s recording window in which no stimulus was presented. The stimulus system contained a free-field loudspeaker (LCY-K100 Ribbon Tweeter, Madisound), an amplifier (HCA-750A, PARASOUND) and a Tucker-Davis Technologies system 3 (RX6 multifunction processor, PA5 programmable attenuator, SigGenRP software, Tucker-Davis Technologies).

Data Analysis

All statistical analyses were accomplished using GraphPad Prism 8 (version 8.4.3., GraphPad). In ABR data, a two-way ANOVA with a Tukey post-test was used to compare thresholds at the three experimental time points. For the extracellular recording data, a Mann-Whitney test was used to compare the Control and Sound Exposure groups. For multiple comparisons, a Kruskal-Wallis test was used with a Dunn's *post hoc* test. A simple linear regression was utilized to determine the relationship between the characteristic frequency and recording depth. Data are presented as mean with standard deviation (*SD*) or standard error of the mean (SEM) and $p < 0.05$ criteria was used to determine statistical significance.

RESULTS

The ABR Thresholds Were Temporary Shift in the Exposed Ear After Unilateral Acoustic Trauma

To assess the effect of unilateral acoustic trauma on hearing, the ABR thresholds were determined in four mice before, directly following, and 1 month post-exposure in both ears. We found a temporary threshold increase at 12.5, 20, 30, and 40 kHz right after sound exposure in the exposed ear which recovered to control levels 1 month later (**Figure 1A**). In contrast, ABR thresholds in the unexposed (blocked) ear were not affected by sound exposure (**Figure 1B**).

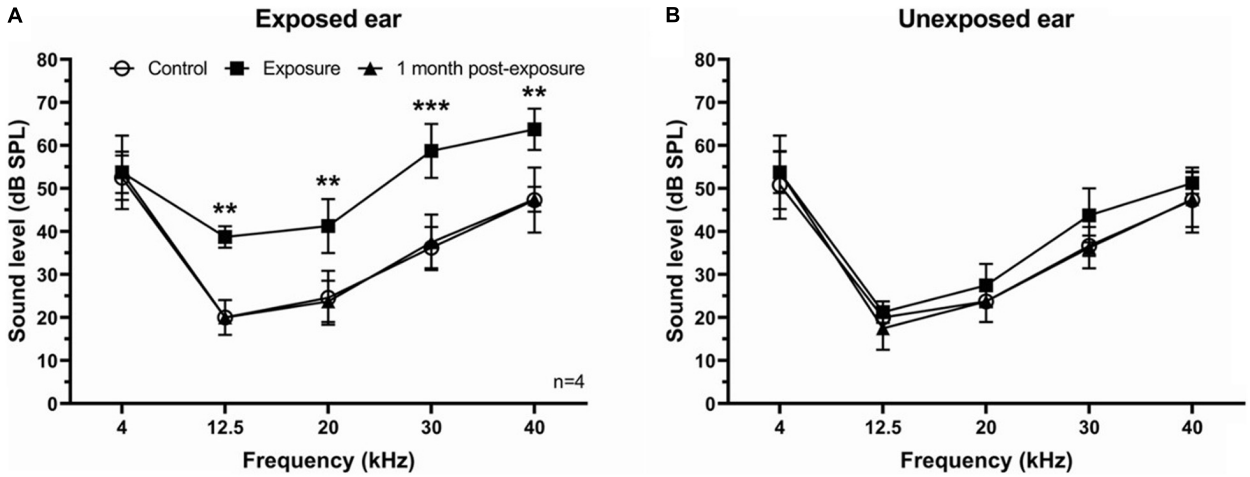

FIGURE 1 | ABR thresholds in SE group. **(A)** ABR thresholds were temporary increased immediately following sound exposure in the exposed ear and recovered back to the control level 1 month post-exposure. **(B)** ABR thresholds showed no difference after sound exposure in the unexposed ear. Mean ± *SD*. Significant changes indicated with (**) at $p = 0.001$ level or (***) at $p = 0.0001$ level.

Unilateral Acoustic Trauma Increases Spontaneous Firing Rate of IC Neurons

To determine the effect of unilateral acoustic trauma on SFR, extracellular single unit responses of 371 neurons were recorded in control (unexposed) and sound exposed mice in contra- and ipsilateral ICs relative to the side of exposure (**Figures 2A,B**). We found that the mean SFRs of IC neurons in the control group was 8.9 ± 1.3 spikes/s and was no different between right and left ICs (right, 8.9 ± 2.2 spikes/s; left, 8.5 ± 1.5 spikes/s, $p = 0.61$). The average SFR, however, was significantly increased in the SE group compared to control (**Figure 2C**, control, 8.9 ± 1.3 spikes/s; SE, 16.78 ± 1.66 spikes/s). These changes were not uniformly distributed across neurons with different characteristic frequencies (CFs; compare **Figures 2A,B**). To determine whether IC neurons within the CF range showed more pronounced increase in SFR, we divided neurons with different CFs into 4 roughly equal frequency ranges ($n = 48$, 79, 73, and 60, respectively). In our study mice were exposed to one octave narrow-band noise (8–17 kHz) with a center frequency of 12.5 kHz. Previous research demonstrated that the neurons most affected by exposure have CFs at or above the center frequency of exposure (Mulders and Robertson, 2009; Longenecker and Galazyuk, 2011; Turner et al., 2012; Coomber et al., 2014; Ropp et al., 2014). Therefore, the frequency range from 0 to 12.5 kHz (all CFs below the center frequency of exposure) defined the size of the frequency step to partition the four ranges (<12.5, 12.5–25, 25–37.5, and >37.5 kHz). In agreement with previous studies, the IC neurons having CFs within the range of sound exposure (12.5–25 kHz) showed the most robust increase in SFR (**Figure 2D**, Control, 12.59 ± 3.77 spikes/s; SE, 25.49 ± 4.72 spikes/s).

Previous research reveals a tonotopic map in the IC with a spatial gradient of CFs oriented in a dorsolateral (low frequencies) to ventromedial (high frequencies) direction. Consistent with this organization, we found a linear relationship between the CF and recording depth of IC neurons in the SE group (**Figure 2E**, $Y = 17.37^*X + 338.7$, $R^2 = 0.55$). These regressions allowed us to identify the depth (550–780 μm) within the IC where the neurons with more pronounced SFR increase were found following a narrow-band (8–17 kHz) noise exposure.

After Unilateral Sound Exposure Ipsilateral IC Neurons Demonstrate Higher SFR Compared to Contralateral IC

To determine whether one side of IC was more affected than the other, we separated and compared neurons recorded in contra- (130 neurons) (**Figure 3A**) and ipsilateral (93 neurons) (**Figure 3B**) IC. Although SFR was increased in both contra- and ipsilateral IC neurons, the ipsilateral IC was more affected by exposure (**Figure 3C**, Control, 8.9 ± 1.3 spikes/s; Contra-, 15.41 ± 2.1 spikes/s; Ipsi-, 18.7 ± 2.69 spikes/s). The SFR increase was most evident in the CF range 12.5–25 kHz of both contra- and ipsilateral IC. This change was statistically significant in ipsilateral (33.01 ± 8.45 spikes/s) but not in contralateral IC (22.48 ± 3.77 spikes/s) compared to controls (**Figure 3D**).

Acoustic Trauma Increases Spontaneous Bursting Activity of IC Neurons

To assess the effect of unilateral acoustic trauma on spontaneous bursting activity in IC neurons, we adopted the burst definition from Bauer et al. (2008). To be defined as a bursting event, each burst needed to satisfy the following 6 criteria: (1) maximum allowable burst duration: 310 ms; (2) maximum ISI at burst start: 500 ms; (3) maximum within-burst ISI: 10 ms; (4) minimum interval between bursts: 50 ms; (5) minimum burst duration: 5 ms; (6) minimum number of spikes in a burst: 2. In addition, the present data was arbitrarily divided into three bursting levels: no bursting (NB), low bursting (LB) (< 20%) and high bursting (HB) (≥20%) (**Figure 4A**). In the control group (147

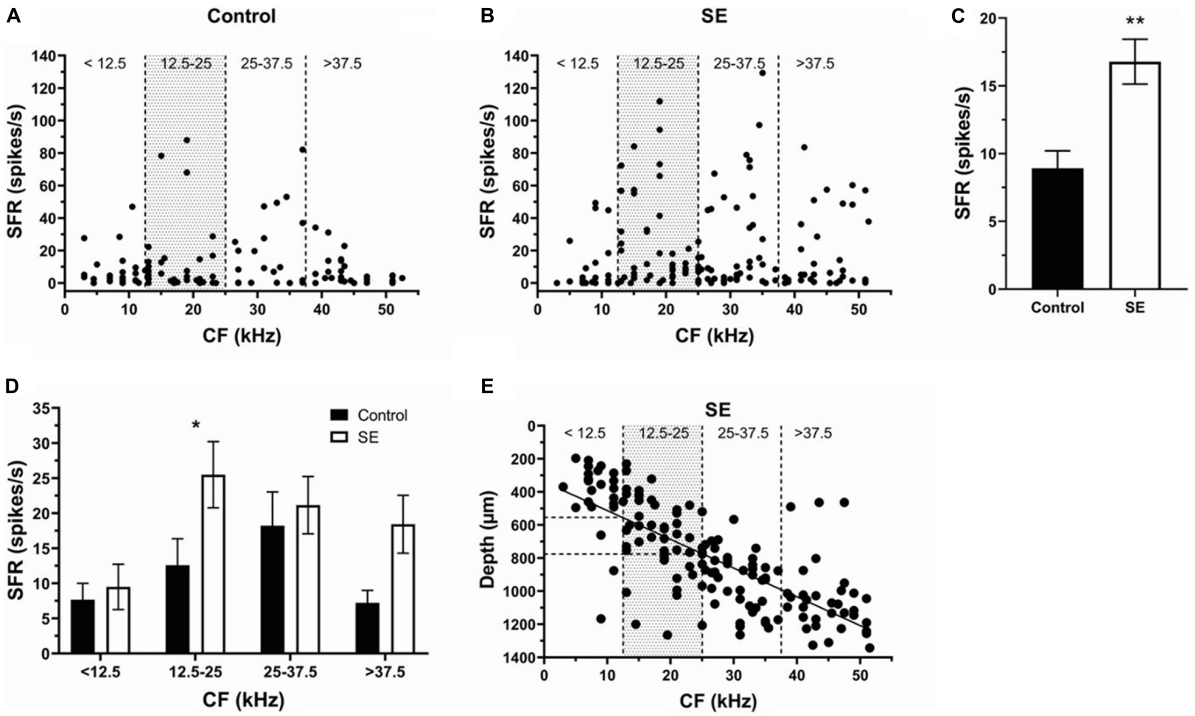

FIGURE 2 | Sound exposure increases SFRs in IC neurons with CFs at or above the center frequency of exposure. **(A,B)** The SFR is plotted against the CF of each neuron in the control (n = 107) and SE groups (n = 153). **(C)** Mean SFR in the control (8.9 ± 1.3 spikes/s) and SE group (16.78 ± 1.66 spikes/s). **(D)** Mean SFR in the four frequency ranges of control and SE groups. **(E)** The relationship between CF and recording depth of IC neurons in SE group. Mean ± SEM. Significant SFR changes indicated with (*) at p = 0.05 level or (**) at p = 0.001 level.

neurons), 66.67% of neurons showed bursting activity (47.62% LB, 19.05% HB), whereas 33.33% of neurons did not (**Figure 4A**). In the sound exposed group (224 neurons), 72.0% of IC neurons were classified as bursting while 28.0% of neurons showed no bursting. The bursting neurons (72%) were then divided into low bursting and high bursting groups (38.67 and 33.33%, respectively) (**Figure 4A**). We found that after sound exposure, the proportion of high bursting neurons was increased while low bursting decreased compared to controls. Further, the mean bursting level was elevated only in the neurons having CFs in the range of 12.5–25 kHz (**Figure 4B**). Regarding bursting parameters, the SE group showed significant increases in both bursting duration and mean spikes in a burst compared to the control group (**Figures 4C,E**, control, 8.76 ± 0.2 ms, 2.47 ± 0.06 spikes; SE, 9.75 ± 0.21 ms, 2.66 ± 0.05 spikes). Again, these changes were most evident and significant within the CF range of 12.5–25 kHz (**Figures 4D,F**).

Unilateral Acoustic Trauma Differentially Affects Spontaneous Bursting Activity in Contralateral and Ipsilateral IC Neurons

The proportion of no bursting (control: 49 neurons; contra: 44 neurons; Ipsi: 19 neurons), low bursting (control: 70 neurons; contra: 47 neurons; ipsi: 40 neurons), and high bursting neurons (control:28 neurons; contra: 40 neurons; ipsi: 34 neurons) was differentially altered by unilateral sound exposure (**Figure 5A**). The percentage of NB neurons in the contralateral IC was similar to controls after exposure, but decreased in the ipsilateral IC (control—33.33%, contralateral—33.59% ipsilateral—20.21%). The proportion of LB neurons was decreased in both ICs in SE mice compared to control mice. However, this decrease was more pronounced in the contralateral IC (control—47.62%; contra–35.88%; ipsi—42.55%). In contrast, the percent of HB neurons increased in both ICs with a larger change in ipsilateral IC (control–19.05%; contra–30.53%; ipsi—37.24%). Although the mean bursting level tended to increase in both contra and ipsilateral ICs in neurons with a wide range of CFs, this increase was most evident in the range of 12.5–25 kHz in the ipsilateral IC (**Figure 5B**). Similarly, the bursting duration increased in both ICs (**Figure 5C**), whereas this increase was most noticeable in the range of 12.5–25 kHz in the ipsilateral IC (**Figure 5D**). The mean number spikes per burst was also slightly elevated in both ICs after sound exposure but was significant in the ipsilateral IC (**Figure 5E**). In accordance with other parameters of bursting this increase was significant in the ipsilateral IC in the range of 12.5–25 kHz (**Figure 5F**).

DISCUSSION

The main goal of this research was to determine changes in firing activity of the auditory midbrain neurons of mice following a unilateral sound overexposure. Changes in spontaneous firing

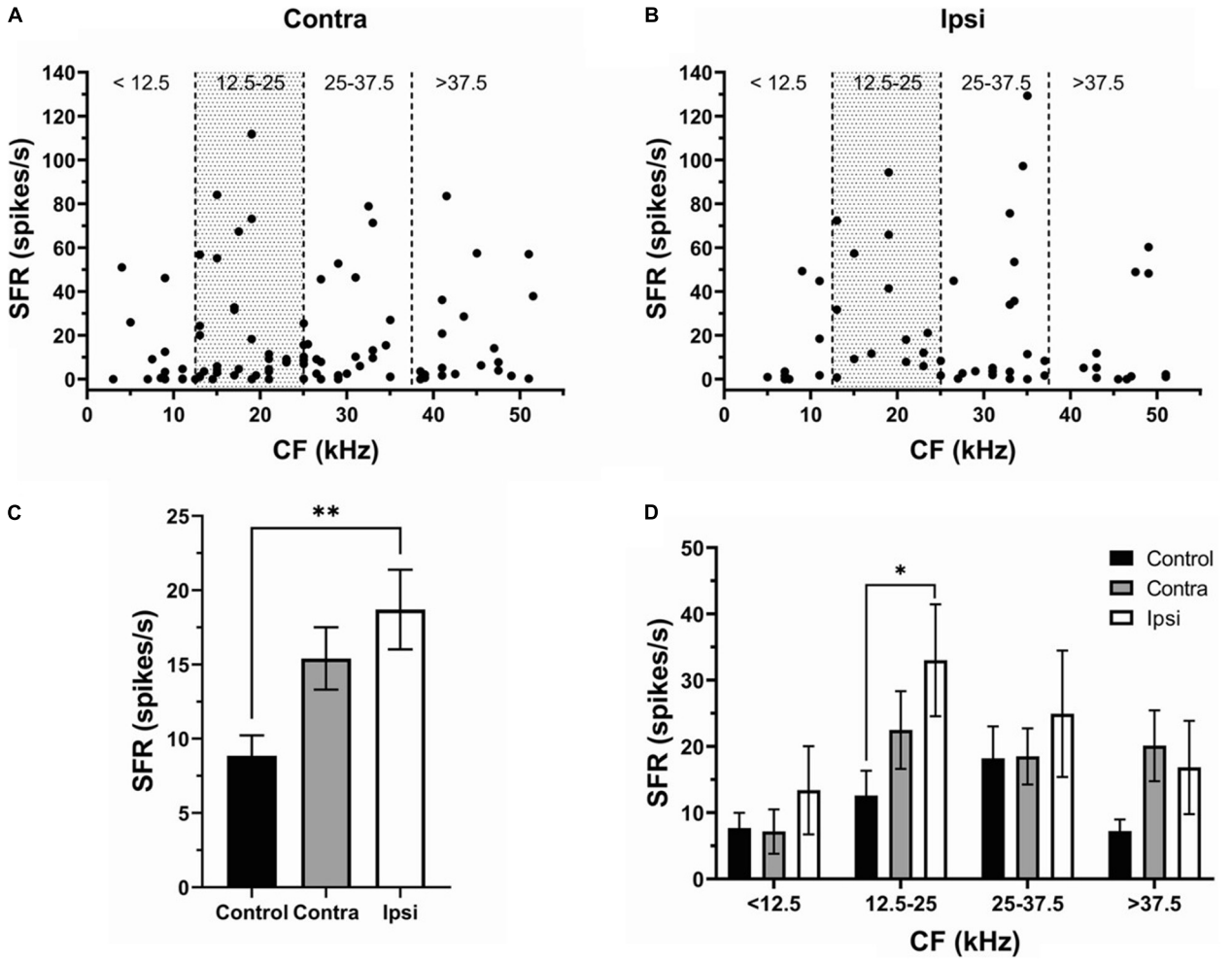

FIGURE 3 | The effect of sound exposure on SFR is more robust in the ipsilateral IC. **(A,B)** The SFR against the CF in neurons of contralateral (n = 97) and ipsilateral IC (n = 56). **(C)** Mean SFR in IC neurons of the control (8.9 ± 1.3 spikes/s), contralateral SE (15.41 ± 2.1 spikes/s) and ipsilateral SE (18.7 ± 2.69 spikes/s) groups. **(D)** Mean SFR in control, contra- and ipsilateral SE IC at four frequency ranges (<12.5 kHz; 12.5–25 kHz; 25–37.5 kHz; and > 37.5 kHz). Mean ± SEM. (*) p = 0.05 level or (**) at p = 0.001 level.

rate and bursting were assessed in contralateral and ipsilateral ICs relative to the side of exposure and then compared. In accordance with previous reports the spontaneous firing rate and bursting were increased in IC neurons by exposure (Ma et al., 2006; Bauer et al., 2008; Mulders and Robertson, 2013; Ropp et al., 2014; Ma et al., 2020). Remarkably, this increase was evident in both the contralateral and ipsilateral ICs, with a more robust effect in the ipsilateral IC.

ABR Threshold Were Temporary Increase and Recovery in the Exposed Ear

The main goals of ABR testing were to confirm three expected outcomes of sound exposure. First, that our unilateral exposure affected the exposed ear only, with little or no effect on the unexposed ear. Second, that our exposure caused an ABR threshold shift, indicating that the sound exposure was effective in inducing an acoustic trauma. Third, that this threshold shift was temporary, which after several weeks returned to the level before exposure. Therefore, we tested ABR thresholds in the ipsilateral and contralateral ears relative to the side of exposure independently before, immediately after, and 1 month following sound exposure. Our data indicate that all expected outcomes were confirmed.

Sound Exposure Induces Hyperactivity in the IC

At present, there is an agreement in the field of tinnitus research that hyperactivity in the auditory system is an underlying mechanism of tinnitus. On the other hand, some laboratory animals or human subjects exhibiting hyperactivity do not show tinnitus. Thus, hyperactivity is a necessary, but not a sufficient, condition for a phantom sound percept or tinnitus.

Studies utilizing both tinnitus animal models and human research advocate that hyperactivity in the auditory system often

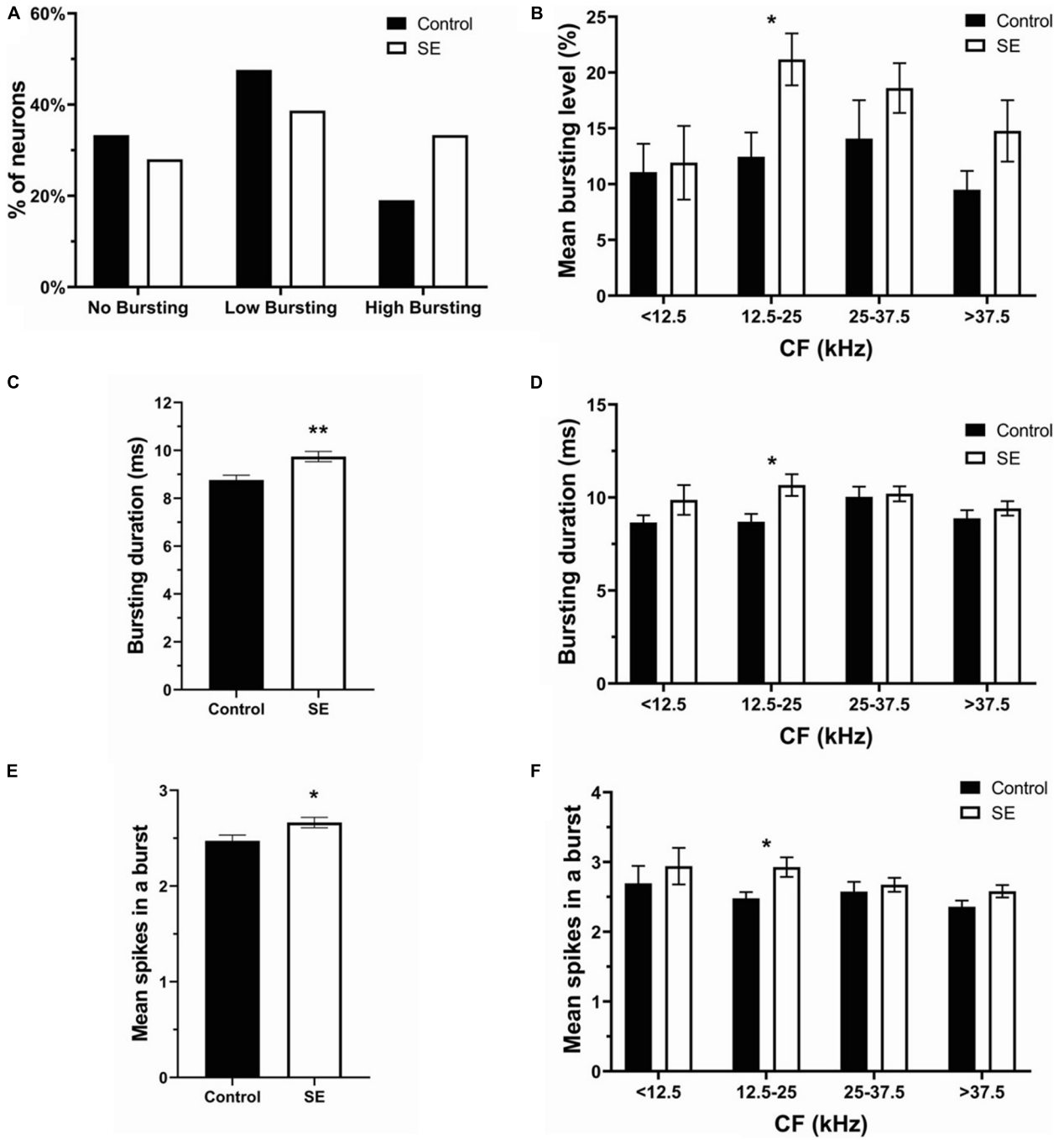

FIGURE 4 | Bursting activity was elevated in the SE group especially within the CF frequency range of 12.5–25 kHz. **(A)** The percentage of no bursting, low bursting and high bursting neurons in control and SE groups. **(B)** Mean bursting level vs. four CF ranges in control and SE groups. **(C)** Bursting duration and **(E)** mean spikes in a burst in control (8.76 ± 0.2 ms; 2.47 ± 0.06 spikes) and SE groups (9.75 ± 0.21 ms; 2.66 ± 0.05 spikes). **(D)** Bursting duration and **(F)** mean spikes in a burst vs. four CF ranges in control and SE groups. Mean ± SEM. (*) $p = 0.05$ level or (**) at $p = 0.001$ level.

correlates with tinnitus. Although such hyperactivity has been demonstrated for all levels of the central auditory pathway, the most affected specific nuclei differ between studies. Research from multiple labs using different animal models found that hyperactivity in the cochlear nucleus correlates with behavioral evidence of tinnitus (see review Wu et al., 2016). Tinnitus-related hyperactivity in the dorsal cochlear nucleus (DCN) has been associated with reduced inhibition as well as increased excitation from the non-auditory circuitry following cochlear injury (Wang et al., 2009; Middleton et al., 2011; Dehmel et al., 2012;

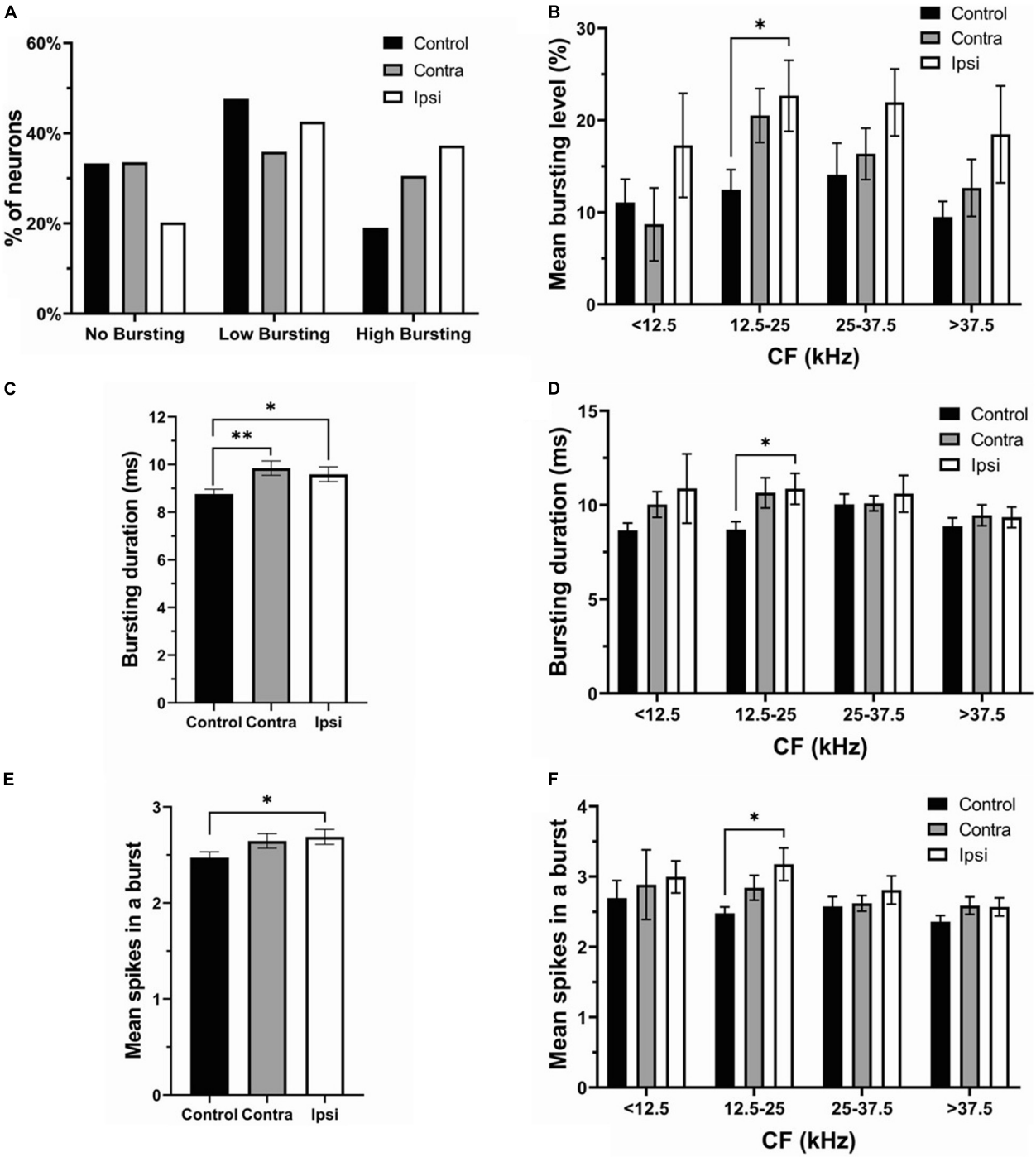

FIGURE 5 | The ipsilateral IC contributed to the changes in bursting activity after unilateral acoustic trauma. **(A)** The percentage of no bursting, low bursting and high bursting neurons in control, contra- and ipsilateral SE ICs. **(B)** Mean bursting level vs. CF range in control, contra- and ipsilateral SE ICs. **(C)** Bursting duration in all recorded neurons in control (both ICs), contra and ipsilateral SE ICs. **(D)** Bursting duration in four different CF frequency ranges. **(E)** Mean spikes in a burst in control (both ICs), contra and ipsilateral SE ICs. **(F)** Mean spikes in a burst in four different CF frequency ranges. Mean ± SEM. (*) $p = 0.05$ level or (**) at $p = 0.001$ level.

Koehler and Shore, 2013). The presence of hyperactivity in sound exposed animals in the IC is still debated. On one hand, several studies showed that increased SFR occurred in neurons with best frequencies (BFs) overlapping the regions of hearing loss (Ma et al., 2006; Mulders and Robertson, 2009; Longenecker and Galazyuk, 2011; Manzoor et al., 2013) or widespread increases in SFR without frequency specificity (Bauer et al., 2008; Berger et al., 2014; Ropp et al., 2014). On the other hand, one study failed to

find a significant change in SFR of IC neurons following a sound exposure in mice (Shaheen and Liberman, 2018).

Our results reveal that hyperactivity is present in the exposed mice. After unilateral exposure, both the SFR and bursting were increased in both the contra and ipsilateral ICs (**Figures 2C**, **4C,E**) and these changes were linked to the frequency range of exposure (**Figures 2D**, **4D,F**). However, the elevation in SFR and bursting was significant only in the ipsilateral IC compared to controls (**Figures 3C**, **5E**). Although not significant, the presence of consistent increases in SFR and bursting in the contralateral IC suggests that these effects would reach statistical significance with a substantial increase in the sample size of recorded neurons. It is possible that the absence of significant changes in hyperactivity in several studies might also be explained by a small sample size and/or the focus on data from the contralateral IC relative to the side of exposure. The fact that we observed this hyperactivity several months after exposure makes us confident that this is a chronic sign of an acoustic trauma.

The Ipsilateral Dominance in Hyperactivity

The most unexpected finding of this study is that both the contralateral and ipsilateral ICs showed clear signs of hyperactivity, and that the ipsilateral IC was more affected following a unilateral sound exposure. Consistent with these results, an ipsilateral dominance has been reported for elevation of bursting firing in IC neurons after unilateral exposure (Longenecker and Galazyuk, 2016). Despite the consistent trend of ipsilateral dominance in the present study, the difference between ipsilateral and contralateral IC was not statistically significant. These findings are surprising, because unilateral sound exposure is expected to cause damage mostly in the affected ear, as was confirmed by a temporary ABR threshold shift immediately following sound exposure (**Figure 1**). As a result, the sensorineural hearing loss induced by exposure should lead to a reduction of the sensory input from the cochlea to the central auditory system. To compensate for the loss, the neurons in the cochlear nucleus on the exposed side should increase their activity. This compensatory increase in the central auditory activity in response to the loss of sensory input is referred to as central gain enhancement (see review by Auerbach et al., 2014). Enhanced central gain is hypothesized to give rise to hyperactivity in the central auditory system which is believed to be responsible for development of hyperacusis and/or tinnitus. Hyperactivity has been well characterized for the fusiform neurons of the dorsal cochlear nucleus after sound exposure (Brozoski et al., 2002; Shore et al., 2008; Finlayson and Kaltenbach, 2009; Pilati et al., 2012; Wu et al., 2016). DCN neurons mainly project to the contralateral IC (see review of Cant and Benson, 2003). An ipsilateral projection is described by most authors, although it appears to be small. Therefore, after unilateral sound exposure we should expect hyperactivity mainly to be present in the contralateral IC. In contrast, in the present study we observe hyperactivity in both ICs with ipsilateral dominance. Thus, bilateral projection from affected cochlear nucleus to both ICs after unilateral exposure cannot explain our findings. A possible explanation for this result is that unilateral exposure leads to maladaptive changes in neuronal firing or hyperactivity in both the ipsilateral and contralateral cochlear nuclei, which then project this hyperactivity to both ICs.

Unilateral Exposure Induces Hyperactivity in Both Cochlear Nuclei and Therefore in Both ICs

In our study there were bilateral changes in the SFR and bursting firing properties of IC neurons. Such changes might be inherited from ascending projections from both ipsilateral and contralateral cochlear nuclei. Unilateral sound exposure could directly alter firing properties of neurons in the ipsilateral cochlear nucleus, one of the main inputs to IC, and also indirectly affect the contralateral cochlear nucleus via crossed connections between the cochlear nuclei (Cant and Benson, 2003). Previous research reveal the likelihood of crossed inhibitory connections between the cochlear nuclei (Cant and Gaston, 1982; Wenthold, 1987; Schofield and Cant, 1996b; Alibardi, 2000). Cant and Gaston (1982) reported connections between the dorsal and ventral cochlear nuclei projecting to the contralateral, anteroventral, and posteroventral cochlear nucleus, as well as to the dorsal cochlear nucleus fusiform cell layer. Schofield and Cant (1996a) described labeled boutons that made contacts in the contralateral fusiform neurons and deep layers of the dorsal cochlear nucleus. Potashner et al. (2000) found that unilateral manipulation of peripheral input altered glycine neurotransmission in both the contralateral and ipsilateral dorsal cochlear nuclei. Therefore, plastic changes in one cochlear nucleus are likely to cause either direct or indirect changes in the contralateral cochlear nucleus. More direct evidence for plastic changes in the contralateral cochlear nucleus to unilateral auditory depravation comes from two studies where changes in glutamatergic synapses were identified in both the affected and unaffected cochlear nuclei (Rubio, 2006; Whiting et al., 2009). In an earlier study the AMPA receptors were found to be redistributed in DCN neurons receiving direct contact from the auditory nerve on the side of the auditory nerve lesion and also in the neurons of the contralateral DCN which receives an intact auditory nerve synaptic input (Rubio, 2006). In a following study, similar bilateral changes were observed in response to a mild (∼20 dB) conductive unilateral hearing loss in rats (Whiting et al., 2009). They detected that auditory nerve synapses on bushy and fusiform neurons of the ventral and dorsal cochlear nucleus, respectively, upregulated the GLU3 AMPA receptor subunit, whereas inhibitory synapses showed decreased expression of the GlyRa1 subunit. These changes, however, were fully reversible once the earplug causing conductive hearing loss was removed. Hence, multiple studies provide evidence for the mechanism

by which unilateral acoustic trauma can cause bilateral changes in firing activity of auditory neurons throughout the central auditory system. On the other hand, it is still unclear why in the present study such changes were more evident in the ipsilateral IC. Future research is needed to shed light on this phenomenon.

In summary, the present study has demonstrated that a unilateral acoustic trauma leads to development of hyperactivity in both contralateral and ipsilateral ICs with a greater ipsilateral effect several months after exposure. In both ICs, an increase in SFR and bursting is linked to the frequency range of exposure. These results confirm that an acoustic trauma reliably induces chronic hyperactivity in the auditory midbrain. They also highlight the importance for research on hyperactivity to evaluate the side of recording within the auditory pathway.

DATA AVAILABILITY STATEMENT

The raw data supporting the conclusions of this article will be made available by the authors, without undue reservation.

ETHICS STATEMENT

The animal study was reviewed and approved by the Institutional Animal Care and Use Committee at the Northeast Ohio Medical University.

AUTHOR CONTRIBUTIONS

AG contributed to conception and design of the study and wrote sections of the manuscript. C-JH organized the database, performed the statistical analysis, and wrote the first draft of the manuscript. Both authors contributed to manuscript revision, read, and approved the submitted version.

FUNDING

This research was supported by grant R01 DC016918 from the National Institute on Deafness and Other Communication Disorders of the U.S. Public Health Service.

REFERENCES

Alibardi, L. (2000). Cytology, synaptology and immunocytochemistry of commissural neurons and their putative axonal terminals in the dorsal cochlear nucleus of the rat. *Ann. Anat.* 182, 207–220. doi: 10.1016/S0940-9602(00)80023-0

Auerbach, B. D., Rodrigues, P. V., and Salvi, R. J. (2014). Central gain control in tinnitus and hyperacusis. *Front. Neurol.* 5:206. doi: 10.3389/fneur.2014.00206

Bauer, C. A., Turner, J. G., Caspary, D. M., Myers, K. S., and Brozoski, T. J. (2008). Tinnitus and inferior colliculus activity in chinchillas related to three distinct patterns of cochlear trauma. *J. Neurosci. Res.* 86, 2564–2578. doi: 10.1002/jnr.21699

Berger, J. I., Coomber, B., Wells, T. T., Wallace, M. N., and Palmer, A. R. (2014). Changes in the response properties of inferior colliculus neurons relating to tinnitus. *Front. Neurol.* 5:203. doi: 10.3389/fneur.2014.00203

Brozoski, T. J., and Bauer, C. A. (2005). The effect of dorsal cochlear nucleus ablation on tinnitus in rats. *Hear. Res.* 206, 227–236. doi: 10.1016/j.heares.2004.12.013

Brozoski, T. J., Bauer, C. A., and Caspary, D. M. (2002). Elevated fusiform cell activity in the dorsal cochlear nucleus of chinchillas with psychophysical evidence of tinnitus. *J. Neurosci.* 22, 2383–2390. doi: 10.1523/jneurosci.22-06-02383.2002

Cant, N. B., and Benson, C. G. (2003). Parallel auditory pathways: projection patterns of the different neuronal populations in the dorsal and ventral cochlear nuclei. *Brain Res. Bull.* 60, 457–474. doi: 10.1016/s0361-9230(03)00050-9

Cant, N. B., and Gaston, K. C. (1982). Pathways connecting the right and left cochlear nuclei. *J. Comp. Neurol.* 212, 313–326. doi: 10.1002/cne.902120308

Coomber, B., Berger, J. I., Kowalkowski, V. L., Shackleton, T. M., Palmer, A. R., and Wallace, M. N. (2014). Neural changes accompanying tinnitus following unilateral acoustic trauma in the guinea pig. *Eur. J. Neurosci.* 40, 2427–2441. doi: 10.1111/ejn.12580

Dehmel, S., Pradhan, S., Koehler, S., Bledsoe, S., and Shore, S. (2012). Noise overexposure alters long-term somatosensory-auditory processing in the dorsal cochlear nucleus — possible basis for tinnitus-related hyperactivity? *J. Neurosci.* 32, 1660–1671. doi: 10.1523/jneurosci.4608-11.2012

Eggermont, J. J., and Roberts, E. (2004). The neuroscience of tinnitus. *Trends Neurosci.* 27, 676–682. doi: 10.1016/j.tins.2004.08.010

Finlayson, P. G., and Kaltenbach, J. A. (2009). Alterations in the spontaneous discharge patterns of single units in the dorsal cochlear nucleus following intense sound exposure. *Hear. Res.* 256, 104–117. doi: 10.1016/j.heares.2009.07.006

Galazyuk, A. V., Wenstrup, J. J., and Hamid, M. A. (2012). Tinnitus and underlying brain mechanisms. *Curr. Opin. Otolaryngol. Head Neck Surg.* 20, 409–415. doi: 10.1097/MOO.0b013e3283577b81

Galazyuk, A., and Hébert, S. (2015). Gap-Prepulse Inhibition of the Acoustic Startle Reflex (GPIAS) for tinnitus assessment: current status and future directions. *Front. Neurol.* 6:88. doi: 10.3389/fneur.2015.00088

Gerken, G. M. (1996). Central tinnitus and lateral inhibition: an auditory brainstem model. *Hear. Res.* 97, 75–83. doi: 10.1016/s0378-5955(96)80009-8

Gröschel, M., Ryll, J., Götze, R., Ernst, A., and Basta, D. (2014). Acute and long-term effects of noise exposure on the neuronal spontaneous activity in cochlear nucleus and inferior colliculus brain slices. *BioMed. Res. Int.* 2014:909260. doi: 10.1155/2014/909260

Kalappa, B. I., Brozoski, T. J., Turner, J. G., and Caspary, D. M. (2014). Single unit hyperactivity and bursting in the auditory thalamus of awake rats directly correlates with behavioural evidence of tinnitus. *J. Physiol.* 592, 5065–5078. doi: 10.1113/jphysiol.2014.278572

Kaltenbach, J. A., and Afman, C. E. (2000). Hyperactivity in the dorsal cochlear nucleus after intense sound exposure and its resemblance to tone-evoked activity: a physiological model for tinnitus. *Hear. Res.* 140, 165–172. doi: 10.1016/s0378-5955(99)00197-5

Koehler, S. D., and Shore, S. E. (2013). Stimulus-timing dependent multisensory plasticity in the guinea pig dorsal cochlear nucleus. *PLoS One* 8:e59828. doi: 10.1371/journal.pone.0059828

Kujawa, S. G., and Liberman, M. C. (2009). Adding Insult to injury: cochlear nerve degeneration after "Temporary" noise-induced hearing loss. *J. Neurosci.* 29, 14077–14085. doi: 10.1523/jneurosci.2845-09.2009

Liberman, M. C., and Kiang, N. Y. (1978). Acoustic trauma in cats. Cochlear pathology and auditory-nerve activity. *Acta Otolaryngol. Suppl.* 358, 1–63.

Longenecker, R. J., and Galazyuk, A. V. (2011). Development of tinnitus in CBA/CaJ mice following sound exposure. *J. Assoc. Res. Otolaryngol.* 12, 647–658. doi: 10.1007/s10162-011-0276-1

Longenecker, R. J., and Galazyuk, A. V. (2016). Variable Effects of acoustic trauma on behavioral and neural correlates of tinnitus in individual animals. *Front. Behav. Neurosci.* 10:207. doi: 10.3389/fnbeh.2016.00207

Ma, L., Ono, M., Qin, L., and Kato, N. (2020). Acoustic trauma induced the alteration of the activity balance of excitatory and inhibitory neurons in the inferior colliculus of mice. *Hear. Res.* 391:107957. doi: 10.1016/j.heares.2020.107957

Ma, W. L., Hidaka, H., and May, B. J. (2006). Spontaneous activity in the inferior colliculus of CBA/J mice after manipulations that induce tinnitus. *Hear. Res.* 212, 9–21. doi: 10.1016/j.heares.2005.10.003

Manzoor, N. F., Gao, Y., Licari, F., and Kaltenbach, J. A. (2013). Comparison and contrast of noise-induced hyperactivity in the dorsal cochlear nucleus and inferior colliculus. *Hear. Res.* 295, 114–123. doi: 10.1016/j.heares.2012.04.003

Manzoor, N. F., Licari, F. G., Klapchar, M., Elkin, R. L., Gao, Y., Chen, G., et al. (2012). Noise-induced hyperactivity in the inferior colliculus: its relationship with hyperactivity in the dorsal cochlear nucleus. *J. Neurophysiol.* 108, 976–988. doi: 10.1152/jn.00833.2011

Middleton, J. W., Kiritani, T., Pedersen, C., Turner, J. G., Shepherd, G. M. G., and Tzounopoulos, T. (2011). Mice with behavioral evidence of tinnitus exhibit dorsal cochlear nucleus hyperactivity because of decreased GABAergic inhibition. *Proc. Natl. Acad. Sci. U.S.A.* 108, 7601–7606. doi: 10.1073/pnas.1100223108

Mulders, W. H., and Robertson, D. (2009). Hyperactivity in the auditory midbrain after acoustic trauma: dependence on cochlear activity. *Neuroscience* 164, 733–746. doi: 10.1016/j.neuroscience.2009.08.036

Mulders, W. H., and Robertson, D. (2011). Progressive centralization of midbrain hyperactivity after acoustic trauma. *J. Neurosci.* 192, 753–760. doi: 10.1016/j.neuroscience.2011.06.046

Mulders, W. H., and Robertson, D. (2013). Development of hyperactivity after acoustic trauma in the guinea pig inferior colliculus. *Hear. Res.* 298, 104–108. doi: 10.1016/j.heares.2012.12.008

Noreña, A. J., and Eggermont, J. J. (2003). Changes in spontaneous neural activity immediately after an acoustic trauma: implications for neural correlates of tinnitus. *Hear. Res.* 183, 137–153. doi: 10.1016/s0378-5955(03)00225-9

Pilati, N., Large, C., Forsythe, I. D., and Hamann, M. (2012). Acoustic overexposure triggers burst firing in dorsal cochlear nucleus fusiform cells. *Hear. Res.* 283, 98–106. doi: 10.1016/j.heares.2011.10.008

Potashner, S. J., Suneja, S. K., and Benson, C. G. (2000). Altered glycinergic synaptic activities in guinea pig brain stem auditory nuclei after unilateral cochlear ablation. *Hear. Res.* 147, 125–136. doi: 10.1016/s0378-5955(00)00126-x

Roberts, L. E., Eggermont, J. J., Caspary, D. M., Shore, S. E., Melcher, J. R., and Kaltenbach, J. A. (2010). Ringing ears: the neuroscience of tinnitus. *J. Neurosci.* 30, 14972–14979. doi: 10.1523/jneurosci.4028-10.2010

Robertson, D., and Irvine, D. R. (1989). Plasticity of frequency organization in auditory cortex of guinea pigs with partial unilateral deafness. *J. Comp. Neurol.* 282, 456–471. doi: 10.1002/cne.902820311

Robertson, D., Bester, C., Vogler, D., and Mulders, W. H. A. M. (2013). Spontaneous hyperactivity in the auditory midbrain: relationship to afferent input. *Hear. Res.* 295, 124–129. doi: 10.1016/j.heares.2012.02.002

Ropp, T. J., Tiedemann, K. L., Young, E. D., and May, B. J. (2014). Effects of unilateral acoustic trauma on tinnitus-related spontaneous activity in the inferior colliculus. *J. Assoc. Res. Otolaryngol.* 15, 1007–1022. doi: 10.1007/s10162-014-0488-2

Rubio, M. E. (2006). Redistribution of synaptic AMPA receptors at glutamatergic synapses in the dorsal cochlear nucleus as an early response to cochlear ablation in rats. *Hear. Res.* 216-217, 154–167. doi: 10.1016/j.heares.2006.03.007

Salloum, R. H., Sandridge, S., Patton, D. J., Stillitano, G., Dawson, G., Niforatos, J., et al. (2016). Untangling the effects of tinnitus and hypersensitivity to sound (hyperacusis) in the gap detection test. *Hear. Res.* 331, 92–100. doi: 10.1016/j.heares.2015.10.005

Salvi, R. J., Wang, J., and Ding, D. (2000). Auditory plasticity and hyperactivity following cochlear damage. *Hear. Res.* 147, 261–274. doi: 10.1016/s0378-5955(00)00136-2

Schaette, R., and McAlpine, D. (2011). Tinnitus with a normal audiogram: physiological evidence for hidden hearing loss and computational model. *J. Neurosci.* 31, 13452–13457. doi: 10.1523/JNEUROSCI.2156-11.2011

Schofield, B. R., and Cant, N. B. (1996a). Origins and targets of commissural connections between the cochlear nuclei in guinea pigs. *J. Comp. Neurol.* 375, 128–146. doi: 10.1002/(sici)1096-9861(19961104)375:1<128::aid-cne8>3.0.co;2-5

Schofield, B. R., and Cant, N. B. (1996b). Projections from the ventral cochlear nucleus to the inferior colliculus and the contralateral cochlear nucleus in guinea pigs. *Hear. Res.* 102, 1–14. doi: 10.1016/s0378-5955(96)00121-9

Shaheen, L. A., and Liberman, M. C. (2018). Cochlear synaptopathy changes sound-evoked activity without changing spontaneous discharge in the mouse inferior colliculus. *Front. Syst. Neurosci.* 12:59. doi: 10.3389/fnsys.2018.00059

Shore, S. E., Koehler, S., Oldakowski, M., Hughes, L. F., and Syed, S. (2008). Dorsal cochlear nucleus responses to somatosensory stimulation are enhanced after noise-induced hearing loss. *Eur. J. Neurosci.* 27, 155–168. doi: 10.1111/j.1460-9568.2007.05983.x

Shore, S. E., Roberts, L. E., and Langguth, B. (2016). Maladaptive plasticity in tinnitus–triggers, mechanisms and treatment. *Nat. Rev. Neurol.* 12, 150–160. doi: 10.1038/nrneurol.2016.12

Syka, J., and Rybalko, N. (2000). Threshold shifts and enhancement of cortical evoked responses after noise exposure in rats. *Hear. Res.* 139, 59–68. doi: 10.1016/s0378-5955(99)00175-6

Turner, J. G., Brozoski, T. J., Bauer, C. A., Parrish, J. L., Myers, K., Hughes, L. F., et al. (2006). Gap detection deficits in rats with tinnitus: a potential novel screening tool. *Behav. Neurosci.* 120, 188–195. doi: 10.1037/0735-7044.120.1.188

Turner, J. G., Larsen, D., Hughes, L., Moechars, D., and Shore, S. (2012). Time course of tinnitus development following noise exposure in mice. *J. Neurosci. Res.* 90, 1480–1488. doi: 10.1002/jnr.22827

Wang, H., Brozoski, T. J., Turner, J. G., Ling, L., Parrish, J. L., Hughes, L. F., et al. (2009). Plasticity at glycinergic synapses in dorsal cochlear nucleus of rats with behavioral evidence of tinnitus. *Neuroscience* 164, 747–759. doi: 10.1016/j.neuroscience.2009.08.026

Wenthold, R. J. (1987). Evidence for a glycinergic pathway connecting the two cochlear nuclei: an immunocytochemical and retrograde transport study. *Brain Res.* 415, 183–187. doi: 10.1016/0006-8993(87)90285-x

Whiting, B., Moiseff, A., and Rubio, M. E. (2009). Cochlear nucleus neurons redistribute synaptic AMPA and glycine receptors in response to monaural conductive hearing loss. *Neuroscience* 163, 1264–1276. doi: 10.1016/j.neuroscience.2009.07.049

Wu, C., Stefanescu, R. A., Martel, D. T., and Shore, S. E. (2016). Tinnitus: maladaptive auditory-somatosensory plasticity. *Hear Res.* 334, 20–29. doi: 10.1016/j.heares.2015.06.005

Zhao, Y., Song, Q., Li, X., and Li, C. (2016). Neural hyperactivity of the central auditory system in response to peripheral damage. *Neural Plast.* 2016:2162105. doi: 10.1155/2016/2162105

Conflict of Interest: The authors declare that the research was conducted in the absence of any commercial or financial relationships that could be construed as a potential conflict of interest.

frontiers in Synaptic Neuroscience

ORIGINAL RESEARCH
published: 18 November 2021
doi: 10.3389/fnsyn.2021.748929

Neuron Type-Dependent Synaptic Activity in the Spinal Dorsal Horn of Opioid-Induced Hyperalgesia Mouse Model

*Austin Kearns[1], Jazmine Jayasi[1], Xin Liu[2], Jigong Wang[2], Yuqiang Shi[2], Jin Mo Chung[2], Jun-Ho La[2], Shao-Jun Tang[2] and Chilman Bae[1,2]**

[1] School of Electrical, Computer, and Biomedical Engineering, Southern Illinois University, Carbondale, IL, United States,
[2] Department of Neuroscience, Cell Biology, and Anatomy, University of Texas Medical Branch, Galveston, TX, United States

Opioids are widely used for pain relief; however, chronic opioid use causes a paradoxical state of enhanced pain sensitivity, termed "Opioid-induced hyperalgesia (OIH)." Despite the clinical importance of OIH, the detailed mechanism by which it enhances pain sensitivity remains unclear. In this study, we tested whether repeated morphine induces a neuronal circuit polarization in the mouse spinal dorsal horn (SDH). Transgenic mice expressing GFP to neurokinin 1 receptor-expressing neurons (sNK1Rn) and GABAergic interneurons (sGABAn) that received morphine [20 mg/kg, once daily for four consecutive days (i.p.)] developed mechanical hypersensitivity. Repeated morphine altered synaptic strengths in the SDH as a specific cell-type but not in a gender-dependent manner. In sNK1Rn and non-tonic firing neurons, repeated morphine treatment significantly increased frequency of spontaneous excitatory postsynaptic current (sEPSC) and evoked EPSC (eEPSC). In addition, repeated morphine treatment significantly decreased evoked inhibitory postsynaptic current (eIPSC) in sNK1Rn. Conversely, in sGABAn and tonic firing neurons, repeated morphine treatment significantly decreased sEPSC frequency and eEPSC, but had no change of eIPSC in sGABAn. Interestingly, repeated morphine treatment significantly decreased neuronal rheobase of sNK1Rn but had no effect on sGABAn. These findings suggest that spinal neuronal circuit polarization maybe the mechanism of OIH and identify a potential therapeutic mechanism to prevent or treat opioid-induced pain.

Keywords: opioid-induced hyperalgesia, spinal cord dorsal horn, neurokinin 1 receptor, GABAergic interneurons, central sensitization, morphine, pain, neuronal circuit polarization

OPEN ACCESS

Edited by:
Michael Telias, University of California, Berkeley, United States

Reviewed by:
Asaf Keller, University of Maryland, Baltimore, United States
Sascha R. Alles, University of New Mexico School of Medicine, United States

***Correspondence:**
Chilman Bae
chilman.bae@siu.edu

Received: *28 July 2021*
Accepted: *26 October 2021*
Published: *18 November 2021*

Citation:
Kearns A, Jayasi J, Liu X, Wang J, Shi Y, Chung JM, La J-H, Tang S-J and Bae C (2021) Neuron Type-Dependent Synaptic Activity in the Spinal Dorsal Horn of Opioid-Induced Hyperalgesia Mouse Model. Front. Synaptic Neurosci. 13:748929. doi: 10.3389/fnsyn.2021.748929

INTRODUCTION

Chronic pain is a significant health problem. Globally, 1 in 5 adults suffer from pain, and 1 in 10 adults are diagnosed with chronic pain each year (Goldberg and McGee, 2011). Paradoxically, patients who are repeatedly treated with opioids are routinely diagnosed with enhanced acute and/or chronic pain, an exacerbated pain condition known as opioid-induced hyperalgesia (OIH; Angst and Clark, 2006; Chu et al., 2006). OIH is clinically prevalent and patients who receive

repeated opioid treatment experience significant hyperalgesia (Cohen et al., 2008; Chen et al., 2009; Hay et al., 2009). However, the underlying mechanism of OIH remains to be elucidated.

Recently, synaptic at excitatory and inhibitory synapses have been characterized as a prime mechanism of chronic pain (Luo et al., 2014). In neuropathic pain conditions, synaptic plasticity in the spinal dorsal horn (SDH) is present in the long-term potentiation (LTP) of spinothalamic tract projection plasticity neurons (Ikeda et al., 2009) and long-term depression (LTD) of GABAergic neurons (GABAn; Bittar et al., 2017). Our recent studies revealed differential synaptic plasticity between spinothalamic tract projection neurons and GABAn in SDH of spinal nerve ligation mouse model (Kim et al., 2015; Bittar et al., 2017). Recent studies revealed that ablation of spinal neurokinin-1 receptor neuron (NK1Rn) prevents the development of hyperalgesia (Mantyh et al., 1997; Nichols et al., 1999), and OIH (Vera-Portocarrero et al., 2007), and spinal administration of an NK1R antagonist reverses OIH (King et al., 2005). In addition, synaptic response of spinal NK1Rn to afferent inputs increases with disinhibition (Torsney and MacDermott, 2006).

Due to the critical role of spinal NK1Rn and GABAn in chronic pain including OIH, we hypothesized that repeated morphine use may alter neuron type-dependent synaptic strengths in the SDH, thus leading to OIH. To test this hypothesis, we performed mechanical behavior test and *ex vivo* electrophysiological recording on SDH neurons. We found that in the OIH mouse model, excitatory synaptic strength increased in excitatory neurons but decreased in inhibitory neurons, while inhibitory synaptic strength and neuronal rheobase were depressed in only excitatory neurons. These findings suggest that neuronal type-dependent central sensitization may be a mechanism of OIH.

MATERIALS AND METHODS

Animals

All mice were maintained in Association for Assessment and Accreditation of Laboratory Animal Care International-accredited UTMB animal facility. The mice were housed in a plastic cage with standard bedding and free access to food and water on a 12/12-h light/dark cycle. Six to 8-week-old transgenic mice tagged with GFP to neurokinin 1 receptor-expressing neurons (sNK1Rn) (NK1R-GFP) (Green et al., 2019) and GABAergic interneurons (sGABAn) (FVB-Tg(GAD67-GFP) 45704Swn/J, Jackson Laboratory) in the SDH were used for behavior tests and electrophysiological recordings. For the morphine-treated groups, morphine was administered (i.p.) at a dose of 20 mg/kg by a single injection each day for four consecutive days (**Figure 1A**, blue arrow).

Behavioral Testing

Mechanical nociceptive hypersensitivity in mice was measured as previously described (Callahan et al., 2008). The hind paw between the third and fourth toe in a resting state was stimulated with calibrated von Frey filaments (Stoelting, Wood Dale, IL, United States), and paw withdrawal threshold (PWT) was determined using the Dixon up and down paradigm. For thermal nociceptive sensitivity testing, paw withdrawal latency to a 52°C stimulus was measured using the hot plate test as previously described (Espejo and Mir, 1993). The latency to hind paw licking and/or shaking or jumping were determined. All tests were conducted 2 h prior to drug administration in order to avoid the antinociceptive effect of morphine. The experimenter was blind to the treatments received by individual animals (**Figure 1A**, black arrow). Given that sex is an important factor in pain studies and analgesia, we measured PWT in both male and female mice (Melchior et al., 2016; Roeckel et al., 2017).

Spinal Cord Slice Preparation and Electrophysiological Recording of Dorsal Horn Neurons

Spinal cord slices were taken from OIH mouse model 1 day after the last morphine injection (**Figure 1A**, red arrow) and prepared as previously described (Bae et al., 2018). Briefly, the spinal cord was sliced transversely at a thickness of 350 μm using a vibratome (Leica VT1200S, Buffalo Grove, IL, United States) in cold (∼4°C) NMDG (N-methyl-D-glucamine) solution (in mM: 93 NMDG, 2.5 KCl, 1.2 NaH_2PO_4, 30 $NaHCO_3$, 20 HEPES, 25 glucose, 5 sodium ascorbate, 2 thiourea, 3 sodium pyruvate, 10 $MgSO_4$ and 0.5 $CaCl_2$, pH 7.4), saturated with 95% O_2 and 5% CO_2. Whole-cell patch clamp recordings were made on random or GFP fluorescently identified neurons in lamina II in artificial cerebrospinal fluid (ACSF in mM: 124 NaCl, 2.5 KCl, 1.2 NaH_2PO_4, 24 $NaHCO_3$, 5 HEPES, 12.5 glucose, 2 $MgSO_4$, and 2 $CaCl_2$, pH 7.4) using Multiclamp 700B amplifier, DigiDATA, and pClamp software (version 10.6 Molecular Device, Sunnyvale, CA, United States) at a 10 kHz sampling rate and a 2 kHz filtering rate. The patch-pipettes (4 – 8 MΩ) were filled with internal solution (in mM: 120 K-gluconate, 10 KCl, 2 Mg-ATP, 0.5 Na-GTP, 0.5 EGTA, 20 HEPES, and 10 phosphocreatine, pH 7.3).

Spinal dorsal horn neurons were identified by their action potential (AP) firing patterns upon depolarizing current injections (Lee et al., 2020) or using transgenic mice. After making whole-cell recording configuration, step currents (10 pA step, 300 ms duration, and 5-s intervals) were injected through the patch electrode to determine rheobase and AP firing patterns. We recorded the whole cell membrane capacitance, membrane resistance, access resistance, and resting membrane potential (**Table 1**). The spontaneous excitatory postsynaptic currents (sEPSC) were recorded for 60 s at −65 mV in ACSF (Bae et al., 2018; Lee et al., 2020). To minimize the contamination of IPSC by outward EPSC through ionotropic glutamate receptors, we recorded the IPSC at the reported reversal potential (0 mV) of EPSC through those receptors. EPSCs and IPSCs were evoked by focal electrical stimulation in the vicinity of recorded neurons with a metal bipolar electrode (MicroProbes, Gaithersburg, MD, United States). Test pulses were given for 0.5 ms at 5-s intervals and stimulation intensities ranging from 20 to 200 μA (20 μA step). Monosynaptic evoked EPSCs (eEPSC) and IPSC (eIPSC) were determined based on three criteria: constant short latency, a smooth waveform with a single peak (without jitter), and consistent responses without failure to repeated stimuli

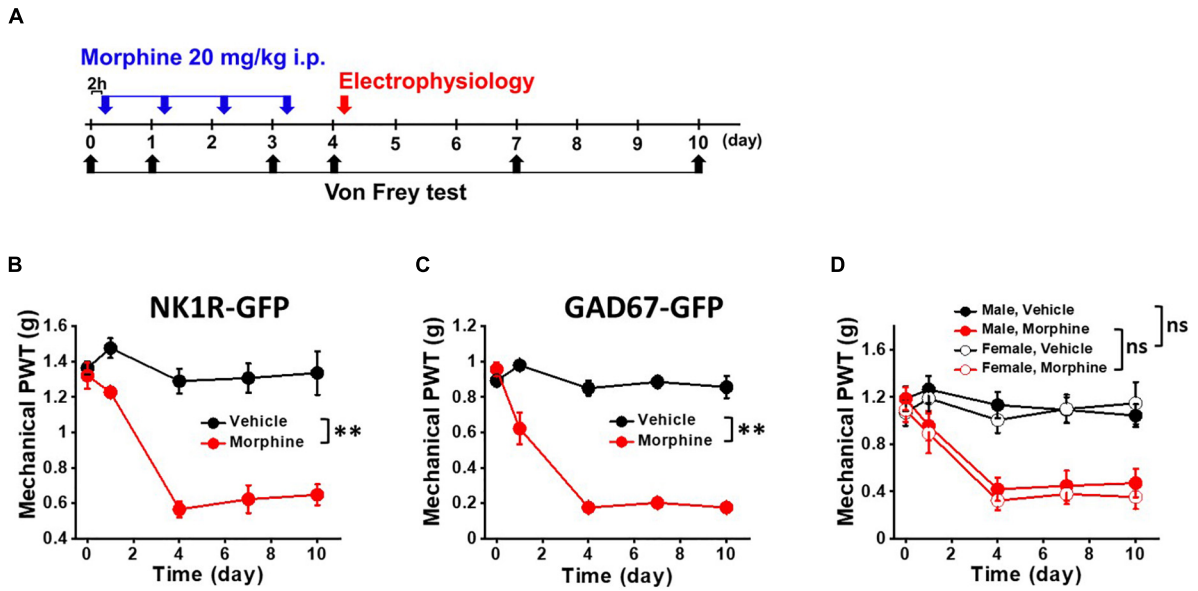

FIGURE 1 | Repeated morphine treatment induced mechanical hypersensitivity in NK1R-GFP and GAD67-GFP transgenic mice. **(A)** Temporal diagram of drug administration and experiments. Morphine (blue arrow, 20 mg/kg) were administrated by intraperitoneal injection. At day 4, the mice were euthanized for electrophysiological recordings (red arrow). Pain behavioral test was performed 2 h post-morphine injection. Paw withdrawal threshold (PWT) was measured by von Frey tests (black arrow) using **(B)** NK1R-GFP mice for sNK1Rn ($N = 6$ for each group) and **(C)** GAD67-GFP mice for sGABAn ($N = 6$ for each group). **(D)** No gender effect on the repeated morphine induced mechanical hypersensitivity (Male,Vehicle ($N = 3$); Male, Morphine ($N = 3$); Female, Vehicle ($N = 3$); Female, Morphine ($N = 3$). ns: not significant, $^{**}p < 0.01$ vs. vehicle by Sidak's multiple comparison test following multilevel analysis.

TABLE 1 | Comparison of the principal passive electrophysiological properties of vehicle and morphine treatments in sNK1Rn and sGABAn.

	sNK1Rn		sGABAn	
	Vehicle	**Morphine**	**Vehicle**	**Morphine**
Membrane capacitance (pF)	30.1 ± 1.5	29.8 ± 2.6	28.9 ± 1.4	27.2 ± 1.3
Membrane resistance (MΩ)	376.7 ± 35.0	394.7 ± 47.6	420.2 ± 25.3	446.4 ± 30.7
Access resistance (MΩ)	15.0 ± 1.6	17.3 ± 1.7	14.5 ± 0.8	14.3 ± 0.9
Resting membrane potential (mV)	−64.8 ± 1.8	−64.5 ± 1.7	−61.9 ± 1.1	−60.7 ± 1.3
Number of mice (N), cells (n)	N:5, n:27	N:4, n:24	N:7, n:65	N:8,n:48

Values of membrane capacitance, membrane resistance, access resistance, and resting membrane potential for vehicle and morphine treatments are reported as mean ± SEM and were statistically compared by Mann–Whitney t test.

(Kim et al., 2015; Bittar et al., 2017). All recordings showing polysynaptic responses were disregarded.

Statistical Analysis

All data were expressed as the mean ± standard error of the mean (SEM) with n, the number of cells and N, the number of mice. For electrophysiology data, all neurons from each individual mice were averaged and considered as a single data point. Means of vehicle and morphine-treated sEPSC frequency and amplitude were compared by Welch's *t* test. The behavioral and eEPSC/eIPSC data were analyzed with Sidak's multiple comparison test following multilevel analysis. Rheobase data were analyzed using Welch's *t* test and ordinary one-way ANOVA with Tukey's multiple comparisons test. Results were considered statistically significant when $p < 0.05$. We used Hedges' g as a measure of effect size. Hedges' g is Cohen's d multiplied by a correction factor and takes each sample size into consideration.

RESULTS

Repeated Morphine Treatment Induced Mechanical Hypersensitivity

For OIH mouse model, we modeled the systemic administration of morphine in patients by i.p. injection (Cai et al., 2016). We first tested whether repeated morphine treatment induced mechanical hypersensitivity in our transgenic mice for allowing identification of sNK1Rn and sGABAn. After the fourth daily injection of morphine (**Figure 1A**, blue arrows), OIH was successfully established in both strains (**Figures 1B,C**). PWTs were significantly reduced by repeated morphine in the mice for sNKR1n (**Figure 1B**) ($F_{(1,5.67)} = 61.85$, $p < 0.001$, $N = 6$ for each group) and for sGABAn (**Figure 1C**) ($F_{(1,10)} = 106.55$, $p < 0.001$, $N = 6$ for each group) in comparison to vehicle. Behavioral tests were performed on male and female from both strains and showed no significant difference (**Figure 1D**) [Morphine: $F_{(1,10)} = 0.36$, $p = 0.561$, Male ($N = 6$), Female ($N = 6$)] [Vehicle: ($F_{(1,\ 10)} = 0.07$, $p = 0.800$, Male ($N = 6$), Female

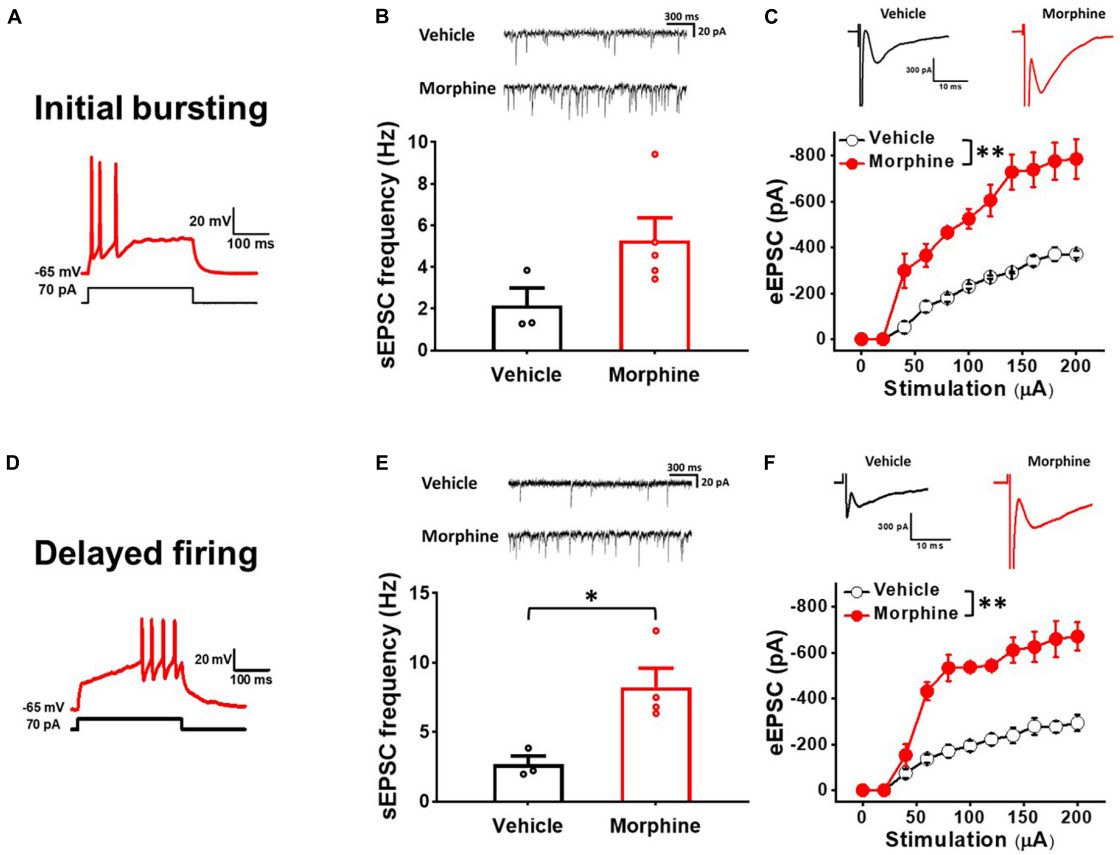

FIGURE 2 | Repeated morphine treatment increased excitatory synaptic strength in non-tonic firing (Initial bursting and Delayed) neurons in the SDH. **(A)** Representative trace of initial bursting neurons. **(B)** (top) Representative traces of spontaneous excitatory postsynaptic current (sEPSC) and (bottom) sEPSC frequency in initial bursting neurons (effect size: 1.47, $p = 0.063$; Vehicle: $N = 3$, $n = 16$; Morphine: $N = 5$, $n = 36$). **(C)** (top) Representative traces of eEPSC in initial bursting neurons and (bottom) stimulus-responsive curve of eEPSC ($F_{(1,29.13)} = 211.78$, $p < 0.001$; Vehicle: $N = 3$, $n = 13$; Morphine: $N = 3$, $n = 8$). $^{**}p < 0.01$ vs. vehicle by Sidak's multiple comparison test following multilevel analysis. **(D)** Representative trace of delayed firing neurons. **(E)** (top) Representative traces of sEPSC and (bottom) sEPSC frequency in delayed firing neurons (effect size: 2.50, p = 0.020; Vehicle: $N = 3$, $n = 7$; Morphine: $N = 4$, $n = 11$). $^{*}p < 0.05$ by Welch's t test. **(F)** (top) Representative traces of eEPSC in delayed firing neurons and (bottom) stimulus-responsive curve of eEPSC ($F_{(1,5.84)} = 82.81$, $p < 0.001$). $^{**}p < 0.01$ vs. vehicle by Sidak's multiple comparison test following multilevel analysis (Vehicle: $N = 3$, $n = 9$; Morphine: $N = 3$, $n = 7$).

($N = 6$)]. Thus, all *ex vivo* electrophysiological recordings were performed on any gender.

Repeated Morphine Treatment Increased Excitatory Synaptic Strength in Non-tonic Firing Neurons in the Spinal Dorsal Horn

To determine whether repeated morphine alters synaptic strengths as a cell-type manner, we performed electrophysiological recordings on non-tonic firing neurons (presumably excitatory neurons) in the laminae II of the SDH (Lee et al., 2020). In initial bursting neurons (**Figure 2A**), the frequency of sEPSC was increased, but not significantly, by repeated morphine when compared to vehicle (**Figure 2B**) [effect size: 1.47, $p = 0.063$; Vehicle: 2.15 ± 0.85 Hz ($N = 3$, $n = 16$); Morphine: 5.29 ± 1.08 Hz ($N = 5$, $n = 36$)]. However, eEPSC in initial bursting neurons was significantly increased by morphine when compared to vehicle (**Figure 2C**) [$F_{(1,29.13)} = 211.78$, $p < 0.001$; Vehicle ($N = 3$, $n = 13$); Morphine ($N = 3$, $n = 8$)]. The stimulus-response curve was left shifted by repeated morphine. In delayed firing neurons (**Figure 2D**), the frequency of sEPSC was significantly increased by repeated morphine when compared to vehicle (**Figure 2E**) [effect size: 2.50, $p = 0.020$; Vehicle: 2.68 ± 0.59 Hz ($N = 3$, $n = 7$); Morphine: 8.24 ± 1.57 Hz ($N = 4$, $n = 11$)]. eEPSC in delayed firing neurons was also significantly increased by morphine when compared to vehicle (**Figure 2F**) [$F_{(1,5.84)} = 82.81$, $p < 0.001$; Vehicle ($N = 3$, $n = 9$); Morphine ($N = 3$, $n = 7$)].

Repeated Morphine Treatment Increased Excitatory Synaptic Strength in sNK1Rn

To confirm whether repeated morphine alters synaptic strengths as neuronal type-specific manner, we performed electrophysiological recordings on fluorescently identified sNK1Rn (**Figure 3**). sEPSC frequency in sNK1Rn was significantly increased by repeated morphine when compared

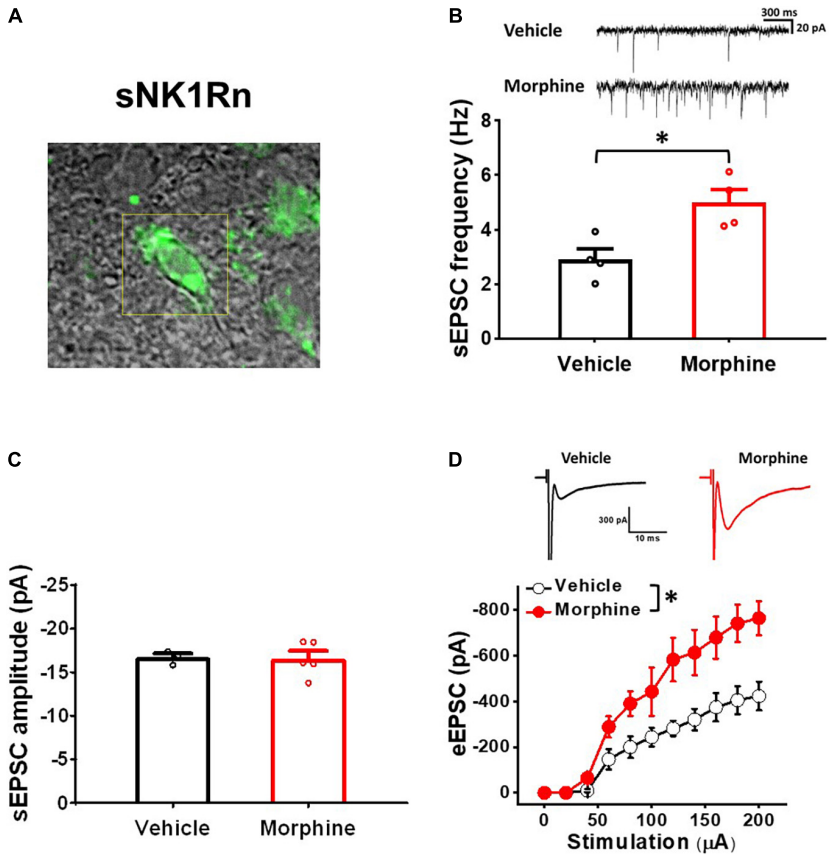

FIGURE 3 | Repeated morphine treatment increased excitatory synaptic strength in sNK1Rn. **(A)** Fluorescent identification of sNK1Rn. **(B)** (top) Representative traces of sEPSC and (bottom) sEPSC frequency (effect size: 2.38, $p = 0.016$; Vehicle: $N = 4$, $n = 27$; Morphine: $N = 4$, $n = 35$). *$p < 0.05$ by Welch's t test **(C)** sEPSC amplitude (effect size: 0.09, $p = 0.891$; Vehicle: $N = 3$, $n = 24$; Morphine: $N = 5$, $n = 41$). **(D)** (top) Representative traces of eEPSC and (bottom) stimulus-response curve of eEPSC [$F_{(1,5.56)} = 9.37$, $p = 0.024$; Vehicle ($N = 4$, $n = 24$), Morphine ($N = 4$, $n = 26$)]. *$p < 0.05$ vs. vehicle by Sidak's multiple comparison test following multilevel analysis.

to vehicle (**Figure 3B**) [effect size: 2.38, $p = 0.016$; Vehicle: 2.90 ± 0.39 Hz ($N = 4$, $n = 27$); Morphine: 4.99 ± 0.48 Hz ($N = 4$, $n = 35$)] but showed no significant difference in sEPSC amplitude (**Figure 3C**) [effect size:0.09, $p = 0.891$; Vehicle: −16.72 ± 0.46 pA ($N = 3$, $n = 24$); Morphine: −16.58 ± 0.88 pA ($N = 5$, $n = 41$)]. eEPSC in sNK1Rn was also significantly increased by morphine when compared to vehicle (**Figure 3D**) [$F_{(1,5.56)} = 9.37$, $p = 0.024$; Vehicle ($N = 4$, $n = 24$); Morphine ($N = 4$, $n = 26$)]. The stimulus-response curve was left shifted by repeated morphine. Together, results from non-tonic firing neurons and sNK1Rn suggest that repeated morphine increases excitatory synaptic strength to excitatory neurons in SDH.

Repeated Morphine Treatment Decreased Excitatory Synaptic Strength in Tonic Firing Neurons in Spinal Dorsal Horn

To ensure that repeated morphine alters synaptic strengths as neuron type-manner, we repeated the above experiments using tonic firing neurons (presumably inhibitory neurons) in the laminae II of the SDH (**Figure 4**) (Lee et al., 2020). The frequency of sEPSC in tonic firing neurons was significantly decreased by repeated morphine when compared to vehicle (**Figure 4B**) [effect size:−3.44, $p = 0.018$; Vehicle: 1.34 ± 0.20 Hz ($N = 3$, $n = 12$); Morphine: 0.34 ± 0.12 Hz ($N = 5$, $n = 16$)]. eEPSC in tonic firing neurons was also significantly decreased by morphine when compared to vehicle (**Figure 4C**) [$F_{(1,5.92)} = 25.56$, $p = 0.002$; Vehicle ($N = 4$, $n = 9$); Morphine ($N = 3$, $n = 7$)]. The stimulus-response curve was right shifted by repeated morphine.

Repeated Morphine Treatment Decreased Excitatory Synaptic Strength in GABAergic Interneurons

To confirm whether repeated morphine alters synaptic strengths in inhibitory neurons in the SDH, we performed electrophysiological recordings on fluorescently identified sGABAn (**Figure 5**). sEPSC frequency in sGABAn was significantly decreased by repeated morphine when compared to vehicle (**Figure 5A**) [effect size:−1.46, $p = 0.012$; Vehicle: 1.2 ± 0.2 Hz ($N = 9$, $n = 143$); Morphine: 0.7 ± 0.1 Hz ($N = 10$,

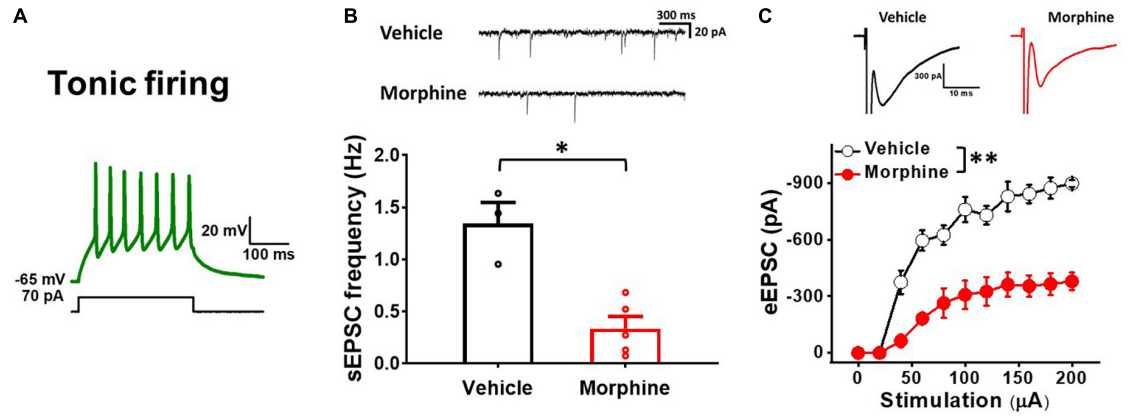

FIGURE 4 | Repeated morphine treatment decreases excitatory synaptic strength in tonic firing neurons in SDH. **(A)** Representative trace of tonic firing neurons. **(B)** (top) Representative traces of sEPSC and (bottom) sEPSC frequency (effect size:–3.44, $p = 0.018$; Vehicle: $N = 3$, $n = 12$; Morphine: $N = 5$, $n = 16$). $^{*}p < 0.05$ by Welch's t test. **(C)** (top) Representative traces of eEPSC and (bottom) Stimulus-responsive curve of eEPSC [$F_{(1,5.92)} = 25.56$, $p = 0.002$; Vehicle ($N = 4$, $n = 9$); Morphine ($N = 3$, $n = 7$)]. $^{**}p < 0.01$ vs. vehicle by Sidak's multiple comparison test following multilevel analysis.

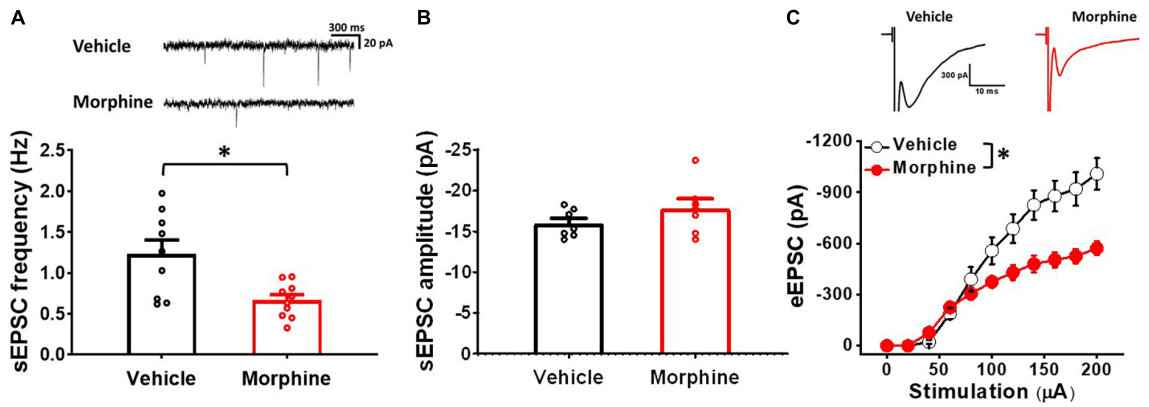

FIGURE 5 | Repeated morphine treatment decreased excitatory synaptic strength in sGABAn. **(A)** (top) Representative traces of sEPSC and (bottom) sEPSC frequency (effect size:–1.46, $p = 0.012$; Vehicle: $N = 9$, $n = 143$; Morphine: $N = 10$, $n = 123$). $^{*}p < 0.05$ by Welch's t test. **(B)** sEPSC amplitude (effect size:–0.71, $p = 0.214$; Vehicle: $N = 7$, $n = 104$; Morphine: $N = 7$, $n = 102$). **(C)** (top) Representative traces of eEPSC and (bottom) stimulus-response curve of eEPSC (**Figure 5C**) [$F_{(1,17.47)} = 4.96$, $p = 0.039$; Vehicle ($N = 9$, $n = 32$); Morphine ($N = 10$, $n = 87$)]. $^{*}p < 0.05$ vs. vehicle by Sidak's multiple comparison test following multilevel analysis.

$n = 123$)] but showed no significant difference in sEPSC amplitude (**Figure 5B**) [effect size:−0.71, $p = 0.214$; Vehicle: -15.98 ± 0.64 pA ($N = 7$, $n = 104$); Morphine: -17.81 ± 1.20 pA ($N = 7$, $n = 102$)]. eEPSC in sGABAn was also significantly decreased by morphine when compared to vehicle (**Figure 5C**) [$F_{(1,17.47)} = 4.96$, $p = 0.039$; Vehicle ($N = 9$, $n = 32$); Morphine ($N = 10$, $n = 87$)]. The stimulus-response curve was right shifted by repeated morphine. Together, results from tonic firing neurons and sGABAn suggest that repeated morphine decreases excitatory synaptic strength to inhibitory neurons in SDH.

Gender Did Not Affect Repeated Morphine-Induced Changes of Synaptic Strength in Spinal Dorsal Horn

We examined whether neuron-type dependent synaptic strength changes in SDH is gender dependent (**Figure 6**). Even though morphine significantly affected sEPSC frequency and eEPSC in each gender, there was no significant difference between both genders in either vehicle or morphine treated group. In non-tonic firing neurons, vehicle treated mice had sEPSC frequency of 2.36 ± 0.72 Hz in male mice ($N = 3$, $n = 20$) and 2.67 ± 0.38 Hz in female mice ($N = 3$, $n = 9$) (effect size: 0.31, $p = 0.728$) (**Figure 6A**). Morphine treated mice had sEPSC frequency of 5.57 ± 0.47 Hz in male mice ($N = 3$, $n = 25$) and 5.62 ± 0.19 Hz in female mice ($N = 3$, $n = 29$) (effect size: 0.08, $p = 0.930$). eEPSC also showed no gender difference in vehicle group and morphine treated group (**Figure 6B**). In sGABAn, vehicle treated mice had sEPSC frequency of 1.43 ± 0.43 Hz in male mice ($N = 6$, $n = 97$) and 1.45 ± 0.17 Hz in female mice ($N = 3$, $n = 46$) (effect size: 0.05, $p = 0.929$). Morphine treated mice had sEPSC frequency of 0.67 ± 0.14 Hz in male mice ($N = 5$, $n = 50$) and 0.57 ± 0.14 Hz in female mice ($N = 5$, $n = 71$) (effect size:−0.67 $p = 0.465$)

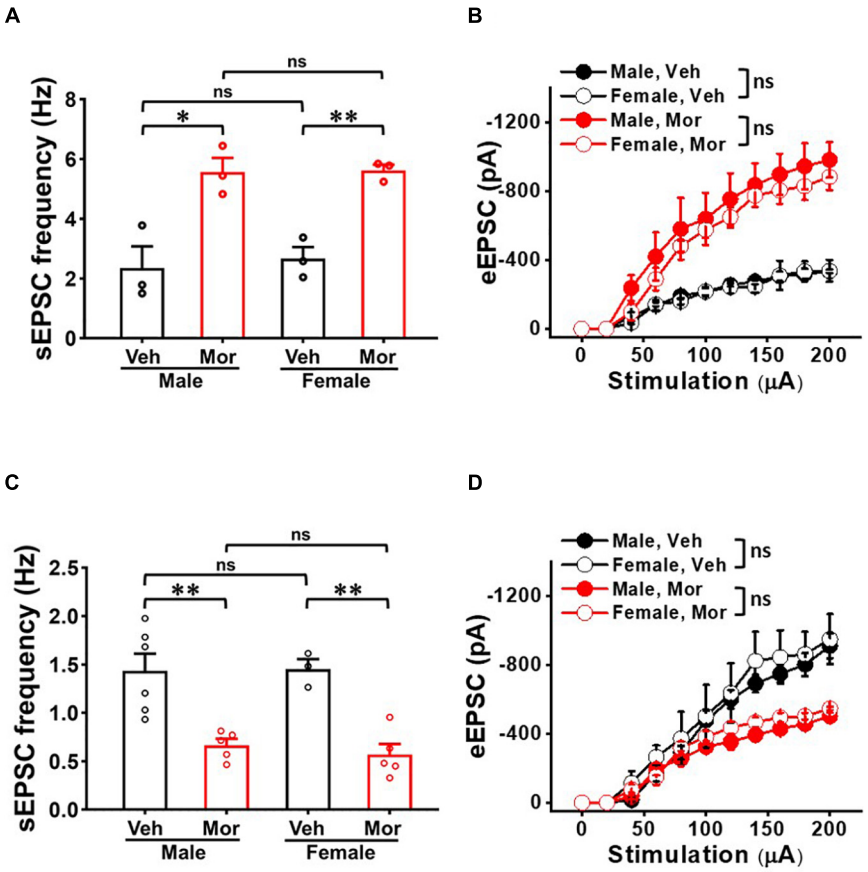

FIGURE 6 | No gender effect on the repeated morphine-induced synaptic strength in SDH. **(A)** sEPSC frequency [effect size: 0.31, $p = 0.728$; Veh: Male ($N = 3$, $n = 20$) vs. Female ($N = 3$, $n = 9$) and effect size: 0.08, $p = 0.930$; Mor: Male ($N = 3$, $n = 25$) vs. Female ($N = 3$, $n = 29$)] and **(B)** eEPSC (Veh: Male ($N = 3$, $n = 15$) vs. Female ($N = 3$, $n = 7$); Mor: Male ($N = 3$, $n = 8$) vs. Female ($N = 3$, $n = 13$) in non-tonic firing neurons. **(C)** sEPSC frequency (Veh: Male ($N = 6$, $n = 97$) vs. Female ($N = 3$, $n = 46$); effect size: 0.05, $p = 0.929$ and Mor: Male ($N = 7$, $n = 66$) vs. Female ($N = 3$, $n = 53$); effect size: –0.02, $p = 0.874$) and **(D)** eEPSC (Veh: Male ($N = 3$, $n = 19$) vs. Female ($N = 3$, $n = 13$), $F_{(1,\ 6.09)} = 0.41$, $p = 0.544$. Mor: Male ($N = 3$, $n = 19$) vs. Female ($N = 3$, $n = 13$), $F_{(1,6.09)} = 0.41$, $p = 0.544$) in sGABAn. $^{*}p < 0.05$ or $^{**}p < 0.01$; Welch's t test. ns: not significant. Sidak's multiple comparison test following multilevel analysis. Veh: Vehicle, Mor: Morphine.

(**Figure 6C**). In addition, eEPSC showed no gender difference in vehicle group and morphine treated group (**Figure 6D**) (Vehicle: Male ($N = 3$, $n = 19$) vs. Female ($N = 3$, $n = 13$), $F_{(1,6.09)} = 0.41$, $p = 0.544$; Morphine: Male ($N = 3$, $n = 23$) vs. Female ($N = 3$, $n = 22$), $F_{(1,9.01)} = 0.95$, $p = 0.355$).

Repeated Morphine Treatment Decreased Inhibitory Synaptic Strength in sNK1Rn

To determine whether repeated morphine alters inhibitory synaptic strengths, we measured eIPSC on sNK1Rn and sGABAn (**Figure 7**). eIPSC in sNK1Rn was significantly reduced by morphine compared to vehicle (**Figures 7A,B**) [$F_{(1,3.23)} = 19.84$, $p = 0.018$; Vehicle ($N = 4$, $n = 9$); Morphine ($N = 4$, $n = 19$)] and showed a right shift in the stimulus-response curve. However, eIPSC in sGABAn showed no significant difference by morphine (**Figure 7C**) [$F_{(1,11.32)} = 0.10$, $p = 0.757$; Vehicle ($N = 7$, $n = 48$); Morphine ($N = 6$, $n = 26$)]. Interestingly, in vehicle groups, eIPSC at 140 μA stimulation was significantly larger in sNK1Rn in comparison to sGABAn (**Figure 7D**) [effect size: −6.73, $p = 0.002$; sNK1Rn (425.68 ± 48.08 pA, $N = 4$, $n = 9$); sGABAn (15.48 ± 11.67 pA, $N = 7$, $n = 48$)].

Repeated Morphine Treatment Decreased Rheobase of sNK1Rn

To determine whether the altered synaptic strengths can change neuronal excitability, we measured rheobase of sNK1Rn and sGABAn (**Figure 8**). Rheobase of sNK1Rn was significantly reduced by morphine compared to vehicle [effect size: −2.48, $p = 0.022$; Vehicle: 48.68 ± 7.30 μA ($N = 4$, $n = 21$); Morphine: 20.21 ± 3.54 μA ($N = 4$, $n = 17$)]. However, rheobase of sGABAn showed no significant difference by morphine [effect size: 0.15, $p = 0.812$; Vehicle: 20.69 ± 2.28 μA ($N = 4$, $n = 45$); Morphine: 22.29 ± 5.98 μA ($N = 5$, $n = 28$)]. Interestingly, in vehicle groups, rheobase of sGABAn was significantly smaller in comparison to sNK1Rn (effect size: −2.55, $p = 0.026$). These results suggest that repeated morphine preferentially sensitizes sNK1Rn excitability. Throughout the experiments we recorded the passive

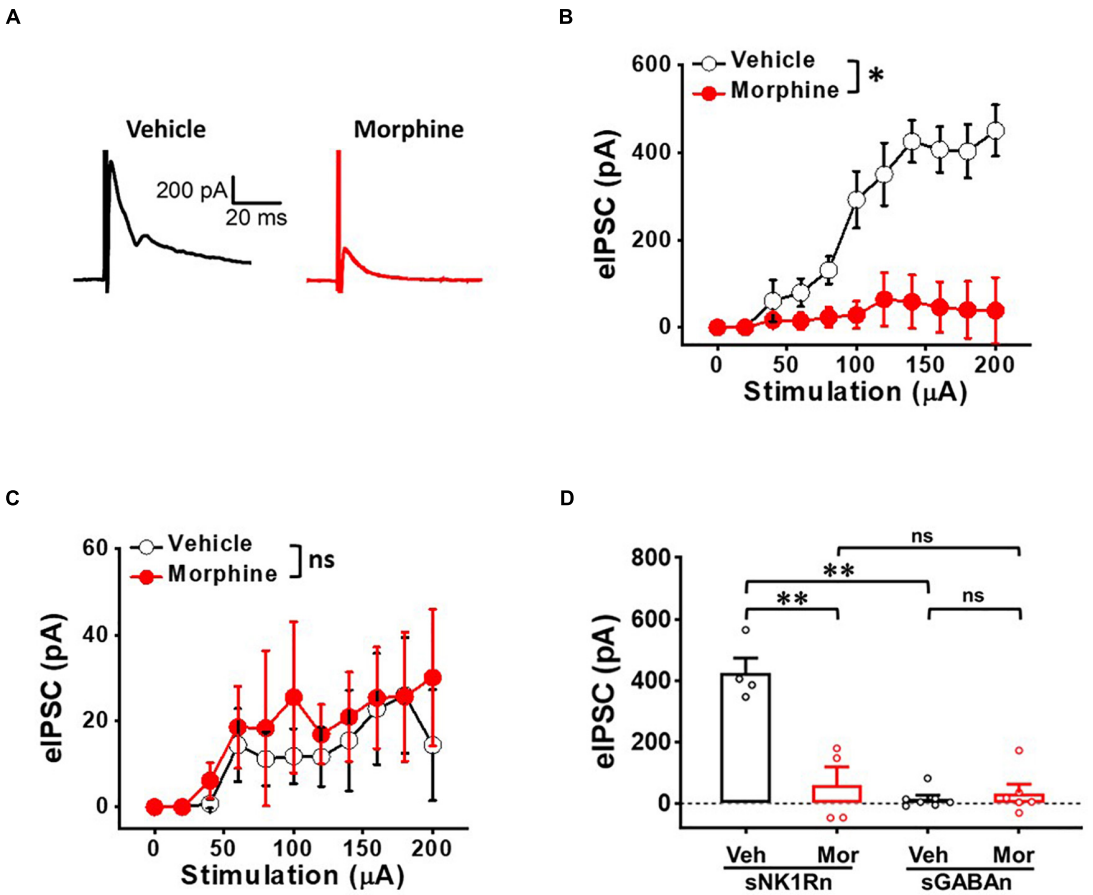

FIGURE 7 | Repeated morphine treatment decreases inhibitory synaptic strength in sNK1Rn. **(A)** Representative traces of evoked inhibitory postsynaptic current (eIPSC) from sNK1Rn. Stimulus-response curve of eIPSC from panel **(B)** sNK1Rn (Vehicle: $N = 4$, $n = 9$; Morphine: $N = 4$, $n = 19$) and **(C)** sGABAn (Vehicle: $N = 7$, $n = 48$; Morphine: $N = 6$, $n = 26$). ns: not significant, $^{*}p < 0.05$ vs. vehicle by Sidak's multiple comparison test following multilevel analysis. **(D)** eIPSC (at 140 μA) of sNK1Rn and sGABAn from panels **(B,C)**, respectively. Effect size: –3.34, $p = 0.0037$ for sNK1Rn: Vehicle vs. Morphine. Effect size: 0.37, $p = 0.5718$ for sGABAn: Vehicle vs. Morphine. Effect size: –6.73, $p = 0.002$ between Veh:sNK1Rn and Veh:sGABAn. Effect size: –0.27, $p = 0.734$ between Mor:sNK1Rn and Mor:sGABAn. $^{**}p < 0.01$; Welch's t test.

electrophysiological properties (cell membrane resistance and capacitance, access resistance, and resting membrane potential) and found that there were no difference in neurons from different groups (**Table 1**).

DISCUSSION

In this study, we determined whether repeated morphine treatment changes synaptic strength in the SDH. An OIH mouse model was developed through repeated morphine injection and confirmed using mechanical hypersensitivity testing (**Figure 1**). We performed *ex vivo* whole-cell recordings on the SDH neurons identified by their firing patterns and fluorescently identified excitatory and inhibitory neurons (sNK1Rn and sGABAn). We found that changes in synaptic strength were dependent on neuron type in the OIH mouse model. Results obtained using sNK1Rn and sGABAn were congruous with the results obtained using identification by neuronal firing patterns.

The laminae II in the SDH is a major terminal region for primary afferent fibers that are important for transmitting information related to pain (Todd, 2010). It has been proven that the SDH contains neurons that selectively respond to noxious stimuli (Grudt and Perl, 2002). However, at present, we have a limited understanding about their functional relationship featuring interconnections and morphological types of neurons from the SDH region (Todd, 2017). The Laminae II neurons have been broadly accepted into morphological classification of four main types: islet, vertical, radial and central cells (Grudt and Perl, 2002; Heinke et al., 2004; Yasaka et al., 2007). Islet cells are inhibitory, while radial and vertical cells are excitatory. Nevertheless, certain morphological types have been found in each group (Yasaka et al., 2010). Previous investigations have reported electrophysiological heterogeneity in the laminae II. Rodent SDH neurons were classified according to their depolarization-induced AP firing patterns (Grudt and Perl, 2002; Lu and Perl, 2003) and identified their cell types based on monosynaptic evoked EPSCs and eIPSCs responses, which is in

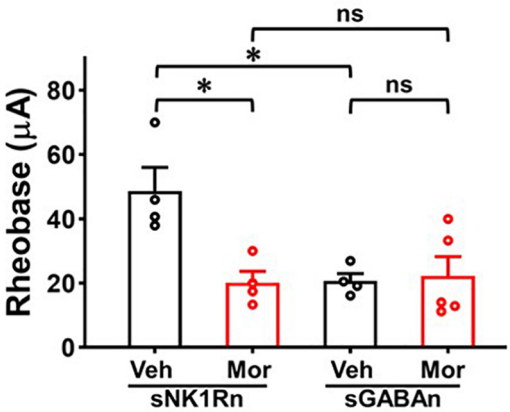

FIGURE 8 | Rheobase of sNK1Rn and sGABAn. Repeated morphine treatment decreased sNK1Rn rheobase (Effect size: –2.48, $p = 0.022$; Vehicle: $N = 4$, $n = 21$, Morphine: $N = 4$, $n = 17$) but had no significant effect on sGABAn rheobase (Effect size: 0.15, $p = 0.812$; Vehicle: $N = 4$, $n = 45$, Morphine: $N = 5$, $n = 28$) $^*p < 0.05$ vs. vehicle by Welch's t test. ns: not significant. In vehicle groups, rheobase of sGABAn was significantly smaller in comparison to sNK1Rn (Effect size: –2.55, $p = 0.026$). $^*p < 0.05$ vs. vehicle of sNK1Rn by ordinary one-way ANOVA with Tukey's multiple comparisons test.

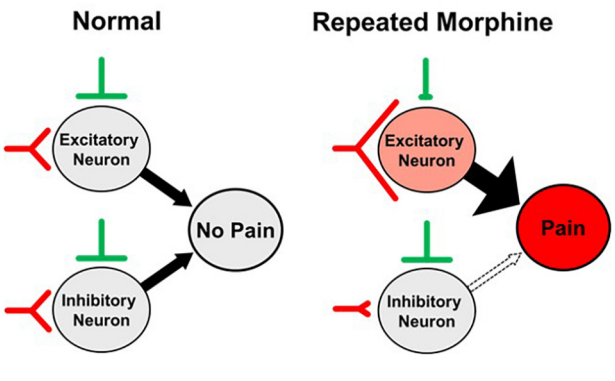

FIGURE 9 | Proposed synaptic mechanism of opioid-induced hyperalgesia (OIH). Repeated morphine causes hyperalgesia (pain) by increasing excitatory input and decreasing inhibitory input to excitatory neurons but disinhibition of inhibitory neurons in the spinal dorsal horn (SDH), leading to differential effects on cell excitability.

accordance with our findings. Moreover, Yasaka et al. grouped neurons based on their discharge patterns and reported that 82% (18 of 22) of non-tonic neurons were excitatory neurons (Yasaka et al., 2010). In this OIH study, based on AP firing pattern results from electrophysiological recordings, 90% (35 of 39 neurons) of sNK1Rn were non-tonic firing neurons [49% initial bursting (17 of 35) and 51% of delayed firing (18 of 35)] and 88% (52 of 59 neurons) of sGABAn were tonic firing neurons. Our OIH model confirmed that sNK1Rn and sGABAn were in accord with our non-tonic and tonic firing neurons results based on their firing patterns. Interestingly, it has been suggested that noxious stimulation leads to the production of phosphorylated ERK in excitatory neurons, resulting in Kv4.2 phosphorylation and changes increased excitability patterns from delayed to tonic firing in the lamina II (Yasaka et al., 2010). Likely, it is possible that morphine may alter firing patterns. Thus, we examined the firing patterns of sNK1Rn and sGABAn treated with vehicle or morphine. We found that sNK1Rn had 50% initial bursting (9 of 18) and 50% delayed firing (9 of 18) in vehicle group and 47% initial bursting (8 of 17) and 53% delayed firing (9 of 17) in morphine group. 96% of sGABAn showed tonic firing in vehicle group and 83% in morphine group, indicating that morphine did not alter the firing patterns.

Opioid-induced hyperalgesia has been suggested to develop differently for various types of pain (Chu et al., 2008). It is important to note that only mechanical, not thermal (data not shown), hypersensitivity was induced after multiple morphine injections in this experiment. In HIV-associated pain, repeated morphine injections in the gp120 mouse pain model induced mechanical hypersensitivity that was present for 18 days (Shi et al., 2019). Other studies also have reported that repeated morphine treatments induced mechanical hypersensitivity but showed no effect on thermal hypersensitivity in mouse model (Roeckel et al., 2017; Fisher et al., 2019; Sasaki et al., 2021). In addition, an opioid related study in healthy human volunteers failed to induce hypersensitivity to noxious heat following the use of remifentanil, whereas mechanical hyperalgesia was progressively enlarged (Angst et al., 2003; Hood et al., 2003). Our results are in line with these previous studies suggesting that the strength of synapses involved in mechanical sensory processing may be more affected by repeated exposure to morphine. However, it has been noted that heat hypersensitivity occurred after 8 days of repeated opioid administration in a study by Mao et al. (1994). Moreover, hyperalgesia associated with withdrawal of opioid has been shown to induce thermal hypersensitivity in rodents (Cabanero et al., 2013).

Spontaneous and evoked EPSC have been used to measure synaptic activity changes. sEPSC frequency is indicative of spontaneous synaptic vesicle transmission (Taylor et al., 1995; Rosenmund and Stevens, 1996; Grabner and Moser, 2018) and of synaptic status in pain conditions including spinal nerve ligation (Gao et al., 2009), painful diabetic neuropathy (Chen et al., 2011), central and peripheral inflammatory pain from TNF-α (Zhang et al., 2011), and chemotherapy-induced peripheral neuropathy (Sisignano et al., 2016). Similarly, eEPSC is a measure of synaptic strength that correspond with the number of presynaptic vesicles and/or post-synaptic receptors for excitatory neurotransmitters (Atasoy et al., 2008). In our previous studies, changes of eEPSC were used as a marker of LTP and LTD in neuropathic pain models (Kim et al., 2015; Bittar et al., 2017). In neuropathic pain conditions, eEPSC was increased in randomly patched neurons in lamina II of the SDH (Chen et al., 2011) and excitatory spinothalamic tract neurons in the SDH (Bittar et al., 2017) but was decreased in GABAergic neurons (Leitner et al., 2013). Our results are in line with these findings. sEPSC frequency and eEPSC increased in sNK1Rn (**Figure 3**) and decreased in sGABAn (**Figure 5**) by repeated morphine indicating that changes of neuron type-dependent synaptic strength correlates with hypersensitivity in the OIH mouse model.

Evoked IPSC is a measure of inhibitory synaptic strength in which stimulus-evoked binding of inhibitory neurotransmitters

opens chloride channels, hyperpolarizing the cell and decreasing the likelihood of AP propagation. eIPSC was decreased in studies of various neuropathic conditions. eIPSC was decreased in randomly patched lamina II neurons in spared nerve injury and chronic constriction injury models (Moore et al., 2002). eIPSC was also decreased in excitatory neurons located in the lamina II of SDH in the partial sciatic nerve ligation model (Imlach et al., 2016). These findings indicate that decreased inhibition of excitatory neurons can be a mechanism of neuropathic pain. In addition, the synaptic response of sNK1Rn to afferent inputs increased when inhibition was suppressed (Torsney and MacDermott, 2006). In rats, excitatory neurons were more disinhibited than inhibitory neurons in SDH (Stikova et al., 2019). In accordance with these findings, our results showed that repeated morphine decreased eIPSC preferentially in sNK1Rn (**Figures 7A,B**). Although pharmacological inhibition was not implemented in this study, sNK1Rn had strong excitatory inputs but significant loss of inhibitory inputs (**Figure 7B**) causing a right-shift in the eIPSC dose-response curve by repeated morphine when recorded at the reversal potential (0 mV), indicating that eIPSC was well isolated. This finding suggests that augmenting synaptic sensitization in excitatory neurons and disinhibition of inhibitory neurons may be an underlying mechanism of OIH.

Rheobase is an indicator of neuronal excitability which represents the threshold current for eliciting neural AP discharge (Li et al., 2009). In neuropathic pain, rheobase was decreased in injured DRG neurons (Kim et al., 1998) and in spared nerve injury model SDH neurons treated with TNF-alpha (Li et al., 2009). In our OIH mouse model, decreased sNK1Rn rheobase (**Figure 8**) indicates increased neural excitability. These findings are in accord with the results of our sEPSC, eEPSC, and eIPSC experiments, indicating the increase in sNK1Rn excitability may be due to the synaptic strength changes. After repeated morphine treatment, sGABAn rheobase showed no significant change but appeared to trend toward depression. Nevertheless, a decrease in sNK1Rn rheobase relative to sGABAn rheobase strongly indicates a net increase in excitability of spinal nociceptive circuits after repeated morphine treatment.

It has been reported that neuron type-dependent synaptic changes are involved in pain. Studies investigating neuropathic pain (Chen et al., 2011; Bittar et al., 2017), inflammatory pain (Park et al., 2011; Zhang et al., 2011), and chemotherapy-induced pain (Sisignano et al., 2016) found that sEPSC frequency and/or eEPSC amplitude were increased in excitatory or randomly patched neurons (Chen et al., 2011; Zhang et al., 2011). Specifically, GABAn and spinothalamic track neurons synaptic plasticity in mouse SDH has been observed in neuropathic pain (Bittar et al., 2017) which is known as an indicator of central sensitization (Kim et al., 2015; Bittar et al., 2017), a phenomenon in which increased membrane excitability and decreased inhibition sensitize nociceptive circuits and contribute to the development of hyperalgesia (Woolf, 2011). Nearly all chronic pain conditions show aspects of central sensitization (Harte et al., 2018), and central sensitization of nociceptive pathways is thought to be an important mechanism in a plethora of pain conditions. Important mechanisms of action of OIH are thought to involve changes in spinal plasticity (Chu et al., 2008; Lee et al., 2011), the central glutaminergic system (Chu et al., 2008), spinal dynorphins (Lee et al., 2011), mu opioid receptor signaling pathways (Roeckel et al., 2016), descending pain facilitation (Vera-Portocarrero et al., 2007; Chu et al., 2008; Roeckel et al., 2016), and decreased neurotransmitter reuptake with enhanced nociceptive response (Lee et al., 2011). Previous studies determined whether NK1Rn is involved in OIH. However, the detailed mechanism of how this NK1Rn is involved in OIH is unknown. Our findings on sNK1Rn and sGABAn indicate that central sensitization caused by neuron type-dependent synaptic activity changes is the underlying mechanism behind hyperalgesia in OIH, and a common and convergent mechanism across many chronic pain conditions.

Interestingly, studies have reported that astrocytes (Sasaki et al., 2021) and reactive oxygen species (ROS) (Shi et al., 2021) in the SDH are critical for OIH. It would be very interesting to test how they may influence neuron type-dependent synaptic activities. For future studies, it is important to also consider studying whether neuron type-dependent synaptic activities are regulated in withdrawal-induced hyperalgesia mouse model.

In conclusion, we investigated the effects of repeated morphine use on mechanical sensitivity and synaptic strength in SDH neurons of OIH mouse model. Our findings suggest that the proposed mechanism of OIH (**Figure 9**) is caused by altered synaptic strengths in the SDH as a cell-type manner, increase of excitatory input and decrease of inhibitory input to excitatory neurons but disinhibition to inhibitory neurons, thus leading to differential effects on cell excitability.

DATA AVAILABILITY STATEMENT

The raw data supporting the conclusions of this article will be made available by the authors, without undue reservation.

ETHICS STATEMENT

The animal study was reviewed and approved by the University of Texas Medical Branch.

AUTHOR CONTRIBUTIONS

S-JT, J-HL, JC, and CB: conceptualization. AK, XL, JW, YS, and CB: methodology. AK, JJ, J-HL, S-JT, and CB: writing. All authors contributed to the article and approved the submitted version.

FUNDING

This study was funded by the National Institutes of Health under award numbers R01DA036165, R01NS079166, R01NS095747, and R01DA050530 to S-JT and Southern Illinois University new faculty start-up grant to CB.

REFERENCES

Angst, M. S., and Clark, J. D. (2006). Opioid-induced hyperalgesia: a qualitative systematic review. *Anesthesiology* 104, 570–587. doi: 10.1097/00000542-200603000-00025

Angst, M. S., Koppert, W., Pahl, I., Clark, D. J., and Schmelz, M. (2003). Short-term infusion of the mu-opioid agonist remifentanil in humans causes hyperalgesia during withdrawal. *Pain* 106, 49–57. doi: 10.1016/s0304-3959(03)00276-8

Atasoy, D., Ertunc, M., Moulder, K. L., Blackwell, J., Chung, C., Su, J., et al. (2008). Spontaneous and evoked glutamate release activates two populations of NMDA receptors with limited overlap. *J. Neurosci.* 28, 10151–10166. doi: 10.1523/JNEUROSCI.2432-08.2008

Bae, C., Wang, J., Shim, H. S., Tang, S. J., Chung, J. M., and La, J. H. (2018). Mitochondrial superoxide increases excitatory synaptic strength in spinal dorsal horn neurons of neuropathic mice. *Mol. Pain* 14:1744806918797032. doi: 10.1177/1744806918797032

Bittar, A., Jun, J., La, J. H., Wang, J., Leem, J. W., and Chung, J. M. (2017). Reactive oxygen species affect spinal cell type-specific synaptic plasticity in a model of neuropathic pain. *Pain* 158, 2137–2146. doi: 10.1097/j.pain.0000000000001014

Cabanero, D., Baker, A., Zhou, S., Hargett, G. L., Irie, T., Xia, Y., et al. (2013). Pain after discontinuation of morphine treatment is associated with synaptic increase of GluA4-containing AMPAR in the dorsal horn of the spinal cord. *Neuropsychopharmacology* 38, 1472–1484. doi: 10.1038/npp.2013.46

Cai, Y., Yang, L., Hu, G., Chen, X., Niu, F., Yuan, L., et al. (2016). Regulation of morphine-induced synaptic alterations: role of oxidative stress, ER stress, and autophagy. *J. Cell Biol.* 215, 245–258. doi: 10.1083/jcb.201605065

Callahan, B. L., Gil, A. S., Levesque, A., and Mogil, J. S. (2008). Modulation of mechanical and thermal nociceptive sensitivity in the laboratory mouse by behavioral state. *J. Pain* 9, 174–184. doi: 10.1016/j.jpain.2007.10.011

Chen, L., Malarick, C., Seefeld, L., Wang, S., Houghton, M., and Mao, J. (2009). Altered quantitative sensory testing outcome in subjects with opioid therapy. *Pain* 143, 65–70. doi: 10.1016/j.pain.2009.01.022

Chen, S. R., Chen, H., Yuan, W. X., and Pan, H. L. (2011). Increased presynaptic and postsynaptic alpha2-adrenoceptor activity in the spinal dorsal horn in painful diabetic neuropathy. *J. Pharmacol. Exp. Ther.* 337, 285–292. doi: 10.1124/jpet.110.176586

Chu, L. F., Angst, M. S., and Clark, D. (2008). Opioid-induced hyperalgesia in humans: molecular mechanisms and clinical considerations. *Clin. J. Pain* 24, 479–496. doi: 10.1097/AJP.0b013e31816b2f43

Chu, L. F., Clark, D. J., and Angst, M. S. (2006). Opioid tolerance and hyperalgesia in chronic pain patients after one month of oral morphine therapy: a preliminary prospective study. *J. Pain* 7, 43–48. doi: 10.1016/j.jpain.2005.08.001

Cohen, S. P., Christo, P. J., Wang, S., Chen, L., Stojanovic, M. P., Shields, C. H., et al. (2008). The effect of opioid dose and treatment duration on the perception of a painful standardized clinical stimulus. *Reg. Anesth. Pain Med.* 33, 199–206. doi: 10.1016/j.rapm.2007.10.009

Espejo, E. F., and Mir, D. (1993). Structure of the rat's behaviour in the hot plate test. *Behav. Brain Res.* 56, 171–176. doi: 10.1016/0166-4328(93)90035-o

Fisher, C., Johnson, K., Okerman, T., Jurgenson, T., Nickell, A., Salo, E., et al. (2019). Morphine efficacy, tolerance, and hypersensitivity are altered after modulation of SUR1 subtype KATP channel activity in mice. *Front. Neurosci.* 13:1122. doi: 10.3389/fnins.2019.01122

Gao, Y. J., Zhang, L., Samad, O. A., Suter, M. R., Yasuhiko, K., Xu, Z. Z., et al. (2009). JNK-induced MCP-1 production in spinal cord astrocytes contributes to central sensitization and neuropathic pain. *J. Neurosci.* 29, 4096–4108. doi: 10.1523/JNEUROSCI.3623-08.2009

Goldberg, D. S., and McGee, S. J. (2011). Pain as a global public health priority. *BMC Public Health* 11:770. doi: 10.1186/1471-2458-11-770

Grabner, C. P., and Moser, T. (2018). Individual synaptic vesicles mediate stimulated exocytosis from cochlear inner hair cells. *Proc. Natl. Acad. Sci. U.S.A.* 115, 12811–12816. doi: 10.1073/pnas.1811814115

Green, D. P., Limjunyawong, N., Gour, N., Pundir, P., and Dong, X. (2019). A mast-cell-specific receptor mediates neurogenic inflammation and pain. *Neuron* 101, 412–420.e413. doi: 10.1016/j.neuron.2019.01.012

Grudt, T. J., and Perl, E. R. (2002). Correlations between neuronal morphology and electrophysiological features in the rodent superficial dorsal horn. *J. Physiol.* 540(Pt 1), 189–207. doi: 10.1113/jphysiol.2001.012890

Harte, S. E., Harris, R. E., and Clauw, D. J. (2018). The neurobiology of central sensitization. *J. Appl. Biobehav. Res.* 23:e12137. doi: 10.1111/jabr.12137

Hay, J. L., White, J. M., Bochner, F., Somogyi, A. A., Semple, T. J., and Rounsefell, B. (2009). Hyperalgesia in opioid-managed chronic pain and opioid-dependent patients. *J. Pain* 10, 316–322. doi: 10.1016/j.jpain.2008.10.003

Heinke, B., Ruscheweyh, R., Forsthuber, L., Wunderbaldinger, G., and Sandkuhler, J. (2004). Physiological, neurochemical and morphological properties of a subgroup of GABAergic spinal lamina II neurones identified by expression of green fluorescent protein in mice. *J. Physiol.* 560(Pt 1), 249–266. doi: 10.1113/jphysiol.2004.070540

Hood, D. D., Curry, R., and Eisenach, J. C. (2003). Intravenous remifentanil produces withdrawal hyperalgesia in volunteers with capsaicin-induced hyperalgesia. *Anesth. Analg.* 97, 810–815. doi: 10.1213/01.ane.0000078811.80093.88

Ikeda, H., Kiritoshi, T., and Murase, K. (2009). Synaptic plasticity in the spinal dorsal horn. *Neurosci. Res.* 64, 133–136. doi: 10.1016/j.neures.2009.03.004

Imlach, W. L., Bhola, R. F., Mohammadi, S. A., and Christie, M. J. (2016). Glycinergic dysfunction in a subpopulation of dorsal horn interneurons in a rat model of neuropathic pain. *Sci. Rep.* 6:37104. doi: 10.1038/srep37104

Kim, H. Y., Jun, J., Wang, J., Bittar, A., Chung, K., and Chung, J. M. (2015). Induction of long-term potentiation and long-term depression is cell-type specific in the spinal cord. *Pain* 156, 618–625. doi: 10.1097/01.j.pain.0000460354.09622.ec

Kim, Y. I., Na, H. S., Kim, S. H., Han, H. C., Yoon, Y. W., Sung, B., et al. (1998). Cell type-specific changes of the membrane properties of peripherally-axotomized dorsal root ganglion neurons in a rat model of neuropathic pain. *Neuroscience* 86, 301–309. doi: 10.1016/s0306-4522(98)00022-0

King, T., Gardell, L. R., Wang, R., Vardanyan, A., Ossipov, M. H., Malan, T. P., et al. (2005). Role of NK-1 neurotransmission in opioid-induced hyperalgesia. *Pain* 116, 276–288. doi: 10.1016/j.pain.2005.04.014

Lee, K. Y., Bae, C., Lee, D., Kagan, Z., Bradley, K., Chung, J. M., et al. (2020). Low-intensity, kilohertz frequency spinal cord stimulation differently affects excitatory and inhibitory neurons in the rodent superficial dorsal horn. *Neuroscience* 428, 132–139. doi: 10.1016/j.neuroscience.2019.12.031

Lee, M., Silverman, S. M., Hansen, H., Patel, V. B., and Manchikanti, L. (2011). A comprehensive review of opioid-induced hyperalgesia. *Pain Physician* 14, 145–161.

Leitner, J., Westerholz, S., Heinke, B., Forsthuber, L., Wunderbaldinger, G., Jäger, T., et al. (2013). Impaired excitatory drive to spinal gabaergic neurons of neuropathic mice. *PLoS One* 8:e73370. doi: 10.1371/journal.pone.0073370

Li, J., Xie, W., Zhang, J. M., and Baccei, M. L. (2009). Peripheral nerve injury sensitizes neonatal dorsal horn neurons to tumor necrosis factor-alpha. *Mol. Pain* 5:10. doi: 10.1186/1744-8069-5-10

Lu, Y., and Perl, E. R. (2003). A specific inhibitory pathway between substantia gelatinosa neurons receiving direct C-fiber input. *J. Neurosci.* 23, 8752–8758.

Luo, C., Kuner, T., and Kuner, R. (2014). Synaptic plasticity in pathological pain. *Trends Neurosci.* 37, 343–355. doi: 10.1016/j.tins.2014.04.002

Mantyh, P. W., Rogers, S. D., Honore, P., Allen, B. J., Ghilardi, J. R., Li, J., et al. (1997). Inhibition of hyperalgesia by ablation of lamina I spinal neurons expressing the substance P receptor. *Science* 278, 275–279. doi: 10.1126/science.278.5336.275

Mao, J., Price, D. D., and Mayer, D. J. (1994). Thermal hyperalgesia in association with the development of morphine tolerance in rats: roles of excitatory amino acid receptors and protein kinase C. *J. Neurosci.* 14, 2301–2312.

Melchior, M., Poisbeau, P., Gaumond, I., and Marchand, S. (2016). Insights into the mechanisms and the emergence of sex-differences in pain. *Neuroscience* 338, 63–80. doi: 10.1016/j.neuroscience.2016.05.007

Moore, K. A., Kohno, T., Karchewski, L. A., Scholz, J., Baba, H., and Woolf, C. J. (2002). Partial peripheral nerve injury promotes a selective loss of GABAergic inhibition in the superficial dorsal horn of the spinal cord. *J. Neurosci.* 22, 6724–6731.

Nichols, M. L., Allen, B. J., Rogers, S. D., Ghilardi, J. R., Honore, P., Luger, N. M., et al. (1999). Transmission of chronic nociception by spinal neurons expressing the substance P receptor. *Science* 286, 1558–1561. doi: 10.1126/science.286.5444.1558

Park, C. K., Lu, N., Xu, Z. Z., Liu, T., Serhan, C. N., and Ji, R. R. (2011). Resolving TRPV1- and TNF-alpha-mediated spinal cord synaptic plasticity

and inflammatory pain with neuroprotectin D1. *J. Neurosci.* 31, 15072–15085. doi: 10.1523/JNEUROSCI.2443-11.2011

Roeckel, L. A., Le Coz, G. M., Gaveriaux-Ruff, C., and Simonin, F. (2016). Opioid-induced hyperalgesia: cellular and molecular mechanisms. *Neuroscience* 338, 160–182. doi: 10.1016/j.neuroscience.2016.06.029

Roeckel, L. A., Utard, V., Reiss, D., Mouheiche, J., Maurin, H., Robe, A., et al. (2017). Morphine-induced hyperalgesia involves mu opioid receptors and the metabolite morphine-3-glucuronide. *Sci. Rep.* 7:10406. doi: 10.1038/s41598-017-11120-4

Rosenmund, C., and Stevens, C. F. (1996). Definition of the readily releasable pool of vesicles at hippocampal synapses. *Neuron* 16, 1197–1207. doi: 10.1016/s0896-6273(00)80146-4

Sasaki, M., Kamiya, Y., Bamba, K., Onishi, T., Matsuda, K., Kohno, T., et al. (2021). Serotonin plays a key role in the development of opioid-induced hyperalgesia in mice. *J. Pain* 22, 715–729. doi: 10.1016/j.jpain.2020.12.008

Shi, Y., Yuan, S., and Tang, S. J. (2019). Morphine and HIV-1 gp120 cooperatively promote pathogenesis in the spinal pain neural circuit. *Mol. Pain* 15:1744806919868380. doi: 10.1177/1744806919868380

Shi, Y., Yuan, S., and Tang, S. J. (2021). Reactive oxygen species (ROS) are critical for morphine exacerbation of HIV-1 gp120-induced pain. *J. Neuroimmune Pharmacol.* 16, 581–591. doi: 10.1007/s11481-020-09951-6

Sisignano, M., Angioni, C., Park, C. K., Meyer Dos Santos, S., Jordan, H., Kuzikov, M., et al. (2016). Targeting CYP2J to reduce paclitaxel-induced peripheral neuropathic pain. *Proc. Natl. Acad. Sci. U.S.A.* 113, 12544–12549. doi: 10.1073/pnas.1613246113

Stikova, Z., Ptakova, N., Horakova, M., Kostun, J., and Ondic, O. (2019). Inflammatory myofibroblastic tumor of the uterus – case report. *Cesk Patol.* 55, 239–243.

Taylor, W. R., Chen, E., and Copenhagen, D. R. (1995). Characterization of spontaneous excitatory synaptic currents in salamander retinal ganglion cells. *J. Physiol.* 486(Pt 1), 207–221. doi: 10.1113/jphysiol.1995.sp020803

Todd, A. J. (2010). Neuronal circuitry for pain processing in the dorsal horn. *Nat. Rev. Neurosci.* 11, 823–836. doi: 10.1038/nrn2947

Todd, A. J. (2017). Identifying functional populations among the interneurons in laminae I-III of the spinal dorsal horn. *Mol. Pain* 13:1744806917693003. doi: 10.1177/1744806917693003

Torsney, C., and MacDermott, A. B. (2006). Disinhibition opens the gate to pathological pain signaling in superficial neurokinin 1 receptor-expressing neurons in rat spinal cord. *J. Neurosci.* 26, 1833–1843. doi: 10.1523/JNEUROSCI.4584-05.2006

Vera-Portocarrero, L. P., Zhang, E. T., King, T., Ossipov, M. H., Vanderah, T. W., Lai, J., et al. (2007). Spinal NK-1 receptor expressing neurons mediate opioid-induced hyperalgesia and antinociceptive tolerance via activation of descending pathways. *Pain* 129, 35–45. doi: 10.1016/j.pain.2006.09.033

Woolf, C. J. (2011). Central sensitization: implications for the diagnosis and treatment of pain. *Pain* 152(3 Suppl), S2–S15. doi: 10.1016/j.pain.2010.09.030

Yasaka, T., Kato, G., Furue, H., Rashid, M. H., Sonohata, M., Tamae, A., et al. (2007). Cell-type-specific excitatory and inhibitory circuits involving primary afferents in the substantia gelatinosa of the rat spinal dorsal horn *in vitro*. *J. Physiol.* 581(Pt 2), 603–618. doi: 10.1113/jphysiol.2006.123919

Yasaka, T., Tiong, S. Y. X., Hughes, D. I., Riddell, J. S., and Todd, A. J. (2010). Populations of inhibitory and excitatory interneurons in lamina II of the adult rat spinal dorsal horn revealed by a combined electrophysiological and anatomical approach. *Pain* 151, 475–488. doi: 10.1016/j.pain.2010.08.008

Zhang, L., Berta, T., Xu, Z. Z., Liu, T., Park, J. Y., and Ji, R. R. (2011). TNF-alpha contributes to spinal cord synaptic plasticity and inflammatory pain: distinct role of TNF receptor subtypes 1 and 2. *Pain* 152, 419–427. doi: 10.1016/j.pain.2010.11.014

Conflict of Interest: The authors declare that the research was conducted in the absence of any commercial or financial relationships that could be construed as a potential conflict of interest.

Publisher's Note: All claims expressed in this article are solely those of the authors and do not necessarily represent those of their affiliated organizations, or those of the publisher, the editors and the reviewers. Any product that may be evaluated in this article, or claim that may be made by its manufacturer, is not guaranteed or endorsed by the publisher.

frontiers in Molecular Neuroscience

ORIGINAL RESEARCH
published: 22 December 2021
doi: 10.3389/fnmol.2021.796053

Hyperexcitability of Sensory Neurons in Fragile X Mouse Model

Pan-Yue Deng[1], Oshri Avraham[2], Valeria Cavalli[2,3,4] and Vitaly A. Klyachko[1,3]**

[1] Department of Cell Biology and Physiology, Washington University School of Medicine, St. Louis, MO, United States, [2] Department of Neuroscience, Washington University School of Medicine, St. Louis, MO, United States, [3] Hope Center for Neurological Disorders, Washington University School of Medicine, St. Louis, MO, United States, [4] Center of Regenerative Medicine, Washington University School of Medicine, St. Louis, MO, United States

Sensory hypersensitivity and somatosensory deficits represent the core symptoms of Fragile X syndrome (FXS). These alterations are believed to arise from changes in cortical sensory processing, while potential deficits in the function of peripheral sensory neurons residing in dorsal root ganglia remain unexplored. We found that peripheral sensory neurons exhibit pronounced hyperexcitability in *Fmr1* KO mice, manifested by markedly increased action potential (AP) firing rate and decreased threshold. Unlike excitability changes found in many central neurons, no significant changes were observed in AP rising and falling time, peak potential, amplitude, or duration. Sensory neuron hyperexcitability was caused primarily by increased input resistance, without changes in cell capacitance or resting membrane potential. Analyses of the underlying mechanisms revealed reduced activity of HCN channels and reduced expression of HCN1 and HCN4 in *Fmr1* KO compared to WT. A selective HCN channel blocker abolished differences in all measures of sensory neuron excitability between WT and *Fmr1* KO neurons. These results reveal a hyperexcitable state of peripheral sensory neurons in *Fmr1* KO mice caused by dysfunction of HCN channels. In addition to the intrinsic neuronal dysfunction, the accompanying paper examines deficits in sensory neuron association/communication with their enveloping satellite glial cells, suggesting contributions from both neuronal intrinsic and extrinsic mechanisms to sensory dysfunction in the FXS mouse model.

Keywords: hyperexcitability, Fragile X syndrome, action potential, sensory neuron, HCN channel

OPEN ACCESS

Edited by:
Michael Telias, University of California, Berkeley, United States

Reviewed by:
Judith Ann Strong, University of Cincinnati, United States
Sarah Rotschafer, Mercer University, United States
Aleksander Domanski, University of Bristol, United Kingdom

***Correspondence:**
Valeria Cavalli
cavalli@wustl.edu
Vitaly A. Klyachko
klyachko@wustl.edu

Specialty section:
This article was submitted to Neuroplasticity and Development, a section of the journal Frontiers in Molecular Neuroscience

Received: *15 October 2021*
Accepted: *17 November 2021*
Published: *22 December 2021*

Citation:
Deng P-Y, Avraham O, Cavalli V and Klyachko VA (2021) Hyperexcitability of Sensory Neurons in Fragile X Mouse Model. Front. Mol. Neurosci. 14:796053. doi: 10.3389/fnmol.2021.796053

INTRODUCTION

Fragile X syndrome (FXS) is the leading monogenetic cause of intellectual disability (ID) and autism. This disorder most commonly results from transcriptional silencing of the *Fmr1* gene causing loss of expression of Fragile X Mental Retardation Protein (FMRP) (Penagarikano et al., 2007). Individuals with FXS typically present with cognitive dysfunction, learning deficits, social and behavioral problems, neurological deficits, and morphological abnormalities. Among most prevalent FXS deficits is hypersensitivity to sensory stimuli, including auditory, visual, and tactile stimuli. Increasing evidence suggests that sensory hypersensitivity may lead to behavioral alterations such as poor eye contact, anxiety, and impaired social interactions (Rais et al., 2018).

Individuals with FXS commonly exhibit somatosensory deficits, such as hypersensitivity to touch (Cascio, 2010), Self-injurious behaviors in Fragile X individuals (Arron et al., 2011;

Crawford et al., 2019) are also indicative of abnormal pain perception. Impaired pain induction and perception are also observed in the FXS mouse model, including reduced induction of neuropathic pain (Ramirez-Lopez et al., 2021), and insensitivity to visceral pain (Yang et al., 2020). These and other sensory deficits have been largely attributed to alterations in cortical sensory processing with a wide range of excitability deficits identified in somatosensory cortex of FXS models at neuronal, circuit, and network levels (Contractor et al., 2015). For example, *Fmr1* KO mice have abnormal encoding of tactile stimulation frequency and enlarged receptive fields in the somatosensory cortex (Juczewski et al., 2016). However, recent studies in other monogenetic models of autism suggest that many core cognitive and sensory deficits may arise from an earlier abnormality in sensory inputs that drive subsequent abnormal development of cortical circuits (Orefice et al., 2016, 2019). A hyperexcitable state of somatosensory neurons has been suggested to be a part of the core developmental pathology in autism models, leading to region-specific brain abnormalities during the critical period (Orefice et al., 2019). Indeed, the formation of the cortical receptive fields depends on sensory experience (Allen et al., 2003). The enlarged receptive fields in *Fmr1* KO mice and altered perception of sensory information may be a consequence, in part, of altered sensory inputs during development. Yet little is known about alterations in the peripheral neural system that receives the primary sensory inputs. Research in Fragile X field has almost exclusively focused on central defects in processing of somatosensory information and dysfunction of the central neurons and circuits. Whether dysfunction of peripheral sensory neurons is present and contributes to FXS pathophysiology remains largely unexplored.

Peripheral sensory neurons in the dorsal root ganglia (DRG) play critical roles in receiving direct sensory information from the environment and conveying it to the central nervous system (CNS). Structurally, these are pseudo-unipolar neurons with one axon projecting into peripheral nerve and the other axon ascending in the dorsal root and spinal cord. Sensory neurons express FMRP, which localize to the soma and axons (Price et al., 2006). While the gross development of DRG is normal in the absence of FMRP (Price and Melemedjian, 2012), there is evidence for functional defects in sensory neurons including an increased surface expression of voltage-gated calcium channels leading to increased somatic glutamate release (Ferron et al., 2014, 2020). However, whether and how excitability of peripheral sensory neurons is altered by the loss of FMRP remains unexplored.

In this study we performed recordings from the DRG neurons isolated from adolescent mice in a short-term culture to examine changes in sensory neuron excitability caused by loss of FMRP.

RESULTS

Hyperexcitable State of Sensory Neurons in *Fmr1* KO Mice

Firing patterns of sensory neurons situated in the DRG convey information from external and internal environment of the body to the CNS. Thus, these neurons play a critical role in transducing sensory information to neuronal signals. Accordingly, we first asked how excitability of sensory neurons is affected in *Fmr1* KO mice. Whole-cell recordings were performed in short-term cultures of sensory neurons, as described (Avraham et al., 2020). Neurons were separated for analysis by size into two groups with a cutoff at 30 μm diameter (Yousuf et al., 2019) into small/medium vs. large diameter neurons. We found that most of the small/medium diameter neurons [mean diameter: 19.14 ± 0.53 μm (WT), 19.84 ± 0.54 μm (KO)] in the short-term DRG cultures exhibit tonic action potential (AP) firing (multiple APs fired in a stimulus intensity-dependent manner, **Figure 1A**), whereas all tested large neurons (>30 μm) show phasic AP firing (a single AP fired regardless of stimulus intensity, data not shown). To better understand how and to what extent the excitability of somatosensory neurons is affected in *Fmr1* KO mice, we therefore used the small/medium diameter sensory neurons as a model neuron. In our culture conditions, the majority of the cells we recorded from are small/medium diameter IB4-positive neurons (Avraham et al., 2020). IB4 positive neurons represent non-peptidergic C- and Aδ-nociceptive neurons and some Aδ-low threshold mechanoreceptors (Wang et al., 1998; Li et al., 2011; Olson et al., 2016), a subset of which detect gentle touch (Liu et al., 2007; Olson et al., 2016).

Action potentials were evoked by multi-step current injections (from 25 to 150 pA with a step size of 25 pA, **Figure 1A**). Only the first APs were used to determine AP latency, threshold, and rheobase to avoid AP parameters being affected by cumulative Na^+ channel inactivation during subsequent APs. We found that excitability of sensory neurons was markedly increased in the absence of FMRP, as evident by decreased latency to the first AP ($p < 0.01$, **Figure 1B**, all values here and throughout are summarized in **Supplementary Table 1**), lower voltage threshold ($p < 0.01$, **Figure 1D**), and reduced rheobase charge transfer ($p < 0.01$, **Figure 1C**) which represents a measure of current threshold. Sensory neurons in *Fmr1* KO mice also fired more APs at lower stimulus intensity steps ($p < 0.01$, **Figure 1E**), and had a shortened inter-AP interval ($p < 0.05$, **Figure 1F**). Unlike excitability changes observed in many central neurons (Contractor et al., 2015) we observed no significant changes in AP rising and falling time, AP peak potential, and AP amplitude, as well as in AP duration (**Figure 2**). It is noteworthy that the threshold and rheobase values were largely independent of step current intensities within genotypes, indicating that these are reliable parameters for evaluating neuronal excitability.

We further confirmed the increased excitability of sensory neurons in *Fmr1* KO mice by examining AP parameters in a ramp-current evoked AP traces, using a previously reported approach (Deng and Klyachko, 2016a,b; Deng et al., 2019). As expected, we found that excitability of DRG neurons was indeed increased in *Fmr1* KO mice, as evident by a significantly larger number of APs fired in KO neurons ($p = 0.014$; **Figures 3A,C**); a large hyperpolarizing shift of threshold potential ($p = 0.0015$; **Figures 3A–C**), and reduced AP rheobase ($p < 0.0001$; **Figure 3C**).

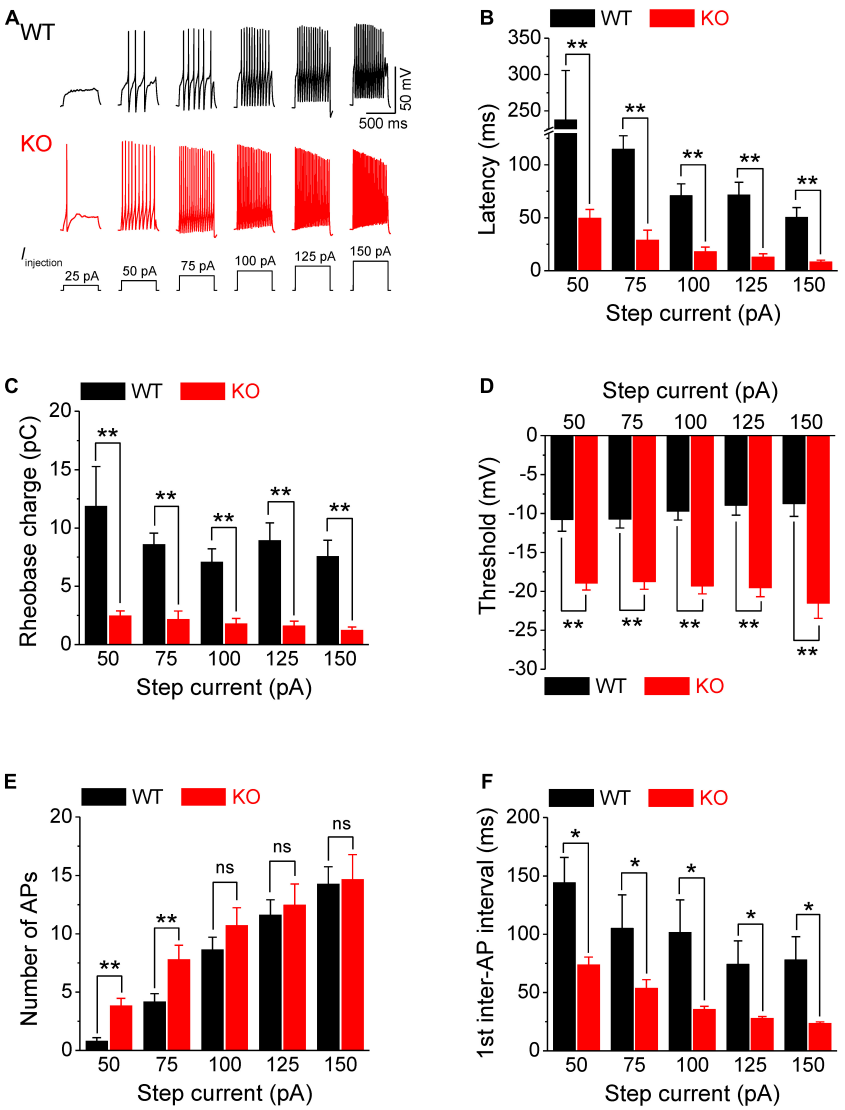

FIGURE 1 | Increased excitability of sensory neurons in *Fmr1* KO mice. **(A)** Sample AP traces evoked by step-current injection. Note, that for a 25-pA step, there was no AP observed in any of tested WT neurons, and in ∼50% of KO neurons. Thus, in the following panels we analyzed AP parameters starting from 50 pA step. **(B–F)** Analysis of AP parameters in measurements from panel **(A)**. Latency to the first AP **(B)**, rheobase charge transfer **(C)**, threshold **(D)**, number of AP fired **(E)**, and first inter-AP interval **(F)** in WT and *Fmr1* KO neurons. *T*-test; $*p < 0.05$; $**p < 0.01$; ns, not significant.

Together, these observations demonstrate a state of marked hyperexcitability of peripheral sensory neurons in the absence of FMRP.

Hyperexcitability of Sensory Neurons in *Fmr1* KO Mice Is Associated With Increased Input Resistance, but Is Not Due to Kv7 Channel Deficits

Because the intrinsic membrane properties play a major role in setting neuronal excitability, we examined the resting membrane potential (RMP), cell size, membrane capacitance, and input resistance of sensory neurons in *Fmr1* KO and WT animals. While no significant differences were observed in cell size, capacitance, and RMP between genotypes (**Figure 3D**), we found a significant increase in input resistance in *Fmr1* KO neurons ($p = 0.0097$; **Figure 3D**). Increased input resistance is consistent with the reduced rheobase in the absence of FMRP and may thus be a direct cause of hyperexcitability of KO neurons.

To understand the mechanisms of these excitability defects, we first considered that absence of significant changes in RMP or AP waveform suggests that the voltage-gated Na^+ and K^+ channels active near RMP or above threshold are unlikely to be strongly affected in sensory neurons of *Fmr1* KO mice. Thus, the changes in input resistance may result from alterations in some voltage-dependent sub-threshold conductance, such as M current (carried by Kv7 channels) and/or h current (carried by HCN channels) that are abundantly expressed in sensory

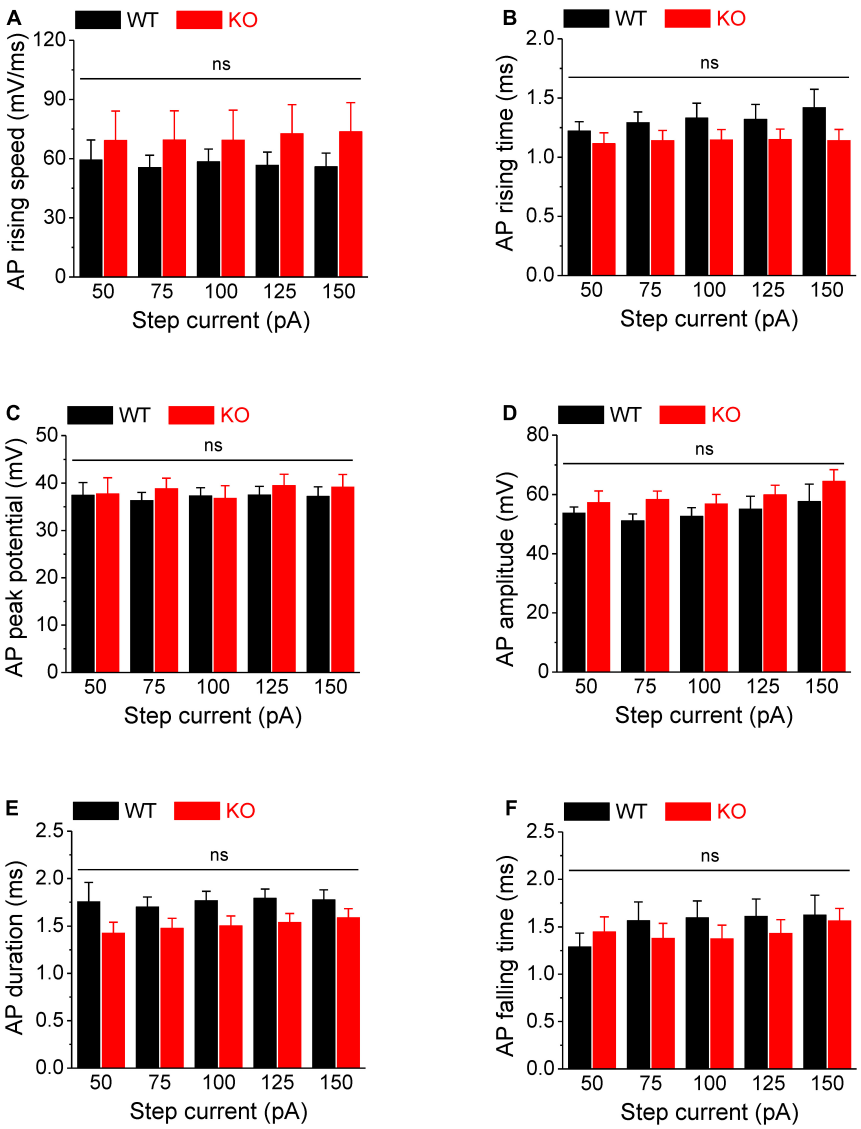

FIGURE 2 | No changes in AP rising and falling time, duration, and amplitude in *Fmr1* KO neurons. **(A–F)** Loss of FMRP did not affect AP rising speed **(A)**, 10–90% rising time **(B)**, AP peak potential **(C)**, AP amplitude **(D)**, AP duration **(E)**, and 90–10% AP falling time **(F)**. *T*-test; ns, not significant.

neurons (de Moraes et al., 2017). We examined contributions from Kv7 channels and found that the Kv7 channel blocker XE991 (10 μM) failed to abolish the differences between genotypes in either the voltage threshold ($p = 0.012$, **Supplementary Figure 1A**), or in the rheobase charge transfer ($p < 0.0001$; **Supplementary Figure 1B**). This observation suggests that Kv7 channels are unlikely to underlie excitability changes observed in *Fmr1* KO neurons.

HCN Channel Dysfunction Causes Hyperexcitability of Sensory Neurons in *Fmr1* KO Mice

Next, we examined the HCN channel activity in sensory neurons. HCN channels are activated by a membrane hyperpolarization, and cells with active HCN channels are characterized by voltage sag in current clamp recordings in response to a hyperpolarizing current. As expected, negative current injection produced marked voltage sags in WT neurons (**Figure 4A**). Most importantly, the voltage sag in *Fmr1* KO neurons was significantly decreased compared to WT in all tested steps for both absolute values and sag ratios ($p < 0.01$ for all steps; **Figures 4A–C**). These differences were not due to the basal RMP differences between genotypes ($p = 0.52$, **Supplementary Table 1**).

Given that the HCN channels contribute significantly to input resistance, these results suggest that the reduced HCN channel function might be the major cause of hyperexcitability in sensory neurons of *Fmr1* KO mice. If this is the case, inhibition of HCN channels should eliminate the differences in input resistance and

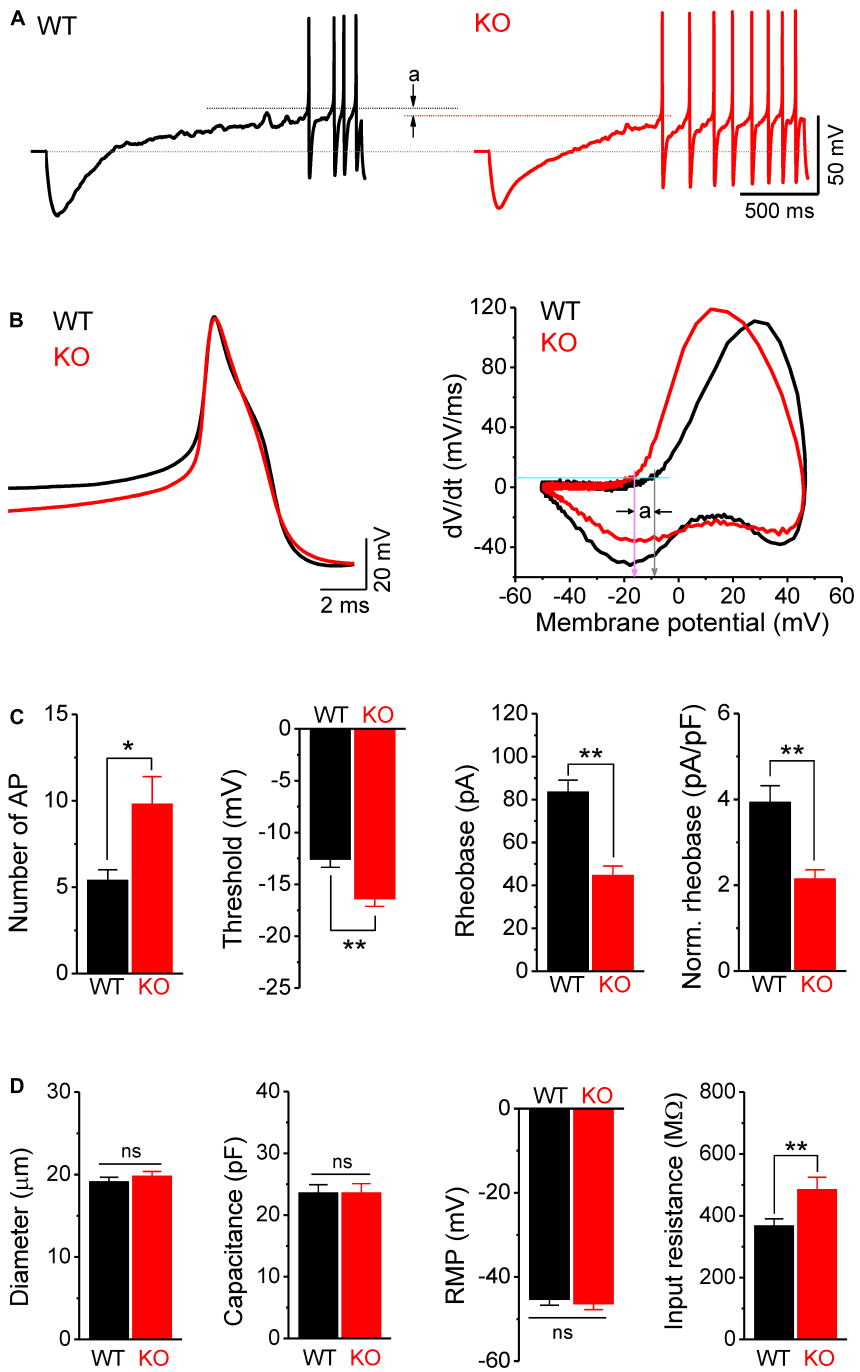

FIGURE 3 | Hyperexcitability of sensory neurons in *Fmr1* KO mice is associated with increased input resistance. **(A)** Sample traces of ramp-evoked APs. Note the differences in number of APs and threshold (a) between WT and KO neurons. Short dot-lines indicate the threshold levels of WT (black) and KO (red) neurons. Long dot-line is the resting membrane potential (RMP) level. **(B)** The first APs from panel **(A)** and their corresponding phase plots, indicating decreased AP threshold in *Fmr1* KO mice (a). Cyan line is the membrane depolarizing speed of 5 mV/ms, the corresponding voltages of its intersections with phase plot were thresholds for WT (gray arrow) and KO (pink arrow) neurons. **(C)** Summarized data for the number of APs, threshold, rheobase, and membrane capacitance-normalized rheobase for the measurements in panel **(A)**. **(D)** Summarized data for cell size, membrane capacitance, RMP, and membrane input resistance for the measurements in panel **(A)**. *T*-test; $*p < 0.05$; $**p < 0.01$; ns, not significant.

in excitability of sensory neurons between genotypes. In line with this prediction, the HCN channel blocker ZD7288 (10 μM), which potently blocks all HCN channels without preference for a specific HCN subunit, abolished the difference in input resistance between WT and KO neurons ($p = 0.73$; **Figure 4D**). Most importantly, ZD7288 also abolished differences in sensory

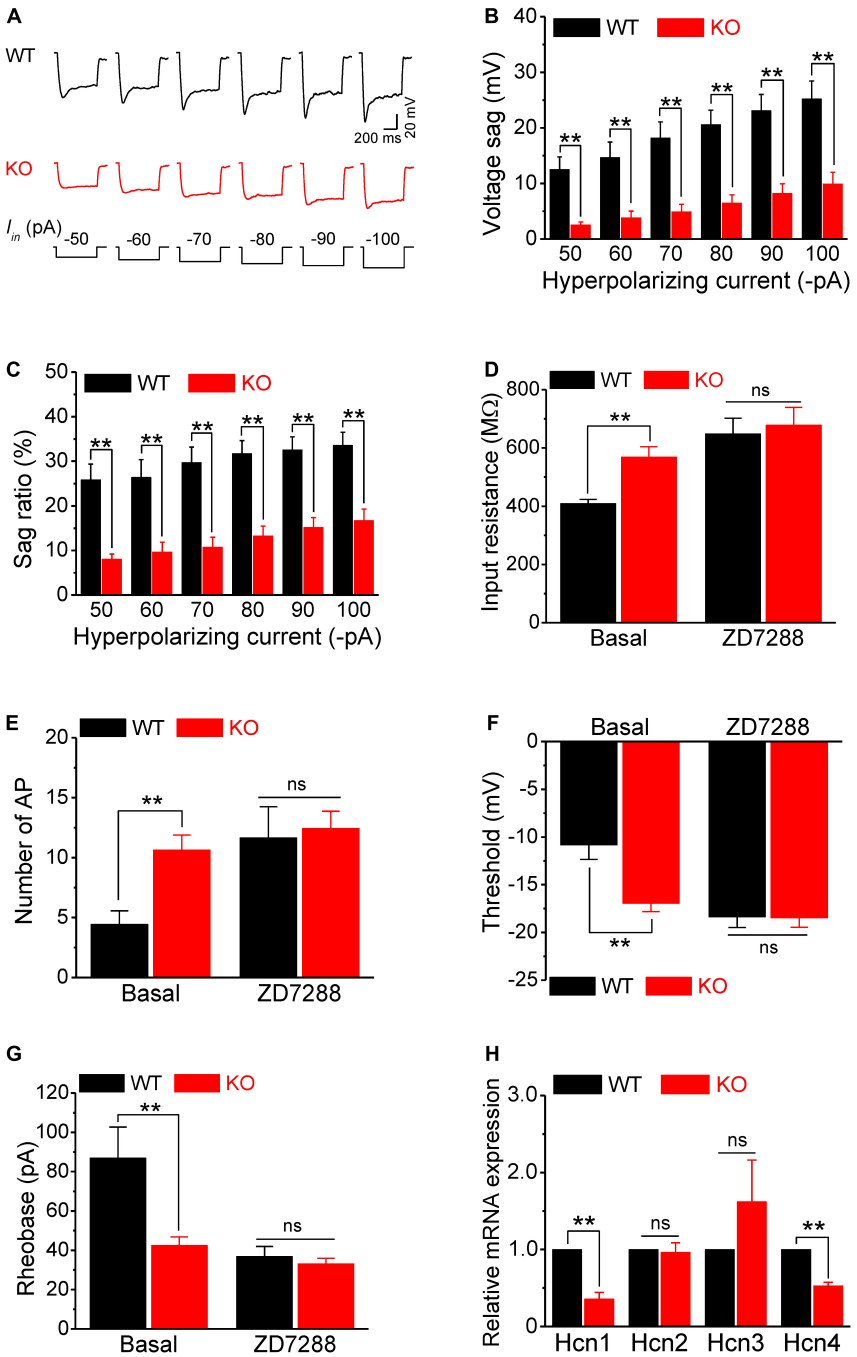

FIGURE 4 | HCN channel dysfunction causes hyperexcitability of sensory neurons in *Fmr1* KO mice. **(A)** Example traces of hyperpolarization-induced voltage sag in sensory neurons. I_{in} is the injected hyperpolarizing current with intensities indicated in the lower panel. **(B,C)** Quantification of voltage sag in WT and KO neurons in absolute values **(B)** and as a sag ratio **(C)** for all tested hyperpolarizing current levels. **(D)** A selective HCN channel blocker ZD7288 abolished the differences in input resistance between genotypes. **(E–G)** HCN channel blocker ZD7288 abolished the differences in the number of APs fired **(E)**, threshold **(F)**, and rheobase **(G)** between genotypes. **(H)** qPCR analysis of the relative mRNA expression of *Hcn1–4* in *Fmr1* KO compared to WT DRGs. $N = 3$ biologically independent animals. *T*-test; $^{**}p < 0.01$; ns, not significant.

neuron excitability between WT and KO neurons, including the number of AP fired ($p = 0.78$; **Figure 4E**), AP threshold ($p = 0.94$; **Figure 4F**), as well as rheobase ($p = 0.50$; **Figures 4G,H**). Together, these results confirmed that reduced HCN channel function causes increased input resistance, which in turn leads to hyperexcitability of sensory neurons in *Fmr1* KO mice.

Fragile X mental retardation protein regulates expression and activity of multiple ion channels (Deng and Klyachko, 2021)

and HCN channels are a known target of FMRP translational control (Darnell et al., 2011; Brager et al., 2012; Zhang et al., 2014; Orefice et al., 2016, 2019). We thus examined by quantitative PCR (qPCR) if *Hcn* channel expression was altered in sensory neurons of *Fmr1* KO mice. We used whole DRG for these experiments, since HCN channels are selectively expressed in neurons in the DRG (Moosmang et al., 2001; Biel et al., 2009), with HCN1, HCN2, and to a lesser extent HCN4 being most abundant (Moosmang et al., 2001; Chaplan et al., 2003). We found that mRNA levels of *Hcn1* and *Hcn4* were significantly reduced in *Fmr1* KO DRG (*Hcn1*, $p = 0.0018$; *Hcn4*, $p = 0.0004$) (**Figure 4H**) while levels of *Hcn2* and *Hcn3* were not strongly affected (*Hcn2*, $p = 0.78$; *Hcn3*, $p = 0.32$) (**Figure 4H**). Together with the above results, this observation suggests that neuronal hyperexcitability in the absence of FMRP is caused by reduced HCN channel expression in sensory neurons.

DISCUSSION

Sensory hypersensitivity in FXS has thus far been largely attributed to sensory processing abnormalities in the brain circuits (Contractor et al., 2015). Our results revealed a contribution to sensory abnormalities from peripheral deficits in the FXS mouse model. We found a hyperexcitable state of peripheral sensory neurons characterized by markedly increased AP frequency and reduced threshold caused by loss of FMRP. Altered sensory neuron excitability in *Fmr1* KO mice arises, at least in part, from intrinsic neuronal mechanisms involving increased input resistance caused by HCN channel dysfunction.

HCN channels are active at rest and play a crucial role in controlling input resistance, and thus neuronal excitability (Shah, 2014). Voltage dependence of HCN channels is regulated by a number of intracellular factors. Other voltage-gated channels have a strong influence on HCN channel activity. The resulting action of HCN channels on membrane excitability in a given cell type is thus determined by a delicate balance of these factors. For example, in the CA1 neurons, through interaction with Kv7 channels, HCN channels can enhance AP firing in response to an EPSP when AP threshold is low and can inhibit AP firing when AP threshold is high (George et al., 2009). The AP threshold of DRG neurons is comparatively high, thus reduction of HCN channel activity in *Fmr1* KO neurons is consistent with increased firing. Also, HCN channels have two separate influences on membrane excitability: one is the channel-mediated inward current (i.e., excitatory influence), the second one is a shunting effect (inhibitory influence). The overall effect might be complicated or even "paradoxical" (George et al., 2009). Given that the input resistance is a direct determinant of AP rheobase, our observations of reduced rheobase in *Fmr1* KO neurons support the notion that HCN channels in sensory neurons function through the shunting effect to reduce input resistance.

Cell-type specific HCN channel defects have been previously implicated in excitability alterations of central neurons in the FXS models. For example, the elevated HCN1 subunit expression and increased Ih current were found in dendrites of CA1 pyramidal cells from *Fmr1* KO mice leading to decreased input resistance and reduced temporal summation (Brager et al., 2012), while the opposite changes in HCN1 expression, Ih and excitability were observed in the layer 5 pyramidal cells of somatosensory cortex (Zhang et al., 2014) or layer 4 stellate cells of *Fmr1* KO mice (Booker et al., 2019). Reduced HCN1 expression and decreased Ih were also found in large (mechanosensory) but not small diameter DRG neurons in Shank3 deletion model of Phelan–McDermid syndrome often associated with ASD (Orefice et al., 2016, 2019). Here we observed that *Hcn1* and *Hcn4* expression is strongly reduced in the DRG of *Fmr1* KO mice. Together with the observations that a selective HCN channel blocker abolished differences in all measures of excitability between *Fmr1* KO and WT mice, these observations suggest that reduced HCN channel expression is the major cause of hyperexcitability of sensory DRG neurons caused by FMRP loss. Notably, in central neurons, FMRP is also known to exert powerful control over ion channel activity *via* protein–protein interactions (Brown et al., 2010; Deng et al., 2013, 2019; Deng and Klyachko, 2021). In the case of HCN channels, FMRP can regulate the channel's surface levels in a tissue-specific manner *via* protein–protein interactions with the HCN-TRIP8b complexes (Brandalise et al., 2020). Whether this interaction is present in sensory neurons and contribute to neuronal excitability defects remains to be determined.

Interestingly, HCN channel expression and Ih current show age-dependent increase in thalamic neurons (Kanyshkova et al., 2009) which dampens their excitability as these neurons mature. Furthermore, there is evidence of maturation-dependent regulation of HCN channels in spiral ganglia in the auditory pathway (Shen et al., 2018) and immature neurons are known to exhibit higher intrinsic excitability and plasticity (Schmidt-Hieber et al., 2004; Oh et al., 2010). Can hyperexcitability of peripheral sensory neurons be a consequence, in part, of the delayed neuronal maturation in *Fmr1* KO mice? The age-dependent changes in excitability have been reported in central neurons of *Fmr1* KO mice: the CA3 pyramidal neurons show increased excitability in young *Fmr1* KO mice (3–4 weeks) (Deng et al., 2019; Dwivedi et al., 2019), but this was not seen in the older animals (6–8 weeks) (Dwivedi et al., 2019). Further, a delay in neuronal maturation and immature state of dendritic spines is widely documented in central neurons of *Fmr1* KO mice (Comery et al., 1997; Harlow et al., 2010; Guo et al., 2015; Moskalyuk et al., 2020), resulting in delayed maturation of local networks (Vislay et al., 2013; Nomura et al., 2017) and a developmental delay in somatosensory map formation (Till et al., 2012). This is also consistent with abnormal neurogenesis and altered differentiation of neural stem cells in *Fmr1* KOs, leading to poor neuronal maturation and high gliogenic development (Castren et al., 2005; Telias et al., 2013, 2015). Our single-cell RNA-seq analyses described in detail in the accompanying paper indeed suggest that maturation of sensory neurons in the DRG is delayed/aberrant, as evident in upregulation of progenitor markers and downregulation of neuronal differentiation/neuronal identity markers. Thus, the delayed maturation of sensory neurons in the DRG could be an underlying or contributing factor driving their hyperexcitability.

The increased intrinsic excitability of sensory neurons is only one of complex multifaceted changes that occur in the peripheral sensory system in the absence of FMRP. For example, the excitability changes we observed here will combine with the increased glutamate release from the soma and terminals of these neurons, which occurs independently due to excessive surface expression of N-type calcium channels (Ferron et al., 2014, 2020), further multiplying the excessive output from sensory neurons. Moreover, morphological changes of neuronal processes, such as axon structure or axon initial segment length, which are affected centrally in *Fmr1* KO mice (Booker et al., 2020), can also contribute to sensory neuron excitability. Given the long-range projections of the sensory neurons of the DRG, future central and peripheral projection tracing will be needed to define the precise morphological changes in sensory neuron processes. In addition to these intrinsic mechanisms, in the accompanying paper, we describe extrinsic mechanisms that may contribute to sensory deficits due to disruption of the peripheral neurons' association/communication with their enveloping satellite glial cells. Thus, an interplay of multiple peripheral deficits needs to be considered to fully understand sensory deficits caused by FMRP loss. Notably, our measurements of neuronal excitability are limited to short-term cultures in which neurons do not develop full length long-range projections and do not get enveloped by the satellite glia cells. Thus how the complex interplay between the intrinsic and extrinsic changes influences sensory processing *in vivo* remains to be elucidated. This includes defining how sensory transduction is affected in the intact DRG and whether distorted cortical maps in *Fmr1* KOs (Till et al., 2012) are a consequence of altered sensory receptive fields. Moreover, *in vivo* measurements will also be needed to define the extent to which peripheral deficits contribute to the abnormal processing of repeating sensory stimuli (Domanski et al., 2019). Such measurements will present a technical challenge because sensory DRG neurons in more intact settings (*ex vivo* slices or *in vivo*) are entirely surrounded by the satellite glia coat.

What is the relevance of sensory neuron hyperexcitability to clinical FXS phenotypes? The majority of cells analyzed in our experiments were small/medium diameter IB4-positive nociceptors (Avraham et al., 2020). A previous study showed that loss of FMRP decreases nociceptive sensitization in adult mice, even though the basal nociceptive thresholds were intact (Price et al., 2007). Recent evidence also indicates impaired pain induction and perception in the FXS mouse model, including reduced neuropathic pain (Ramirez-Lopez et al., 2021), and visceral pain (Yang et al., 2020). Future *in vivo* studies will be needed to determine whether and how increased excitability of nociceptive neurons in adolescent mice we observed here is linked to abnormal pain induction or perception in FXS mice. Notably, IB4-positive sensory neurons also include a subset of mechanoreceptors that detect gentle touch (Liu et al., 2007). Thus, our observations could be relevant to the clinical FXS phenotypes beyond the pain induction/perception, since individuals with Fragile X are known to experience hypersensitivity to touch (Arnett et al., 2014; He et al., 2017).

MATERIALS AND METHODS

Animals and Dorsal Root Ganglia Neuronal Culture

Fmr1 KO (FVB.129P2-Pde6b^{+}Tyr^{c-ch}Fmr1^{tm1Cgr}/J; stock #004624) and WT control (FVB.129P2-Pde6b^{+}Tyr^{c-ch}/AntJ; stock #004828) mice on FVB background were obtained from The Jackson Laboratory. Male mice (28- to 30-day old) were used for DRG cultures since male FXS individuals typically have more severe symptoms than do female individuals (Hagerman et al., 2009). Lumbar DRG (L1–L5) were dissected from *Fmr1* KO and WT control mice and collected into cold Hank's balanced salt solution (HBSS) with 5% Hepes, then transferred to warm papain solution and incubated for 20 min in 37°C. DRG's were washed in HBSS and incubated with collagenase for 20 min in 37°C. Ganglia were then mechanically dissociated to a single cell suspension by triturating in culture medium (Neurobasal medium), with Glutamax, PenStrep, and B-27. Cells were then cultured on 100 μg/ml poly-D-lysine coated cover slips and used for electrophysiological recording 24 h after plating. All animal procedures were in compliance with the NIH Guide for the Care and Use of Laboratory Animals and conformed to Washington University Animal Studies Committee guidelines.

Electrophysiology

Action Potential Recording and Analysis

Whole-cell patch-clamp recordings in a current-clamp mode were performed using a MultiClamp 700B amplifier (Molecular Devices) from short-term cultures (24 h after plating) of isolated DRG neurons, visually identified with infrared video microscopy and differential interference contrast optics (Olympus BX51WI). Current-clamp recordings were made with pipette capacitance compensation and bridge-balance compensation. Recordings were conducted at near-physiological temperature (33–34°C). In these conditions, the majority of cells analyzed were small/medium diameter IB4-positive neurons (Avraham et al., 2020). The recording electrodes were filled with the following (in mM): 130 K-gluconate, 10 KCl, 0.1 EGTA, 2 $MgCl_2$, 2 $ATPNa_2$, 0.4 GTPNa, and 10 HEPES, pH 7.3. The extracellular solution contained (in mM): 145 NaCl, 3 KCl, 10 HEPES, 2.5 $CaCl_2$, 1.2 $MgCl_2$, and 7 glucose, pH 7.4 (saturated with 95% O_2 and 5% CO_2). APs were evoked either by multiple-step-current injection (from 25 to 150 pA with step duration of 600 ms and step size 25 pA) or by a ramp-current injection (0.1 pA/ms) with a hyperpolarizing onset. To determine the number of APs, all APs for each step were counted (step-evoked APs), but for the ramp-evoked APs, only APs within the first 2 s from beginning of the ramp were counted. AP threshold was defined as voltage where the AP rise speed reaches 5 mV/ms. The AP threshold was determined only from the first APs in the trace. For ramp-evoked APs, AP rheobase was determined as current amplitude difference from baseline to threshold point. Rheobase charge transfer was the integration of the current over the time interval, which was from the beginning of the steps (or ramp cross baseline) to the first AP threshold point. AP latency was defined as the time duration

from the beginning of step-current to the first AP threshold point. AP duration was defined as the time interval between AP rising and falling parts at a membrane potential of +15 mV level. When the number of APs was more than 2, the first inter-AP interval was defined as the time duration between the peaks of first and second APs. All data were averaged over 5–8 trials for each cell. All chemicals for internal solution and bath solution were from Sigma-Aldrich. The channel blockers ZD7288 and XE991 were from Tocris. Different cells were used to test the effect of blockers (ZD7288 or XE991) to minimize the influence from "washout effect" due to recording time limitations (recordings in DRG cultures have a fast rundown during whole cell recordings).

Determination of Resting Membrane Potential, Capacitance, and Input Resistance

Resting membrane potential was measured immediately after whole-cell formation. Cell capacitance was determined by the amplifier's auto whole-cell compensation function with slight manual adjustment to optimize the measurement if needed. Under current-clamp mode, a negative current (−50 pA for 500 ms) was injected every 5 s to assess the input resistance. The voltage difference between baseline and steady state was used to calculate input resistance.

Measurements of HCN Channel Activity

For evaluation of HCN channel activity, hyperpolarization-evoked voltage sag was determined by step-current injection (from −50 to −100 pA with step size −10 pA and duration 600 ms). Sag amplitude was defined as the voltage difference between the lowest point of voltage trace and steady-state part (average 50 ms) immediate before the end of step. Sag ratio was calculated as 100% × (sag amplitude) ÷ (voltage difference between baseline and the lowest point of voltage trace).

RNA Isolation and Quantitative PCR

Dorsal root ganglia were lysed and total RNA was extracted using Trizol reagent (Thermo Fisher, Cat# 15596026). Next, RNA concentration was determined using a NanoDrop 2000 (Thermo Fisher Scientific). First strand synthesis was then performed using the High Capacity cDNA Reverse Transcription kit (Applied Biosystems). qPCR was performed using PowerUp SYBR Green master mix (Thermo Fisher, Cat# a25742) using 5 ng of cDNA per reaction. Plates were run on a QuantStudio 6 Flex system. Quantification of relative gene expression was performed using an automated software package (QuantStudio, ThermoFisher Scientific) following a standard $2^{-\Delta\Delta Ct}$ method as described (Rao et al., 2013). Briefly, the cycle threshold (Ct) information generated by the qPCR system is directly used to determine relative gene expression in target and reference samples, using a reference gene as the normalizing factor (Rao et al., 2013). The Ct for the mRNA of a housekeeping gene (*Rpl13a*) was first subtracted from the Ct for the mRNA of the different *Hcn* isoforms in the same sample to normalize for variation in the amount and quality of mRNA between different samples. This normalization procedure (ΔCt) permits comparison of expression of a gene of interest among different samples. The average ΔCt value from three technical replicates was calculated for each of the biological replicates ($n = 3$). The final outcome of this quantification was calculated as the fold change of *Hcn* isoforms expression in the KO samples relative to their expression in the WT samples ($\Delta\Delta Ct$). The relative gene expression is usually set to 1 for reference samples (WT) because $\Delta\Delta Ct$ is equal to 0 and therefore 2^0 is equal to 1 (Rao et al., 2013).

Primer sequences were obtained from PrimerBank or published literature and product size validated using agarose gel electrophoresis.

Rpl13a (PrimerBank ID 334688867c2) Forward Primer AGCCTACCAGAAAGTTTGCTTAC Reverse Primer GCTTCTTCTTCCGATAGTGCATC.

Hcn1 Forward Primer ACATGCTGTGCATTGGTTATGGCG, Reverse PrimerAACAAACATTGCGTAGCAGGTGGC.

Hcn2 Forward Primer ACTTCCGCACCGGCATTGTTATTG, Reverse Primer TCGATTCCCTTCTCCACTATG AGG.

Hcn3 Forward Primer TGGGAACCACTGGTGCACG, Reverse Primer TGAGCGTCTAGCAGATCGAG.

Hcn4 Forward Primer GCATGATGCTTCTGCTGTGTCACT, Reverse Primer TTCACCATGCCATTGATGGACACC.

Statistical Analysis

Data are presented as mean ± SEM. Student's *T*-test was used for statistical analysis as appropriate. Significance was set as $p < 0.05$. The *n* was number of cells tested. All statistical values and tests used in each experiment are given in **Supplementary Table 1** for each panel.

DATA AVAILABILITY STATEMENT

The raw data supporting the conclusions of this article will be made available by the authors, without undue reservation.

ETHICS STATEMENT

All animal procedures were reviewed and approved by the Washington University School of Medicine Institutional Animal Care and Use Committee (IACUC) under protocol A-3381-01. All experiments were performed in accordance with the relevant guidelines and regulations. All experimental protocols involving mice were approved by the Washington University School of Medicine (protocol #21-0104 and #20-0173). Mice were housed and cared for in the Washington University School of Medicine animal care facility. This facility is accredited by the Association for Assessment and Accreditation of Laboratory Animal Care (AALAC) and conforms to the PHS guidelines for Animal Care. Accreditation - 7/18/97, USDA Accreditation: Registration # 43-R-008.

AUTHOR CONTRIBUTIONS

P-YD, OA, VC, and VK conceived and designed the experiments and wrote the manuscript. P-YD and OA performed

the experiments and data analysis. VC and VK secured the funding. All authors contributed to the article and approved the submitted version.

FUNDING

This work was funded in part by the NIH grant R35 NS111596 to VK, and by the NIH grant R01 NS111719 and R35 NS122260 to VC.

ACKNOWLEDGMENTS

We would like to thank members of the Klyachko and Cavalli Lab for valuable discussions.

SUPPLEMENTARY MATERIAL

The Supplementary Material for this article can be found online at: https://www.frontiersin.org/articles/10.3389/fnmol.2021.796053/full#supplementary-material

REFERENCES

Allen, C. B., Celikel, T., and Feldman, D. E. (2003). Long-term depression induced by sensory deprivation during cortical map plasticity in vivo. *Nat. Neurosci.* 6, 291–299. doi: 10.1038/nn1012

Arnett, M. T., Herman, D. H., and McGee, A. W. (2014). Deficits in tactile learning in a mouse model of fragile X syndrome. *PLoS One* 9:e109116. doi: 10.1371/journal.pone.0109116

Arron, K., Oliver, C., Moss, J., Berg, K., and Burbidge, C. (2011). The prevalence and phenomenology of self-injurious and aggressive behaviour in genetic syndromes. *J. Intellect. Disabil. Res.* 55, 109–120. doi: 10.1111/j.1365-2788.2010.01337.x

Avraham, O., Deng, P. Y., Jones, S., Kuruvilla, R., Semenkovich, C. F., Klyachko, V. A., et al. (2020). Satellite glial cells promote regenerative growth in sensory neurons. *Nat. Commun.* 11:4891. doi: 10.1038/s41467-020-18642-y

Biel, M., Wahl-Schott, C., Michalakis, S., and Zong, X. (2009). Hyperpolarization-activated cation channels: from genes to function. *Physiol. Rev.* 89, 847–885. doi: 10.1152/physrev.00029.2008

Booker, S. A., Domanski, A. P. F., Dando, O. R., Jackson, A. D., Isaac, J. T. R., Hardingham, G. E., et al. (2019). Altered dendritic spine function and integration in a mouse model of fragile X syndrome. *Nat. Commun.* 10:4813. doi: 10.1038/s41467-019-11891-6

Booker, S. A., Simoes de Oliveira, L., Anstey, N. J., Kozic, Z., Dando, O. R., Jackson, A. D., et al. (2020). Input-output relationship of CA1 pyramidal neurons reveals intact homeostatic mechanisms in a mouse model of fragile X syndrome. *Cell Rep.* 32:107988. doi: 10.1016/j.celrep.2020.107988

Brager, D. H., Akhavan, A. R., and Johnston, D. (2012). Impaired dendritic expression and plasticity of h-channels in the fmr1(−/y) mouse model of fragile X syndrome. *Cell Rep.* 1, 225–233. doi: 10.1016/j.celrep.2012.02.002

Brandalise, F., Kalmbach, B. E., Mehta, P., Thornton, O., Johnston, D., Zemelman, B. V., et al. (2020). Fragile X mental retardation protein bidirectionally controls dendritic I_h in a cell-type specific manner between mouse hippocampus and prefrontal cortex. *J. Neurosci.* 40, 5327–5340. doi: 10.1523/JNEUROSCI.1670-19.2020

Brown, M. R., Kronengold, J., Gazula, V. R., Chen, Y., Strumbos, J. G., Sigworth, F. J., et al. (2010). Fragile X mental retardation protein controls gating of the sodium-activated potassium channel Slack. *Nat. Neurosci.* 13, 819–821. doi: 10.1038/nn.2563

Cascio, C. J. (2010). Somatosensory processing in neurodevelopmental disorders. *J. Neurodev. Dis.* 2, 62–69. doi: 10.1007/s11689-010-9046-3

Castren, M., Tervonen, T., Karkkainen, V., Heinonen, S., Castren, E., Larsson, K., et al. (2005). Altered differentiation of neural stem cells in fragile X syndrome. *Proc. Natl. Acad. Sci. U.S.A.* 102, 17834–17839. doi: 10.1073/pnas.0508995102

Chaplan, S. R., Guo, H. Q., Lee, D. H., Luo, L., Liu, C., Kuei, C., et al. (2003). Neuronal hyperpolarization-activated pacemaker channels drive neuropathic pain. *J. Neurosci.* 23, 1169–1178. doi: 10.1523/jneurosci.23-04-01169.2003

Comery, T. A., Harris, J. B., Willems, P. J., Oostra, B. A., Irwin, S. A., Weiler, I. J., et al. (1997). Abnormal dendritic spines in fragile X knockout mice: maturation and pruning deficits. *Proc. Natl. Acad. Sci. U.S.A.* 94, 5401–5404. doi: 10.1073/pnas.94.10.5401

Contractor, A., Klyachko, V. A., and Portera-Cailliau, C. (2015). Altered neuronal and circuit excitability in fragile X syndrome. *Neuron* 87, 699–715. doi: 10.1016/j.neuron.2015.06.017

Crawford, H., Karakatsani, E., Singla, G., and Oliver, C. (2019). The persistence of self-injurious and aggressive behavior in males with fragile X syndrome over 8 years: a longitudinal study of prevalence and predictive risk markers. *J. Autism Dev. Disord.* 49, 2913–2922. doi: 10.1007/s10803-019-04002-3

Darnell, J. C., Van Driesche, S. J., Zhang, C., Hung, K. Y., Mele, A., Fraser, C. E., et al. (2011). FMRP stalls ribosomal translocation on mRNAs linked to synaptic function and autism. *Cell* 146, 247–261. doi: 10.1016/j.cell.2011.06.013

de Moraes, E. R., Kushmerick, C., and Naves, L. A. (2017). Morphological and functional diversity of first-order somatosensory neurons. *Biophys. Rev.* 9, 847–856. doi: 10.1007/s12551-017-0321-3

Deng, P. Y., Carlin, D., Oh, Y. M., Myrick, L. K., Warren, S. T., Cavalli, V., et al. (2019). Voltage-independent SK-channel dysfunction causes neuronal hyperexcitability in the hippocampus of Fmr1 knock-out mice. *J. Neurosci.* 39, 28–43. doi: 10.1523/JNEUROSCI.1593-18.2018

Deng, P. Y., and Klyachko, V. A. (2016a). Genetic upregulation of BK channel activity normalizes multiple synaptic and circuit defects in a mouse model of fragile X syndrome. *J. Physiol.* 594, 83–97. doi: 10.1113/JP271031

Deng, P. Y., and Klyachko, V. A. (2016b). Increased persistent sodium current causes neuronal hyperexcitability in the entorhinal cortex of Fmr1 knockout mice. *Cell Rep.* 16, 3157–3166. doi: 10.1016/j.celrep.2016.08.046

Deng, P. Y., and Klyachko, V. A. (2021). Channelopathies in fragile X syndrome. *Nat. Rev. Neurosci.* 22, 275–289. doi: 10.1038/s41583-021-00445-9

Deng, P. Y., Rotman, Z., Blundon, J. A., Cho, Y., Cui, J., Cavalli, V., et al. (2013). FMRP regulates neurotransmitter release and synaptic information transmission by modulating action potential duration via BK channels. *Neuron* 77, 696–711. doi: 10.1016/j.neuron.2012.12.018

Domanski, A. P. F., Booker, S. A., Wyllie, D. J. A., Isaac, J. T. R., and Kind, P. C. (2019). Cellular and synaptic phenotypes lead to disrupted information processing in Fmr1-KO mouse layer 4 barrel cortex. *Nat. Commun.* 10:4814. doi: 10.1038/s41467-019-12736-y

Dwivedi, D., Chattarji, S., and Bhalla, U. S. (2019). Impaired reliability and precision of spiking in adults but not juveniles in a mouse model of fragile X syndrome. *eNeuro* 6:ENEURO.0217-19.2019. doi: 10.1523/ENEURO.0217-19.2019

Ferron, L., Nieto-Rostro, M., Cassidy, J. S., and Dolphin, A. C. (2014). Fragile X mental retardation protein controls synaptic vesicle exocytosis by modulating N-type calcium channel density. *Nat. Commun.* 5:3628. doi: 10.1038/ncomms4628

Ferron, L., Novazzi, C. G., Pilch, K. S., Moreno, C., Ramgoolam, K., and Dolphin, A. C. (2020). FMRP regulates presynaptic localization of neuronal voltage gated calcium channels. *Neurobiol. Dis.* 138:104779. doi: 10.1016/j.nbd.2020.104779

George, M. S., Abbott, L. F., and Siegelbaum, S. A. (2009). HCN hyperpolarization-activated cation channels inhibit EPSPs by interactions with M-type K(+) channels. *Nat. Neurosci.* 12, 577–584. doi: 10.1038/nn.2307

Guo, W., Polich, E. D., Su, J., Gao, Y., Christopher, D. M., Allan, A. M., et al. (2015). Fragile X proteins FMRP and FXR2P control synaptic GluA1 expression and neuronal maturation via distinct mechanisms. *Cell Rep.* 11, 1651–1666. doi: 10.1016/j.celrep.2015.05.013

Hagerman, R. J., Berry-Kravis, E., Kaufmann, W. E., Ono, M. Y., Tartaglia, N., Lachiewicz, A., et al. (2009). Advances in the treatment of fragile X syndrome. *Pediatrics* 123, 378–390.

Harlow, E. G., Till, S. M., Russell, T. A., Wijetunge, L. S., Kind, P., and Contractor, A. (2010). Critical period plasticity is disrupted in the barrel cortex of FMR1 knockout mice. *Neuron* 65, 385–398. doi: 10.1016/j.neuron.2010.01.024

He, C. X., Cantu, D. A., Mantri, S. S., Zeiger, W. A., Goel, A., and Portera-Cailliau, C. (2017). Tactile defensiveness and impaired adaptation of neuronal activity in the Fmr1 knock-out mouse model of autism. *J. Neurosci.* 37, 6475–6487. doi: 10.1523/JNEUROSCI.0651-17.2017

Juczewski, K., von Richthofen, H., Bagni, C., Celikel, T., Fisone, G., and Krieger, P. (2016). Somatosensory map expansion and altered processing of tactile inputs in a mouse model of fragile X syndrome. *Neurobiol. Dis.* 96, 201–215. doi: 10.1016/j.nbd.2016.09.007

Kanyshkova, T., Pawlowski, M., Meuth, P., Dube, C., Bender, R. A., Brewster, A. L., et al. (2009). Postnatal expression pattern of HCN channel isoforms in thalamic neurons: relationship to maturation of thalamocortical oscillations. *J. Neurosci.* 29, 8847–8857. doi: 10.1523/JNEUROSCI.0689-09.2009

Li, L., Rutlin, M., Abraira, V. E., Cassidy, C., Kus, L., Gong, S., et al. (2011). The functional organization of cutaneous low-threshold mechanosensory neurons. *Cell* 147, 1615–1627. doi: 10.1016/j.cell.2011.11.027

Liu, Q., Vrontou, S., Rice, F. L., Zylka, M. J., Dong, X., and Anderson, D. J. (2007). Molecular genetic visualization of a rare subset of unmyelinated sensory neurons that may detect gentle touch. *Nat. Neurosci.* 10, 946–948. doi: 10.1038/nn1937

Moosmang, S., Stieber, J., Zong, X., Biel, M., Hofmann, F., and Ludwig, A. (2001). Cellular expression and functional characterization of four hyperpolarization-activated pacemaker channels in cardiac and neuronal tissues. *Eur. J. Biochem.* 268, 1646–1652. doi: 10.1046/j.1432-1327.2001.02036.x

Moskalyuk, A., Van De Vijver, S., Verstraelen, P., De Vos, W. H., Kooy, R. F., and Giugliano, M. (2020). Single-cell and neuronal network alterations in an in vitro model of fragile X syndrome. *Cereb. Cortex* 30, 31–46. doi: 10.1093/cercor/bhz068

Nomura, T., Musial, T. F., Marshall, J. J., Zhu, Y., Remmers, C. L., Xu, J., et al. (2017). Delayed maturation of fast-spiking interneurons is rectified by activation of the TrkB receptor in the mouse model of fragile X syndrome. *J. Neurosci.* 37, 11298–11310. doi: 10.1523/JNEUROSCI.2893-16.2017

Oh, M. M., Oliveira, F. A., and Disterhoft, J. F. (2010). Learning and aging related changes in intrinsic neuronal excitability. *Front. Aging Neurosci.* 2:2. doi: 10.3389/neuro.24.002.2010

Olson, W., Dong, P., Fleming, M., and Luo, W. (2016). The specification and wiring of mammalian cutaneous low-threshold mechanoreceptors. *Wiley Interdiscip. Rev. Dev. Biol.* 5, 389–404. doi: 10.1002/wdev.229

Orefice, L. L., Mosko, J. R., Morency, D. T., Wells, M. F., Tasnim, A., Mozeika, S. M., et al. (2019). Targeting peripheral somatosensory neurons to improve tactile-related phenotypes in ASD models. *Cell* 178, 867–886.e24. doi: 10.1016/j.cell.2019.07.024

Orefice, L. L., Zimmerman, A. L., Chirila, A. M., Sleboda, S. J., Head, J. P., and Ginty, D. D. (2016). Peripheral mechanosensory neuron dysfunction underlies tactile and behavioral deficits in mouse models of ASDs. *Cell* 166, 299–313. doi: 10.1016/j.cell.2016.05.033

Penagarikano, O., Mulle, J. G., and Warren, S. T. (2007). The pathophysiology of fragile X syndrome. *Annu. Rev. Genomics Hum. Genet.* 8, 109–129.

Price, T. J., Flores, C. M., Cervero, F., and Hargreaves, K. M. (2006). The RNA binding and transport proteins staufen and fragile X mental retardation protein are expressed by rat primary afferent neurons and localize to peripheral and central axons. *Neuroscience* 141, 2107–2116. doi: 10.1016/j.neuroscience.2006.05.047

Price, T. J., and Melemedjian, O. K. (2012). Fragile X mental retardation protein (FMRP) and the spinal sensory system. *Res. Prob. Cell Differ.* 54, 41–59. doi: 10.1007/978-3-642-21649-7_4

Price, T. J., Rashid, M. H., Millecamps, M., Sanoja, R., Entrena, J. M., and Cervero, F. (2007). Decreased nociceptive sensitization in mice lacking the fragile X mental retardation protein: role of mGluR1/5 and mTOR. *J. Neurosci.* 27, 13958–13967. doi: 10.1523/JNEUROSCI.4383-07.2007

Rais, M., Binder, D. K., Razak, K. A., and Ethell, I. M. (2018). Sensory processing phenotypes in fragile X syndrome. *ASN Neuro* 10:1759091418801092. doi: 10.1177/1759091418801092

Ramirez-Lopez, A., Pastor, A., de la Torre, R., La Porta, C., Ozaita, A., Cabanero, D., et al. (2021). Role of the endocannabinoid system in a mouse model of Fragile X undergoing neuropathic pain. *Eur. J. Pain* 25, 1316–1328. doi: 10.1002/ejp.1753

Rao, X., Huang, X., Zhou, Z., and Lin, X. (2013). An improvement of the $2^{-\Delta\Delta CT}$ method for quantitative real-time polymerase chain reaction data analysis. *Biostat. Bioinforma. Biomath.* 3, 71–85.

Schmidt-Hieber, C., Jonas, P., and Bischofberger, J. (2004). Enhanced synaptic plasticity in newly generated granule cells of the adult hippocampus. *Nature* 429, 184–187. doi: 10.1038/nature02553

Shah, M. M. (2014). Cortical HCN channels: function, trafficking and plasticity. *J. Physiol.* 592, 2711–2719. doi: 10.1113/jphysiol.2013.270058

Shen, H., Liu, W., Geng, Q., Li, H., Lu, M., Liang, P., et al. (2018). Age-dependent up-regulation of HCN channels in spiral ganglion neurons coincide with hearing loss in mice. *Front. Aging Neurosci.* 10:353. doi: 10.3389/fnagi.2018.00353

Telias, M., Kuznitsov-Yanovsky, L., Segal, M., and Ben-Yosef, D. (2015). Functional deficiencies in fragile X neurons derived from human embryonic stem cells. *J. Neurosci.* 35, 15295–15306. doi: 10.1523/JNEUROSCI.0317-15.2015

Telias, M., Segal, M., and Ben-Yosef, D. (2013). Neural differentiation of fragile X human Embryonic Stem Cells reveals abnormal patterns of development despite successful neurogenesis. *Dev. Biol.* 374, 32–45. doi: 10.1016/j.ydbio.2012.11.031

Till, S. M., Wijetunge, L. S., Seidel, V. G., Harlow, E., Wright, A. K., Bagni, C., et al. (2012). Altered maturation of the primary somatosensory cortex in a mouse model of fragile X syndrome. *Hum. Mol. Genet.* 21, 2143–2156. doi: 10.1093/hmg/dds030

Vislay, R. L., Martin, B. S., Olmos-Serrano, J. L., Kratovac, S., Nelson, D. L., Corbin, J. G., et al. (2013). Homeostatic responses fail to correct defective amygdala inhibitory circuit maturation in fragile X syndrome. *J. Neurosci.* 33, 7548–7558. doi: 10.1523/JNEUROSCI.2764-12.2013

Wang, H. F., Shortland, P., Park, M. J., and Grant, G. (1998). Retrograde and transganglionic transport of horseradish peroxidase-conjugated cholera toxin B subunit, wheatgerm agglutinin and isolectin B4 from *Griffonia simplicifolia* I in primary afferent neurons innervating the rat urinary bladder. *Neuroscience* 87, 275–288. doi: 10.1016/s0306-4522(98)00061-x

Yang, L. K., Lu, L., Feng, B., Wang, X. S., Yue, J., Li, X. B., et al. (2020). FMRP acts as a key messenger for visceral pain modulation. *Mol. Pain* 16:1744806920972241. doi: 10.1177/1744806920972241

Yousuf, M. S., Noh, M. C., Friedman, T. N., Zubkow, K., Johnson, J. C., Tenorio, G., et al. (2019). Sensory neurons of the dorsal root ganglia become hyperexcitable in a T-cell-mediated MOG-EAE model of multiple sclerosis. *eNeuro* 6:ENEURO.0024-19.2019. doi: 10.1523/ENEURO.0024-19.2019

Zhang, Y., Bonnan, A., Bony, G., Ferezou, I., Pietropaolo, S., Ginger, M., et al. (2014). Dendritic channelopathies contribute to neocortical and sensory hyperexcitability in Fmr1(−/y) mice. *Nat. Neurosci.* 17, 1701–1709. doi: 10.1038/nn.3864

Conflict of Interest: The authors declare that the research was conducted in the absence of any commercial or financial relationships that could be construed as a potential conflict of interest.

Publisher's Note: All claims expressed in this article are solely those of the authors and do not necessarily represent those of their affiliated organizations, or those of the publisher, the editors and the reviewers. Any product that may be evaluated in this article, or claim that may be made by its manufacturer, is not guaranteed or endorsed by the publisher.

frontiers in Molecular Neuroscience

ORIGINAL RESEARCH
published: 04 January 2022
doi: 10.3389/fnmol.2021.796070

Disrupted Association of Sensory Neurons With Enveloping Satellite Glial Cells in Fragile X Mouse Model

Oshri Avraham[1], Pan-Yue Deng[2], Dario Maschi[2], Vitaly A. Klyachko[2,3] and Valeria Cavalli[1,3,4]**

[1] Department of Neuroscience, Washington University School of Medicine, St. Louis, MO, United States, [2] Department of Cell Biology and Physiology, Washington University School of Medicine, St. Louis, MO, United States, [3] Hope Center for Neurological Disorders, Washington University School of Medicine, St. Louis, MO, United States, [4] Center of Regenerative Medicine, Washington University School of Medicine, St. Louis, MO, United States

Among most prevalent deficits in individuals with Fragile X syndrome (FXS) is hypersensitivity to sensory stimuli and somatosensory alterations. Whether dysfunction in peripheral sensory system contributes to these deficits remains poorly understood. Satellite glial cells (SGCs), which envelop sensory neuron soma, play critical roles in regulating neuronal function and excitability. The potential contributions of SGCs to sensory deficits in FXS remain unexplored. Here we found major structural defects in sensory neuron-SGC association in the dorsal root ganglia (DRG), manifested by aberrant covering of the neuron and gaps between SGCs and the neuron along their contact surface. Single-cell RNAseq analyses demonstrated transcriptional changes in both neurons and SGCs, indicative of defects in neuronal maturation and altered SGC vesicular secretion. We validated these changes using fluorescence microscopy, qPCR, and high-resolution transmission electron microscopy (TEM) in combination with computational analyses using deep learning networks. These results revealed a disrupted neuron-glia association at the structural and functional levels. Given the well-established role for SGCs in regulating sensory neuron function, altered neuron-glia association may contribute to sensory deficits in FXS.

Keywords: satellite glial cells, fragile X syndrome, sensory neuron, neuron-glia communication, hyperexcitability

OPEN ACCESS

Edited by:
Michael Telias, University of California, Berkeley, United States

Reviewed by:
Yongcheol Cho, Korea University, South Korea
Arkady Khoutorsky, McGill University, Canada

****Correspondence:***
Valeria Cavalli
cavalli@wustl.edu
Vitaly A. Klyachko
klyachko@wustl.edu

Specialty section:
This article was submitted to Neuroplasticity and Development, a section of the journal Frontiers in Molecular Neuroscience

Received: *15 October 2021*
Accepted: *17 November 2021*
Published: *04 January 2022*

Citation:
Avraham O, Deng P-Y, Maschi D, Klyachko VA and Cavalli V (2022) Disrupted Association of Sensory Neurons With Enveloping Satellite Glial Cells in Fragile X Mouse Model. Front. Mol. Neurosci. 14:796070. doi: 10.3389/fnmol.2021.796070

INTRODUCTION

Fragile X syndrome (FXS) is the most common heritable cause of intellectual disability and the leading monogenetic cause of autism spectrum disorders (ASD). This condition stems from loss of fragile X mental retardation protein (FMRP), which regulates a wide range of neuronal functions *via* translational control and protein-protein interactions. Some of the most prevalent symptoms of FXS include hypersensitivity to a wide range of sensory stimuli, such as tactile, auditory, and visual stimuli (Cascio, 2010). Sensory hypersensitivity may contribute or even cause behavioral deficits such as anxiety and impaired social interactions (Rais et al., 2018). These sensory deficits have been thus far largely attributed to alterations in sensory processing abnormalities in brain circuits

(Contractor et al., 2015). Yet the mechanisms of sensory deficits in FXS and ASD remain elusive. Recent studies suggest that many core cognitive deficits in ASD may arise from earlier deficits in sensory inputs that subsequently drive abnormal development of cortical circuits (Orefice et al., 2016, 2019). Whether and how dysfunction of peripheral sensory system that receive and convey primary sensory information contribute to FXS pathophysiology remains largely unexplored.

In the accompanying manuscript we described a state of profound hyperexcitability of primary sensory neurons in the dorsal root ganglia (DRG) driven, at least in part, by intrinsic neuronal deficits in HCN channels. In addition to neuronal intrinsic mechanisms, glial cells can modulate neuronal structure and function, and are implicated in many neurodevelopmental diseases (Kim et al., 2020). In the brain, astrocytes express FMRP and accumulating evidence suggests widespread alterations in astrocyte-neuronal communication in FXS models (Pacey and Doering, 2007; Jacobs and Doering, 2010; Jacobs et al., 2012, 2016; Yang et al., 2012; Pacey et al., 2015; Cheng et al., 2016; Sourial and Doering, 2016; Wallingford et al., 2017; Krasovska and Doering, 2018). Moreover, astrocyte-selective loss of FMRP contributes to cortical synaptic deficits in FXS through the dysregulated astroglial glutamate transporter GLT1 and impaired glutamate uptake (Higashimori et al., 2016). In the peripheral sensory circuit, satellite glial cells (SGCs) share many functional similarities with astrocytes despite a great diversity in morphology (Avraham et al., 2020, 2021b; Hanani and Spray, 2020; Hanani and Verkhratsky, 2021). As many as 8–10 SGCs completely envelop each DRG neuron (Pannese, 1964). SGCs contribute to abnormal neuronal hyperexcitability in many pain syndromes (Hanani and Spray, 2020) and we recently showed that these cells also contribute to promote peripheral axon regeneration (Avraham et al., 2020, 2021b). While contribution of astrocytes to synaptic and neuronal dysfunction in the brain of FXS models has received a lot of recent attention, the potential contributions of SGCs in FXS remains unexplored.

In this study we combined ultrastructural analyses and single-cell RNAseq to examine changes in sensory neuron association with their enveloping SGCs caused by FMRP loss.

RESULTS

Structural Changes in Sensory Neuron-Satellite Glial Cell Association in *Fmr1* KO Mice

In adult animals, SGCs tightly enwrap the soma of each sensory neuron (Pannese, 1964). The gap between the two cell surfaces can often be as small as ∼20–50 nm. This close association between the two cell types is essential for efficient mutual neuron–SGC interactions (Hanani and Spray, 2020), although the mechanisms regulating and maintaining this close association remain poorly understood. We thus determined the impact of FMRP loss on the structural organization of SGCs surrounding sensory neurons. Transmission Electron Microscopy (TEM) demonstrated the tight contact between SGCs and neurons in WT control mice, whereas the *Fmr1* KOs presented an aberrant covering of the neuron with multiple large gaps between the glia and the neuron along their contact surface (**Figure 1A**, all values and statistical information is provided in **Supplementary Table 1**). We found a significant increase in the number of neurons with large gaps along neuron-glia contact surface in the *Fmr1* KO mice compared to WT (**Figure 1B**). Quantification of the distance between each neuron and the SGC coat further revealed significant defects in the *Fmr1* KO mice with a marked increase in the neuron-glia distances (**Figure 1C**). However, other aspects of neuronal morphology were similar between *Fmr1* KO and WT mice, with no detectable changes in neuronal diameter, area, and shape (**Figures 1D–F**). Additionally, immunostaining of sections of DRG from *Fmr1* KO and WT mice for the apoptotic marker cleaved caspase 3 revealed no change in apoptotic cell death in *Fmr1* KO compared to WT mice (**Figures 1G–I**), indicating that loss of FMRP does not cause excessive neuronal apoptotic cell death. These observations suggest that loss of FMRP results in a failure of SGCs to envelop the neurons tightly. Such a major structural defect might disrupt the neuron-SGC communication. Whether all sensory neurons or only specific subtypes present this aberrant interaction with their surrounding SGC remains to be determined.

Transcriptional Changes in Dorsal Root Ganglia Cells Caused by Loss of Fragile X Mental Retardation Protein

To begin to define the changes in the molecular profile of sensory neurons and SGCs in *Fmr1* KO mice associated with the structural alterations we observed above, we performed single-cell RNA-seq (scRNAseq) from the DRGs of *Fmr1* KO and WT, using the Chromium Single Cell Gene Expression Solution (10x Genomics). This method allows characterization of DRG cells at the molecular level, as described previously (Avraham et al., 2020, 2021b). While scRNAseq captures transcriptional events, changes in RNA stability may also contribute to the different profiles obtained, and the depth of sequencing obtained in scRNAseq analyses might not allow to capture low level transcripts. The number of sequenced cells in *Fmr1* KO mice was 11,060 from 2 biological replicates with an average of 105,076 mean reads per cell, 2,141 mean genes per cell and a total of 20,219 genes detected. The number of sequenced cells from WT mice was 10,856 from 2 biological replicates with an average of 94,139 mean reads per cell, 2,239 mean genes per cell, and a total of 20,066 genes detected. Low quality cells with less than 600 genes per cell and doublets were filtered out from downstream analysis (see filtering criteria in the section "Materials and Methods"). To identify cluster-specific genes, we calculated the expression difference of each gene between that cluster and the average in the rest of the clusters (ANOVA fold change threshold $>$ 1.5). Examination of the cluster-specific marker genes in t-distributed stochastic neighbor embedding (t-SNE) plot, revealed major cellular subtypes including medium/small neurons (*Trpv1*), large neurons (*Nefh*/Nf200), SGCs (*Kcnj10*, *Fabp7*), Schwann cells (*Ncmap*), pericytes (*Kcnj8*), endothelial

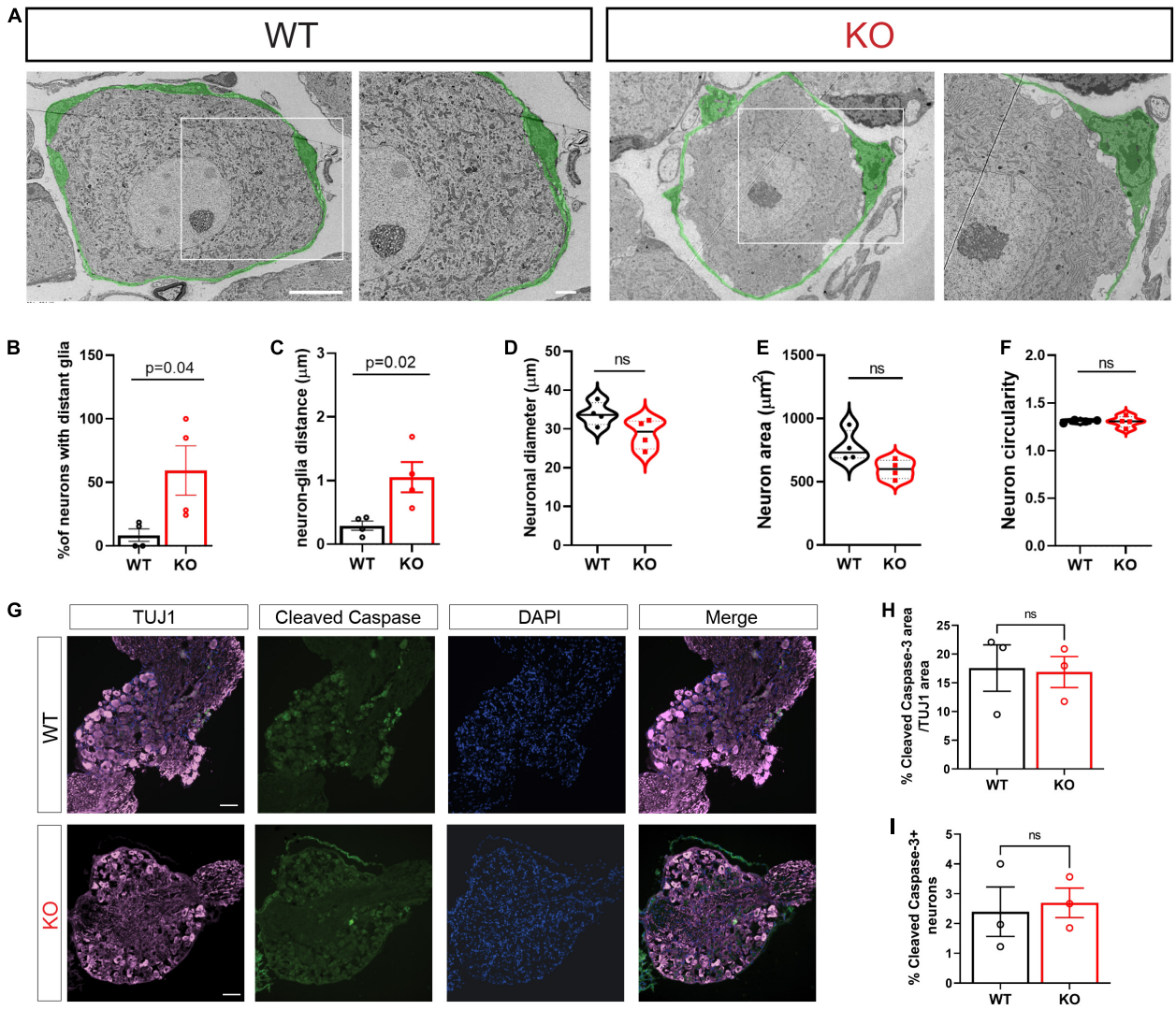

FIGURE 1 | Structural alterations in neuron-SGC association in *Fmr1* KO DRGs with no changes in neuronal morphology. **(A)** Representative TEM images of a neuron-SGC unit in DRG sections from WT and *Fmr1* KO. In total, 4 biologically independent animals. Scale bar: 10 μm (left panel), 2 μm (right panel). The SGCs surrounding sensory neurons are pseudo-colored in green. **(B)** Quantification of percentage of neurons which have gaps between the neuron membrane and the covering SGC, out of the total number of neurons imaged. $n = 4$ biologically independent animals. **(C)** Measurements of the distance between the neuron membrane and the covering SGC membrane (μm). In total, 3 measurements were taken from each neuron. $n = 4$ biologically independent animals. **(D–F)** Measurements of neuronal diameter **(D)**, neuronal area **(E)**, and neuronal circularity **(F)** [ratio between major axis (X) and minor axis (Y). 1 = circular, 1 > elliptic]. $n = 4$ biologically independent animals. **(G)** Representative images of DRG sections co-stained with TUJ1 (magenta) and the apoptotic marker Cleaved Caspase3 (green). $n = 3$ biologically independent animals. Scale bar: 100 μm. **(H)** Quantification of percentage of Cleaved Caspase 3 fluorescence intensity normalized to TUJ1 intensity. $n = 3$ biologically independent animals. **(I)** Quantification of the percentage of cleaved caspase 3 positive neurons out of all neurons per section. $n = 3$ biologically independent animals.

cells (*Pecam*/Cd31), macrophages (*Cd68*), and mesenchymal cells (*Pdgfra*) (**Figures 2A,B** and **Supplementary Table 2**). An unbiased (Graph-based) clustering identified 17 distinct cell clusters (**Figure 2C**). We then compared the cell clustering between WT and *Fmr1* KO DRGs and found that unique cell clusters were not altered by loss of FMRP (**Figure 2D**), with similarity in cell cluster distribution between samples and genotypes (**Figures 2E,F**). To uncover the transcriptional changes that occur within DRG cell clusters in *Fmr1* KO compared to WT control, we calculated the differentially expressed (DE) genes for every cluster (FDR ≤ 0.05, FC ≥ 1.5) and found that loss of FMRP induced substantial gene expression changes in many cell types in the DRG (**Figure 2G** and **Supplementary Tables 3–13**).

Delayed/Aberrant Sensory Neuron Maturation Caused by Loss of Fragile X Mental Retardation Protein

The number of neurons recovered in our scRNAseq analysis was ∼3%, whereas neurons represent ∼12% of cells in the

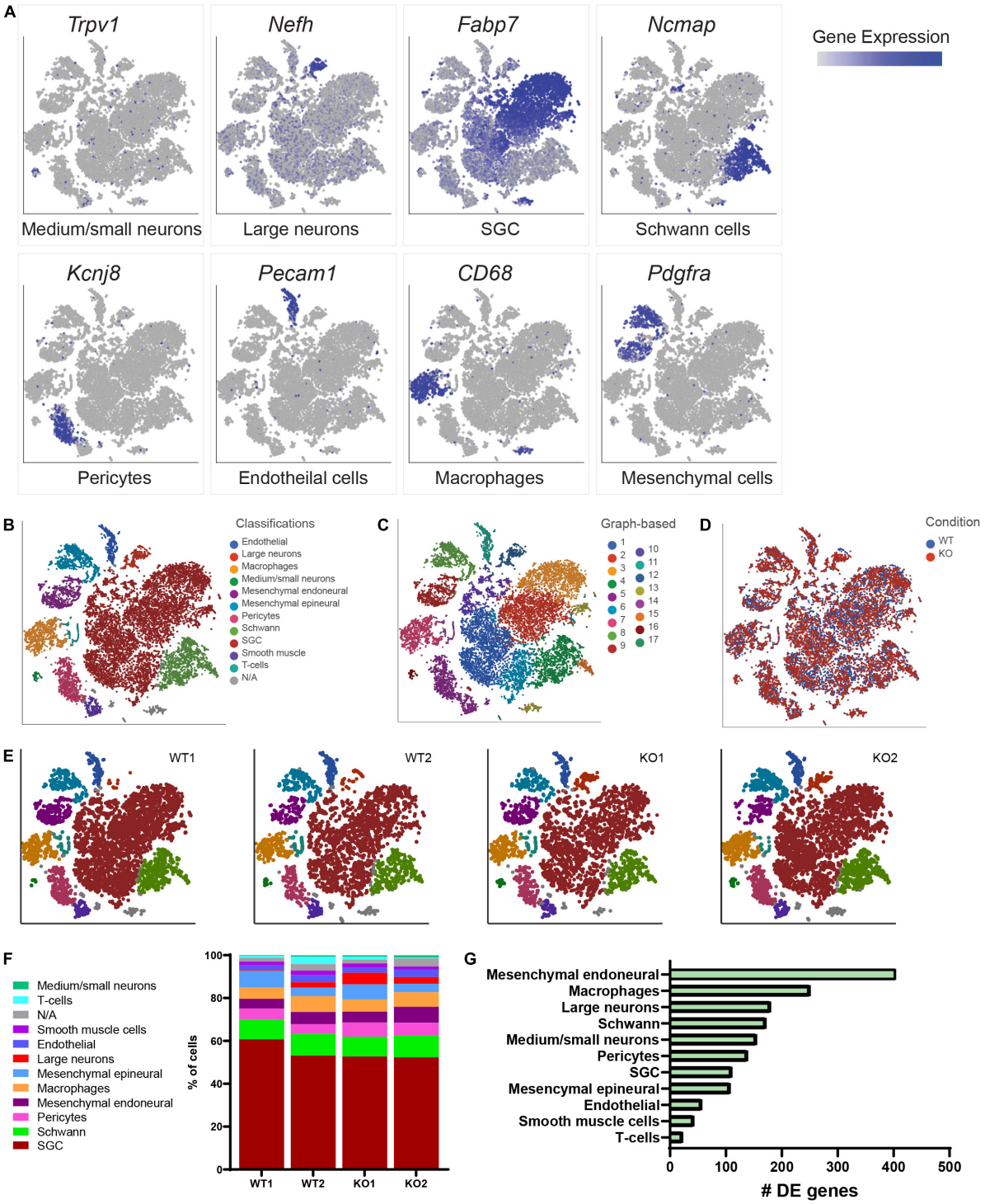

FIGURE 2 | Cluster analysis from scRNAseq of DRGs. **(A)** t-SNE overlay for expression of marker genes for different cell populations in all cells from WT and *Fmr1* KO including Trpv1 for small/medium neurons, Nefh for large neurons, Fabp7 for SGCs, Ncmap for Schwann cells, Kcnj8 for pericytes, Pecam for endothelial cells, CD68 for Macrophages and Pdgfra for mesenchymal cells. The relative levels of expression are presented as a blue color gradient on the left. $n = 3$ biologically independent animals. **(B)** t-SNE plot of 18,000 cells from *Fmr1* KO and WT dissociated DRG. Classifications were assigned based on known marker genes. Low quality cells (3,916 cells from a total of 21,916) with less than 600 genes per cell and doublets were filtered out from analysis (see filtering criteria in the section "Materials and Methods"). In total, 11 distinct cell clusters were assigned based on known marker genes. **(C)** Unbiased, Graph based clustering with 17 distinct cell clusters. **(D)** t-SNE plot colored by genotype. **(E)** t-SNE plots separated by biological sample in WT and KO, colored by cell type. **(F)** Fraction of each cell type within WT (8,970 cells), and *Fmr1* KO (9,038 cells) conditions. **(G)** Plot of the number of differentially regulated genes in each cell type in *Fmr1* KO compared to WT (FDR $\leq$ 0.05, fold-change $\geq$ 1.5).

DRG (Avraham et al., 2021b). The relatively low number of neurons recovered might be due to the fact that sensory neurons are relatively large cells, which might be destroyed when passed through microfluidic device and to the potential neuronal damage during tissue dissociation process (Avraham et al., 2020). However, we collected a sufficient number of neurons (248 in WT and 659 in KO) that allowed comparison between genotypes. Since in the accompanying paper we found significant changes in excitability of small/medium *Fmr1* KO neurons, we pooled all cells classified as small/medium neurons (cluster 16; 139 cells in WT and 304 in KO). According to the classification of adult DRG neurons at the single cell level (Sharma et al., 2020), small/medium neurons in our data set included CGRP-α neurons (*Avpr1a, Slc6a7*), CGRP-γ neurons (*Ctcflos, Greb1l*), C-LTMR (*Cacna1i*), Trmp8 neurons (*Trm8*), and excluded proprioceptors (*CGRP*θ, ζ and ε), Aβ LTMR and Aδ LTMR neurons (**Supplementary Table 2**).

We found 155 differentially expressed (DE) genes in the *Fmr1* KO small/medium neurons compared to WT (**Figure 2G**). In total, 61 genes were upregulated and 94 genes were downregulated (FDR $\leq$ 0.05 FC $\geq$ 1.5) (**Figure 3A** and **Supplementary Table 3**). We next performed pathway enrichment analysis to reveal the biological function underlying the molecular changes in the *Fmr1* KO neurons (**Figure 3B**, GO biological process). The upregulated genes were related to nervous system development, cell proliferation, glial cell differentiation and mRNA metabolism (**Figure 3B** and **Table 1**). Downregulated genes were related to neuronal differentiation, microtubule and intermediate filament cytoskeleton, axonal transport, neurotransmitter secretion and cholesterol and steroid biosynthesis (**Figure 3B** and **Table 1**). Among the transcriptional changes associated with FMRP loss are notable alterations in genes regulating neuronal differentiation and elaboration. Both peripheral neurons and glia arise from neural crest cells. Upon differentiation, sensory neurons acquire neuronal identity by upregulating neuronal markers. Neuronal differentiation markers such as *Ntrk1*; *Ndrg4*; *Avil*; *Stmn2*and markers of axonal/dendritic elaboration such as *Nefl*, *Prph*, *Tubb3*/TUJ1, and

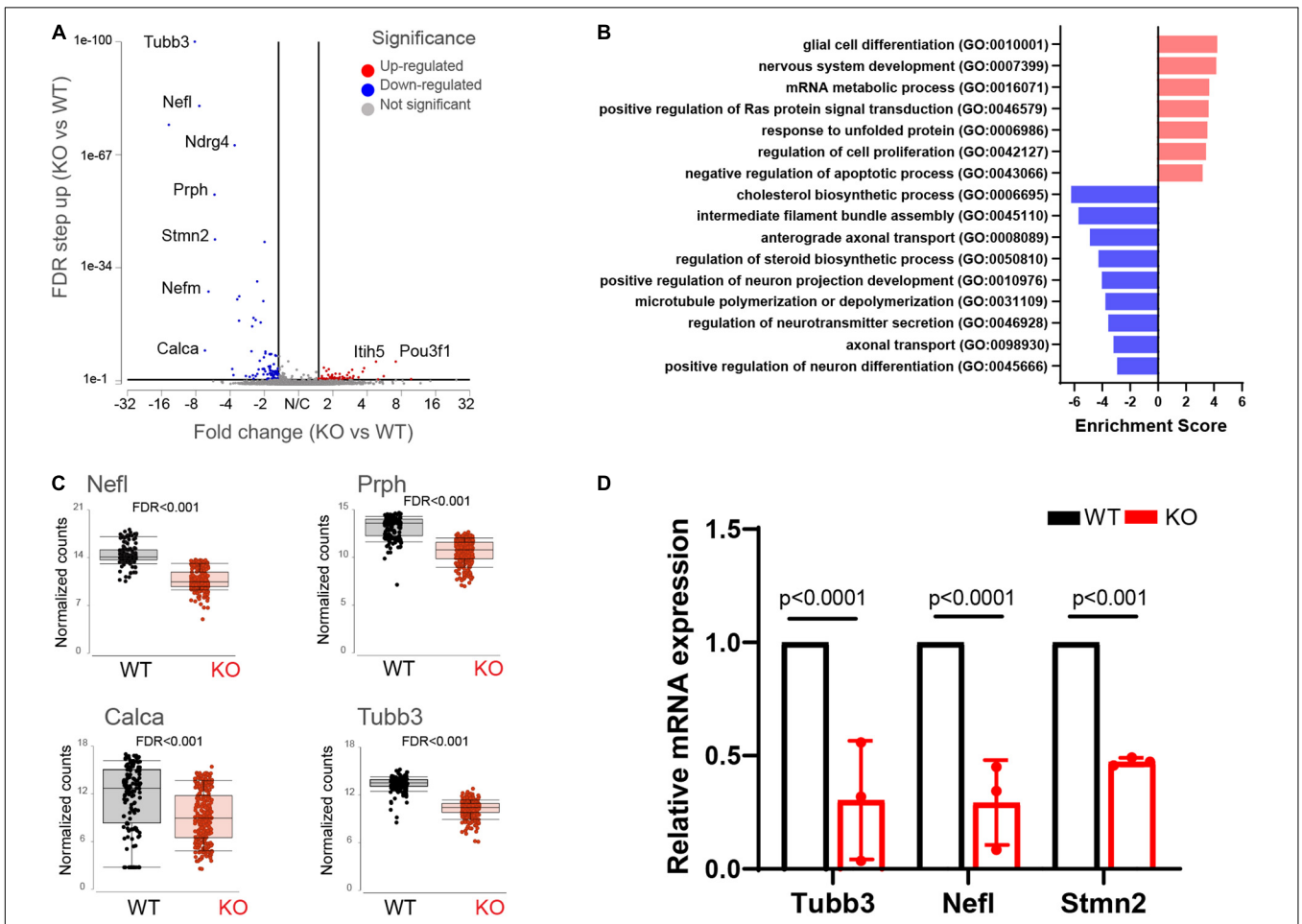

FIGURE 3 | Molecular changes in *Fmr1* KO small/medium sensory neurons indicate delayed differentiation. **(A)** Volcano plot of DE genes in small/medium neurons from *Fmr1* KO compared to WT. **(B)** Enriched pathways in *Fmr1* KO compared to WT (GO Biological Process) for up-regulated (red) and down-regulated (blue) genes. **(C)** Mean expression of the neuronal markers *Nefl*, *Prph*, *Tubb3*, and *Calca* in WT (black) and *Fmr1* KO (red). **(D)** qPCR analysis of the relative mRNA expression of *Tubb3*, *Nefl*, and *Stmn2* in *Fmr1* KO compared to WT DRGs. *n* = 3 biologically independent animals.

TABLE 1 | Enriched biological processes (GO 2018) for differentially up and down regulated genes in *Fmr1* KO small/medium neurons.

GO biological process term	Genes
Up regulated	
Glial cell differentiation (GO:0010001)	RELN; ERBB3; SOX10
Nervous system development (GO:0007399)	EDNRB; RELN; ERBB3; B3GNT5; FABP7; NAB2; VLDLR; P OU3F2
mRNA metabolic process (GO:0016071)	SON; ZFP36L2; HSPA1B; HSPA1A
Positive regulation of Ras protein signal transduction (GO:0046579)	COL3A1; NOTCH1; LPAR1
Response to unfolded protein (GO:0006986)	DNAJA1; HSPA1B; HSPA1A
Regulation of cell proliferation (GO:0042127)	TCF7L2; CXCL10; NOTCH1; CDK6; ERBB3; FABP7; POU3 F2; HSPA1B; HSPA1A
Negative regulation of apoptotic process (GO:0043066)	DNAJA1; NOTCH1; SON; ERBB3; ANGPTL4; HSPA1B; HS PA1A
Down regulated	
Cholesterol biosynthetic process (GO:0006695)	FDPS; SQLE; MVD; ACAT2; FDFT1
Intermediate filament bundle assembly (GO:0045110)	NEFL; NEFM; NEFH
Anterograde axonal transport (GO:0008089)	FMR1; HSPB1; NEFL; AP3B2
Regulation of steroid biosynthetic process (GO:0050810)	FDPS; SQLE; MVD; FDFT1
Positive regulation of neuron projection development (GO:0010976)	RIMS2; NTRK1; NDRG4; AVIL; STMN2
Microtubule polymerization or depolymerization (GO:0031109)	TPPP3; STMN2; STMN3
Regulation of neurotransmitter secretion (GO:0046928)	RIMS2; FMR1; CPLX1
Axonal transport (GO:0098930)	FMR1; NEFL; AP3B2
Positive regulation of neuron differentiation (GO:0045666)	NTRK1; NDRG4; AVIL; STMN2

Calca/CGRP were down regulated in *Fmr1* KO small/medium neurons (**Figures 3A,C**). We validated these findings by qPCR experiments, which confirmed that the neuronal markers *Tubb3*, *Stmn2*, and *Nefl* were downregulated in *Fmr1* KO DRG compared to WT DRG (**Figure 3D**).

Upon differentiation, sensory neurons also normally downregulate glial and progenitor markers. We found that progenitor markers such as *Sox10*, *Fabp7*, *Foxd3*, and *Notch1* were abnormally upregulated in the *Fmr1* KO neurons compared to WT (**Figure 4A**). We previously showed that *Fabp7* is highly expressed in all SGCs in adult mice (Avraham et al., 2020, 2021b). However, *Fabp7* is also expressed in radial glial cells as well as neuronal progenitors and is critical for neurogenesis in the CNS (Feng et al., 1994; Matsumata et al., 2012). We thus examined by immunofluorescence if FABP7 was upregulated in neurons of *Fmr1* KO DRG compared to WT. As expected, there was minimal spatial overlap of FABP7 and TUJ1 staining in WT, confirming very low neuronal expression of FABP7 in developed sensory neurons (**Figures 4B–D**). In contrast, overlap of FABP7 and TUJ1 staining was clearly evident in *Fmr1* KO, highlighting a greatly increased number of neurons expressing FABP7 (**Figures 4B–D**), and validating the scRNAseq data.

To further explore changes in neuronal maturation caused by FMRP loss, we compared the lineage profiles of neurons in *Fmr1* KO and WT, using a differential trajectory map based on "Monocle2." This analysis can order a set of individual cells along a path/trajectory/lineage, and assign a pseudo-time value to each cell that represents where the cell is along that path. This trajectory analysis further revealed the different developmental stage of neurons in WT vs. *Fmr1* KO (**Figure 4E**). These results suggest a delayed or aberrant sensory neuronal development process resulting from the loss of FMRP. These observations are consistent with developmental delays suggested in mouse cortical neurons (Tervonen et al., 2009; Saffary and Xie, 2011; Edens et al., 2019), as well as in human neurons and forebrain organoids (Sunamura et al., 2018; Kang et al., 2021).

Transcriptional Changes in Satellite Glial Cells Caused by Loss of Fragile X Mental Retardation Protein Are Related to Vesicle Organization and Secretion

We next examined the transcriptional profile of SGCs in *Fmr1* KO and WT mice. We pooled all cells classified as SGCs (9,917 cells, 5,173 in WT and 4,744 in *Fmr1* KO) and compared the gene expression in *Fmr1* KO and WT SGCs (FDR $\leq$ 0.05 FC $\geq$ 1.5). We found 111 genes that were differentially upregulated in *Fmr1* KO SGCs and 19 genes that were downregulated (**Figure 5A** and **Supplementary Table 4**). Pathway enrichment analysis (GO biological process) revealed that the upregulated genes were related to calcium signaling, vesicle organization and chemical synaptic transmission (**Figure 5B** and **Table 2**). Downregulated pathways were related to response to cytokine stimulus and inflammatory response (**Figure 5B** and **Table 2**). These downregulated pathways are consistent with the reduced serum levels of pro-inflammatory chemokines in FXS individuals (Van Dijck et al., 2020). Interestingly, the chemokine *Ccl2* was downregulated in both SGC and macrophages in *Fmr1* KO mice compared to WT (**Supplementary Tables 4, 6**), and is also reduced in the serum of FXS patients (Van Dijck et al., 2020).

We then determine if the SGC subtypes and their similarity to astrocytes we previously characterized (Avraham et al., 2021b) were affected by FMRP loss. Trajectory analysis revealed major differences between WT and *Fmr1* KO SGCs (**Figure 5C**), that might be indicative of a different developmental process in SGC in the absence of FMRP. Despite these major differences in

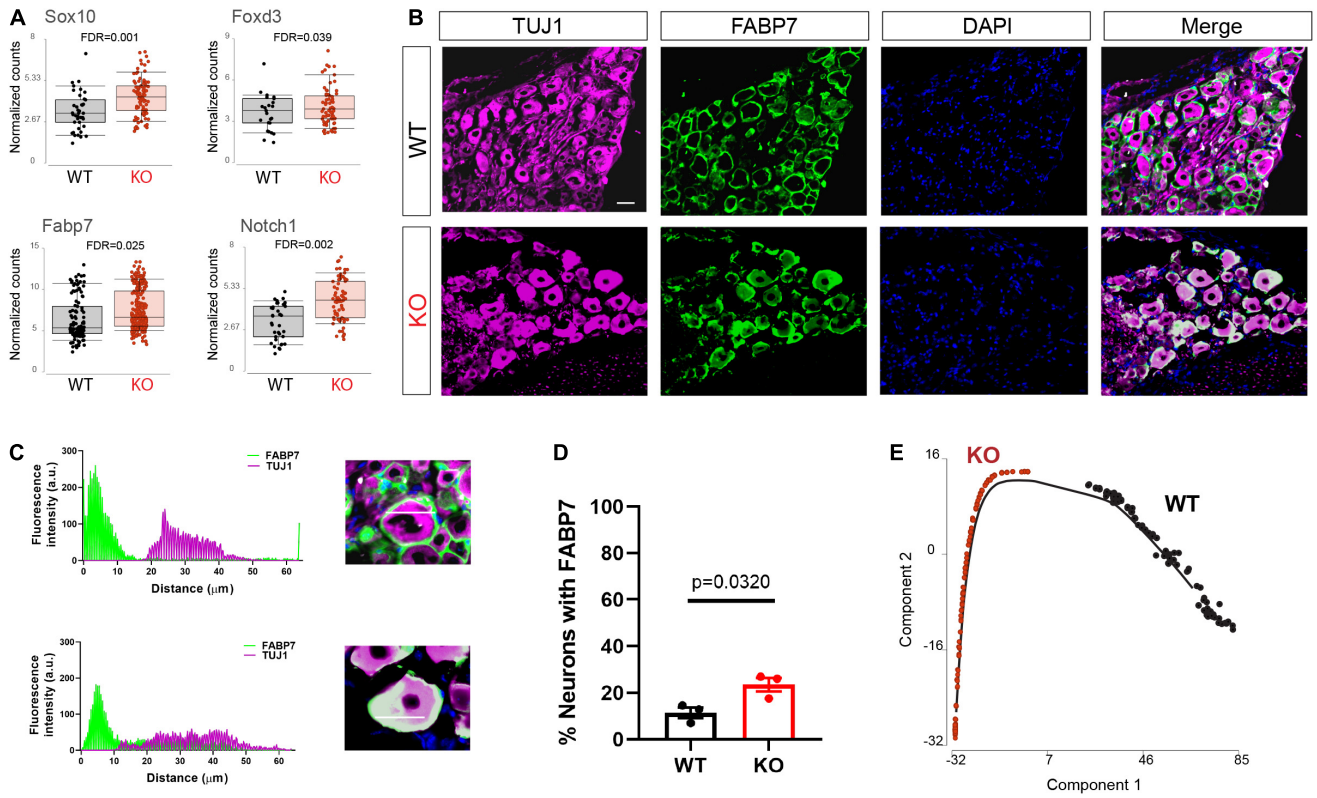

FIGURE 4 | Dysregulated neuronal maturation in *Fmr1* KO DRG. **(A)** Mean expression of the progenitor markers *Sox10*, *Fabp7*, *Notch1*, and *Foxd3* in WT (black) and *Fmr1* KO (red). **(B)** Representative immunofluorescence images of DRG sections from WT and *Fmr1* KO mice co-stained with TUJ1 (magenta) and the SGC marker FABP7 (green). $n = 3$ biologically independent animals. Scale bar: 50 μm. **(C)** Representative images of fluorescence intensity of FABP7/TUJ1 measured across neuron-SGC units (white line in inset image). **(D)** Percentage of neurons with detectable FABP7 expression in WT and *Fmr1* KO. $n = 3$ biologically independent animals, 10–15 cells from each animal were used for measurements. **(E)** Trajectory analysis of small/medium neurons colored by genotype.

trajectories, an unbiased clustering of SGCs in WT and *Fmr1* KO revealed similarity in SGC subtype distribution (**Figure 5D**). Overlay of top marker genes for each SGC cluster paralleled our previous findings of SGC subtypes (Avraham et al., 2021b; **Figure 5E**), with the exception for an additional cluster 5 in both *Fmr1* KO and WT, which was enriched in proliferation markers such as *Top2a*, *Cdk1*, and *Mki67* (**Figure 5E** and **Supplementary Table 14**) and could result from the mice being younger in the current study (4-weeks old), compared to our previous studies using more mature mice (8–12 weeks old). A differential expression analysis between *Fmr1* KO and WT for each SGC cluster revealed larger changes in clusters 2 and 5, moderate changes in clusters 3 and 4 and minor in cluster 1 (FDR $\leq$ 0.05 FC $\geq$ 1.5) (**Figure 5F**). We examined the SGC cluster 3 in more details, since cluster 3 shared the most genes with astrocytes (**Figure 5G**), consistent with our previous findings (Avraham et al., 2021b). Loss of FMRP in astrocytes induces developmental delays in maturation and elaboration of neuronal dendrites and altered synaptic protein expression (Jacobs et al., 2010; Yang et al., 2012; Wang et al., 2016). Enriched pathways of the differentially expressed genes in cluster 3 in *Fmr1* KO compared to WT suggested a role in neuronal growth and differentiation as well as stress-activated responses (**Figure 5H**). These results thus further support the notion that SGCs' role in supporting sensory neuron development might be impaired in *Fmr1* KO.

Fragile X Mental Retardation Protein Loss Leads to Altered Vesicle Organization in Satellite Glial Cells

How SGCs communicate with sensory neurons remains poorly understood. There is evidence that SGCs can secrete factors such as TNFα, ATP, and GABA in certain conditions (Bowery et al., 1976; Hosli and Hosli, 1978; Hanani and Spray, 2020), but whether glial secretion occurs through vesicular release is not well-studied. The transcriptome analysis of SGCs indicated enrichment for genes related to vesicle organization and secretion as one of the most predominant changes in *Fmr1* KO SGCs (**Figure 5B**). Thus, we sought to verify this observation using ultrastructural measurements. We used TEM to image the SGC cytoplasm at high-resolution and observed multiple vesicular profiles of ∼50 nm diameter in both WT and *Fmr1* KO SGCs (**Figures 6A,B**). We then applied deep learning network algorithms (Selvaraju et al., 2020) to quantify the number of vesicular profiles in the SGC cytoplasm (**Figures 6A,B**; see section

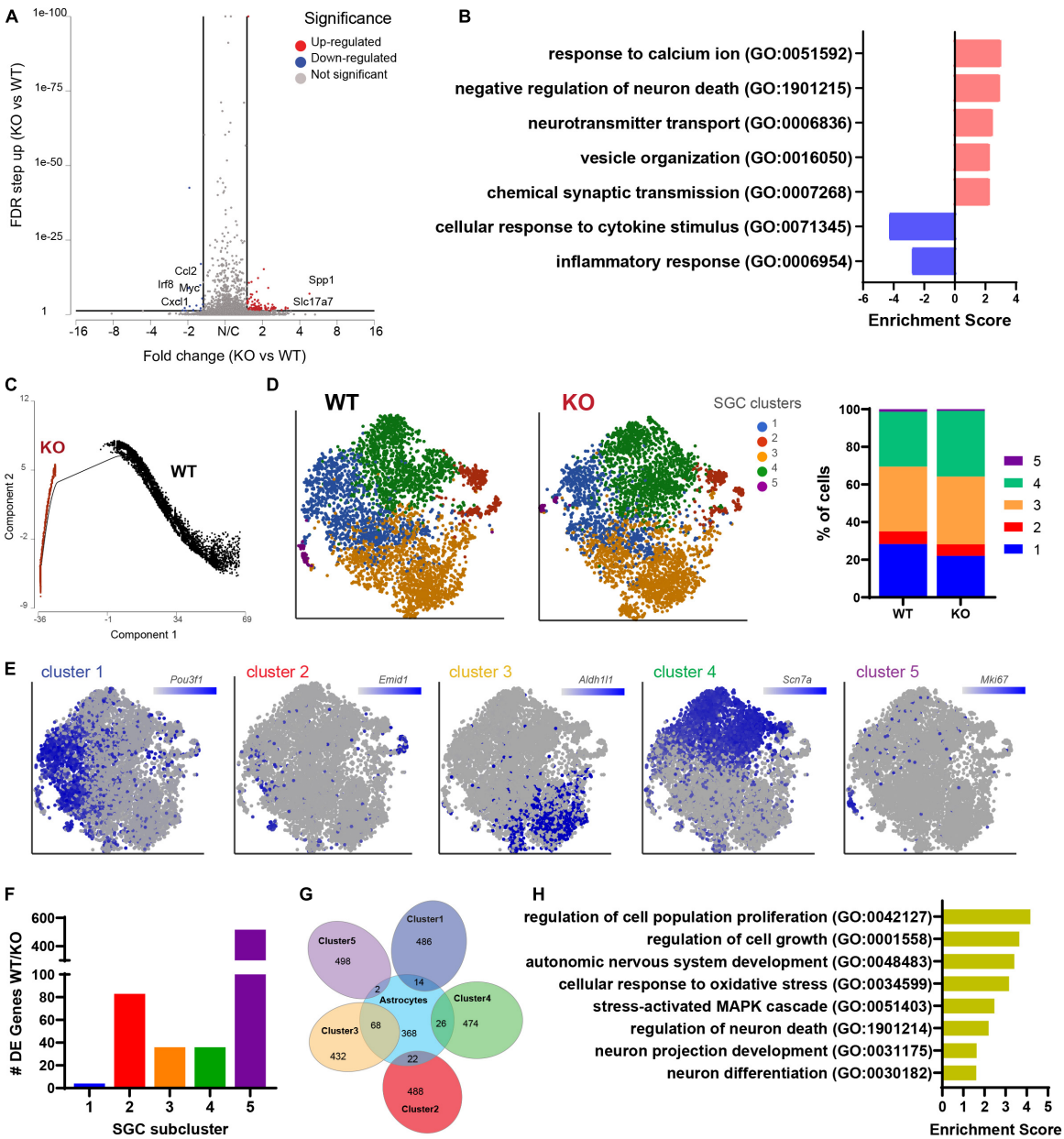

FIGURE 5 | Molecular changes in *Fmr1* KO SGCs are related to vesicle organization and secretion. **(A)** Volcano plot of DE genes in SGCs from *Fmr1* KO compared to WT. **(B)** Enriched pathways in *Fmr1* KO (GO Biological Process) for up-regulated (red) and down-regulated (blue) genes. **(C)** Trajectory analysis of SGCs colored by genotype. **(D)** t-SNE plot of SGC cluster colored by subclusters (unbiased, Graph based clustering) with quantification of the fraction of cells in the different SGC subclusters out of total number of SGC. **(E)** t-SNE overlay with SGC cluster specific genes. **(F)** Quantification of the number of differentially expressed genes in each SGC subcluster in *Fmr1* KO compared to WT (FDR ≤ 0.05, fold-change ≥ 1.5). **(G)** Venn diagram comparing signature genes in SGC subclusters and astrocytes. **(H)** Enriched pathways (GO Biological process) for top differentially upregulated genes in subcluster3 in *Fmr1* KO compared to WT (FDR ≤ 0.05, fold-change ≥ 1.5).

"Materials and Methods" for details). This analysis revealed a significant increase in the number of vesicles in *Fmr1* KO SGCs cytoplasm compared to WT (**Figures 6C,D**), validating the scRNAseq data. These results suggest that loss of FMRP causes SGCs to upregulate pathways related to vesicular secretion and thus communication with neurons, which could be a compensation for the disrupted glia-neuron association at the structural level.

DISCUSSION

Our results revealed major ultra-structural and transcriptional changes caused by loss of FMRP in the peripheral sensory system, including sensory neurons and their enveloping SGCs. Our analyses suggest structural disruption of sensory neuron-SGC association in the absence of FMRP, which is accompanied by aberrant transcriptional changes in pathways involved in vesicle

TABLE 2 | Enriched biological processes (GO 2018) for differentially up and down regulated genes in *Fmr1* KO SGCs.

GO biological process term	Genes
Up regulated	
Response to calcium ion (GO:0051592)	TRPC3; SYT1; DPEP1; KCNH1
Negative regulation of neuron death (GO:1901215)	CHGA; UNC5B; VSTM2L; ISL1
Neurotransmitter transport (GO:0006836)	SLC17A6; SLC17A7
Vesicle organization (GO:0016050)	RPH3A; SYT1; VAMP1; DNM1
Chemical synaptic transmission (GO:0007268)	GABBR2; SYT1; PLP1; SLC17A6; SLC17A7; GABRG2
Down regulated	
Cellular response to cytokine stimulus (GO:0071345)	MYC; LCN2; CCL2; IRF8; CXCL1
Inflammatory response (GO:0006954)	CYBB; CCL2; CXCL1

secretion and neuron-glia communication. These abnormalities are also accompanied by transcriptional changes indicative of delayed/altered maturation of neurons and SGCs. Given the well-established role for SGCs in regulating sensory neurons functions (Hanani and Spray, 2020), and the similarity between human and mouse SGCs (Avraham et al., 2021a), the structural and functional disruption of neuron-SGC communication may have important contribution to sensory dysfunctions in FXS.

Many aspects of neuronal function in the DRG are regulated by neuron-SGC interactions (Hanani and Spray, 2020). Thus, the disruption of neuron-glia association and altered vesicular communication could contribute to sensory defects *via* several mechanisms. First, SGC share functional similarities with astrocytes (Avraham et al., 2020; Hanani and Spray, 2020; Hanani and Verkhratsky, 2021) and loss of FMRP in astrocytes induces developmental delays in maturation and elaboration of hippocampal neuron dendrites and altered synaptic protein expression (Jacobs et al., 2010; Yang et al., 2012; Wang et al., 2016). Our results reveal that, similarly to central neurons, peripheral sensory neurons in *Fmr1* KO have a markedly delayed developmental trajectory. Interestingly, we observed that SGC cluster 3, which shares the most similarities with astrocytes, is altered by the loss of FMRP, with enriched pathways related to neuronal differentiation and development. Disruption of SGCs-neuron association and communication, if present during early development, could thus contribute to the developmental delay in maturation of sensory neurons in the absence of FMRP. Whether all sensory neuron subtypes present aberrant interaction with their surrounding SGC in the *Fmr1* KO mouse model, or specific subtypes are preferentially affected remains to be elucidated. This will be interesting to pursue in future studies, as various subtypes of sensory neurons encode different sensory modalities, such as pain and touch, that are affected in FXS individuals.

Second, SGCs are well-known to regulate neural excitability in normal conditions and to lead to pathological neuronal hyperexcitability in many pain syndromes (Hanani and Spray, 2020). SGCs can regulate neuronal excitability *via* ATP release (Du et al., 2011; Yousuf et al., 2011). Also, both sensory neurons and SGCs express glutamate receptors (Kung et al., 2013), although whether SGCs release glutamate has not been established definitively. Interestingly, it has long been known that SGCs can uptake and release GABA in a calcium-dependent manner (Minchin and Iversen, 1974; Minchin, 1975; Bowery et al., 1976; Hosli and Hosli, 1978) and that sensory neurons express $GABA_A$ and $GABA_B$ receptors (Labrakakis et al., 2003; Du et al., 2017). A recent study found that a subpopulation of SGCs in the DRG express GABA, the Bestrophin-1 (Best1), a Ca^{2+} dependent chloride channel, and enzymes of the putrescine pathway responsible for an alternative route of GABA biosynthesis, suggesting that SGCs may be the source of endogenous GABA released in the DRG (Vargas-Parada et al., 2021). Importantly, SGC-mediated inhibition is dependent on a close association between neurons and SGCs (Shoji et al., 2010; Vargas-Parada et al., 2021). Thus, structural disruption of neuron-SGCs association, as we observed in *Fmr1* KO mice, can contribute to sensory neuron hyperexcitability, in part, by reducing effects of GABA release from SGCs. Future studies will be needed to define the complex secretome of SGCs, which may include ATP, GABA, and glutamate.

Third, signaling pathways which are down-regulated in SGCs of *Fmr1* KO mice are primarily linked to inflammatory and cytokine response. This is consistent with findings of cytokine imbalance in FXS individuals (Van Dijck et al., 2020), children with autism (Yu et al., 2020) and the growing evidence that neuro-inflammatory mechanisms may contribute to the pathogenesis of FXS as well as other autism-associated disorders (Di Marco et al., 2016; Yu et al., 2020). This observation is particularly intriguing in a view of a growing number of reports that cytokines may specifically interact with neuronal ion channels regulating excitability (Viviani et al., 2007; Schafers and Sorkin, 2008). Pro-inflammatory cytokines are known to modulates L- and N-type Ca^{2+}channels, Na^{+}-channels, and $GABA_A$ receptors, and to regulate trafficking of AMPA and $GABA_A$ receptors in central neurons as well as glutamate uptake by glial transporters (Viviani et al., 2007; Schafers and Sorkin, 2008). Thus, dysregulation of the inflammatory and cytokine response in SGCs in *Fmr1* KO mice could contribute to sensory neuronal dysfunction *via* multiple mechanisms.

In summary, our results uncover major defects in neuron-SGCs association and communication, suggesting that manipulation of SGCs function maybe a viable new strategy to normalize function of peripheral sensory neurons in FXS.

MATERIALS AND METHODS

Animals

Fmr1 KO and WT control mice on FVB background were obtained from The Jackson Laboratory. Male mice (28–30-day old) were used. All animal procedures were in compliance with the NIH Guide for the Care and Use of Laboratory Animals and conformed to Washington University Animal Studies Committee guidelines.

Transmission Electron Microscopy

Mice were perfused with 2.5% glutaraldehyde and 4% paraformaldehyde in 0.1 M Cacodylate buffer, followed by

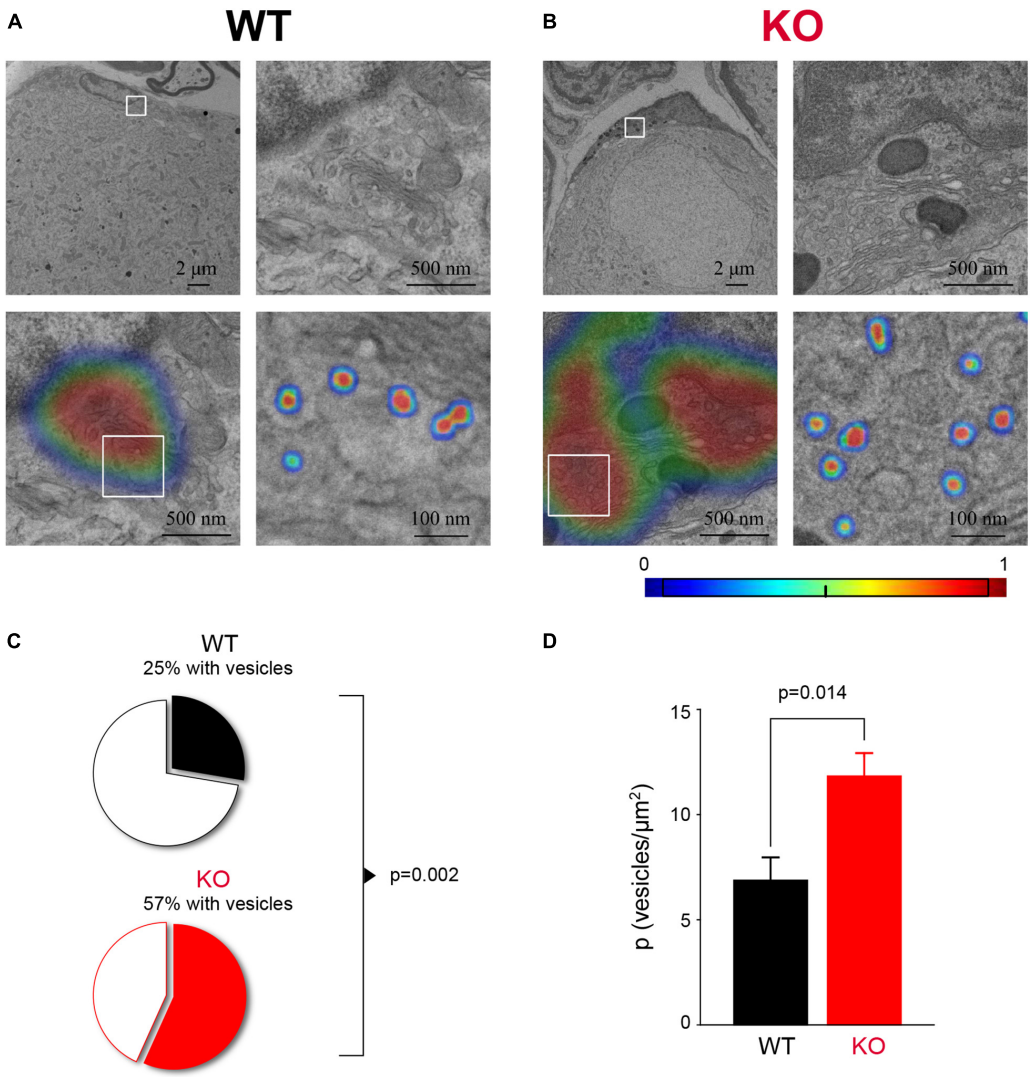

FIGURE 6 | Increased vesicle number in *Fmr1* KO SGC cytoplasm. **(A)** Example of SGC cytoplasmic area next to the SGC nucleus from WT mice (top left) with a boxed area zoomed-in (top, right). The area of interest (bottom left, same area as top right) with the heat-map showing the probability to identify an area with vesicles determined with a gradient-weighted class activation mapping approach. Boxed area is zoomed-in showing segmentation of vesicles using a separate deep learning network (bottom, right). **(B)** The same as panel **(A)**, but for *Fmr1* KO SGCs. **(C)** The proportion of SGCs with detectable vesicles ($P = 0.0021$, Chi-square test). $n = 4$ biologically independent animals. **(D)** Average vesicle density in SGC ($P = 0.014$, KS test). $n = 4$ biologically independent animals.

post fix. A secondary fix was done with 1% osmium tetroxide. For TEM, tissue was dehydrated with ethanol and embedded with spurr's resin. Thin sections (70 nm) were mounted on mesh grids and stained with 8% uranyl acetate followed by Sato's lead stain. Sections were imaged on a Jeol (JEM-1400) electron microscope and acquired with an AMT V601 digital camera (Washington University Center for Cellular Imaging). For measurements of the number of neurons with distant glia, neurons were counted as 0 (no distant glia) or 1 (obvious distant glia). To quantify the distance between the neuron outer membrane and the SGC, we performed 3 measurements per neuron, where we detected the largest visible gaps between the neuron membrane and the SGC membrane. Neuron's diameter was measured at the neuron's largest point across. Neuron circularity was measured as a ratio between major axis (X) and minor axis (Y) (1 = circular, 1 < elliptic). Neuronal area was measured by manually tracing the neuron outer membrane. For all measurements ImageJ software was used.

Vesicle Detection in Transmission Electron Microscopy Sections With Deep Learning Neural Networks

Customized two-step deep learning algorithm utilizing GoogLeNet network was developed to detect and count SGC vesicles in TEM sections. First, we used the gradient-weighted class activation mapping (Grad-CAM) technique to scan the images to produce a localization map identifying regions of

interest with vesicles in the image. We then used a second trained network to identify and segment individual vesicles (Selvaraju et al., 2020). The first network was trained with 2,671 pre-label images, 20% of the data was randomly assigned to the validation group. Network was trained using a mini-batch of 25 and a maximum epoch of 500, obtaining an accuracy of over 99% in the validation group. In order to prevent over fitting, we perform data augmentation by randomly resizing by 10% and reflecting the image. The second network was trained with 4,425 pre-label images, 20% of the data was randomly assigned to the validation group. This network was trained using a mini-batch of 100 and a maximum epoch of 1,000 obtaining an accuracy of 98.2% in the validation group. Given the small number of pixels that define a vesicle, data augmentation was prone to generate image artifacts that reduce the performance of the network. To overcome this problem, we limited the data augmentation to 5% resizing and used reflection and pixel shift in addition. The vesicle density was determined using a clustering algorithm and the area was defined as the smallest convex set that contains all the vesicles (convex hull area).

Single Cell RNAseq

DRG collected from 3 mice from each genotype for two biological replicates were dissociated into single cell suspension as describe (Avraham et al., 2020, 2021b). Cells were then washed in HBSS + Hepes + 0.1%BSA solution, passed through a 70-micron cell strainer. Hoechst dye was added to distinguish live cells from debris and cells were FACS sorted using MoFlo HTS with Cyclone (Beckman Coulter, Indianapolis, IN). Sorted cells were washed in HBSS + Hepes + 0.1%BSA solution and manually counted using hemocytometer. Solution was adjusted to a concentration of 500 cell/microliter and loaded on the 10X Chromium system. Single-cell RNA-Seq libraries were prepared using GemCode Single-Cell 3' Gel Bead and Library Kit (10x Genomics). A digital expression matrix was obtained using 10X's CellRanger pipeline (Build version 2.1.0) (Washington University Genome Technology Access Center). Quantification and statistical analysis were done with Partek Flow package (Build version 9.0.20.0417).

Filtering Criteria

Low quality cells and potential doublets were filtered out from analysis using the following parameters; total reads per cell: 600–15,000, expressed genes per cell: 500–4,000, mitochondrial reads < 10%. A noise reduction was applied to remove low expressing genes = 1 count. Counts were normalized and presented in logarithmic scale in CPM (count per million) approach. An unbiased clustering (graph based clustering) was done and presented as t-SNE (t-distributed stochastic neighbor embedding) plot, using a dimensional reduction algorithm that shows groups of similar cells as clusters on a scatter plot. Differential gene expression analysis performed using an ANOVA model; a gene is considered differentially expressed (DE) if it has a false discovery rate (FDR) step-up (p-value adjusted). $p \leq 0.05$ and a fold-change $\geq \pm 1.5$. Lowering the cutoff of fold-change down to $\geq \pm$ 1.3, result in similar gene sets and pathway analysis. The data was subsequently analyzed for enrichment of GO terms using Partek flow pathway analysis. Partek was also used to generate figures for t-SNE plots using a statistical method for visualizing high-dimensional data by giving each data point a location in a two-dimensional map.

Trajectory Analysis

We performed a differential trajectory mapping using "Monocle2" with standard settings. The algorithm orders a set of individual cells along a path/trajectory/lineage, and assigns a pseudo-time value to each cell that represents where the cell is along that path. This method identifies intermediate states during a biological process as well as bifurcation between two alternative cellular fates.

Immunohistochemistry

After isolation of DRG, tissue was fixed using 4% paraformaldehyde for 1 h at room temperature. Tissue was then washed in PBS and cryoprotected using 30% sucrose solution at 4°C overnight. Next, the tissue was embedded in O.C.T., frozen, and mounted for cryosectioning. All frozen sections were cut to a width of 12 μm for subsequent staining. Slides were washed 3× in PBS and then blocked for in solution containing 10% goat serum in 0.2% Triton-PBS for 1 h. Next, sections were incubated overnight in blocking solution containing primary antibody. The next day, sections were washed 3× with PBS and then incubated in blocking solution containing a secondary antibody for 1 h at room temperature. Finally, sections were washed 3× with PBS and mounted using ProLong Gold antifade (Thermo Fisher Scientific). For immunofluorescence on cultured cells, DRG cells were cultured on 100 μg/ml poly-D-lysine coated cover slips for 4 days in neurobasal media. Cells were then fixed using 4% paraformaldehyde for 20 min at room temperature. Cover slips were incubated for 1 h in 0.1% Triton-PBS containing primary antibody washed 3× with PBS and then incubated in 0.1% Triton-PBS solution containing a secondary antibody for 1 h at room temperature followed by 3 washes in PBS. Images were acquired at 10× or 20× using a Nikon TE2000E inverted microscope and images were analyzed using Nikon Elements. To determine the cleaved caspase staining area, a binary was generated to fit the positive signal, and positive staining area was measured. We noticed that the cleaved caspase signal was mainly in neuronal cells, therefore that area was internally normalized to TUJ1 positive staining area (ImageJ). To measure the number of cleaved caspase 3 positive neurons we manually selected all neurons (TUJ1 positive cells) with signal of cleaved caspase-3 above background (ImageJ). To measure the intensity of FABP7 signal in neurons, a 60 μm line was drawn across the neuron. Fluorescence intensity for FABP7 and TUJ1 was measured along the line (Nikon Elements).

Antibodies were as follow: Tubb3 (TUJ1) antibody (BioLegend catalog #802001, RRID:AB_291637), FABP7 (Thermo Fisher Scientific Cat# PA5-24949, RRID:AB_2542449), cleaved caspase 3 (CST Cat# 9664, RRID:AB_2070042).

RNA Isolation and Quantitative PCR

DRG and nerves were lysed and total RNA was extracted using Trizol reagent (Thermo Fisher Scientific, Cat# 15596026).).

Next, RNA concentration was determined using a NanoDrop 2000 (Thermo Fisher Scientific). First strand synthesis was then performed using the High Capacity cDNA Reverse Transcription kit (Applied Biosystems). Quantitative PCR was performed using PowerUp SYBR Green master mix (Thermo Fisher Scientific, Cat# a25742) using 5 ng of cDNA per reaction. Plates were run on a QuantStudio 6 Flex and analyzed in Microsoft Excel. The average Ct value from three technical replicates was averaged and normalized to the internal control Rpl13a. All primer sequences were obtained from PrimerBank and product size validated using agarose gel electrophoresis.

Rpl13a (PrimerBank ID 334688867c2) Forward Primer AGCCTACCAGAAAGTTTGCTTAC Reverse Primer GCTTCTTCTTCCGATAGTGCATC

Tubb3 (PrimerBank ID12963615a1) Forward Primer TAGACCCCAGCGGCAACTA

Reverse Primer GTTCCAGGTTCCAAGTCCACC

Nefl1 (PrimerBank ID 200038a1) Forward Primer CCGTACTTTTCGACCTCCTACA

Reverse Primer CTTGTGTGCGGATAGACTTGAG

Stmn2 (PrimerBank ID 118130361c1) Forward Primer CAGAGGAGCGAAGAAAGTCTCA

Reverse Primer CTAGATTAGCCTCACGGTTTTCC

Statistical Analysis

Data are presented as means ± SEM. Student's paired or unpaired *t*-test, KS test or Chi-square test were used for statistical analysis as appropriate; significance was set as $p < 0.05$. The n was number of cells tested, unless otherwise stated. All statistical values and tests used in each experiment are given in **Supplementary Table 1** for each panel, as well as in each figure legend.

DATA AVAILABILITY STATEMENT

The datasets generated in this study can be found in online repositories. The names of the repository/repositories and accession number(s) can be found below: https://www.ncbi.nlm.nih.gov/search/all/?term=GSE176449.

ETHICS STATEMENT

All animal procedures were reviewed and approved by the Washington University School of Medicine Institutional Animal Care and Use Committee (IACUC) under protocol A-3381-01. All experiments were performed in accordance with the relevant guidelines and regulations. All experimental protocols involving mice were approved by the Washington University School of Medicine (protocol #21-0104 and #20-0173). Mice were housed and cared for in the Washington University School of Medicine animal care facility. This facility is accredited by the Association for Assessment and Accreditation of Laboratory Animal Care (AALAC) and conforms to the PHS guidelines for Animal Care. Accreditation - 7/18/97, USDA Accreditation: Registration #43-R-008.

AUTHOR CONTRIBUTIONS

OA, P-YD, VC, and VK conceived and designed the experiments. P-YD and OA performed the experiments. DM contributed deep learning analysis tools. P-YD, OA, and DM performed data analysis. VC and VK secured the funding. All authors wrote the manuscript and approved the submitted version.

FUNDING

This work was supported in part by NIH R35 grant NS111596 to VK, and R01 NS111719 and R35 NS122260 to VC.

ACKNOWLEDGMENTS

We would like to thank Klyachko and Cavalli lab members for valuable discussions. We gratefully acknowledge Greg Strout, Ross Kossina, and James Fitzpatrick from the Washington University Center for Cellular Imaging (WUCCI), which is supported in part by Washington University School of Medicine, the Children's Discovery Institute of Washington University, and St. Louis Children's Hospital (CDI-CORE-2015-505 and CDI-CORE-2019-813) and the Foundation for Barnes-Jewish Hospital (3770) for assistance in acquiring and interpreting Transmission Electron Microscopy (TEM) data.

SUPPLEMENTARY MATERIAL

The Supplementary Material for this article can be found online at: https://www.frontiersin.org/articles/10.3389/fnmol.2021.796070/full#supplementary-material

Supplementary Table 1 | Data values and statistical analyses. Columns represent (from left to right): figure/panel number; experimental conditions; mean values and SEM; number of samples, statistical test used for comparison; *P*-value resulting from the statistical comparison.

Supplementary Table 2 | Differentially expressed (DE) genes per cell type relative to all other cell clusters (ANOVA Fold change > 1.5).

Supplementary Table 3 | Differentially expressed (DE) genes in *Fmr1* KO small/medium neurons (FDR < 0.05, Fold change > 1.5).

Supplementary Table 4 | Differentially expressed (DE) genes in *Fmr1* KO SGCs (FDR < 0.05, Fold change > 1.5).

Supplementary Tables 5–13 | Differentially expressed (DE) genes in *Fmr1* KO for endothelial cells, macrophages, mesenchymal endoneural, mesenchymal epineural, pericytes, Schwann cells, smooth muscle cells, large neurons and T-cells (FDR < 0.05, Fold change > 1.5).

Supplementary Table 14 | Differentially expressed (DE) genes per SGC cluster relative to all other SGC clusters (ANOVA Fold change > 1.5). Shared genes with astrocytes for each SGC subcluster and DE genes in *Fmr1* KO SGC for cluster 3.

REFERENCES

Avraham, O., Feng, R., Ewan, E. E., Rustenhoven, J., Zhao, G., and Cavalli, V. (2021b). Profiling sensory neuron microenvironment after peripheral and central axon injury reveals key pathways for neural repair. *eLife* 10:e68457. doi: 10.7554/eLife.68457

Avraham, O., Chamessian, A., Feng, R., Halevi, A. E., Moore, A. M., Gereau, R. W., et al. (2021a). Profiling the molecular signature of Satellite Glial Cells at the single cell level reveals high similarities between rodent and human. *bioRxiv* [Preprint]. doi: 10.1101/2021.04.17.440274

Avraham, O., Deng, P. Y., Jones, S., Kuruvilla, R., Semenkovich, C. F., Klyachko, V. A., et al. (2020). Satellite glial cells promote regenerative growth in sensory neurons. *Nat. Commun.* 11:4891. doi: 10.1038/s41467-020-18642-y

Bowery, N. G., Brown, D. A., Collins, G. G., Galvan, M., Marsh, S., and Yamini, G. (1976). Indirect effects of amino-acids on sympathetic ganglion cells mediated through the release of gamma-aminobutyric acid from glial cells. *Br. J. Pharmacol.* 57, 73–91. doi: 10.1111/j.1476-5381.1976.tb07658.x

Cascio, C. J. (2010). Somatosensory processing in neurodevelopmental disorders. *J. Neurodev. Disord.* 2, 62–69. doi: 10.1007/s11689-010-9046-3

Cheng, C., Lau, S. K., and Doering, L. C. (2016). Astrocyte-secreted thrombospondin-1 modulates synapse and spine defects in the fragile X mouse model. *Mol. Brain* 9:74. doi: 10.1186/s13041-016-0256-9

Contractor, A., Klyachko, V. A., and Portera-Cailliau, C. (2015). Altered Neuronal and Circuit Excitability in Fragile X Syndrome. *Neuron* 87, 699–715. doi: 10.1016/j.neuron.2015.06.017

Di Marco, B., Bonaccorso, C. M., Aloisi, E., D'Antoni, S., and Catania, M. V. (2016). Neuro-inflammatory mechanisms in developmental disorders associated with intellectual disability and autism spectrum disorder: a neuro- immune perspective. *CNS Neurol. Disord. Drug Targets* 15, 448–463. doi: 10.2174/1871527315666160321105039

Du, X., Hao, H., Yang, Y., Huang, S., Wang, C., Gigout, S., et al. (2017). Local GABAergic signaling within sensory ganglia controls peripheral nociceptive transmission. *J. Clin. Invest.* 127, 1741–1756. doi: 10.1172/JCI86812

Du, X., Wang, C., and Zhang, H. (2011). Activation of ATP-sensitive potassium channels antagonize nociceptive behavior and hyperexcitability of DRG neurons from rats. *Mol. Pain* 7:35. doi: 10.1186/1744-8069-7-35

Edens, B. M., Vissers, C., Su, J., Arumugam, S., Xu, Z., Shi, H., et al. (2019). FMRP modulates neural differentiation through m(6)A-Dependent mRNA nuclear export. *Cell Rep.* 28, 845–854.e5. doi: 10.1016/j.celrep.2019.06.072

Feng, L., Hatten, M. E., and Heintz, N. (1994). Brain lipid-binding protein (BLBP): a novel signaling system in the developing mammalian CNS. *Neuron* 12, 895–908. doi: 10.1016/0896-6273(94)90341-7

Hanani, M., and Spray, D. C. (2020). Emerging importance of satellite glia in nervous system function and dysfunction. *Nat. Rev. Neurosci.* 21, 485–498.

Hanani, M., and Verkhratsky, A. (2021). Satellite glial cells and astrocytes, a comparative review. *Neurochem. Res.* 46, 2525–2537. doi: 10.1007/s11064-021-03255-8

Higashimori, H., Schin, C. S., Chiang, M. S., Morel, L., Shoneye, T. A., Nelson, D. L., et al. (2016). Selective deletion of Astroglial FMRP Dysregulates glutamate transporter GLT1 and contributes to Fragile X syndrome phenotypes *in vivo*. *J. Neurosci.* 36, 7079–7094. doi: 10.1523/JNEUROSCI.1069-16.2016

Hosli, E., and Hosli, L. (1978). Autoradiographic localization of the uptake of [(3)H]- GABA and [(3)H]L-glutamic acid in neurones and glial cells of cultured dorsal root ganglia. *Neurosci. Lett.* 7, 173–176. doi: 10.1016/0304-3940(78)90163-5

Jacobs, S., Cheng, C., and Doering, L. C. (2012). Probing astrocyte function in fragile X syndrome. *Results Probl. Cell Differ.* 54, 15–31. doi: 10.1007/978-3-642-21649-7_2

Jacobs, S., Cheng, C., and Doering, L. C. (2016). Hippocampal neuronal subtypes develop abnormal dendritic arbors in the presence of Fragile X astrocytes. *Neuroscience* 324, 202–217. doi: 10.1016/j.neuroscience.2016.03.011

Jacobs, S., and Doering, L. C. (2010). Astrocytes prevent abnormal neuronal development in the fragile x mouse. *J. Neurosci.* 30, 4508–4514. doi: 10.1523/JNEUROSCI.5027-09.2010

Jacobs, S., Nathwani, M., and Doering, L. C. (2010). Fragile X astrocytes induce developmental delays in dendrite maturation and synaptic protein expression. *BMC Neurosci.* 11:132. doi: 10.1186/1471-2202-11-132

Kang, Y., Zhou, Y., Li, Y., Han, Y., Xu, J., Niu, W., et al. (2021). A human forebrain organoid model of fragile X syndrome exhibits altered neurogenesis and highlights new treatment strategies. *Nat. Neurosci.* 24, 1377–1391. doi: 10.1038/s41593-021-00913-6

Kim, Y. S., Choi, J., and Yoon, B. E. (2020). Neuron-glia interactions in neurodevelopmental disorders. *Cells* 9:2176. doi: 10.3390/cells9102176

Krasovska, V., and Doering, L. C. (2018). Regulation of IL-6 Secretion by Astrocytes via TLR4 in the Fragile X Mouse Model. *Front. Mol. Neurosci.* 11:272. doi: 10.3389/fnmol.2018.00272

Kung, L. H., Gong, K., Adedoyin, M., Ng, J., Bhargava, A., Ohara, P. T., et al. (2013). Evidence for glutamate as a neuroglial transmitter within sensory ganglia. *PLoS One* 8:e68312. doi: 10.1371/journal.pone.0068312

Labrakakis, C., Tong, C. K., Weissman, T., Torsney, C., and MacDermott, A. B. (2003). Localization and function of ATP and GABAA receptors expressed by nociceptors and other postnatal sensory neurons in rat. *J. Physiol.* 549, 131–142. doi: 10.1113/jphysiol.2002.031963

Matsumata, M., Sakayori, N., Maekawa, M., Owada, Y., Yoshikawa, T., and Osumi, N. (2012). The effects of Fabp7 and Fabp5 on postnatal hippocampal neurogenesis in the mouse. *Stem Cells* 30, 1532–1543. doi: 10.1002/stem.1124

Minchin, M. C. (1975). Factors influencing the efflux of [3H]gamma-aminobutyric acid from satellite glial cells in rat sensory ganglia. *J. Neurochem.* 24, 571–577. doi: 10.1111/j.1471-4159.1975.tb07676.x

Minchin, M. C., and Iversen, L. L. (1974). Release of (3H)gamma-aminobutyric acid from glial cells in rat dorsal root ganglia. *J. Neurochem.* 23, 533–540. doi: 10.1111/j.1471-4159.1974.tb06056.x

Orefice, L. L., Mosko, J. R., Morency, D. T., Wells, M. F., Tasnim, A., Mozeika, S. M., et al. (2019). Targeting peripheral somatosensory neurons to improve tactile-related phenotypes in ASD Models. *Cell* 178, 867–886.e24. doi: 10.1016/j.cell.2019.07.024

Orefice, L. L., Zimmerman, A. L., Chirila, A. M., Sleboda, S. J., Head, J. P., and Ginty, D. D. (2016). Peripheral mechanosensory neuron dysfunction underlies tactile and behavioral deficits in mouse models of ASDs. *Cell* 166, 299–313. doi: 10.1016/j.cell.2016.05.033

Pacey, L. K., and Doering, L. C. (2007). Developmental expression of FMRP in the astrocyte lineage: implications for fragile X syndrome. *Glia* 55, 1601–1609. doi: 10.1002/glia.20573

Pacey, L. K., Guan, S., Tharmalingam, S., Thomsen, C., and Hampson, D. R. (2015). Persistent astrocyte activation in the fragile X mouse cerebellum. *Brain Behav.* 5:e00400. doi: 10.1002/brb3.400

Pannese, E. (1964). Number and structure of perisomatic satellite cells of spinal ganglia under normal conditions or during axon regeneration and neuronal hypertrophy. *Z. Zellforsch. Mikrosk. Anat.* 63, 568–592. doi: 10.1007/BF00339491

Rais, M., Binder, D. K., Razak, K. A., and Ethell, I. M. (2018). Sensory processing phenotypes in Fragile X Syndrome. *ASN Neuro* 10:1759091418801092. doi: 10.1177/1759091418801092

Saffary, R., and Xie, Z. (2011). FMRP regulates the transition from radial glial cells to intermediate progenitor cells during neocortical development. *J. Neurosci.* 31, 1427–1439. doi: 10.1523/JNEUROSCI.4854-10.2011

Schafers, M., and Sorkin, L. (2008). Effect of cytokines on neuronal excitability. *Neurosci. Lett.* 437, 188–193. doi: 10.1016/j.neulet.2008.03.052

Selvaraju, R. R., Cogswell, M., Das, A., Vedantam, R., Parikh, D., and Batra, D. (2020). Grad-CAM: visual explanations from deep networks via gradient-based localization. *Int. J. Comput. Vis.* 128, 336–359.

Sharma, N., Flaherty, K., Lezgiyeva, K., Wagner, D. E., Klein, A. M., and Ginty, D. D. (2020). The emergence of transcriptional identity in somatosensory neurons. *Nature* 577, 392–398. doi: 10.1038/s41586-019-1900-1

Shoji, Y., Yamaguchi-Yamada, M., and Yamamoto, Y. (2010). Glutamate- and GABA-mediated neuron-satellite cell interaction in nodose ganglia as revealed by intracellular calcium imaging. *Histochem. Cell Biol.* 134, 13–22. doi: 10.1007/s00418-010-0711-0

Sourial, M., and Doering, L. C. (2016). Astrocyte-secreted factors selectively alter neural stem and progenitor cell proliferation in the Fragile X Mouse. *Front. Cell. Neurosci.* 10:126. doi: 10.3389/fncel.2016.00126

Sunamura, N., Iwashita, S., Enomoto, K., Kadoshima, T., and Isono, F. (2018). Loss of the fragile X mental retardation protein causes aberrant differentiation in human neural progenitor cells. *Sci. Rep.* 8:11585. doi: 10.1038/s41598-018-30025-4

Tervonen, T. A., Louhivuori, V., Sun, X., Hokkanen, M. E., Kratochwil, C. F., Zebryk, P., et al. (2009). Aberrant differentiation of glutamatergic cells in neocortex of mouse model for fragile X syndrome. *Neurobiol. Dis.* 33, 250–259. doi: 10.1016/j.nbd.2008.10.010

Van Dijck, A., Barbosa, S., Bermudez-Martin, P., Khalfallah, O., Gilet, C., Martinuzzi, E., et al. (2020). Reduced serum levels of pro-inflammatory chemokines in fragile X syndrome. *BMC Neurol.* 20:138. doi: 10.1186/s12883-020-01715-2

Vargas-Parada, A., Loeza-Alcocer, E., Gonzalez-Ramirez, R., Rodriguez-Sanchez, M., Raya-Tafolla, G., Floran, B., et al. (2021). γ-Aminobutyric acid (GABA) from satellite glial cells tonically depresses the excitability of primary afferent fibers. *Neurosci. Res.* 170, 50–58. doi: 10.1016/j.neures.2020.08.007

Viviani, B., Gardoni, F., and Marinovich, M. (2007). Cytokines and neuronal ion channels in health and disease. *Int. Rev. Neurobiol.* 82, 247–263. doi: 10.1016/S0074-7742(07)82013-7

Wallingford, J., Scott, A. L., Rodrigues, K., and Doering, L. C. (2017). Altered developmental expression of the astrocyte-secreted factors Hevin and SPARC in the Fragile X Mouse Model. *Front. Mol. Neurosci.* 10:268. doi: 10.3389/fnmol.2017.00268

Wang, L., Wang, Y., Zhou, S., Yang, L., Shi, Q., Li, Y., et al. (2016). Imbalance between Glutamate and GABA in Fmr1 knockout astrocytes influences neuronal development. *Genes* 7:45. doi: 10.3390/genes7080045

Yang, Q., Feng, B., Zhang, K., Guo, Y. Y., Liu, S. B., Wu, Y. M., et al. (2012). Excessive astrocyte-derived neurotrophin-3 contributes to the abnormal neuronal dendritic development in a mouse model of fragile X syndrome. *PLoS Genet.* 8:e1003172. doi: 10.1371/journal.pgen.1003172

Yousuf, A., Klinger, F., Schicker, K., and Boehm, S. (2011). Nucleotides control the excitability of sensory neurons via two P2Y receptors and a bifurcated signaling cascade. *Pain* 152, 1899–1908. doi: 10.1016/j.pain.2011.04.016

Yu, K. H., Palmer, N., Fox, K., Prock, L., Mandl, K. D., Kohane, I. S., et al. (2020). The phenotypical implications of immune dysregulation in fragile X syndrome. *Eur. J. Neurol.* 27, 590–593. doi: 10.1111/ene.14146

Conflict of Interest: The authors declare that the research was conducted in the absence of any commercial or financial relationships that could be construed as a potential conflict of interest.

Publisher's Note: All claims expressed in this article are solely those of the authors and do not necessarily represent those of their affiliated organizations, or those of the publisher, the editors and the reviewers. Any product that may be evaluated in this article, or claim that may be made by its manufacturer, is not guaranteed or endorsed by the publisher.

frontiers in Molecular Neuroscience

REVIEW
published: 06 January 2022
doi: 10.3389/fnmol.2021.805929

Hyperexcitability and Homeostasis in Fragile X Syndrome

Xiaopeng Liu[1,2], *Vipendra Kumar*[1], *Nien-Pei Tsai*[1] *and Benjamin D. Auerbach*[1,2]*

[1]Deparment of Molecular & Integrative Physiology, University of Illinois at Urbana-Champaign, Urbana, IL, United States,
[2]Beckman Institute for Advanced Science & Technology, University of Illinois at Urbana-Champaign, Urbana, IL, United States

Fragile X Syndrome (FXS) is a leading inherited cause of autism and intellectual disability, resulting from a mutation in the *FMR1* gene and subsequent loss of its protein product FMRP. Despite this simple genetic origin, FXS is a phenotypically complex disorder with a range of physical and neurocognitive disruptions. While numerous molecular and cellular pathways are affected by FMRP loss, there is growing evidence that circuit hyperexcitability may be a common convergence point that can account for many of the wide-ranging phenotypes seen in FXS. The mechanisms for hyperexcitability in FXS include alterations to excitatory synaptic function and connectivity, reduced inhibitory neuron activity, as well as changes to ion channel expression and conductance. However, understanding the impact of *FMR1* mutation on circuit function is complicated by the inherent plasticity in neural circuits, which display an array of homeostatic mechanisms to maintain activity near set levels. FMRP is also an important regulator of activity-dependent plasticity in the brain, meaning that dysregulated plasticity can be both a cause and consequence of hyperexcitable networks in FXS. This makes it difficult to separate the direct effects of *FMR1* mutation from the myriad and pleiotropic compensatory changes associated with it, both of which are likely to contribute to FXS pathophysiology. Here we will: (1) review evidence for hyperexcitability and homeostatic plasticity phenotypes in FXS models, focusing on similarities/differences across brain regions, cell-types, and developmental time points; (2) examine how excitability and plasticity disruptions interact with each other to ultimately contribute to circuit dysfunction in FXS; and (3) discuss how these synaptic and circuit deficits contribute to disease-relevant behavioral phenotypes like epilepsy and sensory hypersensitivity. Through this discussion of where the current field stands, we aim to introduce perspectives moving forward in FXS research.

Keywords: fragile X syndrome, circuit hyperexcitability, homeostatic plasticity, E/I balance, sensory hypersensitivity, epilepsy

OPEN ACCESS

Edited by:
Michael Telias, University of Rochester, United States

Reviewed by:
Caleb Doll, University of Colorado Hospital, United States
Christina Gross, Cincinnati Children's Hospital Medical Center, United States
Maria Vincenza Catania, Italian National Research Council, Italy

***Correspondence:**
Benjamin D. Auerbach
bda5@illinois.edu

Specialty section:
This article was submitted to Brain Disease Mechanisms, a section of the journal Frontiers in Molecular Neuroscience

Received: *31 October 2021*
Accepted: *14 December 2021*
Published: *06 January 2022*

Citation:
Liu X, Kumar V, Tsai N-P and Auerbach BD (2022) Hyperexcitability and Homeostasis in Fragile X Syndrome. Front. Mol. Neurosci. 14:805929. doi: 10.3389/fnmol.2021.805929

INTRODUCTION

Fragile X syndrome (FXS) is the most common inherited form of intellectual disability (ID) and one of the leading known genetic causes of autism spectrum disorders (ASD; Hagerman et al., 2017). FXS is most commonly caused by the expansion and hyper-methylation of CGG-repeats around

the *FMR1* gene, leading to its transcriptional silencing and the subsequent loss of its protein product, Fragile x mental retardation protein (FMRP; Bhakar et al., 2012). In rare cases, FXS can also arise from point mutations or deletions in the *FMR1* gene (Hammond et al., 1997; Myrick et al., 2014, 2015; Suhl and Warren, 2015). FMRP is a well-conserved neuronal RNA-binding protein involved in the transport and translational regulation of a large number of mRNA in the brain (Ashley et al., 1993; Siomi et al., 1993; Stefani et al., 2004; Santoro et al., 2012). The known genetics of FXS and the evolutionarily conserved nature of FMRP have allowed for the development of well-validated animals models of the disorder (Bhogal and Jongens, 2010; Schroeder et al., 2017). FXS has thus emerged as a prototype for a molecular medicine approach to neuropsychiatric disorders, i.e., treating diseases with complex pathophysiology by targeting underlying molecular and cellular alterations identified in pre-clinical models (Krueger and Bear, 2011). However, recent clinical trial failures in FXS have also underscored the potential pitfalls of attempting to translate therapies developed from molecular pathology identified in animal models into suitable clinical treatments (Berry-Kravis et al., 2018). These setbacks highlight the need for further understanding of how cellular and molecular perturbations caused by loss of FMRP contribute to neural circuit dysfunction in FXS, as these circuit abnormalities are most relevant to understanding how the behavioral phenotypes associated with FXS arise. Elucidating the consequences of *FMR1* mutation at the circuit and behavioral level is complicated by the wide-ranging, multifunctional role of FMRP as well as the vast compensatory mechanisms utilized by the brain to maintain neuronal function within an optimal range.

FMRP is highly enriched in neurons and expressed across various cell compartments, cell-types, and brain regions (Abitbol et al., 1993; Devys et al., 1993; Verheij et al., 1995; Feng et al., 1997; Christie et al., 2009; Olmos-Serrano et al., 2010). FMRP expression is also developmentally regulated in both humans (Abitbol et al., 1993) and mice (Saffary and Xie, 2011), with expression starting at early embryonic stages, peaking during early post-natal developmental critical periods, but remaining at sustained levels throughout adulthood (Till, 2010; Bonaccorso et al., 2015; Gholizadeh et al., 2015). Most evidence indicates that FMRP is a translation repressor, with the ability to inhibit both translation initiation (Napoli et al., 2008) and elongation (Ceman et al., 2003). Indeed, a majority of FMRP is associated with stalled polyribosomes (Feng et al., 1997; Stefani et al., 2004; Darnell et al., 2011) and loss of FMRP often results in increased cerebral protein synthesis rate (Osterweil et al., 2010; Qin et al., 2013; Jacquemont et al., 2018). Several high-throughput approaches have indicated that FMRP associates with thousands of mRNA targets (approximately 4–8% of all brain mRNA) with wide-ranging effects on neuronal function (Brown et al., 2001; Darnell et al., 2011; Ascano et al., 2012). Targets include a large fraction of the synaptic proteome in both pre- and post-synaptic compartments, ion channels important for regulation of cellular excitability, as well as transcription factors and chromatin-modifying proteins that can broadly affect the genetic and proteomic content of cells. FMRP can also influence cell excitability through direct protein–protein interactions with voltage- and ligand-gated ion channels (Deng and Klyachko, 2021).

Because of its ubiquitous expression and ability to regulate a large portion of the neuronal proteome, it is perhaps not surprising that loss of FMRP has far-reaching consequences on neuronal function. However, accumulating evidence suggests that neuronal hyperexcitability and network hyperactivity are important points of convergence for FXS pathophysiology (Contractor et al., 2015). In many instances, neuronal hyperexcitability is likely the direct result of loss of FMRP and its canonical role in regulating mRNA translation or ion channel function. However, a number of studies have also indicated that hyperexcitability in FXS can occur as a result of aberrant activity-dependent and/or homeostatic plasticity mechanisms, especially in early post-natal weeks when the neuronal circuits undergo immense changes owing to sensory experiences. In yet other cases, synaptic and cellular alterations that appear to promote hyperexcitability in FXS models may actually be compensatory changes that act to stabilize network activity. Loss of FMRP function is therefore likely to have multiple and sometimes even contradictory effects on circuit function, and interpreting these circuit level complexities requires an understanding of both the pleiotropic effects of *FMR1* mutation as well as the adaptive and maladaptive homeostatic responses to these primary changes. This balancing act is not unique to FXS either, as altered network and cellular homeostasis are thought to contribute to the pathogenesis of genetically-diverse forms of ASD (Bourgeron, 2015; Nelson and Valakh, 2015) as well as other neurodevelopmental and neurocognitive disorders (Frere and Slutsky, 2018; Kavalali and Monteggia, 2020). Thus, the goal of this review is to use FXS as a model for understanding the dynamic and varied processes that contribute to emergent circuit dysfunction in neuropsychiatric disorders. Below we will examine the evidence for altered excitability and plasticity in FXS models, primarily focusing on the *Fmr1* KO mouse. We will pay particular attention to the complex interplay between excitability and plasticity phenotypes, and discuss how these synaptic and circuit deficits contribute to disease-relevant behavioral phenotypes like epilepsy and sensory hypersensitivity.

HYPEREXCITABLE NEURONS AND NETWORKS IN FRAGILE X SYNDROME

Many FXS phenotypes can be understood through the lens of neuronal hyperexcitability, with the prevalence of sensory hypersensitivity, hyperactive/aggressive behavior, epileptic seizures, and abnormal EEGs in FXS individuals and *FMR1* KO animal models confirming neuronal network hyperexcitability as a characteristic defect owing to FMRP deficiency (Musumeci et al., 2000; Berry-Kravis, 2002; Lozano et al., 2014). While hyperexcitability is observed across many cortical and subcortical brain regions, the exact mechanisms generating this phenotype appear to vary by brain region and this may have important implications for the treatment of the disorder. A wide range of studies have pointed out that the loss of FMRP disrupts innumerable signaling pathways essential for the maintenance of normal synaptic function and neuronal network stability

(Bhakar et al., 2012). Hyperexcitability in FXS can be explained as a function of a number of changes, including: (1) abnormal activity-dependent refinement of synaptic connectivity leading to elevated numbers of excitatory synapses in certain neuronal populations; (2) impaired inhibitory neuron function and/or synaptic properties leading to an altered balance between excitatory and inhibitory strength (E/I imbalance); and (3) disruption in ion channel function or expression, leading to increased intrinsic excitability and altered dendritic integration. Indeed, there is evidence for changes in all of these processes in the *FMR1* deficient brain (**Figure 1**) and that they interact with one another in a complex fashion.

Altered Excitatory Synaptic Function and Plasticity in FXS

One of the earliest synaptic phenotypes identified in FXS was the presence of abnormal dendritic spines, where the majority of excitatory synapses are formed in the brain. Golgi stain studies have found an overabundance of immature spines in both *FMR1* KO mice (Comery et al., 1997; Galvez and Greenough, 2005; Mckinney et al., 2005) and FXS human tissue (Hinton et al., 1991; Wisniewski et al., 1991; Irwin et al., 2001). Subsequent live-imaging experiments using two-photon microscopy have found spine density and/or shape phenotypes to be more variably expressed in FXS models, being sensitive to brain region, developmental age, and genetic background (Nimchinsky et al., 2001; Meredith et al., 2007; Cruz-Martín et al., 2010; Harlow et al., 2010; Pan et al., 2010; He and Portera-Cailliau, 2013). However, these live-imaging studies also highlighted the fact that, regardless of overall number or shape differences, dendritic spines in *FMR1* KO animals exhibit atypical dynamics and were much less sensitive to changes in activity levels or sensory experience (Wisniewski et al., 1991; Antar et al., 2006; Goel et al., 2006; Pan et al., 2010). Thus, loss of FMRP leads to impaired activity-dependent changes to spine structure and number, resulting in abnormal synaptic maturation, stabilization, and/or elimination (Comery et al., 1997; Cruz-Martín et al., 2010; Pfeiffer et al., 2010).

Consistent with anatomical studies of spine dynamics, electrophysiological experiments have found differences in excitatory synaptic function in *FMR1* KO models, once again with an emphasis on disrupted activity-dependent modifications (Sidorov et al., 2013). Early studies found no alteration to basal synaptic transmission or long-term potentiation (LTP) in the hippocampus of *FMR1* KO mice (Godfraind et al., 1996; Paradee et al., 1999), although subsequent studies have found subtle LTP deficits in the hippocampus (Lauterborn et al., 2007; Hu et al., 2008) and other brain regions (Meredith et al., 2007; Koga et al., 2015). The most prominent synaptic plasticity phenotype observed in *FMR1* KO models is excessive group 1 metabotropic glutamate receptor (mGluR1/5)-dependent long-term depression (LTD) at excitatory synapses (Huber et al., 2002; Koekkoek et al., 2005; Hou et al., 2006; Till et al., 2015). Expression of mGluR-LTD in the mature brain is mediated *via* post-synaptic internalization of AMPA receptors (Snyder et al., 2001; Gladding et al., 2009), which is stabilized by rapid *de novo* synthesis of proteins from pre-existing, dendritically-localized mRNA (Huber et al., 2000). Interestingly, FMRP itself is one of the proteins synthesized by mGluR 1/5 activation (Weiler et al., 1997; Antar et al., 2004; Hou et al., 2006). These findings, coupled with FMRP's role in repressing activity-dependent protein synthesis, have led to the idea that FMRP acts as a negative feedback regulator to limit mGluR-mediated protein synthesis (Bear et al., 2004). Consistent with this notion, basal protein synthesis rates are elevated in the hippocampus of *FMR1* KO mice and mGluR5-mediated increases in protein synthesis are occluded in slices from *FMR1* animals (Todd et al., 2003; Osterweil et al., 2010). Similarly, mGluR-LTD is not only exaggerated in *FMR1* KO animals but it no longer requires new protein translation (Hou et al., 2006; Nosyreva and Huber, 2006). Importantly, post-natal re-expression of FMRP in *FMR1* KO slices can restore normal levels of mGluR-LTD (Zeier et al., 2009). It is unclear how exaggerated mGluR-LTD contributes to neuronal hyperexcitability in FXS, as enhanced synaptic depression at excitatory synapses would likely act to decrease excitatory drive onto neurons. However, it may be more informative to view mGluR-LTD as a sensitive functional read-out of mGluR-stimulated protein synthesis in dendrites, which has a number of consequences in addition to LTD that could directly contribute to neuronal hyperexcitability, such as facilitating the persistence of LTP (LTP priming; Raymond et al., 2000) and inducing prolonged epileptiform discharges (Bianchi et al., 2009). Indeed, mGluR-mediated priming of LTP (Auerbach and Bear, 2010) and mGluR-induced epileptiform activity (Chuang et al., 2005; Zhao et al., 2011) are enhanced and/or uncoupled from activity-dependent protein synthesis in the hippocampus of *FMR1* KO mice, both of which would act to increase circuit excitability.

Disrupted Critical Period Plasticity and Synaptic Refinement

Activity-dependent synaptic modification is a crucial step in normal development (Faust et al., 2021). As FMRP is highly expressed during early life critical periods (Till, 2010; Bonaccorso et al., 2015; Gholizadeh et al., 2015), loss of FMRP may lead to altered excitatory synaptic development, which in turn could contribute to hyperexcitability phenotypes in FX. There is indeed evidence for deficient or disrupted critical period plasticity in *FMR1* KO mice. Whole cell recordings from layer 4 stellate cells in barrel cortex slices from juvenile *FMR1* KO mice have found increased persistence of silent synapses, those containing NMDAR but not AMPAR currents, at later developmental time points compared to wild-type (WT) animals, which corresponded with a shift in the temporal window for LTP induction at these synapses (Harlow et al., 2010). Intracortical connections in the barrel cortex of *FMR1* KO mice were also shown to exhibit abnormal development in a temporally restricted manner (Bureau et al., 2008). In the auditory system, passive exposure to tones during the auditory critical period results in shifts to the tonotopic map of sound frequency representation in the auditory cortex (Zhang L. I. et al., 2001). This critical period auditory plasticity was absent in *FMR1* KO mice (Kim et al., 2013), potential due to impaired stabilization of LTP at auditory thalamocortical synapses at this development

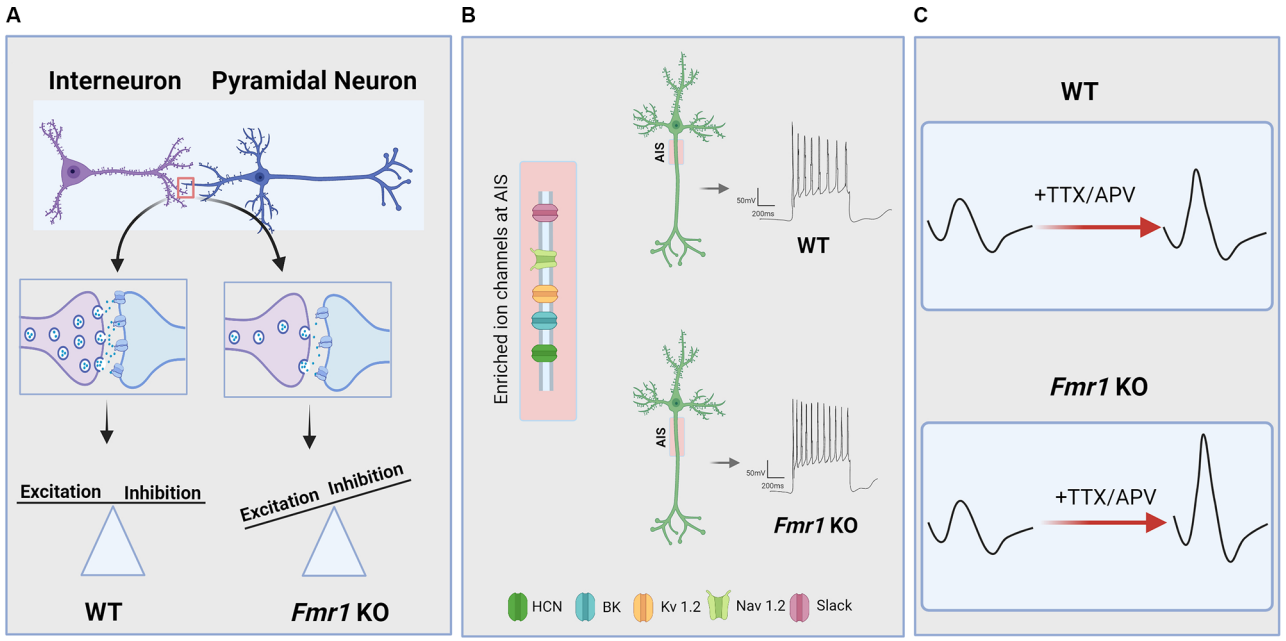

FIGURE 1 | Neuronal and circuit hyperexcitability in Fragile X Syndrome (FXS). Hyperexcitability owing to loss of function of the *FMR1* gene and its protein product FMRP manifests across levels of the CNS *via* a variety of mechanisms. **(A)** Several lines of evidence indicate that disrupted excitatory/inhibitory synaptic balance due to altered activity-dependent refinement of synaptic connectivity and impaired synaptic transmission and plasticity contribute to circuit hyperexcitability in FXS. In particular, there is evidence for a reduction in inhibitory synaptic transmission in several brain regions of *FMR1* KO animals which, in addition to excessive excitatory connectivity in some cases, can result in increased E/I ratio and circuit hyperexcitability. **(B)** FMRP deficiency is also associated with dysregulated ion channel function and expression, resulting in changes to intrinsic excitability, action potential (AP) slope and duration, and increased the axon initial segment (AIS) length in some brain areas. AIS is enriched in many of the ion channels that are directly or indirectly regulated by FMRP. **(C)** Hyperexcitability in FXS can also arise from impaired homeostatic plasticity, which is an essential mechanism for maintaining basal network activity and preventing circuit hypo- or hyperexcitability. For instance, *FMR1* KO neurons exhibit dysregulated homeostatic changes to intrinsic excitability in response to activity blockade, resulting in increased AP slope and cellular hyperexcitability compared to WT neurons.

time-point (Yang et al., 2014). It is also important to note that FMRP's role in circuit development is not restricted to the cortex, as post-synaptic reduction of FMRP in chick auditory brainstem *via in utero* electroporation leads to a delay in dendrite branch retraction and the prevention of presynaptic endbulb development (Wang et al., 2018). These studies indicate that FMRP is important for defining the critical window for neuronal circuit refinement during development.

How might dysregulated critical period plasticity result in hyperexcitable circuits? A central mechanism for developmental refinement of neural circuits is synaptic pruning, i.e., the activity-dependent elimination of synapses (Sakai, 2020; Faust et al., 2021). Several studies have indicated that synapse elimination is disrupted in *FMR1* KO animals. In drosophila, loss of FMRP has been shown to alter dendritic complexity and synapse growth at glutamatergic neuromuscular junctions (Zhang Y. Q. et al., 2001) and in the central nervous system (Pan et al., 2004; Kennedy et al., 2020). Dual patch experiments have found evidence for overconnectivity of excitatory neurons in acute slices from the somatosensory cortex of *FMR1* KO mice (Patel et al., 2014). Interestingly, this hyperconnectivity phenotype was not due to increased development of synaptic connections in *FMR1* KO mice but rather to a failure in activity-dependent synaptic elimination between 3 and 5 weeks postnatal. Similar synaptic pruning deficits have been observed in hippocampal slice cultures, where it was shown that synapse elimination *via* the activity-dependent transcription factor MEF2 is absent in slices from *FMR1* KO mice (Pfeiffer et al., 2010). Importantly, acute post-synaptic re-expression of FMRP was able to restore MEF2-dependent synapse elimination in KO slices, suggesting FMRP regulates excitatory synapse elimination in a cell-autonomous manner. FMRP was subsequently shown to regulate MEF2-dependent synapse elimination *via* PP2A-mediated dephosphorylation of the ubiquitin E3 ligase murine double minute-2 (Mdm2), which promotes the degradation of the synaptic scaffolding protein PSD-95 (Tsai et al., 2017). Most recently, post-synaptic loss of FMRP in the somatosensory cortex has been shown to result in impaired activity-dependent development of callosal inputs, resulting in increased local intracortical connectivity but impaired long-range cortical-cortical connections (Zhang et al., 2021).

FMRP is also expressed in pre-synaptic terminals (Christie et al., 2009), and pre-synaptic loss of FMRP may regulate excitatory post-synaptic development as well (Antar et al., 2006). Indeed, studies using mosaic deletion of *Fmr1* in hippocampal slice culture found that pre-synaptic loss of FMRP was sufficient to increase synaptic connectivity while postsynaptic

deletion did not alter connection probability (Hanson and Madison, 2007). While the mechanisms governing abnormal pre-synaptic development with *FMR1* deletion remain to be fully elucidated, there is intriguing evidence that FMRP can regulate pre-synaptic transmitter release via direct modulation of ion channel function independent of its role in translation regulation (see Section "Ion Channel Dysregulation and Altered Intrinsic Excitability in FXS"; Ferron et al., 2014; Myrick et al., 2015). Whether pre- or post-synaptic in nature, deficient synapse elimination has the potential to lead to hyperexcitability in mature circuits. For instance, *in vivo* recordings from the lateral superior olive (LSO), an auditory brainstem area important for sound localization, found evidence for increased sound-evoked activity and hyperexcitability at the population level in *FMR1* KO mice (Garcia-Pino et al., 2017). Parallel whole cell slice recordings found no difference in the properties of individual excitatory or inhibitory synapses in this region, but rather that hyperexcitability was the result of an increased number of excitatory connections converging onto individual LSO neurons. Ultrastructure analysis in the somatosensory cortex shows that loss of FMRP results in a three-fold increase in multiply-innervated spines, leading to increased single-spine excitation that promotes circuit hyperexcitability (Booker et al., 2019). Thus, hyperexcitable circuits in FXS could be due in part to failures of synaptic pruning during development as a consequence of dysregulated experience-dependent plasticity.

Altered Inhibitory Neuron Function in FXS

Efficient information processing in neural circuits requires a tightly regulated balance between excitatory and inhibitory activity (E/I balance; Haider et al., 2006; Shew et al., 2011; Yizhar et al., 2011). As discussed above, loss of FMRP alters the development and function of excitatory synapses in a number of ways that could affect neuronal excitability. FMRP is also broadly expressed in GABAergic neurons (Feng et al., 1997; Olmos-Serrano et al., 2010) and many lines of evidence point to altered inhibitory neuronal function in FXS as well. *FMR1* KO mice have reduced levels of several $GABA_A$ receptor subunits, the major fast-acting inhibitory ionotropic receptor in the brain, at both the mRNA (D'hulst et al., 2006; Gantois et al., 2006) and protein levels (El Idrissi et al., 2005; Gantois et al., 2006; Curia et al., 2009). Pre-synaptically, expression of the rate-limiting GABA synthesizing enzyme glutamic acid decarboxylase (GAD) has been shown to be reduced in *FMR1* KO mice (Olmos-Serrano et al., 2010), although other studies have found increased GAD65/67 expression in some brain regions (El Idrissi et al., 2005). Down-regulation of $GABA_A$ receptors and GAD have also been observed in the drosophila fly model of FXS (Gatto et al., 2014). Anatomical defects in GABAergic and/or glycinergic neurons have been observed in the cortex (Selby et al., 2007) and brainstem (Mccullagh et al., 2017) of *FMR1* KO mice. *In vivo* imaging studies have found impaired sensory-evoked activity in inhibitory neuron populations in the cortex of *FMR1* KO mice as well (Goel et al., 2018). Human PET imaging studies have found evidence for diminished $GABA_A$ receptor binding in the brains of FXS individuals (D'hulst et al., 2015). Electroencephalography (EEG; Ethridge et al., 2017; Wang et al., 2017) and transcranial magnetic stimulation studies (TMS; Morin-Parent et al., 2019) have found indirect evidence for reduced inhibition in humans with FXS in the form of altered neuronal oscillations and reduced short-interval suppression of TMS-evoked potentials, which both depend on local intracortical inhibition (Kujirai et al., 1993; Chen et al., 2008; Cardin et al., 2009; Sohal et al., 2009). Thus, there is general agreement that *FMR1* mutation results in a broad dampening of GABAergic inhibition in the brain which could lead to hyperexcitable networks (**Figure 1A**). However, it is also clear that the concept of a single E/I balance is overly simplistic, as there are different sources of inhibition within a single microcircuit that target distinct cellular compartments and affect different aspects of neuronal function (O'donnell et al., 2017). It is also likely that disruptions to excitatory synaptic function in FXS can evoke changes to inhibitory transmission and *vice versa*. Thus, it is important to understand the precise manner in which inhibitory synaptic and circuit function are altered in FXS in order to fully understand the consequences of these changes on network excitability and information processing.

Deficient GABAergic Transmission in FMR1 KO Models

Electrophysiological studies have found evidence for reduced GABAergic inhibition onto excitatory principal cells in *FMR1* KO animals in a variety of brain areas, albeit with region-specific differences. Consistent with evidence for changes to the pre- and post-synaptic machinery for GABAergic signaling in FXS, both the frequency and amplitude of spontaneous and miniature inhibitory post-synaptic potentials (sIPSCs, mIPSCs) are reduced in the amygdala of adult (Olmos-Serrano et al., 2010) and juvenile (Vislay et al., 2013) *FMR1* KO mice. Conversely, GABAergic inhibition was found to be enhanced in the striatum of adult *FMR1* mice *via* increased pre-synaptic transmitter release (Centonze et al., 2008). Basal GABAergic transmission was not altered in layer 2/3 pyramidal neurons in the somatosensory cortex of *FMR1* KO mice, but mGluR-mediated activation of low-threshold spiking (LTS) interneurons was deficient, resulting in reduced activity-dependent inhibition (Paluszkiewicz et al., 2011). mGluR-dependent decreases in inhibitory function *via* retrograde endocannabinoid signaling have also been observed in the hippocampus (Zhang and Alger, 2010), striatum (Maccarrone et al., 2010), and cortex (Rio et al., 2018) of *FMR1* KO mice, once again highlighting the role of FMRP in mGluR-dependent plasticity. Action potential evoked feed-forward inhibitory input to the CA1 region of the hippocampus is reduced in *FMR1* KO mice in an input-specific manner (Wahlstrom-Helgren and Klyachko, 2015, 2016). Decreased feed-forward inhibition onto excitatory neurons has also been observed in the lateral amygdala (Svalina et al., 2021) and the somatosensory cortex (Antoine et al., 2019; Domanski et al., 2019) of *FMR1* KO mice. Loss of feedforward inhibition is associated with marked changes in E/I balance, increased spike probability, and reduced spike precision, all of which are likely to contribute to circuit hyperexcitability and impaired information processing in these areas. However, it should also be noted that, in some cases, decreased inhibitory synaptic transmission and enhanced E/I

ratio in *FMR1* KO mice may actually act to stabilize circuit excitability. For instance, Antoine and colleagues found that *FMR1* KO mice exhibited reduced feedforward inhibition onto layer 2/3 pyramidal neurons in the somatosensory cortex but that this reduction in inhibitory conductance was not associated with increased whisker-evoked spiking activity in these neurons (Antoine et al., 2019). Instead, modeling experiments suggested that rather than promoting network hyperexcitability, altered E/I balance in layer 2/3 neurons may actually reflect a homeostatic process to maintain stable synaptic drive.

$GABA_A$ receptors not only mediate fast-acting, synapse-specific phasic inhibition but in some brain areas can also mediate slower, sustained tonic inhibition involving extrasynaptic $GABA_A$ receptors (Farrant and Nusser, 2005). Both phasic and tonic inhibition were shown to be deficient in the amygdala of *FMR1* KO animals (Olmos-Serrano et al., 2010; Martin et al., 2014), while tonic but not phasic inhibition was disrupted in the subiculum (Curia et al., 2009). Increased tonic inhibition did not alter overall synaptic conductance or E/I balance in *FMR1* KO animals, but it impaired the timing between feedforward excitation and inhibition, and this disruption in the temporal precision of stimulus-evoked E/I balance may contribute to hyperexcitability (Martin et al., 2014). Acute treatment of *FMR1* KO mice with gaboxadol, a $GABA_A$ receptor agonist selective for extrasynaptic receptors mediating tonic currents, rescues hyperexcitability of amygdala principal neurons and rescued certain behavioral phenotypes in *FMR1* KO mice, suggesting reduced tonic GABAergic inhibition in the amygdala contributes to hyperexcitability phenotypes in FXS (Olmos-Serrano et al., 2010, 2011). In fact, recently completed phase 2 clinical trials investigating the use of gaboxadol to treat FXS have shown promising results (Budimirovic et al., 2021). Thus, circuit hyperexcitability in many brain regions of *FMR1* KO animals is likely due in part to decreased basal GABAergic transmission and/or altered activity-dependent changes to inhibitory drive onto excitatory neurons.

$GABA_B$ receptors are metabotropic receptors that can regulate cellular excitability both pre- and post-synaptically by hyperpolarizing neurons and limiting neurotransmitter release *via* activation of inwardly-rectifying K^+ channels and inhibition of voltage-gated Ca^{2+} channels (Pinard et al., 2010). Due to their broad regulation of pre- and post-synaptic excitability, and specifically, their potential to reduce glutamate release and subsequent downstream activation of mGluR5, $GABA_B$ agonists like arbaclofen have been explored as a potential FXS therapy (Berry-Kravis et al., 2012, 2017). Arbaclofen has indeed been shown to normalize protein synthesis rates as well as a variety of physiological and behavioral phenotypes in *FMR1* KO mice (Henderson et al., 2012; Silverman et al., 2015; Sinclair et al., 2017a). However, clinical trials with arbaclofen have proved unsuccessful (Berry-Kravis et al., 2017) and recent animal studies found that chronic baclofen treatment can actually result in exacerbation of FXS phenotypes, potentially due to drug tolerance development (Zeidler et al., 2018). Drug tolerance development may also limit the effectiveness of other potential FXS therapies, like mGluR5 inhibitors (Stoppel et al., 2021). It is also important to note that $GABA_B$ receptors are also expressed at pre-synaptic inhibitory terminals. Indeed, decreased feedforward inhibition in the hippocampus on *FMR1* KO mice was shown to be driven by increased pre-synaptic $GABA_B$ receptor signaling, leading to reduced GABA release (Wahlstrom-Helgren and Klyachko, 2015). Thus, treatments that enhance $GABA_B$ signaling may act to promote FXS hyperexcitability phenotypes in some cases as well.

Finally, in addition to changes in GABAergic synaptic transmission, altered excitatory drive onto inhibitory neurons has been observed in *FMR1* KO animals. Dual patch clamp recordings from directly coupled excitatory and inhibitory neurons in the somatosensory cortex of juvenile *FMR1* KO mice have shown that there is reduced feedforward excitatory input onto layer 4 fast-spiking (FS) inhibitory neurons (Gibson et al., 2008). This decrease in feedforward excitation was also associated with an increase in persistent UP states in both in slice (Gibson et al., 2008) and *in vivo* (Hays et al., 2011), which are brief periods of persistent depolarized firing states in neurons that are indicative of increased network excitability. Transient increases in UP states were also observed in layer 2/3 somatosensory cortical neurons of *FMR1* KO mice during the critical period (Goncalves et al., 2013). Prolonged UP states in *FMR1* KO mice were rescued by genetic reduction or pharmacological inhibition of mGluR5, suggesting this hyperexcitability phenotype may be related to altered glutamatergic signaling (Hays et al., 2011). Interestingly, reduced excitatory input onto FS inhibitory neurons appears to be due to pre-synaptic loss of FMRP, as selective deletion of *Fmr1* in excitatory neurons resulted in prolonged UP states while selective deletion in inhibitory neurons had no effect (Hays et al., 2011). Indeed, mosaic deletion of *Fmr1* demonstrated that pre-synaptic loss of FMRP in the somatosensory cortex resulted in a specific reduction in presynaptic glutamate release onto post-synaptic inhibitory neurons without affecting excitatory-excitatory connections, indicative of target-specific function for presynaptic FMRP (Patel et al., 2013). Coupled with the evidence for deficits in pruning at excitatory-excitatory connections discussed above (Hanson and Madison, 2007; Pfeiffer et al., 2010; Patel et al., 2014), these studies indicate that pre- vs. post-synaptic loss of FMRP may differentially regulate excitatory and inhibitory synaptic connectivity, resulting in an imbalance to E/I connectivity and network hyperexcitability.

Cell-Type-Specific Changes in Inhibitory Neuron Function

Inhibitory interneurons consist of genetically and anatomically diverse cell populations that subserve distinct roles in circuit function. Thus, understanding the consequences of altered inhibitory function in FXS requires understanding the cell-type specific effects of inhibitory neuron sub-populations. The three most common genetically-defined interneuron classes in the cortex are parvalbumin positive (PV), somatostatin positive (SST), and vasoactive intestinal peptide positive (VIP) interneurons (Defelipe et al., 2013). PV neurons largely overlap with FS basket cells that provide strong perisomatic inhibition to regulate excitatory neuron output. Anatomical studies have found a pronounced decrease in PV neuron density in the cortex

of *FMR1* KO animals (Selby et al., 2007), and *in vivo* Ca^{2+} imaging from genetically-identified PV neurons found reduced sensory-evoked activity in PV neuron populations in the visual cortex of *FMR1* KO mice, which corresponded with impaired perceptual learning (Goel et al., 2018).

Fast-spiking PV neurons play an integral role in regulating the synchronization of cortical circuits, particularly in the high frequency gamma range (Cardin et al., 2009; Sohal et al., 2009). Interestingly, EEG studies have observed increased cortical gamma oscillation in FXS individuals (Ethridge et al., 2017; Wang et al., 2017) as well as *FMR1* KO mice (Lovelace et al., 2018) and rats (Kozono et al., 2020). Similar changes in gamma power are observed in acute cortical slices from *FMR1* KO animals as well, suggesting observed EEG abnormalities are driven in part by local alterations in neocortical circuits (Goswami et al., 2019). Interestingly, EEG alterations in *FMR1* KO mice can be rescued by genetic reduction of matrix metallopeptidase 9 (MMP9), an enzyme involved in the degradation of perineuronal nets (PPNs) which preferentially stabilize synaptic connections with PV neurons (Lovelace et al., 2016; Wen et al., 2018) and whose mRNA has been shown to be a target of FMRP (Janusz et al., 2013). As PV neurons strongly overlap with electrophysiologically characterized FS interneurons, reduction in sensory-evoked PV activity and altered EEG oscillations may be due to deficient intracortical excitatory input onto FS interneurons described above (Gibson et al., 2008), potentially as a consequence of altered MMP9 activity (Wen et al., 2018). Consistent with this notion, forebrain deletion of *FMR1* specifically in excitatory neurons recapitulates increased MMP9 activity and a majority of EEG deficits seen in global *FMR1* KO mice (Lovelace et al., 2020). Recent studies have demonstrated that minocycline treatment, an FDA-approved antibiotic that can inhibit MMP9 activity, reverses electrophysiological and/or behavioral disturbances in *FMR1* KO mice (Bilousova et al., 2009; Lovelace et al., 2020), drosophila FXS models (Siller and Broadie, 2011), and FXS individuals (Leigh et al., 2013).

Beyond PV neurons, the function of other inhibitory interneuron subtypes in FXS has been less well-characterized. Slice recordings from the somatosensory cortex found impaired mGluR-dependent activation of SST-expressing LTS neurons that target distal dendrites to regulate the integration of synaptic input. This reduced activity-dependent inhibition onto excitatory neurons resulted in altered cortical synchronization in the form of elevated low-frequency theta oscillations (Paluszkiewicz et al., 2011). Thus, loss of FMRP can have distinct effects on network function *via* differential regulation of distinct inhibitory interneurons subtypes. VIP interneurons are less numerous than PV and SST neurons but can have a broad impact on cortical circuit function *via* targeting of other interneuron subtypes, forming a disinhibitory circuit (Pfeffer et al., 2013). To our knowledge, no studies have directly assessed VIP interneuron function in FXS models to date.

Altered GABAergic System Development in FXS

The above studies suggest that abnormal inhibitory neuron function in *FMR1* KO animals results from a combination of decreased inhibitory drive onto excitatory neurons and decreased excitatory drive onto inhibitory neurons. These changes are associated with marked changes in E/I balance and neuronal processing in diverse brain regions. As discussed in section "Altered Excitatory Synaptic Function and Plasticity", FMRP is an important regulator of activity-dependent refinement of excitatory synaptic function. GABAergic transmission also plays a critical role during early brain development, where it acts *via* paracrine, non-synaptic signaling to depolarize neurons due to high intracellular Cl^- concentration at this developmental time point (Represa and Ben-Ari, 2005). Recent studies have demonstrated that *Fmr1* deletion delays the developmental switch in GABA polarity from depolarizing to hyperpolarizing in the cortex (He et al., 2014) and hippocampus (Tyzio et al., 2014) due to the developmentally elongated expression of the juvenile Cl^- transporter NKCC1. No differences in the expression level of the adult Cl^- transported KCC2 were observed at any post-natal timepoint in *FMR1* KO mice (He et al., 2014). This delayed maturation of GABAergic signaling is likely to have a profound impact on synaptic and circuit development, similar to altered critical period plasticity of excitatory synaptic function observed in *FMR1* KO animals. Indeed, it was recently shown that inhibiting NKCC1 with the FDA-approved drug bumetanide during the somatosensory critical period corrects the development of thalamocortical excitatory synapses and altered whisker-evoked receptive fields in adult *FMR1* KO mice (He et al., 2018).

Inhibitory synapse formation is also developmentally regulated, characterized by a rapid increase in synapse number and maturation around the end of the 4th postnatal week (Micheva and Beaulieu, 1996; Oh and Smith, 2019). This maturation of cortical GABAergic neurons, particularly PV interneurons, is thought to contribute to the closure of developmental critical periods (Pizzorusso et al., 2002; Balmer et al., 2009). Intriguingly, this inhibitory maturation and critical period closure also coincide with the formation of PNNs. Indeed, there is evidence that PNN-dependent stabilization of PV neuron function directly contributes to the closure of critical period plasticity windows (Lee et al., 2017; Lensjo et al., 2017; Murase et al., 2017). Thus, it is possible that the abnormal development of PNNs and PV cells observed in the cortex of *FMR1* KO animals (Selby et al., 2007; Wen et al., 2018) may underly delayed or impaired critical period plasticity seen at excitatory synapses in these animals (Harlow et al., 2010; Kim et al., 2013), although this hypothesis remains to be explicitly tested. Taken together, these studies indicate that altered excitatory circuit development in FXS may be due in part to GABAergic defects.

Ion Channel Dysregulation and Altered Intrinsic Excitability in FXS

FMRP acts through a variety of direct and indirect mechanisms to regulate the expression and function of multiple ion channels in the brain, including: voltage-gated Na^+, K^+, and Ca^{2+} channels; hyperpolarization-activated cyclic nucleotide-gated (HCN) channels; and small- and big- conductance Ca^{2+}-activated (SK, BK) K^+ channels (Deng and Klyachko, 2021; **Figure 1B**). Several ion channels have been identified as FMRP

targets (Darnell et al., 2011), suggesting that *FMR1* deletion can influence cellular excitability through its canonical role as a translation regulator. These include Kv3.1 (Strumbos et al., 2010), Kv4.2 (Lee et al., 2011), and HCN1 channels (Brager et al., 2012). Interestingly, FMRP can also modulate the function of several ion channels *via* direct protein-protein interactions, including the Na^+-activated K^+ channel Slack (Brown et al., 2010), BK (Deng et al., 2013; Myrick et al., 2015), and SK (Deng et al., 2019) channels. Finally, loss of FMRP can influence cellular excitability indirectly through dysregulation of cell signaling pathways (Chuang et al., 2005; Zhao et al., 2011; Deng and Klyachko, 2016a). Thus, ion channel function is altered through a variety of mechanisms in FXS and this is likely to influence a wide-range of neuronal processes, including intrinsic excitability, neurotransmitter release, and dendritic integration.

Increased Intrinsic Excitability in *Fmr1* KO Models

Several studies have demonstrated increased intrinsic excitability across brain regions in *FMR1* KO animals, although as in the case of synaptic disturbances, the effects vary across brain regions. In addition to reduced feedforward excitation onto FS interneurons, a modest increase in the excitability of layer 4 principal neurons in the somatosensory cortex is observed in *FMR1* KO mice as a result of increased membrane capacitance and input resistance (Gibson et al., 2008; Domanski et al., 2019). Several studies have observed increased stimulus-evoked action potential (AP) generation in layer 5 cortical pyramidal neurons, which appears to depend on altered mGluR activity and downstream signaling components (Hays et al., 2011; Osterweil et al., 2013; McCamphill et al., 2020). However, whole-cell recordings from layer 5 pyramidal cells in entorhinal (Deng et al., 2013) and somatosensory (Zhang et al., 2014) cortex found no difference in intrinsic parameters in these neurons, suggesting this stimulus-evoked hyperexcitability may be synaptically generated. Intrinsic hyperexcitability in the entorhinal (Deng and Klyachko, 2016a) and prefrontal (Routh et al., 2017) cortex of *FMR1* KO mice was shown to depend on increased non-inactivating persistent Na^+ current (I_{NaP}). Interestingly, increased I_{NaP} current in the entorhinal cortex was not due to direct modulation of ion channel expression or function by FMRP, but rather through exaggerated mGluR5 signaling (Deng and Klyachko, 2016a). Few studies have directly assessed the intrinsic properties of inhibitory neurons in *FMR1* KO models, but those that have found no differences (Gibson et al., 2008).

FMRP has been shown to directly regulate the expression of the voltage-gated K^+ channel Kv3.1 (Darnell et al., 2011), whose experience-dependent expression gradients are altered in the medial nucleus of the trapezoid body (MNTB) of *FMR1* KO mice (Strumbos et al., 2010). Abnormal expression of Kv3.1 in the MNTB leads to faster repolarization and higher firing rates, indicative of hyperexcitability (El-Hassar et al., 2019). The MNTB is an essential component of the sound localization circuitry of the auditory brainstem, which requires rapid temporal processing of incoming sound information to compute interaural cue differences (Grothe et al., 2010). Thus, tight regulation of neuronal excitability is essential for allowing MNTB principal cells to fire at high rates with high temporal fidelity. Slack channels account for a major component of the total K^+ current in principal neurons of MNTB and some of the first evidence for direct FMRP-ion channel interactions was observed for Slack channels in the MNTB (Brown et al., 2010). Loss of FMRP reduces Slack currents, thereby increasing neuronal excitability and reducing temporal precision of spiking. MNTB principal neurons send glycinergic projections to the LSO, which uses a precise comparison of inhibitory inputs from the MNTB and excitatory inputs from the cochlear nucleus to compute interaural level differences (Park et al., 1996). Interestingly, hyperexcitability is also observed in principal cells of LSO in *FMR1* KO mice, but in the absence of intrinsic property differences (Garcia-Pino et al., 2017). Rather, LSO hyperexcitability was found to be caused by increased excitatory synaptic connectivity from cochlear nucleus afferents, while inhibitory inputs from the MNTB were unchanged. As tightly regulated E/I balance is essential in this sound localization circuit, it is tempting to speculate that altered excitatory connectivity in the LSO may arise to compensate for hyperexcitable inhibitory inputs from the MTNB or *vice versa*.

Effect of Ion Channel Dysregulation on Synaptic Function in FXS

Ion channels are not only involved in setting AP threshold and firing rate but can affect a variety of synaptic processes as well. For instance, BK channels play a critical role not only in regulating neuronal excitability but also in modulating AP duration and neurotransmitter release (Salkoff et al., 2006). FMRP has been shown to regulate BK channel conductance and expression and loss of this regulation in *FMR1* KO mice leads to decreased BK activity, resulting in AP broadening, which in turn leads to elevated presynaptic Ca^{2+} influx, increased glutamate release, and alterations to short-term pre-synaptic plasticity (Deng et al., 2013; Zhang et al., 2014; Myrick et al., 2015). Genetic upregulation of the BK β4 subunit rescues the observed excitability and synaptic defects (Deng and Klyachko, 2016b). Moreover, treatment of *FMR1* KO mice with the BK channel open BMS-204351 corrected a variety of hyperexcitability and behavioral phenotypes, suggesting BK channels may be a valuable therapeutic target to treat FXS (Zhang et al., 2014; Carreno-Munoz et al., 2018). FMRP-dependent AP broadening is observed in both hippocampal and cortical pyramidal neurons and has a cell-autonomous pre-synaptic origin (Deng et al., 2013). Future work must determine how FMRP-BK channel interaction may contribute to alterations in excitatory-excitatory and/or excitatory-inhibitory connectivity observed in the hippocampus and cortex of *FMR1* KO mice that has been shown to depend on pre-synaptic loss of FMRP as well (Hanson and Madison, 2007; Patel et al., 2013). FMRP has also been shown to regulate pre-synaptic GABA release in cerebellar basket cells *via* modulation of the expression and activity of Kv1.2 (Yang et al., 2020). Loss of FMRP-mediated regulation of Kv1.2 leads to enhanced pre-synaptic Ca^{2+} influx and excessive GABA release onto Purkinje neurons. While these changes would appear to counteract hyperexcitability, Purkinje cells themselves are

inhibitory, so the net effect of these changes would be disinhibition of Purkinje targets and thus still promote circuit hyperexcitability.

Ion channel regulation is not only important for pre-synaptic transmitter release, but also for the dendritic integration of post-synaptic signals (Stuart and Spruston, 2015). One of the first channels identified as a target of FMRP was the voltage-gated K^+ channel Kv4.2, whose expression was shown to be elevated in the hippocampus *FMR1* KO mice (Lee et al., 2011). Kv4.2 is a dendritic localized channel that mediates A-type currents that act to suppress AP-backpropagation into dendrites, which is important for modulating LTP induction (Chen et al., 2006). Thus, increased Kv4.2 expression may contribute to elevated thresholds for LTP induction in *FMR1* KO animals (Lauterborn et al., 2007; Meredith et al., 2007). However, other studies have found evidence for reduced Kv4.2 levels in *FMR1* KO mice (Gross et al., 2011) and dendritic recordings from hippocampal pyramidal neurons found decreased A-current in *FMR1* KO mice, which was associated with enhanced rather than impaired LTP induction (Routh et al., 2013). The discrepancies between these studies remain unclear, as similar biochemical techniques and LTP induction protocols were used. One potential explanation is a difference in the properties of more proximal synapses near the soma compared to distal dendritic synapses examined by Routh and colleagues. It will be important for future studies to examine both somatic and dendritic excitability in *FMR1* KO animals in combination with plasticity levels. A recent study has added another element to these contrary findings by demonstrating that FMRP can also directly interact with Kv4 channels to change their gating properties, resulting in reduced cellular excitability and increased LTP thresholds in cerebellar granule cells (Zhan et al., 2020). Importantly, reintroduction of an FMRP fragment that can bind Kv4 into *FMR1* KO mice restored deficits in mossy fiber LTP induction and behavioral hyperactivity assessed *via* open field test (Zhan et al., 2020).

HCN channels are cation permeable channels that underly the hyperpolarization-activated inward current (I_h) that plays a crucial role in setting resting membrane potential and dendritic excitability (Shah, 2014). HCN1-subunit expression and dendritic I_h are elevated in CA1 pyramidal neurons of *FMR1* KO mice, resulting in decreased input resistance and reduced temporal summation (Brager et al., 2012). Conversely, in layer 4 stellate and layer 5 pyramidal cells, HCN1 expression and dendritic I_h are reduced, leading to increased dendritic gain and sensory hyperexcitability (Zhang et al., 2014). Interestingly, this cell-type-specific bidirectional regulation of HCN channels may be the result of a cell-autonomous protein-protein interaction between FMRP and HCN, providing a potential mechanism for cell-type-specific differences in *FMR1* deletion (Brandalise et al., 2020). L-type voltage-gated Ca^{2+} channels (VGCCs) are another class of ion channels important for dendritic excitability and the mRNA for several VGCCs have been shown to be targets of FMRP (Chen et al., 2003; Darnell et al., 2011). Interestingly, despite being an FMRP target, expression of Cav1.3 is downregulated in the cortex and cerebellum of *FMR1* KO mice (Chen et al., 2003), and reduced expression of L-type VGCCs is associated with impaired spike-timing-dependent-plasticity (Meredith et al., 2007). While FMRP has been shown to predominantly suppress mRNA translation, there is evidence that FMRP can promote the translation of certain mRNA transcripts (Bechara et al., 2009; Fahling et al., 2009; Gross et al., 2011). Alternatively, reduced VGCC expression in juvenile and adult *FMR1* KO animals could be a compensatory change, as it has been shown that there is increased Ca^{2+} influx through L-type VGCCs in neural progenitor cells from *FMR1* KO mice and FXS human-derived pluripotent stem (iPS) cells (Danesi et al., 2018). Together, these studies indicate the wide-ranging effects that dysregulated ion channel function can have on cellular, synaptic, and circuit properties in FXS models.

HOMEOSTATIC PLASTICITY IN FXS

A confluence of molecular, synaptic, and cellular perturbations contribute to the generation of circuit hyperexcitability in FXS. Some of these disruptions are likely due to abnormal embryonic and early post-natal development of brain circuits, while others appear to be due to persistent loss of FMRP function in adulthood. Because FMRP is involved in a variety of neuronal processes across developmental time-points, it is also important to consider the array of compensatory mechanisms utilized by the brain to maintain optimal activity ranges and circuit stability when attempting to elucidate the consequences of *FMR1* deletion. This is complicated by the fact that FMRP is important for many forms of activity-dependent plasticity as well, and recent evidence has highlighted the role of FMRP in regulating homeostatic plasticity both during development and in the mature brain. In this section, we will review recent findings of how FMRP contributes to homeostatic plasticity and how the loss of this regulation contributes to hyperexcitability phenotypes in FXS.

Homeostatic Mechanisms for Maintaining Circuit Stability

Sensory acquisition in the brain begins as early as the fetal stage and occurs throughout the life of an individual (Partanen et al., 2013). Sensory experience and learning process tend to destabilize the associated neuronal circuit, which is part of a normal plasticity mechanism (Beston et al., 2010; Morgan et al., 2019). However, in order to regain circuit stability, such destabilizing forces need to be balanced by a counteracting process such as homeostatic plasticity. Information storage in neural circuits relies on Hebbian forms of synaptic plasticity, which involve activity-dependent changes in synaptic strength owing to LTP and LTD. These activity-dependent changes in synaptic strength depend on the precisely correlated firing of pre- and post-synaptic neurons. After the onset of LTP induction, the potentiated synapses enter a positive feedback loop, leading to continuous synaptic strengthening and circuit hyperexcitability (Turrigiano and Nelson, 2000; Turrigiano, 2008; Vitureira and Goda, 2013). On the other hand, induction of LTD enforces activity-dependent weakening of synapses and continuous LTD would lead to eventual silencing of synapses (Collingridge et al., 2010). Therefore, in the absence of mechanisms that can

attenuate the hypo- or hyperexcitability owing to uncontrolled LTD or LTP, respectively, robust destabilizing forces in a circuit could pose devastating consequences on network activity (Abbott and Nelson, 2000). Because Hebbian plasticity requires FMRP-dependent protein synthesis (Shang et al., 2009; Sidorov et al., 2013; Guo et al., 2016), homeostatic plasticity may also require FMRP and a deficit of homeostatic plasticity may contribute to imbalanced network activity seen in *FMR1* KO mice (Jewett et al., 2018).

The main purpose of homeostatic plasticity is to sense and regulate network excitability to a set-point value to prevent instability and optimize information processing. Studies have shown that neural network stability can be achieved in a number of ways, such as: (1) maintaining E/I balance in the network (Maffei et al., 2004; Gonzalez-Islas and Wenner, 2006; Landau et al., 2016; Keck et al., 2017); (2) regulating intrinsic neuronal firing rates in an activity-dependent manner (Desai et al., 1999; Marder and Prinz, 2003; Zhang and Linden, 2003; Joseph and Turrigiano, 2017); and (3) synaptic scaling, which up- or down-regulates excitatory synapses to modulate overall synaptic activity while maintaining the balance between synaptic weights (Turrigiano and Nelson, 2004; Davis, 2006). One of the most well-studied forms of homeostatic plasticity operating in CNS excitatory synapses is synaptic scaling. Turrigiano and colleagues were the first to demonstrate the presence of synaptic scaling in cortical neuronal culture, where they showed that tetrodotoxin (TTX)-mediated chronic blockade of neural activity caused upscaling of the strength of individual synapses. On the contrary, chronically inhibiting GABAergic transmission through the use of bicuculline or picrotoxin to promote neural activity causes a homeostatic reduction in the strength of individual excitatory synapses, with firing rates returning to baseline values following an initial elevation (Turrigiano et al., 1998). Moreover, selective activity blockade of a neuron using TTX microperfusion in its soma caused proportionate upscaling of synaptic transmission, suggesting that synaptic scaling is a cell-autonomous phenomenon (Ibata et al., 2008).

Studies investigating the signaling pathway of synaptic scaling have revealed the involvement of both N-Methyl-D-aspartate (NMDA) and α-amino-3-hydroxy-5-methyl-4-isoxazolepropionic acid (AMPA) receptors (AMPARs) in mediating homeostatic synaptic scaling at excitatory synapses (Watt et al., 2000; Maffei et al., 2004; Wierenga et al., 2005; Rodriguez et al., 2019). Synaptic upscaling in response to blocking postsynaptic transmission was shown to be achieved by increased surface expression of AMPARs and it involves the insertion of both GluA1 and GluA2 AMPAR subunits. Activity blockade in cultured neurons by TTX has been shown to enhance phosphorylation of GluA1 at the Ser845 residue. GluA1–Ser845 phosphorylation subsequently led to increased GluA1 surface accumulation in the postsynaptic compartment (Diering et al., 2014). A similar increase in GluA1–Ser845 phosphorylation was also shown to be responsible for synaptic upscaling *via* increased AMPAR–mEPSC in the visual cortex following visual deprivation (Goel et al., 2006, 2011). Apart from GluA1, the C-terminus of GluA2 alone can regulate synaptic scaling following TTX-induced synaptic upscaling *in vivo* (Gainey et al., 2009). Additionally, many other signaling molecules or postsynaptic proteins, such as brain-derived neurotrophic factor (BDNF), Arc (activity-regulated cytoskeleton-associated protein), TNFα (tumor necrosis factor α), MHC1 (major histocompatibility complex class 1), PICK1 (protein interacting with C kinase 1), β3 integrins, PSD93 (postsynaptic density protein 93), and PSD95 (postsynaptic density protein 95), also play important roles in synaptic scaling (Rutherford et al., 1998; Shepherd et al., 2006; Stellwagen and Malenka, 2006; Goddard et al., 2007; Sun and Turrigiano, 2011; Elmer and Mcallister, 2012). Compelling evidence suggests the existence of different forms of homeostatic plasticity in order to operate either as a global mechanism for all synapse types or local and specific to a certain neuronal subtype. In a nutshell, homeostatic plasticity ensures the stability of neural circuits essential for normal brain function. Because many of the genes that encode the aforementioned molecules for homeostatic plasticity are direct targets of FMRP (Niere et al., 2012; Tsai et al., 2012), it is logical to speculate that *FMR1* KO neurons may exhibit altered homeostatic plasticity. Next, we will discuss the discovery and significance of impaired homeostatic plasticity in FXS.

Homeostatic Synaptic Plasticity Is Altered in FXS

As discussed in the previous section, loss of FMRP results in a number of changes to excitatory and inhibitory synaptic function and connectivity. There is also a plethora of studies showing that *FMR1* KO neurons fail to adjust their synaptic strength to a basal set point in response to both unconstrained network activity and activity blockade, indicative of impaired homeostatic synaptic plasticity mechanisms in FXS. In particular, there is evidence for altered regulation of AMPARs during synaptic scaling in *FMR1* KO animals (Soden and Chen, 2010; Lee et al., 2018). The surface expression of GluA1-containing AMPARs, in addition to being mediated by phosphorylation of GluA1 at the Ser845 residue as mentioned above, is also known to be regulated by the ubiquitination of multiple lysine residues in the intracellular C-terminus of GluA1 (Schwarz et al., 2010; Lin et al., 2011). Ubiquitination of GluA1 *via* the E3 ubiquitin ligase named neural precursor cell expressed developmentally down-regulated gene 4-like (Nedd4l, or Nedd4-2) leads to a reduction of surface AMPARs and this has been observed to occur during synaptic downscaling (Jewett et al., 2015). In cortical neuron cultures of *FMR1* KO mice, such Nedd4-2-mediated ubiquitination is deficient, leading to impaired synaptic downscaling (Lee et al., 2018). Mechanistically, Lee and colleagues found that dephosphorylation of Nedd4-2 following the chronic blockade of GABAergic transmission is responsible for the defect, as ectopically expressing a phosphomimetic Nedd4-2 can restore GluA1 ubiquitination and synaptic downscaling in cultured *FMR1* KO cortical neurons.

Another reported mechanism concerning the regulation of surface AMPARs during synaptic scaling is through retinoic acid (RA) and retinoic acid receptor α (RARα) signaling in visual cortical circuits. RA regulates local homeostatic plasticity at the level of individual dendritic spines. In the case of

activity blockade, a drop in Ca^{2+} levels stimulates RA synthesis, which in turn enhances local protein synthesis, increases surface insertion of GluA1-containing AMPARs, and ultimately restores Ca^{2+} levels (Aoto et al., 2008). This entire cascade of events leads to synaptic upscaling at excitatory synapses. This form of synaptic upscaling was absent in *FMR1* KO mice and could be restored by post-synaptic re-expression of FMRP (Soden and Chen, 2010). Research from the same group suggests that, apart from synaptic scaling-up at excitatory synapses (Chen et al., 2014), RA/RARα signaling also mediates inhibitory homeostatic plasticity in the mouse primary visual cortex (Zhong et al., 2018). Treatment with RA causes reduced inhibitory drive onto layer 2/3 pyramidal neurons and similar effects are triggered by visual deprivation. This RA-dependent reduction in inhibition was due to reduced inhibitory synaptic transmission from PV interneurons. Interesting, visual deprivation- and RA-dependent downregulation of inhibition was absent in the visual cortex of *FMR1* KO mice and selective deletion of *Fmr1* in PV neurons recapitulated these deficits in inhibitory synaptic downscaling. Thus, loss of FMRP in excitatory neurons impairs homeostatic up-scaling of excitatory synapses while loss of FMRP in PV inhibitory neurons impairs down-scaling of inhibitory synapses. Similar impairments in RA-dependent homeostatic plasticity were observed in *FMR1* deficient human pluripotent stem cells (Zhang et al., 2018). In addition, a recent study surprisingly revealed a physical interaction between FMRP and RARα, and such interaction mediates transcription-independent RA signaling and homeostatic plasticity (Park et al., 2021). Altogether, these findings suggest that FMRP is crucial for homeostatic synaptic plasticity, and the inability of *FMR1* deficient neurons to regulate E/I balance in the face of changes to overall activity levels may contribute to altered synaptic development and synaptic hyperexcitability in FXS.

Homeostatic Intrinsic Plasticity Is Altered in FXS

Homeostatic synaptic plasticity is essential for preventing network hyperexcitability, particularly during early developmental periods when neuronal networks are undergoing immense modification and refinement. What other homeostatic mechanisms could be responsible for the hyperexcitability of neuronal networks in adult brains, especially in the case of FXS? One possibility lies in the homeostatic control of the intrinsic excitability of the neurons. Many studies have shown basally altered intrinsic excitability in *FMR1* KO mice, as discussed above in "Ion Channel Dysregulation and Altered Intrinsic Excitability in FXS" section. Interestingly, in line with these findings on the intrinsic properties of *FMR1* KO neurons, a recent study indicated that *FMR1* KO neurons show a significant increase in input resistance along with distinct alterations in homeostatic intrinsic plasticity in different subsets of cortical neurons. Bülow et al. (2019) found that, depending on the pattern of spikes following steps of current injections, *FMR1* KO cortical neurons exhibit strikingly different intrinsic scaling phenotypes. In comparison to WT neurons, single-spiking *FMR1* KO neurons show impaired intrinsic upscaling, whereas multispiking *FMR1* KO neurons show exaggerated intrinsic upscaling. Furthermore, Bülow and colleagues demonstrated that activity blockade in *FMR1* KO neurons alters action potential parameters, with an increase in the maximum slope of the AP rising phase (**Figure 1C**). This change in AP parameter in *FMR1* KO neurons may be due to increased activity of Na^+ channels, contributing to abnormal intrinsic excitability. While the molecular mechanism underlying the differences between single-spiking and multispiking neurons during intrinsic upscaling is unclear, the study introduced the first evidence for homeostatic intrinsic plasticity deficits in *FMR1* KO mice.

Although it remains unknown how the altered homeostatic intrinsic plasticity at the single-cell level ultimately affects network stability as a whole, a recent study looking at homeostatic network plasticity may give us a clue. Jewett and colleagues demonstrated that FXS cortical neuron cultures fail to achieve homeostatic network synchronization in response to chronic activity stimulation in a multielectrode array recording (Jewett et al., 2018). This deficit was described by a novel signaling pathway, suggesting the involvement of FMRP-dependent ubiquitination of tumor suppressor p53 by the E3 ligase Mdm2 in response to chronic activity stimulation of cortical neurons. In *FMR1* KO neurons, this signaling is hampered, likely due to basally altered activity of Mdm2 (Tsai et al., 2017), and thus the homeostatic reduction in the amplitude of neuronal network spikes is absent (Jewett et al., 2018). This study, together with other studies using single-neuron recordings, suggests that the cortical neurons and networks in *FMR1* KO mice exhibit impaired homeostatic plasticity which could be responsible, at least in part, for circuit hyperexcitability and associated behavioral defects in FXS. It is likely that homeostatic plasticity disruptions are occurring in other brain areas as well. For example, Svalina and colleagues reported that principal cells in the lateral amygdala show enhanced excitability owing to reduced feed-forward inhibition, indicating a potential deficit in homeostatic plasticity in the amygdala (Svalina et al., 2021), which could be relevant to the anxiety issues in FXS.

Finally, others studies have revealed that some forms of homeostatic plasticity are intact in *FMR1* KO animals. For instance, homeostatic changes at the circuit level are normal *ex vivo* in auditory cortical slice cultures following chronic stimulation (Motanis and Buonomano, 2020). Homeostatic changes to axon initial segment (AIS) length, which plays a crucial role in neuronal excitability, are intact in CA1 hippocampal neurons of *FMR1* KO animals as well (Booker et al., 2020). However, this study also found that AIS length was increased in *FMR1* KO neurons (**Figure 1B**), leading to increased cellular excitability. Interestingly, these neurons had reduced functional input from the entorhinal cortex, suggesting that AIS-dependent hyperexcitability in *FMR1* KO mice may actually be an adaptive homeostatic change to compensate for reduced synaptic input. Thus, in some cases, cellular hyperexcitability observed in FX models may act to stabilize rather than destabilize circuit function, as has been suggested for changes to E/I balance in the somatosensory cortex (Antoine et al., 2019). It should be noted that decreased feed-forward inhibition (Wahlstrom-Helgren and Klyachko, 2015) and altered post-synaptic dendritic integration (Brager et al., 2012) are also observed in this

entorhinal-CA1 circuit in *FMR1* KO mice, and future work must delineate the relationship between these changes to synaptic function, intrinsic properties, and AIS length. In other cases, it appears that intact homeostatic mechanisms fail to correct hyperexcitability in *FMR1* KO animals, as seen in the amygdala, where homeostatic upregulation of inhibitory synaptic transmission during critical stages of development cannot be maintained in the mature brain (Vislay et al., 2013). Therefore, while compelling evidence from the growing body of studies strongly suggests that hyperexcitability in FXS can be partially attributed to impairment in homeostatic plasticity, the contradictory results reiterate the complexity of brain hyperexcitability in FXS. More *in vivo* studies using physiological simulations would be needed to further consolidate the observations about homeostatic plasticity in FXS animal models.

BEHAVIORAL CONSEQUENCES OF HYPEREXCITABLE CIRCUITS IN FXS

The studies highlighted in the previous sections demonstrate that hyperexcitable networks are a common outcome of loss of FMRP, but that the mechanisms leading to this phenotype involve complex changes to synaptic and circuit function and plasticity that are highly region-specific. An important question is how does hyperexcitability ultimately contribute to the neurocognitive phenotypes of FXS, and how can we parse the influence of different cellular and molecular mechanisms across brain regions, as this will have important consequences for clinical treatment. The clinical features of FXS are also quite complex with multiple physical and neuropsychiatric symptoms, including intellectual disability, autistic behavior, social anxiety, perseverative behaviors, hyperactivity/impulsivity/aggression, language deficits, and disrupted sleep (Lozano et al., 2014). In a majority of cases, FX individuals exhibit sensory alterations that range from hypersensitivity to sensory stimuli and hyperarousal to seizures. These last symptoms are particularly relevant for this review, as they may provide a tractable window for understanding how hyperexcitability and homeostatic plasticity in different brain regions may relate to core behavioral impairments in FX.

Elevated Seizure Susceptibility in FXS

Hyperexcitability has been linked to elevated susceptibility to seizures in FXS individuals. Some of the earliest works looking at epilepsy in FXS revealed that 10–20% of FXS individuals become epileptic early in childhood (Musumeci et al., 1999; Berry-Kravis, 2002). Despite an apparent epileptiform abnormality on EEG, studies suggest that the abnormal EEG pattern in FXS patients appear to resemble that of a benign focal epilepsy of childhood (BFEC; Berry-Kravis, 2002; Qiu et al., 2008) in which the patients rarely develop status epilepticus (SE; Gauthey et al., 2010). In addition, the patients usually respond well to anti-epilepsy medicine, and most of the patients enter seizure remission before adulthood (Musumeci et al., 1999; Berry-Kravis, 2002). Although seizures and epilepsy are easily controlled for most patients, these seizures are still considered one of the serious comorbidities of FXS, and the EEG pattern in FXS is used as one of the endophenotypes to guide personalized treatment (Cowley et al., 2016).

Elevated seizure susceptibility has been documented in *FMR1* KO mice as well, with the increased preponderance of audiogenic seizures (AGSs) being one of the most reliable and consistent approaches to assessing hyperexcitability *in vivo*. In AGS experiments, mice are presented with a 110–120 dB siren or alarm sound for a duration of 1–3 min. The mice are then scored for behavioral seizures with SE and death as a common final end point for the *FMR1* KO mice (Musumeci et al., 2000). Interestingly, conditional deletion of *FMR1* in subcortical glutamatergic neurons reproduces the AGS phenotype, while re-expression of FMRP selectively in the inferior colliculus of global *FMR1* KO mice eliminates AGSs (Gonzalez et al., 2019). Thus, while auditory EEG abnormalities that contribute to auditory processing deficits in *FMR1* KO mice appear to depend on altered cortical function (Goswami et al., 2019; Lovelace et al., 2020), AGSs are generated subcortically, likely within the auditory midbrain. It is also worth noting that *FMR1* KO rats did not exhibit AGSs as compared to *FMR1* KO mice (Wong et al., 2020), suggesting that AGS is likely a mouse-specific phenotype. In the model of kindling-induced seizures, despite a similar electrographic seizure threshold between *FMR1* KO mice and their WT littermates, *FMR1* KO mice displayed accelerated seizure progression both behaviorally and electrographically (Qiu et al., 2009). Despite similar susceptibility between *FMR1* KO mice and their WT littermates following systemic injections of kainic acid in the model of chemically-induced seizures, *FMR1* KO mice did not exhibit homeostatic response triggers by the seizures (Liu et al., 2021), suggesting the possibility that the *FMR1* KO mice might exhibit higher susceptibility to multiple or sequential seizures. This finding requires future investigation to validate it.

In summary, elevated seizure susceptibility is common in patients and animal models of FXS. While the seizures are usually not spontaneous, they do indicate a hyperexcitable brain circuit in FXS and provide a means for evaluating excitability imbalance in research models and testing therapeutic interventions for FXS.

Sensory Hypersensitivity in FXS

Atypical sensory processing is a common and debilitating feature of FXS and ASD (Sinclair et al., 2017b). Sensory abnormalities are present early in development and are predictive of disease phenotypes that emerge later in life, such as increased anxiety and abnormal social behavior (Baranek et al., 2008, 2013). Sensory phenotypes in FXS can be complex, typically manifesting across sensory domains and characterized by both over- and under-responsiveness to sensory stimuli as well as avoidance and/or sensory seeking behavior (Rais et al., 2018). However, hypersensitivity to sensory stimuli is often the most common and most disruptive symptom, and this may be directly related to neuronal hyperexcitability in sensory areas. Evidence for heightened sensory sensitivity in FXS comes from validated scales and parental questionnaires, such as the Short Sensory Profile (Rogers et al., 2003;

Baranek et al., 2008), as well objective measures, including increased electrodermal response to stimuli (Miller et al., 1999) and altered event-related brain potentials (ERPs; Sinclair et al., 2017b). In addition to being a clinically important aspect of the FXS phenotype, sensory dysregulation affords an opportunity to link underlying disease mechanisms to behavioral symptoms in animal models of FXS, as sensory systems are relatively well-conserved across species and there are well-characterized behavioral and electrophysiological read-outs of sensory processing.

Some of the first evidence for sensory hypersensitivity in FXS animal models came from examination of the acoustic startle response (ASR), with *FMR1* KO mice exhibiting an increase in this full body reflexive response to loud sound stimuli (Chen and Toth, 2001). More recently, the BK channel opener BMS-204352 was shown to reverse ASR increases in *FMR1* KO mice, providing a link between altered ion channel regulation, neuronal hyperexcitability, and sensory hypersensitivity (Zhang et al., 2014). However, other studies have observed a decrease (Frankland et al., 2004; Paylor et al., 2008) or no change (Mccullagh et al., 2020) in ASR in *FMR1* KO mice. The cause of these discrepancies is unclear but may be due in part to background strain effects (Errijgers et al., 2008) and methodological differences (Lauer et al., 2017). Despite the inherent variability in ASR phenotype, studies have shown that the ASR is directly related to FMRP expression (Yun et al., 2006) and ASR phenotypes in *FMR1* KO animals can be rescued with the reintroduction of the *Fmr1* gene (Paylor et al., 2008), indicating that some aspects of the ASR are directly related to loss of FMRP.

Examination of ASR in FXS humans has found no change in baseline startle responses but impaired pre-pulse inhibition of the ASR (PPI), a modification of the paradigm where a startle-eliciting sound is preceded by a lower level auditory or tactile cue that reflexively reduces ASR magnitude (Frankland et al., 2004; Hessl et al., 2009). PPI alterations are also commonly observed in *FMR1* KO mice, however often in the opposite direction as seen in humans, with enhanced rather than reduced PPI magnitude (Chen and Toth, 2001; Nielsen et al., 2002; Frankland et al., 2004; Paylor et al., 2008; Orefice et al., 2016; Kokash et al., 2019). These discrepancies may once again be due to methodological details (Hessl et al., 2009). A recent study using different PPI cues, such as gaps in sound or different spatial locations of sound sources, found decreased PPI in *FMR1* KO mice (Mccullagh et al., 2020) while no PPI alterations were observed in *FMR1* KO rats using a novel, robust methodological approach (Miller et al., 2021). Despite differences from the human phenotype, PPI alterations in *FMR1* KO animals are sensitive to treatments that also reverse auditory hyperexcitability phenotypes, such as mGluR5 inhibitors (de Vrij et al., 2008) or genetic reduction of MMP9 (Kokash et al., 2019). However, the variability in results across studies using these reflexive assays has limited their utility for understanding sensory processing issues in FX.

Operant perceptual decision-making tasks, where animals are conditioned to respond to specific stimuli, allow for quantitative assessment of sensory processing in a manner that can be directly translated to human studies. A recent study assessed sound hypersensitivity in *FMR1* KO rats using an operant sound detection task (Auerbach et al., 2021). *FMR1* KO rats learned the task at the same rate as WT counterparts and reached similar peak performance for detection of near threshold sounds. However, *FMR1* KO rats exhibited significantly faster auditory reaction times (RT) at suprathreshold intensities, suggestive of increased perceptual sensitivity. Indeed, RT-intensity functions have been shown to be a reliable psychoacoustic measure of loudness growth in both humans (Marshall and Brandt, 1980) and animal models (Radziwon and Salvi, 2020). *FMR1* KO rats also displayed abnormal integration of sound duration and bandwidth in a manner consistent with altered loudness perception. These results provide evidence for aberrant low-level auditory processing and excessive loudness growth in *FMR1* KO animals using a task design with potential for clinical translation. RT differences were also sensitive to mGluR5 inhibition, demonstrating this phenotype is related to a core molecular pathology in FXS. Future work must determine the neurophysiological correlates of this behavioral phenotype, but multiple studies have found evidence of sound-evoked hyperactivity and circuit hyperexcitability in the auditory cortex of *FMR1* KO mice (Rotschafer and Razak, 2013; Lovelace et al., 2018; Goswami et al., 2019) and FXS individuals (Van der Molen et al., 2012; Ethridge et al., 2016). In particular, increased event-related potentials (ERPs) and reduced synchronization to auditory chirp stimuli, an amplitude modulated sound that is modulated by a sinusoid with increasing or decreasing frequency, are observed in *FMR1* KO mice and FX individuals (Ethridge et al., 2017; Lovelace et al., 2018; Jonak et al., 2020). These processing deficits could underly the observed behavioral impairments in loudness perception and temporal integration.

A recent study by Goel and colleagues has provided some of the most complete evidence linking circuit hyperexcitability to sensory processing issues in FXS (Goel et al., 2018). By combining *in vivo* Ca^{2+} imaging from genetically-identified PV interneurons and putative excitatory neurons in the visual cortex of mice performing an orientation discrimination task, they found delayed perceptual learning and impaired fine-tuned discrimination in *FMR1* KO mice that correlated with deficits in orientation tuning of principal cells and reduced stimulus-evoked activity in PV neurons. Chemogenetic activation of PV neurons rescued the behavioral impairments in *FMR1* KO mice, suggesting a causal relationship between disrupted E/I balance and impaired sensory processing. Furthermore, parallel human psychophysics studies using an analogous paradigm to one used in mice found similar visual discrimination impairments in FXS individuals.

Similar hypersensitivity (He et al., 2017) and perceptual learning deficits (Arnett et al., 2014) have been observed in the tactile domain of *FMR1* KO mice. Using a novel assay for tactile defensiveness, He and colleagues found that head-fixed *FMR1* KO mice exhibited an exaggerated motor response in attempts to avoid whisker stimulation.

While numerous *ex vivo* studies have found evidence for hyperexcitability in the somatosensory cortex of *FMR1* KO animals (see Section "Hyperexcitable Neurons and Networks in Fragile X Syndrome"), no differences in overall whisker-evoked activity were seen in *FMR1* KO mice in this study, as assessed by two-photon Ca^{2+} imaging of layer 2/3 neurons (He et al., 2017). This is consistent with *in vivo* cell-attached recordings showing no difference in whisker-evoked spiking activity from this same neuronal population (Antoine et al., 2019). However, He and colleagues did find a pronounced deficit in neuronal adaption to repetitive stimulation in *FMR1* KO animals, suggesting that tactile hypersensitivity may be driven in part by impaired habituation to sensory input. Similar habituation deficits have been observed in the auditory (Lovelace et al., 2016) and visual (Pak et al., 2021) domains of *FMR1* KO mice as well. Interestingly, auditory habituation measured behaviorally using ASR has been shown to depend on intact BK channel function (Typlt et al., 2013). Loss of FMRP-mediated regulation of BK channel conductance (Deng et al., 2013; Deng and Klyachko, 2016b) could therefore conceivably account for impaired habituation in *FMR1* KO animals, although this has not been directly tested yet. While less characterized, there is evidence for altered olfaction in FXS models as well (Bodaleo et al., 2019). Interestingly, studies in *FMR1* KO mice (Schilit Nitenson et al., 2015) and a FXS drosophila model (Franco et al., 2017) both found that FXS animals exhibited decreased odor sensitivity, contrary to findings from other sensory domains.

Animal model studies have highlighted several promising molecular targets for the treatment of FXS and, as discussed above, recent studies have uncovered novel treatment targets aimed at circuit-level disruptions that may work in parallel or perhaps even synergistically with existing molecular therapies. However, an important lesson learned from recent clinical trials in FXS is the need for quantitative, objective behavioral read-outs that translate between pre-clinical animal models and clinical trials (Berry-Kravis et al., 2018). Sensory processing disruptions may provide a unique behavioral platform for pre-clinical drug screening using disease-relevant phenotypes that are relatively well-conserved between humans and animal models.

CONCLUSION

Here we have highlighted the number of ways in which loss of FMRP can lead to neuronal hyperexcitability, and how these cellular and circuit changes contribute to the FXS phenotype. Because FMRP regulates multiple activity-dependent processes and is regulated in an activity-dependent manner itself, it is difficult to disentangle the direct effects of FMRP loss from secondary consequences. While some of the phenotypes described above are likely to be compensatory adaptions rather than direct pathologies related to *FMR1* deletion, it is possible that both these primary and compensatory changes contribute to hyperexcitability phenotypes in FXS. The exact consequence of *FMR1* deletion at the synaptic, cellular, and circuit level also depends greatly on the brain region and developmental time point being examined. However, some general themes have emerged regarding the role of FMRP in neuronal and circuit excitability: (1) FMRP is important for activity-dependent development and refinement of synaptic connectivity and loss of FMRP during early life critical periods can lead to abnormal excitatory and inhibitory synaptic connectivity, resulting in altered E/I balance that is likely to contribute to circuit hyperexcitability; (2) FMRP is required for ongoing activity-dependent plasticity in the mature brain and seems particularly important for regulating mGluR-dependent changes to excitatory synaptic function, inhibitory transmitter release, and cellular excitability; (3) FMRP regulates the expression and function of multiple ion channels through a variety of direct and indirect mechanisms. Changes to ion channel function with loss of FMRP not only directly affect intrinsic excitability in a manner to promote hyperactivity, but can lead to profound changes in pre-synaptic release properties and post-synaptic dendritic integration, which in turn will influence synaptic function and plasticity in a variety of ways; and (4) FMRP is an important regulator of homeostatic plasticity, which is essential for stabilizing activity levels in the brain, and impairments to this stabilization mechanism are likely to contribute to circuit hyperexcitability in FXS. The wide-ranging consequences of *FMR1* deletion underscore the importance of examining multiple aspects of neuronal function (e.g., cellular excitability, synaptic plasticity, and network activity) in *FMR1* KO models under the same experimental conditions, ideally using approaches that span from single neurons to intact circuits to behavior. Future studies must also continue to make use of spatial and temporally restricted deletion of *FMR1* to parse the contribution of different cell-types, brain regions, and developmental timepoints to FXS phenotypes. The development of FMRP-tat peptides to reintroduce different FMRP segments to *FMR1* KO neurons is a powerful tool for dissociating FMRPs function *via* direct protein-protein interactions from its canonical role in translational regulation (Zhan et al., 2020; Park et al., 2021). Finally, the development of novel FXS models—such as the *FMR1* KO rat (Till et al., 2015; Golden et al., 2019; Auerbach et al., 2021) and FXS human derived iPS cells (Telias et al., 2013; Bhattacharyya and Zhao, 2016) and organoids (Kang et al., 2021), will help identify which phenotypes are most highly conserved across species and highlight new treatment strategies.

AUTHOR CONTRIBUTIONS

All authors contributed to the article and approved the submitted version.

FUNDING

This work was supported in part by the National Institute of Deafness and Other Communication Disorders Grant K01DC018310 (to BA) and the National Institute of Mental Health Grant R01MH124827 (to N-PT).

REFERENCES

Abbott, L. F., and Nelson, S. B. (2000). Synaptic plasticity: taming the beast. *Nat. Neurosci.* 3, 1178–1183. doi: 10.1038/81453

Abitbol, M., Menini, C., Delezoide, A.-L., Rhyner, T., Vekemans, M., and Mallet, J. (1993). Nucleus basalis magnocellularis and hippocampus are the major sites of FMR-1 expression in the human fetal brain. *Nat. Genet.* 4, 147–153. doi: 10.1038/ng0693-147

Antar, L. N., Afroz, R., Dictenberg, J. B., Carroll, R. C., and Bassell, G. J. (2004). Metabotropic glutamate receptor activation regulates fragile x mental retardation protein and FMR1 mRNA localization differentially in dendrites and at synapses. *J. Neurosci.* 24, 2648–2655. doi: 10.1523/JNEUROSCI.0099-04.2004

Antar, L. N., Li, C., Zhang, H., Carroll, R. C., and Bassell, G. J. (2006). Local functions for FMRP in axon growth cone motility and activity-dependent regulation of filopodia and spine synapses. *Mol. Cell. Neurosci.* 32, 37–48. doi: 10.1016/j.mcn.2006.02.001

Antoine, M. W., Langberg, T., Schnepel, P., and Feldman, D. E. (2019). Increased excitation-inhibition ratio stabilizes synapse and circuit excitability in four autism mouse models. *Neuron* 101, 648–661.e4. doi: 10.1016/j.neuron.2018.12.026

Aoto, J., Nam, C. I., Poon, M. M., Ting, P., and Chen, L. (2008). Synaptic signaling by all-trans retinoic acid in homeostatic synaptic plasticity. *Neuron* 60, 308–320. doi: 10.1016/j.neuron.2008.08.012

Arnett, M. T., Herman, D. H., and Mcgee, A. W. (2014). Deficits in tactile learning in a mouse model of fragile X syndrome. *PloS One* 9:e109116. doi: 10.1371/journal.pone.0109116

Ascano, M., Jr, Mukherjee, N., Bandaru, P., Miller, J. B., Nusbaum, J. D., Corcoran, D. L., et al. (2012). FMRP targets distinct mRNA sequence elements to regulate protein expression. *Nature* 492, 382–386. doi: 10.1038/nature11737

Ashley, C. T., Jr., Wilkinson, K. D., Reines, D., and Warren, S. T. (1993). FMR1 protein: conserved RNP family domains and selective RNA binding. *Science* 262, 563–566. doi: 10.1126/science.7692601

Auerbach, B. D., and Bear, M. F. (2010). Loss of the fragile X mental retardation protein decouples metabotropic glutamate receptor dependent priming of long-term potentiation from protein synthesis. *J. Neurophysiol.* 104, 1047–1051. doi: 10.1152/jn.00449.2010

Auerbach, B. D., Manohar, S., Radziwon, K., and Salvi, R. (2021). Auditory hypersensitivity and processing deficits in a rat model of fragile X syndrome. *Neurobiol. Dis.* 161:105541. doi: 10.1016/j.nbd.2021.105541

Balmer, T. S., Carels, V. M., Frisch, J. L., and Nick, T. A. (2009). Modulation of perineuronal nets and parvalbumin with developmental song learning. *J. Neurosci.* 29, 12878–12885. doi: 10.1523/JNEUROSCI.2974-09.2009

Baranek, G. T., Roberts, J. E., David, F. J., Sideris, J., Mirrett, P. L., Hatton, D. D., et al. (2008). Developmental trajectories and correlates of sensory processing in young boys with fragile X syndrome. *Phys. Occup. Ther. Pediatr.* 28, 79–98. doi: 10.1300/j006v28n01_06

Baranek, G. T., Watson, L. R., Boyd, B. A., Poe, M. D., David, F. J., and Mcguire, L. (2013). Hyporesponsiveness to social and nonsocial sensory stimuli in children with autism, children with developmental delays and typically developing children. *Dev. Psychopathol.* 25, 307–320. doi: 10.1017/S0954579412001071

Bear, M. F., Huber, K. M., and Warren, S. T. (2004). The mGluR theory of fragile X mental retardation. *Trends Neurosci.* 27, 370–377. doi: 10.1016/j.tins.2004.04.009

Bechara, E. G., Didiot, M. C., Melko, M., Davidovic, L., Bensaid, M., Martin, P., et al. (2009). A novel function for fragile X mental retardation protein in translational activation. *PLoS Biol.* 7:e16. doi: 10.1371/journal.pbio.1000016

Berry-Kravis, E. (2002). Epilepsy in fragile X syndrome. *Dev. Med. Child Neurol.* 44, 724–728. doi: 10.1017/s0012162201002833

Berry-Kravis, E., Hagerman, R., Visootsak, J., Budimirovic, D., Kaufmann, W. E., Cherubini, M., et al. (2017). Arbaclofen in fragile X syndrome: results of phase 3 trials. *J. Neurodev. Disord.* 9:3. doi: 10.1186/s11689-016-9181-6

Berry-Kravis, E. M., Hessl, D., Rathmell, B., Zarevics, P., Cherubini, M., Walton-Bowen, K., et al. (2012). Effects of STX209 (arbaclofen) on neurobehavioral function in children and adults with fragile X syndrome: a randomized, controlled, phase 2 trial. *Sci. Transl. Med.* 4:152ra127. doi: 10.1126/scitranslmed.3004214

Berry-Kravis, E. M., Lindemann, L., Jonch, A. E., Apostol, G., Bear, M. F., Carpenter, R. L., et al. (2018). Drug development for neurodevelopmental disorders: lessons learned from fragile X syndrome. *Nat. Rev. Drug Discov.* 17, 280–299. doi: 10.1038/nrd.2017.221

Beston, B. R., Jones, D. G., and Murphy, K. M. (2010). Experience-dependent changes in excitatory and inhibitory receptor subunit expression in visual cortex. *Front. Synaptic Neurosci.* 2:138. doi: 10.3389/fnsyn.2010.00138

Bhakar, A. L., Dolen, G., and Bear, M. F. (2012). The pathophysiology of fragile X (and what it teaches us about synapses). *Annu. Rev. Neurosci.* 35, 417–443. doi: 10.1146/annurev-neuro-060909-153138

Bhattacharyya, A., and Zhao, X. (2016). Human pluripotent stem cell models of Fragile X Syndrome. *Mol. Cell. Neurosci.* 73, 43–51. doi: 10.1016/j.mcn.2015.11.011

Bhogal, B., and Jongens, T. A. (2010). Fragile X syndrome and model organisms: identifying potential routes of therapeutic intervention. *Dis. Model. Mech.* 3, 693–700. doi: 10.1242/dmm.002006

Bianchi, R., Chuang, S. C., Zhao, W., Young, S. R., and Wong, R. K. (2009). Cellular plasticity for group I mGluR-mediated epileptogenesis. *J. Neurosci.* 29, 3497–3507. doi: 10.1523/JNEUROSCI.5447-08.2009

Bilousova, T. V., Dansie, L., Ngo, M., Aye, J., Charles, J. R., Ethell, D. W., et al. (2009). Minocycline promotes dendritic spine maturation and improves behavioural performance in the fragile X mouse model. *J. Med. Genet.* 46, 94–102. doi: 10.1136/jmg.2008.061796

Bodaleo, F., Tapia-Monsalves, C., Cea-Del Rio, C., Gonzalez-Billault, C., and Nunez-Parra, A. (2019). Structural and functional abnormalities in the olfactory system of fragile X syndrome models. *Front. Mol. Neurosci.* 12:135. doi: 10.3389/fnmol.2019.00135

Bonaccorso, C. M., Spatuzza, M., Di Marco, B., Gloria, A., Barrancotto, G., Cupo, A., et al. (2015). Fragile X mental retardation protein (FMRP) interacting proteins exhibit different expression patterns during development. *Int. J. Dev. Neurosci.* 42, 15–23. doi: 10.1016/j.ijdevneu.2015.02.004

Booker, S. A., Domanski, A. P. F., Dando, O. R., Jackson, A. D., Isaac, J. T. R., Hardingham, G. E., et al. (2019). Altered dendritic spine function and integration in a mouse model of fragile X syndrome. *Nat. Commun.* 10:4813. doi: 10.1038/s41467-019-11891-6

Booker, S. A., Simoes De Oliveira, L., Anstey, N. J., Kozic, Z., Dando, O. R., Jackson, A. D., et al. (2020). Input-output relationship of CA1 pyramidal neurons reveals intact homeostatic mechanisms in a mouse model of fragile X syndrome. *Cell Rep.* 32:107988. doi: 10.1016/j.celrep.2020.107988

Bourgeron, T. (2015). From the genetic architecture to synaptic plasticity in autism spectrum disorder. *Nat. Rev. Neurosci.* 16, 551–563. doi: 10.1038/nrn3992

Brager, D. H., Akhavan, A. R., and Johnston, D. (2012). Impaired dendritic expression and plasticity of h-channels in the fmr1(-/y) mouse model of fragile X syndrome. *Cell Rep.* 1, 225–233. doi: 10.1016/j.celrep.2012.02.002

Brandalise, F., Kalmbach, B. E., Mehta, P., Thornton, O., Johnston, D., Zemelman, B. V., et al. (2020). Fragile X mental retardation protein bidirectionally controls dendritic Ih in a cell type-specific manner between mouse hippocampus and prefrontal cortex. *J. Neurosci.* 40, 5327–5340. doi: 10.1523/JNEUROSCI.1670-19.2020

Brown, V., Jin, P., Ceman, S., Darnell, J. C., O'donnell, W. T., Tenenbaum, S. A., et al. (2001). Microarray identification of FMRP-associated brain mRNAs and altered mRNA translational profiles in fragile X syndrome. *Cell* 107, 477–487. doi: 10.1016/s0092-8674(01)00568-2

Brown, M. R., Kronengold, J., Gazula, V.-R., Chen, Y., Strumbos, J. G., Sigworth, F. J., et al. (2010). Fragile X mental retardation protein controls gating of the sodium-activated potassium channel Slack. *Nat. Neurosci.* 13, 819–821. doi: 10.1038/nn.2563

Budimirovic, D. B., Dominick, K. C., Gabis, L. V., Adams, M., Adera, M., Huang, L., et al. (2021). Gaboxadol in Fragile X syndrome: a 12-week randomized, double-blind, parallel-group, phase 2a study. *Front. Pharmacol.* 12:757825. doi: 10.3389/fphar.2021.757825

Bülow, P., Murphy, T. J., Bassell, G. J., and Wenner, P. (2019). Homeostatic intrinsic plasticity is functionally altered in Fmr1 KO cortical neurons. *Cell Rep.* 26, 1378–1388.e3. doi: 10.1016/j.celrep.2019.01.035

Bureau, I., Shepherd, G. M., and Svoboda, K. (2008). Circuit and plasticity defects in the developing somatosensory cortex of FMR1 knock-out mice. *J. Neurosci.* 28, 5178–5188. doi: 10.1523/JNEUROSCI.1076-08.2008

Cardin, J. A., Carlen, M., Meletis, K., Knoblich, U., Zhang, F., Deisseroth, K., et al. (2009). Driving fast-spiking cells induces gamma rhythm and controls sensory responses. *Nature* 459, 663–667. doi: 10.1038/nature08002

Carreno-Munoz, M. I., Martins, F., Medrano, M. C., Aloisi, E., Pietropaolo, S., Dechaud, C., et al. (2018). Potential involvement of impaired BKCa channel function in sensory defensiveness and some behavioral disturbances induced by unfamiliar environment in a mouse model of fragile X syndrome. *Neuropsychopharmacology* 43, 492–502. doi: 10.1038/npp.2017.149

Ceman, S., O'donnell, W. T., Reed, M., Patton, S., Pohl, J., and Warren, S. T. (2003). Phosphorylation influences the translation state of FMRP-associated polyribosomes. *Hum. Mol. Genet.* 12, 3295–3305. doi: 10.1093/hmg/ddg350

Centonze, D., Rossi, S., Mercaldo, V., Napoli, I., Ciotti, M. T., De Chiara, V., et al. (2008). Abnormal striatal GABA transmission in the mouse model for the fragile X syndrome. *Biol. Psychiatry* 63, 963–973. doi: 10.1016/j.biopsych.2007.09.008

Chen, R., Cros, D., Curra, A., Di Lazzaro, V., Lefaucheur, J. P., Magistris, M. R., et al. (2008). The clinical diagnostic utility of transcranial magnetic stimulation: report of an IFCN committee. *Clin. Neurophysiol.* 119, 504–532. doi: 10.1016/j.clinph.2007.10.014

Chen, L., Lau, A. G., and Sarti, F. (2014). Synaptic retinoic acid signaling and homeostatic synaptic plasticity. *Neuropharmacology* 78, 3–12. doi: 10.1016/j.neuropharm.2012.12.004

Chen, L., and Toth, M. (2001). Fragile X mice develop sensory hyperreactivity to auditory stimuli. *Neuroscience* 103, 1043–1050. doi: 10.1016/s0306-4522(01)00036-7

Chen, L., Yun, S. W., Seto, J., Liu, W., and Toth, M. (2003). The fragile x mental retardation protein binds and regulates a novel class of mRNAs containing u rich target sequences. *Neuroscience* 120, 1005–1017. doi: 10.1016/s0306-4522(03)00406-8

Chen, X., Yuan, L.-L., Zhao, C., Birnbaum, S. G., Frick, A., Jung, W. E., et al. (2006). Deletion of Kv4.2 gene eliminates dendritic A-type K+ current and enhances induction of long-term potentiation in hippocampal CA1 pyramidal neurons. *J. Neurosci.* 26, 12143–12151. doi: 10.1523/JNEUROSCI.2667-06.2006

Christie, S. B., Akins, M. R., Schwob, J. E., and Fallon, J. R. (2009). The FXG: a presynaptic fragile X granule expressed in a subset of developing brain circuits. *J. Neurosci.* 29, 1514–1524. doi: 10.1523/JNEUROSCI.3937-08.2009

Chuang, S. C., Zhao, W., Bauchwitz, R., Yan, Q., Bianchi, R., and Wong, R. K. (2005). Prolonged epileptiform discharges induced by altered group I metabotropic glutamate receptor-mediated synaptic responses in hippocampal slices of a fragile X mouse model. *J. Neurosci.* 25, 8048–8055. doi: 10.1523/JNEUROSCI.1777-05.2005

Collingridge, G. L., Peineau, S., Howland, J. G., and Wang, Y. T. (2010). Long-term depression in the CNS. *Nat. Rev. Neurosci.* 11, 459–473. doi: 10.1038/nrn2867

Comery, T. A., Harris, J. B., Willems, P. J., Oostra, B. A., Irwin, S. A., Weiler, I. J., et al. (1997). Abnormal dendritic spines in fragile X knockout mice: maturation and pruning deficits. *Proc. Natl. Acad. Sci. U S A* 94, 5401–5404. doi: 10.1073/pnas.94.10.5401

Contractor, A., Klyachko, V. A., and Portera-Cailliau, C. (2015). Altered neuronal and circuit excitability in fragile X syndrome. *Neuron* 87, 699–715. doi: 10.1016/j.neuron.2015.06.017

Cowley, B., Kirjanen, S., Partanen, J., and Castrén, M. L. (2016). Epileptic electroencephalography profile associates with attention problems in children with fragile X syndrome: review and case series. *Front. Hum. Neurosci.* 10:353. doi: 10.3389/fnhum.2016.00353

Cruz-Martín, A., Crespo, M., and Portera-Cailliau, C. (2010). Delayed stabilization of dendritic spines in fragile X mice. *J. Neurosci.* 30, 7793–7803. doi: 10.1523/JNEUROSCI.0577-10.2010

Curia, G., Papouin, T., Seguela, P., and Avoli, M. (2009). Downregulation of tonic GABAergic inhibition in a mouse model of fragile X syndrome. *Cereb. Cortex* 19, 1515–1520. doi: 10.1093/cercor/bhn159

D'hulst, C., De Geest, N., Reeve, S. P., Van Dam, D., De Deyn, P. P., Hassan, B. A., et al. (2006). Decreased expression of the GABAA receptor in fragile X syndrome. *Brain Res.* 1121, 238–245. doi: 10.1016/j.brainres.2006.08.115

D'hulst, C., Heulens, I., Aa, N. V. D., Goffin, K., Koole, M., Porke, K., et al. (2015). Positron emission tomography (pet) quantification of GABAA receptors in the brain of fragile X patients. *PLoS One* 10:e0131486. doi: 10.1371/journal.pone.0131486

Danesi, C., Achuta, V. S., Corcoran, P., Peteri, U. K., Turconi, G., Matsui, N., et al. (2018). Increased calcium influx through L-type calcium channels in human and mouse neural progenitors lacking fragile X mental retardation protein. *Stem Cell Rep.* 11, 1449–1461. doi: 10.1016/j.stemcr.2018.11.003

Darnell, J. C., Van Driesche, S. J., Zhang, C., Hung, K. Y., Mele, A., Fraser, C. E., et al. (2011). FMRP stalls ribosomal translocation on mRNAs linked to synaptic function and autism. *Cell* 146, 247–261. doi: 10.1016/j.cell.2011.06.013

Davis, G. W. (2006). Homeostatic control of neural activity: from phenomenology to molecular design. *Ann. Rev. Neurosci.* 29, 307–323. doi: 10.1146/annurev.neuro.28.061604.135751

de Vrij, F. M. S., Levenga, J., Van Der Linde, H. C., Koekkoek, S. K., De Zeeuw, C. I., Nelson, D. L., et al. (2008). Rescue of behavioral phenotype and neuronal protrusion morphology in Fmr1 KO mice. *Neurobiol. Dis.* 31, 127–132. doi: 10.1016/j.nbd.2008.04.002

Defelipe, J., López-Cruz, P. L., Benavides-Piccione, R., Bielza, C., Larrañaga, P., Anderson, S., et al. (2013). New insights into the classification and nomenclature of cortical GABAergic interneurons. *Nat. Rev. Neurosci.* 14, 202–216. doi: 10.1038/nrn3444

Deng, P.-Y., Carlin, D., Oh, Y. M., Myrick, L. K., Warren, S. T., Cavalli, V., et al. (2019). Voltage-independent SK-channel dysfunction causes neuronal hyperexcitability in the hippocampus of Fmr1 knock-out mice. *J. Neurosci.* 39, 28–43. doi: 10.1523/JNEUROSCI.1593-18.2018

Deng, P.-Y., and Klyachko, V. A. (2016a). Increased persistent sodium current causes neuronal hyperexcitability in the entorhinal cortex of Fmr1 knockout mice. *Cell Rep.* 16, 3157–3166. doi: 10.1016/j.celrep.2016.08.046

Deng, P.-Y., and Klyachko, V. A. (2016b). Genetic upregulation of BK channel activity normalizes multiple synaptic and circuit defects in a mouse model of fragile X syndrome. *J. Physiol.* 594, 83–97. doi: 10.1113/JP271031

Deng, P.-Y., and Klyachko, V. A. (2021). Channelopathies in fragile X syndrome. *Nat. Rev. Neurosci.* 22, 275–289. doi: 10.1038/s41583-021-00445-9

Deng, P.-Y., Rotman, Z., Blundon, J. A., Cho, Y., Cui, J., Cavalli, V., et al. (2013). FMRP regulates neurotransmitter release and synaptic information transmission by modulating action potential duration *via* BK channels. *Neuron* 77, 696–711. doi: 10.1016/j.neuron.2012.12.018

Desai, N. S., Rutherford, L. C., and Turrigiano, G. G. (1999). Plasticity in the intrinsic excitability of cortical pyramidal neurons. *Nat. Neurosci.* 2, 515–520. doi: 10.1038/9165

Devys, D., Lutz, Y., Rouyer, N., Bellocq, J. P., and Mandel, J. L. (1993). The FMR-1 protein is cytoplasmic, most abundant in neurons and appears normal in carriers of a fragile X premutation. *Nat. Genet.* 4, 335–340. doi: 10.1038/ng0893-335

Diering, G. H., Gustina, A. S., and Huganir, R. L. (2014). PKA-GluA1 coupling *via* AKAP5 controls AMPA receptor phosphorylation and cell-surface targeting during bidirectional homeostatic plasticity. *Neuron* 84, 790–805. doi: 10.1016/j.neuron.2014.09.024

Domanski, A. P. F., Booker, S. A., Wyllie, D. J. A., Isaac, J. T. R., and Kind, P. C. (2019). Cellular and synaptic phenotypes lead to disrupted information processing in Fmr1–KO mouse layer 4 barrel cortex. *Nat. Commun.* 10:4814. doi: 10.1038/s41467-019-12736-y

El-Hassar, L., Song, L., Tan, W. J. T., Large, C. H., Alvaro, G., Santos-Sacchi, J., et al. (2019). Modulators of Kv3 Potassium channels rescue the auditory function of fragile X mice. *J. Neurosci.* 39, 4797–4813. doi: 10.1523/JNEUROSCI.0839-18.2019

El Idrissi, A., Ding, X.-H., Scalia, J., Trenkner, E., Brown, W. T., and Dobkin, C. (2005). Decreased GABA(A) receptor expression in the seizure-prone fragile X mouse. *Neurosci. Lett.* 377, 141–146. doi: 10.1016/j.neulet.2004.11.087

Elmer, B. M., and Mcallister, A. K. (2012). Major histocompatibility complex class I proteins in brain development and plasticity. *Trends Neurosci.* 35, 660–770. doi: 10.1016/j.tins.2012.08.001

Errijgers, V., Fransen, E., D'hooge, R., De Deyn, P. P., and Kooy, R. F. (2008). Effect of genetic background on acoustic startle response in fragile X knockout mice. *Genet. Res. (Camb)* 90, 341–345. doi: 10.1017/S0016672308009415

Ethridge, L. E., White, S. P., Mosconi, M. W., Wang, J., Byerly, M. J., and Sweeney, J. A. (2016). Reduced habituation of auditory evoked potentials indicate cortical hyper-excitability in Fragile X Syndrome. *Transl. Psychiatry* 6:e787. doi: 10.1038/tp.2016.48

Ethridge, L. E., White, S. P., Mosconi, M. W., Wang, J., Pedapati, E. V., Erickson, C. A., et al. (2017). Neural synchronization deficits linked to cortical hyper-excitability and auditory hypersensitivity in fragile X syndrome. *Mol. Autism* 8:22. doi: 10.1186/s13229-017-0140-1

Fahling, M., Mrowka, R., Steege, A., Kirschner, K. M., Benko, E., Forstera, B., et al. (2009). Translational regulation of the human achaete-scute homologue-1 by fragile X mental retardation protein. *J. Biol. Chem.* 284, 4255–4266. doi: 10.1074/jbc.M807354200

Farrant, M., and Nusser, Z. (2005). Variations on an inhibitory theme: phasic and tonic activation of GABAA receptors. *Nat. Rev. Neurosci.* 6, 215–229. doi: 10.1038/nrn1625

Faust, T. E., Gunner, G., and Schafer, D. P. (2021). Mechanisms governing activity-dependent synaptic pruning in the developing mammalian CNS. *Nat. Rev. Neurosci.* 22, 657–673. doi: 10.1038/s41583-021-00507-y

Feng, Y., Absher, D., Eberhart, D. E., Brown, V., Malter, H. E., and Warren, S. T. (1997). FMRP associates with polyribosomes as an mRNP and the I304N mutation of severe fragile X syndrome abolishes this association. *Mol. Cell* 1, 109–118. doi: 10.1016/s1097-2765(00)80012-x

Ferron, L., Nieto-Rostro, M., Cassidy, J. S., and Dolphin, A. C. (2014). Fragile X mental retardation protein controls synaptic vesicle exocytosis by modulating N-type calcium channel density. *Nat. Commun.* 5:3628. doi: 10.1038/ncomms4628

Franco, L. M., Okray, Z., Linneweber, G. A., Hassan, B. A., and Yaksi, E. (2017). Reduced lateral inhibition impairs olfactory computations and behaviors in a drosophila model of fragile X syndrome. *Curr. Biol.* 27, 1111–1123. doi: 10.1016/j.cub.2017.02.065

Frankland, P. W., Wang, Y., Rosner, B., Shimizu, T., Balleine, B. W., Dykens, E. M., et al. (2004). Sensorimotor gating abnormalities in young males with fragile X syndrome and Fmr1-knockout mice. *Mol. Psychiatry* 9, 417–425. doi: 10.1038/sj.mp.4001432

Frere, S., and Slutsky, I. (2018). Alzheimer's disease: from firing instability to homeostasis network collapse. *Neuron* 97, 32–58. doi: 10.1016/j.neuron.2017.11.028

Gainey, M. A., Hurvitz-Wolff, J. R., Lambo, M. E., and Turrigiano, G. G. (2009). Synaptic scaling requires the GluR2 subunit of the AMPA receptor. *J. Neurosci.* 29, 6479–6489. doi: 10.1523/JNEUROSCI.3753-08.2009

Galvez, R., and Greenough, W. T. (2005). Sequence of abnormal dendritic spine development in primary somatosensory cortex of a mouse model of the fragile X mental retardation syndrome. *Am. J. Med. Genet. A* 135, 155–160. doi: 10.1002/ajmg.a.30709

Gantois, I., Vandesompele, J., Speleman, F., Reyniers, E., D'hooge, R., Severijnen, L.-A., et al. (2006). Expression profiling suggests underexpression of the GABA(A) receptor subunit delta in the fragile X knockout mouse model. *Neurobiol. Dis.* 21, 346–357. doi: 10.1016/j.nbd.2005.07.017

Garcia-Pino, E., Gessele, N., and Koch, U. (2017). Enhanced excitatory connectivity and disturbed sound processing in the auditory brainstem of fragile X mice. *J. Neurosci.* 37, 7403–7419. doi: 10.1523/JNEUROSCI.2310-16.2017

Gatto, C. L., Pereira, D., and Broadie, K. (2014). GABAergic circuit dysfunction in the Drosophila Fragile X syndrome model. *Neurobiol. Dis.* 65, 142–159. doi: 10.1016/j.nbd.2014.01.008

Gauthey, M., Poloni, C. B., Ramelli, G. P., Roulet-Perez, E., and Korff, C. M. (2010). Status epilepticus in fragile X syndrome. *Epilepsia* 51, 2470–2473. doi: 10.1111/j.1528-1167.2010.02761.x

Gholizadeh, S., Halder, S. K., and Hampson, D. R. (2015). Expression of fragile X mental retardation protein in neurons and glia of the developing and adult mouse brain. *Brain Res.* 1596, 22–30. doi: 10.1016/j.brainres.2014.11.023

Gibson, J. R., Bartley, A. F., Hays, S. A., and Huber, K. M. (2008). Imbalance of neocortical excitation and inhibition and altered UP states reflect network hyperexcitability in the mouse model of fragile X syndrome. *J. Neurophysiol.* 100, 2615–2626. doi: 10.1152/jn.90752.2008

Gladding, C. M., Fitzjohn, S. M., and Molnar, E. (2009). Metabotropic glutamate receptor-mediated long-term depression: molecular mechanisms. *Pharmacol. Rev.* 61, 395–412. doi: 10.1124/pr.109.001735

Goddard, C. A., Butts, D. A., and Shatz, C. J. (2007). Regulation of CNS synapses by neuronal MHC class I. *Proc. Natl. Acad. Sci. U S A* 104, 6828–6833. doi: 10.1073/pnas.0702023104

Godfraind, J. M., Reyniers, E., De Boulle, K., D'hooge, R., De Deyn, P. P., Bakker, C. E., et al. (1996). Long-term potentiation in the hippocampus of fragile X knockout mice. *Am. J. Med. Genet.* 64, 246–251. doi: 10.1002/(SICI)1096-8628(19960809)64:2<246::AID-AJMG2>3.0.CO;2-S

Goel, A., Cantu, D. A., Guilfoyle, J., Chaudhari, G. R., Newadkar, A., Todisco, B., et al. (2018). Impaired perceptual learning in a mouse model of Fragile X syndrome is mediated by parvalbumin neuron dysfunction and is reversible. *Nat. Neurosci.* 21, 1404–1411. doi: 10.1038/s41593-018-0231-0

Goel, A., Jiang, B., Xu, L. W., Song, L., Kirkwood, A., and Lee, H. K. (2006). Cross-modal regulation of synaptic AMPA receptors in primary sensory cortices by visual experience. *Nat. Neurosci.* 9, 1001–1003. doi: 10.1038/nn1725

Goel, A., Xu, L. W., Snyder, K. P., Song, L., Goenaga-Vazquez, Y., Megill, A., et al. (2011). Phosphorylation of ampa receptors is required for sensory deprivation-induced homeostatic synaptic plasticity. *PLoS One* 6:e18264. doi: 10.1371/journal.pone.0018264

Golden, C. E. M., Breen, M. S., Koro, L., Sonar, S., Niblo, K., Browne, A., et al. (2019). Deletion of the KH1 domain of Fmr1 leads to transcriptional alterations and attentional deficits in rats. *Cereb. Cortex* 29, 2228–2244. doi: 10.1093/cercor/bhz029

Goncalves, J. T., Anstey, J. E., Golshani, P., and Portera-Cailliau, C. (2013). Circuit level defects in the developing neocortex of Fragile X mice. *Nat. Neurosci.* 16, 903–909. doi: 10.1038/nn.3415

Gonzalez, D., Tomasek, M., Hays, S., Sridhar, V., Ammanuel, S., Chang, C. W., et al. (2019). Audiogenic seizures in the Fmr1 knock-out mouse are induced by Fmr1 deletion in subcortical, VGlut2-expressing excitatory neurons and require deletion in the inferior colliculus. *J. Neurosci.* 39, 9852–9863. doi: 10.1523/JNEUROSCI.0886-19.2019

Gonzalez-Islas, C., and Wenner, P. (2006). Spontaneous network activity in the embryonic spinal cord regulates AMPAergic and GABAergic synaptic strength. *Neuron* 49, 563–575. doi: 10.1016/j.neuron.2006.01.017

Goswami, S., Cavalier, S., Sridhar, V., Huber, K. M., and Gibson, J. R. (2019). Local cortical circuit correlates of altered EEG in the mouse model of Fragile X syndrome. *Neurobiol. Dis.* 124, 563–572. doi: 10.1016/j.nbd.2019.01.002

Gross, C., Yao, X., Pong, D. L., Jeromin, A., and Bassell, G. J. (2011). Fragile X mental retardation protein regulates protein expression and mrna translation of the potassium channel Kv4.2. *J. Neurosci.* 31, 5693–5698. doi: 10.1523/JNEUROSCI.6661-10.2011

Grothe, B., Pecka, M., and Mcalpine, D. (2010). Mechanisms of sound localization in mammals. *Physiol. Rev.* 90, 983–1012. doi: 10.1152/physrev.00026.2009

Guo, W., Molinaro, G., Collins, K. A., Hays, S. A., Paylor, R., Worley, P. F., et al. (2016). Selective disruption of metabotropic glutamate receptor 5-homer interactions mimics phenotypes of fragile X syndrome in mice. *J. Neurosci.* 36, 2131–2147. doi: 10.1523/JNEUROSCI.2921-15.2016

Hagerman, R. J., Berry-Kravis, E., Hazlett, H. C., Bailey, D. B., Moine, H., Kooy, R. F., et al. (2017). Fragile X syndrome. *Nat. Rev. Dis. Primers* 3:17065. doi: 10.1038/nrdp.2017.65

Haider, B., Duque, A., Hasenstaub, A. R., and Mccormick, D. A. (2006). Neocortical network activity *in vivo* is generated through a dynamic balance of excitation and inhibition. *J. Neurosci.* 26, 4535–4545. doi: 10.1523/JNEUROSCI.5297-05.2006

Hammond, L. S., Macias, M. M., Tarleton, J. C., and Shashidhar Pai, G. (1997). Fragile X syndrome and deletions in FMR1: new case and review of the literature. *Am. J. Med. Genet.* 72, 430–434.

Hanson, J. E., and Madison, D. V. (2007). Presynaptic FMR1 genotype influences the degree of synaptic connectivity in a mosaic mouse model of fragile X syndrome. *J. Neurosci.* 27, 4014–4018. doi: 10.1523/JNEUROSCI.4717-06.2007

Harlow, E. G., Till, S. M., Russell, T. A., Wijetunge, L. S., Kind, P., and Contractor, A. (2010). Critical period plasticity is disrupted in the barrel cortex of Fmr1 knockout mice. *Neuron* 65, 385–398. doi: 10.1016/j.neuron.2010.01.024

Hays, S. A., Huber, K. M., and Gibson, J. R. (2011). Altered neocortical rhythmic activity states in Fmr1 KO mice are due to enhanced mGluR5 signaling and involve changes in excitatory circuitry. *J. Neurosci.* 31, 14223–14234. doi: 10.1523/JNEUROSCI.3157-11.2011

He, Q., Arroyo, E. D., Smukowski, S. N., Xu, J., Piochon, C., Savas, J. N., et al. (2018). Critical period inhibition of NKCC1 rectifies synapse plasticity in the somatosensory cortex and restores adult tactile response maps in

fragile X mice. *Mol. Psychiatry* 24, 1732–1747. doi: 10.1038/s41380-018-0048-y

He, C. X., Cantu, D. A., Mantri, S. S., Zeiger, W. A., Goel, A., and Portera-Cailliau, C. (2017). Tactile defensiveness and impaired adaptation of neuronal activity in the Fmr1 knock-out mouse model of autism. *J. Neurosci.* 37, 6475–6487. doi: 10.1523/JNEUROSCI.0651-17.2017

He, Q., Nomura, T., Xu, J., and Contractor, A. (2014). The developmental switch in GABA polarity is delayed in fragile X mice. *J. Neurosci.* 34, 446–450. doi: 10.1523/JNEUROSCI.4447-13.2014

He, C. X., and Portera-Cailliau, C. (2013). The trouble with spines in fragile X syndrome: density, maturity and plasticity. *Neuroscience* 251, 120–128. doi: 10.1016/j.neuroscience.2012.03.049

Henderson, C., Wijetunge, L., Kinoshita, M. N., Shumway, M., Hammond, R. S., Postma, F. R., et al. (2012). Reversal of disease-related pathologies in the fragile X mouse model by selective activation of GABAB receptors with arbaclofen. *Sci. Transl. Med.* 4:152ra128. doi: 10.1126/scitranslmed.3004218

Hessl, D. R., Berry-Kravis, E., Cordeiro, L., Yuhas, J., Ornitz, E. M., Campbell, A., et al. (2009). Prepulse inhibition in fragile X syndrome: feasibility, reliability and implications for treatment. *Am. J. Med. Genet. B. Neuropsychiatr. Genet.* 150B, 545–553. doi: 10.1002/ajmg.b.30858

Hinton, V. J., Brown, W. T., Wisniewski, K., and Rudelli, R. D. (1991). Analysis of neocortex in three males with the fragile X syndrome. *Am. J. Med. Genet.* 41, 289–294. doi: 10.1002/ajmg.1320410306

Hou, L., Antion, M. D., Hu, D., Spencer, C. M., Paylor, R., and Klann, E. (2006). Dynamic translational and proteasomal regulation of fragile X mental retardation protein controls mGluR-dependent long-term depression. *Neuron* 51, 441–454. doi: 10.1016/j.neuron.2006.07.005

Hu, H., Qin, Y., Bochorishvili, G., Zhu, Y., Van Aelst, L., and Zhu, J. J. (2008). Ras signaling mechanisms underlying impaired GluR1-dependent plasticity associated with fragile X syndrome. *J. Neurosci.* 28, 7847–7862. doi: 10.1523/JNEUROSCI.1496-08.2008

Huber, K. M., Gallagher, S. M., Warren, S. T., and Bear, M. F. (2002). Altered synaptic plasticity in a mouse model of fragile X mental retardation. *Proc. Natl. Acad. Sci. U S A* 99, 7746–7750. doi: 10.1073/pnas.122205699

Huber, K. M., Kayser, M. S., and Bear, M. F. (2000). Role for rapid dendritic protein synthesis in hippocampal mGluR-dependent long-term depression. *Science* 288, 1254–1257. doi: 10.1126/science.288.5469.1254

Ibata, K., Sun, Q., and Turrigiano, G. G. (2008). Rapid synaptic scaling induced by changes in postsynaptic firing. *Neuron* 57, 819–826. doi: 10.1016/j.neuron.2008.02.031

Irwin, S. A., Patel, B., Idupulapati, M., Harris, J. B., Crisostomo, R. A., Larsen, B. P., et al. (2001). Abnormal dendritic spine characteristics in the temporal and visual cortices of patients with fragile-X syndrome: a quantitative examination. *Am. J. Med. Genet.* 98, 161–167. doi: 10.1002/1096-8628(20010115)98:2<161::aid-ajmg1025>3.0.co;2-b

Jacquemont, S., Pacini, L., Jønch, A. E., Cencelli, G., Rozenberg, I., He, Y., et al. (2018). Protein synthesis levels are increased in a subset of individuals with fragile X syndrome. *Hum. Mol. Genet.* 27, 2039–2051. doi: 10.1093/hmg/ddy099

Janusz, A., Milek, J., Perycz, M., Pacini, L., Bagni, C., Kaczmarek, L., et al. (2013). The Fragile X mental retardation protein regulates matrix metalloproteinase 9 mRNA at synapses. *J. Neurosci.* 33, 18234–18241. doi: 10.1523/JNEUROSCI.2207-13.2013

Jewett, K. A., Lee, K. Y., Eagleman, D. E., Soriano, S., and Tsai, N. P. (2018). Dysregulation and restoration of homeostatic network plasticity in fragile X syndrome mice. *Neuropharmacology* 138, 182–192. doi: 10.1016/j.neuropharm.2018.06.011

Jewett, K. A., Zhu, J., and Tsai, N. P. (2015). The tumor suppressor p53 guides GluA1 homeostasis through Nedd4–2 during chronic elevation of neuronal activity. *J. Neurochem.* 135, 226–233. doi: 10.1111/jnc.13271

Jonak, C. R., Lovelace, J. W., Ethell, I. M., Razak, K. A., and Binder, D. K. (2020). Multielectrode array analysis of EEG biomarkers in a mouse model of Fragile X Syndrome. *Neurobiol. Dis.* 138:104794. doi: 10.1016/j.nbd.2020.104794

Joseph, A., and Turrigiano, G. G. (2017). All for one but not one for all: Excitatory synaptic scaling and intrinsic excitability are coregulated by CaMKIV, whereas inhibitory synaptic scaling is under independent control. *J. Neurosci.* 37, 6778–6785. doi: 10.1523/JNEUROSCI.0618-17.2017

Kang, Y., Zhou, Y., Li, Y., Han, Y., Xu, J., Niu, W., et al. (2021). A human forebrain organoid model of fragile X syndrome exhibits altered neurogenesis and highlights new treatment strategies. *Nat. Neurosci.* 24, 1377–1391. doi: 10.1038/s41593-021-00913-6

Kavalali, E. T., and Monteggia, L. M. (2020). Targeting homeostatic synaptic plasticity for treatment of mood disorders. *Neuron* 106, 715–726. doi: 10.1016/j.neuron.2020.05.015

Keck, T., Hübener, M., and Bonhoeffer, T. (2017). Interactions between synaptic homeostatic mechanisms: an attempt to reconcile BCM theory, synaptic scaling and changing excitation/inhibition balance. *Curr. Opin. Neurobiol.* 43, 87–93. doi: 10.1016/j.conb.2017.02.003

Kennedy, T., Rinker, D., and Broadie, K. (2020). Genetic background mutations drive neural circuit hyperconnectivity in a fragile X syndrome model. *BMC Biol.* 18:94. doi: 10.1186/s12915-020-00817-0

Kim, H., Gibboni, R., Kirkhart, C., and Bao, S. (2013). Impaired critical period plasticity in primary auditory cortex of fragile X model mice. *J. Neurosci.* 33, 15686–15692. doi: 10.1523/JNEUROSCI.3246-12.2013

Koekkoek, S. K., Yamaguchi, K., Milojkovic, B. A., Dortland, B. R., Ruigrok, T. J., Maex, R., et al. (2005). Deletion of FMR1 in Purkinje cells enhances parallel fiber LTD, enlarges spines and attenuates cerebellar eyelid conditioning in Fragile X syndrome. *Neuron* 47, 339–352. doi: 10.1016/j.neuron.2005.07.005

Koga, K., Liu, M.-G., Qiu, S., Song, Q., O'den, G., Chen, T., et al. (2015). Impaired presynaptic long-term potentiation in the anterior cingulate cortex of Fmr1 knock-out mice. *J. Neurosci.* 35, 2033–2043. doi: 10.1523/JNEUROSCI.2644-14.2015

Kokash, J., Alderson, E. M., Reinhard, S. M., Crawford, C. A., Binder, D. K., Ethell, I. M., et al. (2019). Genetic reduction of MMP-9 in the Fmr1 KO mouse partially rescues prepulse inhibition of acoustic startle response. *Brain Res.* 1719, 24–29. doi: 10.1016/j.brainres.2019.05.029

Kozono, N., Okamura, A., Honda, S., Matsumoto, M., and Mihara, T. (2020). Gamma power abnormalities in a Fmr1-targeted transgenic rat model of fragile X syndrome. *Sci. Rep.* 10:18799. doi: 10.1038/s41598-020-75893-x

Krueger, D. D., and Bear, M. F. (2011). Toward fulfilling the promise of molecular medicine in fragile X syndrome. *Annu. Rev. Med.* 62, 411–429. doi: 10.1146/annurev-med-061109-134644

Kujirai, T., Caramia, M. D., Rothwell, J. C., Day, B. L., Thompson, P. D., Ferbert, A., et al. (1993). Corticocortical inhibition in human motor cortex. *J. Physiol.* 471, 501–519. doi: 10.1113/jphysiol.1993.sp019912

Landau, I. D., Egger, R., Dercksen, V. J., Oberlaender, M., and Sompolinsky, H. (2016). The impact of structural heterogeneity on excitation-inhibition balance in cortical networks. *Neuron* 92, 1106–1121. doi: 10.1016/j.neuron.2016.10.027

Lauer, A. M., Behrens, D., and Klump, G. (2017). Acoustic startle modification as a tool for evaluating auditory function of the mouse: Progress, pitfalls and potential. *Neurosci. Biobehav. Rev.* 77, 194–208. doi: 10.1016/j.neubiorev.2017.03.009

Lauterborn, J. C., Rex, C. S., Kramar, E., Chen, L. Y., Pandyarajan, V., Lynch, G., et al. (2007). Brain-derived neurotrophic factor rescues synaptic plasticity in a mouse model of fragile X syndrome. *J. Neurosci.* 27, 10685–10694. doi: 10.1523/JNEUROSCI.2624-07.2007

Lee, H. H. C., Bernard, C., Ye, Z., Acampora, D., Simeone, A., Prochiantz, A., et al. (2017). Genetic Otx2 mis-localization delays critical period plasticity across brain regions. *Mol. Psychiatry* 22:785. doi: 10.1038/mp.2017.83

Lee, H. Y., Ge, W.-P., Huang, W., He, Y., Wang, G. X., Rowson-Baldwin, A., et al. (2011). Bidirectional regulation of dendritic voltage-gated potassium channels by the fragile X mental retardation protein. *Neuron* 72, 630–642. doi: 10.1016/j.neuron.2011.09.033

Lee, K. Y., Jewett, K. A., Chung, H. J., and Tsai, N. P. (2018). Loss of fragile X protein FMRP impairs homeostatic synaptic downscaling through tumor suppressor p53 and ubiquitin E3 ligase Nedd4–2. *Hum. Mol. Genet.* 27, 2805–2816. doi: 10.1093/hmg/ddy189

Leigh, M. J., Nguyen, D. V., Mu, Y., Winarni, T. I., Schneider, A., Chechi, T., et al. (2013). A randomized double-blind, placebo-controlled trial of minocycline in children and adolescents with fragile x syndrome. *J. Dev. Behav. Pediatr.* 34, 147–155. doi: 10.1097/DBP.0b013e318287cd17

Lensjo, K. K., Lepperod, M. E., Dick, G., Hafting, T., and Fyhn, M. (2017). Removal of perineuronal nets unlocks juvenile plasticity through network mechanisms of decreased inhibition and increased gamma activity. *J. Neurosci.* 37, 1269–1283. doi: 10.1523/JNEUROSCI.2504-16.2016

Lin, A., Hou, Q., Jarzylo, L., Amato, S., Gilbert, J., Shang, F., et al. (2011). Nedd4-mediated AMPA receptor ubiquitination regulates receptor turnover and trafficking. *J. Neurochem.* 119, 27–39. doi: 10.1111/j.1471-4159.2011.07221.x

Liu, D. C., Lee, K. Y., Lizarazo, S., Cook, J. K., and Tsai, N. P. (2021). ER stress-induced modulation of neural activity and seizure susceptibility is impaired in a fragile X syndrome mouse model. *Neurobiol. Dis.* 158:105450. doi: 10.1016/j.nbd.2021.105450

Lovelace, J. W., Ethell, I. M., Binder, D. K., and Razak, K. A. (2018). Translation-relevant EEG phenotypes in a mouse model of Fragile X Syndrome. *Neurobiol. Dis.* 115, 39–48. doi: 10.1016/j.nbd.2018.03.012

Lovelace, J. W., Rais, M., Palacios, A. R., Shuai, X. S., Bishay, S., Popa, O., et al. (2020). Deletion of Fmr1 from forebrain excitatory neurons triggers abnormal cellular, eeg and behavioral phenotypes in the auditory cortex of a mouse model of fragile X syndrome. *Cereb. Cortex* 30, 969–988. doi: 10.1093/cercor/bhz141

Lovelace, J. W., Wen, T. H., Reinhard, S., Hsu, M. S., Sidhu, H., Ethell, I. M., et al. (2016). Matrix metalloproteinase-9 deletion rescues auditory evoked potential habituation deficit in a mouse model of Fragile X Syndrome. *Neurobiol. Dis.* 89, 126–135. doi: 10.1016/j.nbd.2016.02.002

Lozano, R., Rosero, C. A., and Hagerman, R. J. (2014). Fragile X spectrum disorders. *Intractable Rare Dis. Res.* 3, 134–146. doi: 10.5582/irdr.2014.01022

Maccarrone, M., Rossi, S., Bari, M., De Chiara, V., Rapino, C., Musella, A., et al. (2010). Abnormal mGlu 5 receptor/endocannabinoid coupling in mice lacking FMRP and BC1 RNA. *Neuropsychopharmacology* 35, 1500–1509. doi: 10.1038/npp.2010.19

Maffei, A., Nelson, S. B., and Turrigiano, G. G. (2004). Selective reconfiguration of layer 4 visual cortical circuitry by visual deprivation. *Nat. Neurosci.* 7, 1353–1359. doi: 10.1038/nn1351

Marder, E., and Prinz, A. A. (2003). Current compensation in neuronal homeostasis. *Neuron* 37, 2–4. doi: 10.1016/s0896-6273(02)01173-x

Marshall, L., and Brandt, J. F. (1980). The relationship between loudness and reaction time in normal hearing listeners. *Acta Otolaryngol.* 90, 244–249. doi: 10.3109/00016488009131721

Martin, B. S., Corbin, J. G., and Huntsman, M. M. (2014). Deficient tonic GABAergic conductance and synaptic balance in the fragile X syndrome amygdala. *J. Neurophysiol.* 112, 890–902. doi: 10.1152/jn.00597.2013

McCamphill, P. K., Stoppel, L. J., Senter, R. K., Lewis, M. C., Heynen, A. J., Stoppel, D. C., et al. (2020). Selective inhibition of glycogen synthase kinase 3α corrects pathophysiology in a mouse model of fragile X syndrome. *Sci. Transl. Med.* 12:eaam8572. doi: 10.1126/scitranslmed.aam8572

Mccullagh, E. A., Poleg, S., Greene, N. T., Huntsman, M. M., Tollin, D. J., and Klug, A. (2020). Characterization of auditory and binaural spatial hearing in a fragile X syndrome mouse model. *eNeuro* 7:ENEURO.0300-0319.2019. doi: 10.1523/ENEURO.0300-19.2019

Mccullagh, E. A., Salcedo, E., Huntsman, M. M., and Klug, A. (2017). Tonotopic alterations in inhibitory input to the medial nucleus of the trapezoid body in a mouse model of Fragile X syndrome. *J. Comp. Neurol.* 525, 3543–3562. doi: 10.1002/cne.24290

Mckinney, B. C., Grossman, A. W., Elisseou, N. M., and Greenough, W. T. (2005). Dendritic spine abnormalities in the occipital cortex of C57BL/6 Fmr1 knockout mice. *Am. J. Med. Genet. B. Neuropsychiatr. Genet.* 136B, 98–102. doi: 10.1002/ajmg.b.30183

Meredith, R. M., Holmgren, C. D., Weidum, M., Burnashev, N., and Mansvelder, H. D. (2007). Increased threshold for spike-timing-dependent plasticity is caused by unreliable calcium signaling in mice lacking fragile X gene Fmr1. *Neuron* 54, 627–638. doi: 10.1016/j.neuron.2007.04.028

Micheva, K. D., and Beaulieu, C. (1996). Quantitative aspects of synaptogenesis in the rat barrel field cortex with special reference to GABA circuitry. *J. Comp. Neurol.* 373, 340–354. doi: 10.1002/(SICI)1096-9861(19960923)373:3<340::AID-CNE3>3.0.CO;2-2

Miller, E. A., Kastner, D. B., Grzybowski, M. N., Dwinell, M. R., Geurts, A. M., and Frank, L. M. (2021). Robust and replicable measurement for prepulse inhibition of the acoustic startle response. *Mol. Psychiatry* 26, 1909–1927. doi: 10.1038/s41380-020-0703-y

Miller, L. J., Mcintosh, D. N., Mcgrath, J., Shyu, V., Lampe, M., Taylor, A. K., et al. (1999). Electrodermal responses to sensory stimuli in individuals with fragile X syndrome: a preliminary report. *Am. J. Med. Genet.* 83, 268–279.

Morgan, P. J., Bourboulou, R., Filippi, C., Koenig-Gambini, J., and Epsztein, J. (2019). Kv1.1 contributes to a rapid homeostatic plasticity of intrinsic excitability in CA1 pyramidal neurons *in vivo*. *eLife* 8:e49915. doi: 10.7554/eLife.49915

Morin-Parent, F., Champigny, C., Lacroix, A., Corbin, F., and Lepage, J.-F. (2019). Hyperexcitability and impaired intracortical inhibition in patients with fragile-X syndrome. *Transl. Psychiatry* 9:312. doi: 10.1038/s41398-019-0650-z

Motanis, H., and Buonomano, D. (2020). Decreased reproducibility and abnormal experience-dependent plasticity of network dynamics in Fragile X circuits. *Sci. Rep.* 10:14535. doi: 10.1038/s41598-020-71333-y

Murase, S., Lantz, C. L., and Quinlan, E. M. (2017). Light reintroduction after dark exposure reactivates plasticity in adults *via* perisynaptic activation of MMP-9. *eLife* 6:e27345. doi: 10.7554/eLife.27345

Musumeci, S. A., Bosco, P., Calabrese, G., Bakker, C., De Sarro, G. B., Elia, M., et al. (2000). Audiogenic seizures susceptibility in transgenic mice with fragile X syndrome. *Epilepsia* 41, 19–23. doi: 10.1111/j.1528-1157.2000.tb01499.x

Musumeci, S. A., Hagerman, R. J., Ferri, R., Bosco, P., Dalla Bernardina, B., Tassinari, C. A., et al. (1999). Epilepsy and EEG findings in males with fragile X syndrome. *Epilepsia* 40, 1092–1099. doi: 10.1111/j.1528-1157.1999.tb00824.x

Myrick, L. K., Deng, P.-Y., Hashimoto, H., Oh, Y. M., Cho, Y., Poidevin, M. J., et al. (2015). Independent role for presynaptic FMRP revealed by an FMR1 missense mutation associated with intellectual disability and seizures. *Proc. Natl. Acad. Sci. U S A* 112, 949–956. doi: 10.1073/pnas.1423094112

Myrick, L. K., Nakamoto-Kinoshita, M., Lindor, N. M., Kirmani, S., Cheng, X., and Warren, S. T. (2014). Fragile X syndrome due to a missense mutation. *Eur. J. Hum. Genet.* 22, 1185–1189. doi: 10.1038/ejhg.2013.311

Napoli, I., Mercaldo, V., Boyl, P. P., Eleuteri, B., Zalfa, F., De Rubeis, S., et al. (2008). The fragile X syndrome protein represses activity-dependent translation through CYFIP1, a new 4E-BP. *Cell* 134, 1042–1054. doi: 10.1016/j.cell.2008.07.031

Nelson, S. B., and Valakh, V. (2015). Excitatory/inhibitory balance and circuit homeostasis in autism spectrum disorders. *Neuron* 87, 684–698. doi: 10.1016/j.neuron.2015.07.033

Nielsen, D. M., Derber, W. J., Mcclellan, D. A., and Crnic, L. S. (2002). Alterations in the auditory startle response in Fmr1 targeted mutant mouse models of fragile X syndrome. *Brain Res.* 927, 8–17. doi: 10.1016/s0006-8993(01)03309-1

Niere, F., Wilkerson, J. R., and Huber, K. M. (2012). Evidence for a fragile X mental retardation protein-mediated translational switch in metabotropic glutamate receptor-triggered Arc translation and long-term depression. *J. Neurosci.* 32, 5924–5936. doi: 10.1523/JNEUROSCI.4650-11.2012

Nimchinsky, E. A., Oberlander, A. M., and Svoboda, K. (2001). Abnormal development of dendritic spines in FMR1 knock-out mice. *J. Neurosci.* 21, 5139–5146. doi: 10.1523/JNEUROSCI.21-14-05139.2001

Nosyreva, E. D., and Huber, K. M. (2006). Metabotropic receptor-dependent long-term depression persists in the absence of protein synthesis in the mouse model of fragile X syndrome. *J. Neurophysiol.* 95, 3291–3295. doi: 10.1152/jn.01316.2005

O'donnell, C., Goncalves, J. T., Portera-Cailliau, C., and Sejnowski, T. J. (2017). Beyond excitation/inhibition imbalance in multidimensional models of neural circuit changes in brain disorders. *eLife* 6:e26724. doi: 10.7554/eLife.26724

Oh, W. C., and Smith, K. R. (2019). Activity-dependent development of GABAergic synapses. *Brain Res.* 1707, 18–26. doi: 10.1016/j.brainres.2018.11.014

Olmos-Serrano, J. L., Corbin, J. G., and Burns, M. P. (2011). The GABA(A) receptor agonist THIP ameliorates specific behavioral deficits in the mouse model of fragile X syndrome. *Dev. Neurosci.* 33, 395–403. doi: 10.1159/000332884

Olmos-Serrano, J. L., Paluszkiewicz, S. M., Martin, B. S., Kaufmann, W. E., Corbin, J. G., and Huntsman, M. M. (2010). Defective GABAergic neurotransmission and pharmacological rescue of neuronal hyperexcitability in the amygdala in a mouse model of fragile X syndrome. *J. Neurosci.* 30, 9929–9938. doi: 10.1523/JNEUROSCI.1714-10.2010

Orefice, L. L., Zimmerman, A. L., Chirila, A. M., Sleboda, S. J., Head, J. P., and Ginty, D. D. (2016). Peripheral mechanosensory neuron dysfunction underlies tactile and behavioral deficits in mouse models of ASDs. *Cell* 166, 299–313. doi: 10.1016/j.cell.2016.05.033

Osterweil, E. K., Chuang, S. C., Chubykin, A. A., Sidorov, M., Bianchi, R., Wong, R. K., et al. (2013). Lovastatin corrects excess protein synthesis and prevents epileptogenesis in a mouse model of fragile X syndrome. *Neuron* 77, 243–250. doi: 10.1016/j.neuron.2012.01.034

Osterweil, E. K., Krueger, D. D., Reinhold, K., and Bear, M. F. (2010). Hypersensitivity to mGluR5 and ERK1/2 leads to excessive protein synthesis in the hippocampus of a mouse model of fragile X syndrome. *J. Neurosci.* 30, 15616–15627. doi: 10.1523/JNEUROSCI.3888-10.2010

Pak, A., Kissinger, S. T., and Chubykin, A. A. (2021). Impaired adaptation and laminar processing of the oddball paradigm in the primary visual cortex of Fmr1 KO mouse. *Front. Cell. Neurosci.* 15:668230. doi: 10.3389/fncel.2021.668230

Paluszkiewicz, S. M., Olmos-Serrano, J. L., Corbin, J. G., and Huntsman, M. M. (2011). Impaired inhibitory control of cortical synchronization in fragile X syndrome. *J. Neurophysiol.* 106, 2264–2272. doi: 10.1152/jn.00421.2011

Pan, F., Aldridge, G. M., Greenough, W. T., and Gan, W.-B. (2010). Dendritic spine instability and insensitivity to modulation by sensory experience in a mouse model of fragile X syndrome. *Proc. Natl. Acad. Sci. U S A* 107, 17768–17773. doi: 10.1073/pnas.1012496107

Pan, L., Zhang, Y. Q., Woodruff, E., and Broadie, K. (2004). The drosophila fragile X gene negatively regulates neuronal elaboration and synaptic differentiation. *Curr. Biol.* 14, 1863–1870. doi: 10.1016/j.cub.2004.09.085

Paradee, W., Melikian, H. E., Rasmussen, D. L., Kenneson, A., Conn, P. J., and Warren, S. T. (1999). Fragile X mouse: strain effects of knockout phenotype and evidence suggesting deficient amygdala function. *Neuroscience* 94, 185–192. doi: 10.1016/s0306-4522(99)00285-7

Park, T. J., Grothe, B., Pollak, G. D., Schuller, G., and Koch, U. (1996). Neural delays shape selectivity to interaural intensity differences in the lateral superior olive. *J. Neurosci.* 16, 6554–6566. doi: 10.1523/JNEUROSCI.16-20-06554.1996

Park, E., Lau, A. G., Arendt, K. L., and Chen, L. (2021). Fmrp interacts with rarα in synaptic retinoic acid signaling and homeostatic synaptic plasticity. *Int. J. Mol. Sci.* 22:6579. doi: 10.1038/s41386-018-0150-5

Partanen, E., Kujala, T., Naatanen, R., Liitola, A., Sambeth, A., and Huotilainen, M. (2013). Learning-induced neural plasticity of speech processing before birth. *Proc. Natl. Acad. Sci. U S A* 110, 15145–15150. doi: 10.1073/pnas.1302159110

Patel, A. B., Hays, S. A., Bureau, I., Huber, K. M., and Gibson, J. R. (2013). A target cell-specific role for presynaptic Fmr1 in regulating glutamate release onto neocortical fast-spiking inhibitory neurons. *J. Neurosci.* 33, 2593–2604. doi: 10.1523/JNEUROSCI.2447-12.2013

Patel, A. B., Loerwald, K. W., Huber, K. M., and Gibson, J. R. (2014). Postsynaptic FMRP promotes the pruning of cell-to-cell connections among pyramidal neurons in the L5A neocortical network. *J. Neurosci.* 34, 3413–3418. doi: 10.1523/JNEUROSCI.2921-13.2014

Paylor, R., Yuva-Paylor, L. A., Nelson, D. L., and Spencer, C. M. (2008). Reversal of sensorimotor gating abnormalities in Fmr1 knockout mice carrying a human Fmr1 transgene. *Behav. Neurosci.* 122, 1371–1377. doi: 10.1037/a0013047

Pfeffer, C. K., Xue, M., He, M., Huang, Z. J., and Scanziani, M. (2013). Inhibition of inhibition in visual cortex: the logic of connections between molecularly distinct interneurons. *Nat. Neurosci.* 16, 1068–1076. doi: 10.1038/nn.3446

Pfeiffer, B. E., Zang, T., Wilkerson, J. R., Taniguchi, M., Maksimova, M. A., Smith, L. N., et al. (2010). Fragile X mental retardation protein is required for synapse elimination by the activity-dependent transcription factor MEF2. *Neuron* 66, 191–197. doi: 10.1016/j.neuron.2010.03.017

Pinard, A., Seddik, R., and Bettler, B. (2010). GABAB receptors: physiological functions and mechanisms of diversity. *Adv. Pharmacol.* 58, 231–255. doi: 10.1016/S1054-3589(10)58010-4

Pizzorusso, T., Medini, P., Berardi, N., Chierzi, S., Fawcett, J. W., and Maffei, L. (2002). Reactivation of ocular dominance plasticity in the adult visual cortex. *Science* 298, 1248–1251. doi: 10.1126/science.1072699

Qiu, L. F., Hao, Y. H., Li, Q. Z., and Xiong, Z. Q. (2008). Fragile X syndrome and epilepsy. *Neurosci. Bull.* 24, 338–344. doi: 10.1007/s12264-008-1221-0

Qiu, L. F., Lu, T. J., Hu, X. L., Yi, Y. H., Liao, W. P., and Xiong, Z. Q. (2009). Limbic epileptogenesis in a mouse model of fragile X syndrome. *Cereb. Cortex* 19, 1504–1514. doi: 10.1093/cercor/bhn163

Qin, M., Schmidt, K. C., Zametkin, A. J., Bishu, S., Horowitz, L. M., Burlin, T. V., et al. (2013). Altered cerebral protein synthesis in fragile X syndrome: studies in human subjects and knockout mice. *J. Cereb. Blood Flow Metab.* 33, 499–507. doi: 10.1038/jcbfm.2012.205

Radziwon, K., and Salvi, R. (2020). Using auditory reaction time to measure loudness growth in rats. *Hear. Res.* 395:108026. doi: 10.1016/j.heares.2020.108026

Rais, M., Binder, D. K., Razak, K. A., and Ethell, I. M. (2018). Sensory processing phenotypes in fragile X syndrome. *ASN Neuro* 10:1759091418801092. doi: 10.1177/1759091418801092

Raymond, C. R., Thompson, V. L., Tate, W. P., and Abraham, W. C. (2000). Metabotropic glutamate receptors trigger homosynaptic protein synthesis to prolong long-term potentiation. *J. Neurosci.* 20, 969–976. doi: 10.1523/JNEUROSCI.20-03-00969.2000

Represa, A., and Ben-Ari, Y. (2005). Trophic actions of GABA on neuronal development. *Trends Neurosci.* 28, 278–283. doi: 10.1016/j.tins.2005.03.010

Rio, C. A. C.-D., Nunez-Parra, A., Freedman, S., Restrepo, D., and Huntsman, M. M. (2018). Homeostatic inhibitory control of cortical hyperexcitability in fragile X syndrome. *bioRxiv* [Preprint]. doi: 10.1101/459511

Rodriguez, G., Mesik, L., Gao, M., Parkins, S., Saha, R., and Lee, H. K. (2019). Disruption of NMDAR function prevents normal experience-dependent homeostatic synaptic plasticity in mouse primary visual cortex. *J. Neurosci.* 39, 7664–7673. doi: 10.1523/JNEUROSCI.2117-18.2019

Rogers, S. J., Hepburn, S., and Wehner, E. (2003). Parent reports of sensory symptoms in toddlers with autism and those with other developmental disorders. *J. Autism Dev. Disord.* 33, 631–642. doi: 10.1023/b:jadd.0000006000.38991.a7

Rotschafer, S., and Razak, K. (2013). Altered auditory processing in a mouse model of fragile X syndrome. *Brain Res.* 1506, 12–24. doi: 10.1016/j.brainres.2013.02.038

Routh, B. N., Johnston, D., and Brager, D. H. (2013). Loss of functional A-type potassium channels in the dendrites of CA1 pyramidal neurons from a mouse model of fragile X syndrome. *J. Neurosci.* 33, 19442–19450. doi: 10.1523/JNEUROSCI.3256-13.2013

Routh, B. N., Rathour, R. K., Baumgardner, M. E., Kalmbach, B. E., Johnston, D., and Brager, D. H. (2017). Increased transient Na+ conductance and action potential output in layer 2/3 prefrontal cortex neurons of the fmr1-/y mouse. *J. Physiol.* 595, 4431–4448. doi: 10.1113/JP274258

Rutherford, L. C., Nelson, S. B., and Turrigiano, G. G. (1998). BDNF has opposite effects on the quantal amplitude of pyramidal neuron and interneuron excitatory synapses. *Neuron* 21, 521–530. doi: 10.1016/s0896-6273(00)80563-2

Saffary, R., and Xie, Z. (2011). FMRP regulates the transition from radial glial cells to intermediate progenitor cells during neocortical development. *J. Neurosci.* 31, 1427–1439. doi: 10.1523/JNEUROSCI.4854-10.2011

Sakai, J. (2020). Core concept: how synaptic pruning shapes neural wiring during development and, possibly, in disease. *Proc. Nat. Acad. Sci. U S A* 117, 16096–16099. doi: 10.1073/pnas.2010281117

Salkoff, L., Butler, A., Ferreira, G., Santi, C., and Wei, A. (2006). High-conductance potassium channels of the SLO family. *Nat. Rev. Neurosci.* 7, 921–931. doi: 10.1038/nrn1992

Santoro, M. R., Bray, S. M., and Warren, S. T. (2012). Molecular mechanisms of fragile X syndrome: a twenty-year perspective. *Annu. Rev. Pathol.* 7, 219–245. doi: 10.1146/annurev-pathol-011811-132457

Schilit Nitenson, A., Stackpole, E. E., Truszkowski, T. L. S., Midroit, M., Fallon, J. R., and Bath, K. G. (2015). Fragile X mental retardation protein regulates olfactory sensitivity but not odorant discrimination. *Chem. Senses* 40, 345–350. doi: 10.1093/chemse/bjv019

Schroeder, J. C., Reim, D., Boeckers, T. M., and Schmeisser, M. J. (2017). Genetic animal models for autism spectrum disorder. *Curr. Top. Behav. Neurosci.* 30, 311–324. doi: 10.1007/7854_2015_407

Schwarz, L. A., Hall, B. J., and Patrick, G. N. (2010). Activity-dependent ubiquitination of GluA1 mediates a distinct AMPA receptor endocytosis and sorting pathway. *J. Neurosci.* 30, 16718–16729. doi: 10.1523/JNEUROSCI.3686-10.2010

Selby, L., Zhang, C., and Sun, Q.-Q. (2007). Major defects in neocortical GABAergic inhibitory circuits in mice lacking the fragile X mental retardation protein. *Neurosci. Lett.* 412, 227–232. doi: 10.1016/j.neulet.2006.11.062

Shah, M. M. (2014). Cortical HCN channels: function, trafficking and plasticity. *J. Physiol.* 592, 2711–2719. doi: 10.1113/jphysiol.2013.270058

Shang, Y., Wang, H., Mercaldo, V., Li, X., Chen, T., and Zhuo, M. (2009). Fragile X mental retardation protein is required for chemically-induced long-term

potentiation of the hippocampus in adult mice. *J. Neurochem.* 111, 635–646. doi: 10.1111/j.1471-4159.2009.06314.x

Shepherd, J. D., Rumbaugh, G., Wu, J., Chowdhury, S., Plath, N., Kuhl, D., et al. (2006). Arc/Arg3.1 mediates homeostatic synaptic scaling of AMPA receptors. *Neuron* 52, 475–484. doi: 10.1016/j.neuron.2006.08.034

Shew, W. L., Yang, H., Yu, S., Roy, R., and Plenz, D. (2011). Information capacity and transmission are maximized in balanced cortical networks with neuronal avalanches. *J. Neurosci.* 31, 55–63. doi: 10.1523/JNEUROSCI.4637-10.2011

Sidorov, M. S., Auerbach, B. D., and Bear, M. F. (2013). Fragile X mental retardation protein and synaptic plasticity. *Mol. Brain* 6:15. doi: 10.1186/1756-6606-6-15

Siller, S. S., and Broadie, K. (2011). Neural circuit architecture defects in a Drosophila model of Fragile X syndrome are alleviated by minocycline treatment and genetic removal of matrix metalloproteinase. *Dis. Model. Mech.* 4, 673–685. doi: 10.1242/dmm.008045

Silverman, J. L., Pride, M. C., Hayes, J. E., Puhger, K. R., Butler-Struben, H. M., Baker, S., et al. (2015). GABAB receptor agonist R-baclofen reverses social deficits and reduces repetitive behavior in two mouse models of autism. *Neuropsychopharmacology* 40, 2228–2239. doi: 10.1038/npp.2015.66

Sinclair, D., Featherstone, R., Naschek, M., Nam, J., Du, A., Wright, S., et al. (2017a). GABA-B agonist baclofen normalizes auditory-evoked neural oscillations and behavioral deficits in the Fmr1 knockout mouse model of fragile X syndrome. *eNeuro* 4:ENEURO.0380-16.2017. doi: 10.1523/ENEURO.0380-16.2017

Sinclair, D., Oranje, B., Razak, K. A., Siegel, S. J., and Schmid, S. (2017b). Sensory processing in autism spectrum disorders and fragile X syndrome-from the clinic to animal models. *Neurosci. Biobehav. Rev.* 76, 235–253. doi: 10.1016/j.neubiorev.2016.05.029

Siomi, H., Siomi, M. C., Nussbaum, R. L., and Dreyfuss, G. (1993). The protein product of the fragile X gene, FMR1, has characteristics of an RNA-binding protein. *Cell* 74, 291–298. doi: 10.1016/0092-8674(93)90420-u

Snyder, E. M., Philpot, B. D., Huber, K. M., Dong, X., Fallon, J. R., and Bear, M. F. (2001). Internalization of ionotropic glutamate receptors in response to mGluR activation. *Nat. Neurosci.* 4, 1079–1085. doi: 10.1038/nn746

Soden, M. E., and Chen, L. (2010). Fragile X protein FMRP is required for homeostatic plasticity and regulation of synaptic strength by retinoic acid. *J. Neurosci.* 30, 16910–16921. doi: 10.1523/JNEUROSCI.3660-10.2010

Sohal, V. S., Zhang, F., Yizhar, O., and Deisseroth, K. (2009). Parvalbumin neurons and gamma rhythms enhance cortical circuit performance. *Nature* 459, 698–702. doi: 10.1038/nature07991

Stefani, G., Fraser, C. E., Darnell, J. C., and Darnell, R. B. (2004). Fragile X mental retardation protein is associated with translating polyribosomes in neuronal cells. *J. Neurosci.* 24, 7272–7276. doi: 10.1523/JNEUROSCI.2306-04.2004

Stellwagen, D., and Malenka, R. C. (2006). Synaptic scaling mediated by glial TNF-α. *Nature* 440, 1054–1059. doi: 10.1038/nature04671

Stoppel, D. C., Mccamphill, P. K., Senter, R. K., Heynen, A. J., and Bear, M. F. (2021). mGluR5 negative modulators for fragile X: treatment resistance and persistence. *Front. Psychiatry* 12:718953. doi: 10.3389/fpsyt.2021.718953

Strumbos, J. G., Brown, M. R., Kronengold, J., Polley, D. B., and Kaczmarek, L. K. (2010). Fragile X mental retardation protein is required for rapid experience-dependent regulation of the potassium channel Kv3.1b. *J. Neurosci.* 30, 10263–10271. doi: 10.1523/JNEUROSCI.1125-10.2010

Stuart, G. J., and Spruston, N. (2015). Dendritic integration: 60 years of progress. *Nat. Neurosci.* 18, 1713–1721. doi: 10.1038/nn.4157

Suhl, J. A., and Warren, S. T. (2015). Single-nucleotide mutations in FMR1 reveal novel functions and regulatory mechanisms of the fragile X syndrome protein FMRP. *J. Exp. Neurosci.* 9, 35–41. doi: 10.4137/JEN.S25524

Sun, Q., and Turrigiano, G. G. (2011). PSD-95 and PSD-93 play critical but distinct roles in synaptic scaling up and down. *J. Neurosci.* 31, 6800–6808. doi: 10.1523/JNEUROSCI.5616-10.2011

Svalina, M. N., Guthman, E. M., Cea-Del Rio, C. A., Kushner, J. K., Baca, S. M., Restrepo, D., et al. (2021). Hyperexcitability and loss of feedforward inhibition contribute to aberrant plasticity in the Fmr1KO amygdala. *eNeuro* 8:ENEURO.0113–0121.2021. doi: 10.1523/ENEURO.0113-21.2021

Telias, M., Segal, M., and Ben-Yosef, D. (2013). Neural differentiation of Fragile X human embryonic stem cells reveals abnormal patterns of development despite successful neurogenesis. *Dev. Biol.* 374, 32–45. doi: 10.1016/j.ydbio.2012.11.031

Till, S. M. (2010). The developmental roles of FMRP. *Biochem. Soc. Trans.* 38, 507–510. doi: 10.1042/BST0380507

Till, S. M., Asiminas, A., Jackson, A. D., Katsanevaki, D., Barnes, S. A., Osterweil, E. K., et al. (2015). Conserved hippocampal cellular pathophysiology but distinct behavioural deficits in a new rat model of FXS. *Hum. Mol. Genet.* 24, 5977–5984. doi: 10.1093/hmg/ddv299

Todd, P. K., Mack, K. J., and Malter, J. S. (2003). The fragile X mental retardation protein is required for type-I metabotropic glutamate receptor-dependent translation of PSD-95. *Proc. Natl. Acad. Sci. U S A* 100, 14374–14378. doi: 10.1073/pnas.2336265100

Tsai, N. P., Wilkerson, J. R., Guo, W., and Huber, K. M. (2017). FMRP-dependent Mdm2 dephosphorylation is required for MEF2-induced synapse elimination. *Hum. Mol. Genet.* 26, 293–304. doi: 10.1093/hmg/ddw386

Tsai, N. P., Wilkerson, J. R., Guo, W., Maksimova, M. A., Demartino, G. N., Cowan, C. W., et al. (2012). Multiple autism-linked genes mediate synapse elimination *via* proteasomal degradation of a synaptic scaffold PSD-95. *Cell* 151, 1581–1594. doi: 10.1016/j.cell.2012.11.040

Turrigiano, G. G. (2008). The self-tuning neuron: synaptic scaling of excitatory synapses. *Cell* 135, 422–435. doi: 10.1016/j.cell.2008.10.008

Turrigiano, G. G., Leslie, K. R., Desai, N. S., Rutherford, L. C., and Nelson, S. B. (1998). Activity-dependent scaling of quantal amplitude in neocortical neurons. *Nature* 391, 892–896. doi: 10.1038/36103

Turrigiano, G. G., and Nelson, S. B. (2000). Hebb and homeostasis in neuronal plasticity. *Curr. Opin. Neurobiol.* 10, 358–364. doi: 10.1016/s0959-4388(00)00091-x

Turrigiano, G. G., and Nelson, S. B. (2004). Homeostatic plasticity in the developing nervous system. *Nat. Rev. Neurosci.* 5, 97–107. doi: 10.1038/nrn1327

Typlt, M., Mirkowski, M., Azzopardi, E., Ruth, P., Pilz, P. K., and Schmid, S. (2013). Habituation of reflexive and motivated behavior in mice with deficient BK channel function. *Front. Integr. Neurosci.* 7:79. doi: 10.3389/fnint.2013.00079

Tyzio, R., Nardou, R., Ferrari, D. C., Tsintsadze, T., Shahrokhi, A., Eftekhari, S., et al. (2014). Oxytocin-mediated GABA inhibition during delivery attenuates autism pathogenesis in rodent offspring. *Science* 343, 675–679. doi: 10.1126/science.1247190

Van der Molen, M. J., Van der Molen, M. W., Ridderinkhof, K. R., Hamel, B. C., Curfs, L. M., and Ramakers, G. J. (2012). Auditory change detection in fragile X syndrome males: a brain potential study. *Clin. Neurophysiol.* 123, 1309–1318. doi: 10.1016/j.clinph.2011.11.039

Verheij, C., De Graaff, E., Bakker, C. E., Willemsen, R., Willems, P. J., Meijer, N., et al. (1995). Characterization of FMR1 proteins isolated from different tissues. *Hum. Mol. Genet.* 4, 895–901. doi: 10.1093/hmg/4.5.895

Vislay, R. L., Martin, B. S., Olmos-Serrano, J. L., Kratovac, S., Nelson, D. L., Corbin, J. G., et al. (2013). Homeostatic responses fail to correct defective amygdala inhibitory circuit maturation in fragile X syndrome. *J. Neurosci.* 33, 7548–7558. doi: 10.1523/JNEUROSCI.2764-12.2013

Vitureira, N., and Goda, Y. (2013). Cell biology in neuroscience: The interplay between Hebbian and homeostatic synaptic plasticity. *J. Cell Biol.* 203, 175–186. doi: 10.1083/jcb.201306030

Wahlstrom-Helgren, S., and Klyachko, V. A. (2015). GABAB receptor-mediated feed-forward circuit dysfunction in the mouse model of fragile X syndrome. *J. Physiol.* 593, 5009–5024. doi: 10.1113/JP271190

Wahlstrom-Helgren, S., and Klyachko, V. A. (2016). Dynamic balance of excitation and inhibition rapidly modulates spike probability and precision in feed-forward hippocampal circuits. *J. Neurophysiol.* 116, 2564–2575. doi: 10.1152/jn.00413.2016

Wang, J., Ethridge, L. E., Mosconi, M. W., White, S. P., Binder, D. K., Pedapati, E. V., et al. (2017). A resting EEG study of neocortical hyperexcitability and altered functional connectivity in fragile X syndrome. *J. Neurodev. Disord.* 9:11. doi: 10.1186/s11689-017-9191-z

Wang, X., Zorio, D. A. R., Schecterson, L., Lu, Y., and Wang, Y. (2018). Postsynaptic FMRP regulates synaptogenesis *in vivo* in the developing cochlear nucleus. *J. Neurosci.* 38, 6445–6460. doi: 10.1523/JNEUROSCI.0665-18.2018

Watt, A. J., Van Rossum, M. C. W., Macleod, K. M., Nelson, S. B., and Turrigiano, G. G. (2000). Activity coregulates quantal AMPA and NMDA currents at neocortical synapses. *Neuron* 26, 659–670. doi: 10.1016/s0896-6273(00)81202-7

Weiler, I. J., Irwin, S. A., Klintsova, A. Y., Spencer, C. M., Brazelton, A. D., Miyashiro, K., et al. (1997). Fragile X mental retardation protein is translated near synapses in response to neurotransmitter activation. *Proc. Natl. Acad. Sci. U S A* 94, 5395–5400. doi: 10.1073/pnas.94.10.5395

Wen, T. H., Afroz, S., Reinhard, S. M., Palacios, A. R., Tapia, K., Binder, D. K., et al. (2018). Genetic reduction of matrix metalloproteinase-9 promotes formation of perineuronal nets around parvalbumin-expressing interneurons and normalizes auditory cortex responses in developing Fmr1 knock-out mice. *Cereb. Cortex* 28, 3951–3964. doi: 10.1093/cercor/bhx258

Wierenga, C. J., Ibata, K., and Turrigiano, G. G. (2005). Postsynaptic expression of homeostatic plasticity at neocortical synapses. *J. Neurosci.* 25, 2895–2905. doi: 10.1523/JNEUROSCI.5217-04.2005

Wisniewski, K. E., Segan, S. M., Miezejeski, C. M., Sersen, E. A., and Rudelli, R. D. (1991). The Fra(X) syndrome: neurological, electrophysiological and neuropathological abnormalities. *Am. J. Med. Genet.* 38, 476–480. doi: 10.1002/ajmg.1320380267

Wong, H., Hooper, A. W. M., Niibori, Y., Lee, S. J., Hategan, L. A., Zhang, L., et al. (2020). Sexually dimorphic patterns in electroencephalography power spectrum and autism-related behaviors in a rat model of fragile X syndrome. *Neurobiol. Dis.* 146:105118. doi: 10.1016/j.nbd.2020.105118

Yang, Y.-M., Arsenault, J., Bah, A., Krzeminski, M., Fekete, A., Chao, O. Y., et al. (2020). Identification of a molecular locus for normalizing dysregulated GABA release from interneurons in the Fragile X brain. *Mol. Psychiatry* 25, 2017–2035. doi: 10.1038/s41380-018-0240-0

Yang, S., Yang, S., Park, J. S., Kirkwood, A., and Bao, S. (2014). Failed stabilization for long-term potentiation in the auditory cortex of FMR1 knockout mice. *PLoS One* 9:e104691. doi: 10.1371/journal.pone.0104691

Yizhar, O., Fenno, L. E., Prigge, M., Schneider, F., Davidson, T. J., O'shea, D. J., et al. (2011). Neocortical excitation/inhibition balance in information processing and social dysfunction. *Nature* 477, 171–178. doi: 10.1038/nature10360

Yun, S. W., Platholi, J., Flaherty, M. S., Fu, W., Kottmann, A. H., and Toth, M. (2006). Fmrp is required for the establishment of the startle response during the critical period of auditory development. *Brain Res.* 1110, 159–165. doi: 10.1016/j.brainres.2006.06.086

Zeidler, S., Pop, A. S., Jaafar, I. A., de Boer, H., Buijsen, R. A. M., de Esch, C. E. F., et al. (2018). Paradoxical effect of baclofen on social behavior in the fragile X syndrome mouse model. *Brain Behav.* 8:e00991. doi: 10.1002/brb3.991

Zeier, Z., Kumar, A., Bodhinathan, K., Feller, J. A., Foster, T. C., and Bloom, D. C. (2009). Fragile X mental retardation protein replacement restores hippocampal synaptic function in a mouse model of fragile X syndrome. *Gene. Ther.* 16, 1122–1129. doi: 10.1038/gt.2009.83

Zhan, X., Asmara, H., Cheng, N., Sahu, G., Sanchez, E., Zhang, F.-X., et al. (2020). FMRP(1–297)-tat restores ion channel and synaptic function in a model of Fragile X syndrome. *Nat. Commun.* 11:2755. doi: 10.1038/s41467-020-16250-4

Zhang, L., and Alger, B. E. (2010). Enhanced endocannabinoid signaling elevates neuronal excitability in fragile X syndrome. *J. Neurosci.* 30, 5724–5729. doi: 10.1523/JNEUROSCI.0795-10.2010

Zhang, Y. Q., Bailey, A. M., Matthies, H. J. G., Renden, R. B., Smith, M. A., Speese, S. D., et al. (2001). Drosophila fragile X-related gene regulates the MAP1B homolog futsch to control synaptic structure and function. *Cell* 107, 591–603. doi: 10.1016/s0092-8674(01)00589-x

Zhang, L. I., Bao, S., and Merzenich, M. M. (2001). Persistent and specific influences of early acoustic environments on primary auditory cortex. *Nat. Neurosci.* 4, 1123–1130. doi: 10.1038/nn745

Zhang, Y., Bonnan, A., Bony, G., Ferezou, I., Pietropaolo, S., Ginger, M., et al. (2014). Dendritic channelopathies contribute to neocortical and sensory hyperexcitability in Fmr1(-/y) mice. *Nat. Neurosci.* 17, 1701–1709. doi: 10.1038/nn.3864

Zhang, W., and Linden, D. J. (2003). The other side of the engram: experience-driven changes in neuronal intrinsic excitability. *Nat. Rev. Neurosci.* 4, 885–900. doi: 10.1038/nrn1248

Zhang, Z., Marro, S. G., Zhang, Y., Arendt, K. L., Patzke, C., Zhou, B., et al. (2018). The fragile X mutation impairs homeostatic plasticity in human neurons by blocking synaptic retinoic acid signaling. *Sci. Trans. Med.* 10:eaar4338. doi: 10.1126/scitranslmed.aar4338

Zhang, Z., Rumschlag, J., Jonak, C. R., Binder, D. K., Razak, K. A., Gibson, J. R., et al. (2021). FMRP regulates experience-dependent maturation of callosal synaptic connections and bilateral cortical synchrony. *BioRxiv* [Preprint]. doi: 10.1101/2021.06.25.449490

Zhao, W., Chuang, S.-C., Bianchi, R., and Wong, R. K. S. (2011). Dual regulation of fragile X mental retardation protein by group I metabotropic glutamate receptors controls translation-dependent epileptogenesis in the hippocampus. *J. Neurosci.* 31, 725–734. doi: 10.1523/JNEUROSCI.2915-10.2011

Zhong, L. R., Chen, X., Park, E., Südhof, T. C., and Chen, L. (2018). Retinoic acid receptor RARα-dependent synaptic signaling mediates homeostatic synaptic plasticity at the inhibitory synapses of mouse visual cortex. *J. Neurosci.* 38, 10454–10466. doi: 10.1523/JNEUROSCI.1133-18.2018

Conflict of Interest: The authors declare that the research was conducted in the absence of any commercial or financial relationships that could be construed as a potential conflict of interest.

Publisher's Note: All claims expressed in this article are solely those of the authors and do not necessarily represent those of their affiliated organizations, or those of the publisher, the editors and the reviewers. Any product that may be evaluated in this article, or claim that may be made by its manufacturer, is not guaranteed or endorsed by the publisher.

frontiers in Molecular Neuroscience

ORIGINAL RESEARCH
published: 14 February 2022
doi: 10.3389/fnmol.2022.817227

14-3-3 Dysfunction in Dorsal Hippocampus CA1 (dCA1) Induces Psychomotor Behavior *via* a dCA1-Lateral Septum-Ventral Tegmental Area Pathway

*Jiajing Zhang, Meaghan Navarrete, Yuying Wu and Yi Zhou**

Department of Biomedical Sciences, Florida State University College of Medicine, Tallahassee, FL, United States

While hippocampal hyperactivity is implicated in psychosis by both human and animal studies, whether it induces a hyperdopaminergic state and the underlying neural circuitry remains elusive. Previous studies established that region-specific inhibition of 14-3-3 proteins in the dorsal hippocampus CA1 (dCA1) induces schizophrenia-like behaviors in mice, including a novelty-induced locomotor hyperactivity. In this study, we showed that 14-3-3 dysfunction in the dCA1 over-activates ventral tegmental area (VTA) dopaminergic neurons, and such over-activation is necessary for eliciting psychomotor behavior in mice. We demonstrated that such hippocampal dysregulation of the VTA during psychomotor behavior is dependent on an over-activation of the lateral septum (LS), given that inhibition of the LS attenuates over-activation of dopaminergic neurons and psychomotor behavior induced by 14-3-3 inhibition in the dCA1. Moreover, 14-3-3 inhibition-induced neuronal activations within the dCA1-LS-VTA pathway and psychomotor behavior can be reproduced by direct chemogenetic activation of LS-projecting dCA1 neurons. Collectively, these results suggest that 14-3-3 dysfunction in the dCA1 results in hippocampal hyperactivation which leads to psychomotor behavior *via* a dCA1-LS-VTA pathway.

Keywords: 14-3-3, dorsal hippocampus CA1, hippocampal hyperactivity, lateral septum (LS), ventral tegmental area (VTA), psychomotor behavior, chemogenetics, dopamine

OPEN ACCESS

Edited by:
Menahem Segal,
Weizmann Institute of Science, Israel

Reviewed by:
Pawel Matulewicz,
Innsbruck Medical University, Austria
David Bortz,
University of Pittsburgh,
United States

****Correspondence:***
Yi Zhou
yi.zhou@med.fsu.edu

Specialty section:
This article was submitted to Brain Disease Mechanisms, a section of the journal Frontiers in Molecular Neuroscience

Received: *17 November 2021*
Accepted: *14 January 2022*
Published: *14 February 2022*

Citation:
Zhang J, Navarrete M, Wu Y and Zhou Y (2022) 14-3-3 Dysfunction in Dorsal Hippocampus CA1 (dCA1) Induces Psychomotor Behavior via a dCA1-Lateral Septum-Ventral Tegmental Area Pathway. Front. Mol. Neurosci. 15:817227. doi: 10.3389/fnmol.2022.817227

INTRODUCTION

The heterogeneity of psychiatric disorders poses major difficulties in deciphering their underlying etiology. Thus, unraveling the circuitry basis of psychiatric symptoms holds promise for identifying novel circuit-level targets for future treatment development. It is well recognized that the mesolimbic dopamine (DA) system, which originates from DA neurons in the ventral tegmental area (VTA), is critical for salience attribution, which is impaired in patients experiencing psychosis (Laruelle et al., 1999; Abi-Dargham et al., 2009; Howes and Nour, 2016). As the DA system is tightly modulated by excitatory and inhibitory inputs from the cortical and subcortical regions in response to both internal and external stimuli, a pathological DAergic hyperactivation is thought to be secondary to dysfunction in susceptible brain regions that regulate the VTA (Lodge and Grace, 2011; Howes et al., 2015; Howes and Nour, 2016). In particular, cortical and hippocampal

anomalies are highly implicated in psychiatric disorders, which may explain why the brain's failures in processing sensory information could give rise to psychosis.

Alterations in structure and physiology of the hippocampus (HP) have been consistently linked to schizophrenia (Medoff et al., 2001; Schobel et al., 2009a; Talati et al., 2014; McHugo et al., 2019). Specifically, human imaging studies identified hippocampal hyperactivity associated with psychosis (Talati et al., 2014; Dugré et al., 2019; McHugo et al., 2019). Consistent with this, studies using transgenic or developmental rodent models of schizophrenia associate a loss of hippocampal GABAergic interneurons activity (Belforte et al., 2010; Gilani et al., 2014) or increased hippocampal neuronal activity (higher firing rate, increased c-Fos, etc.) with psychomotor behavior (Lodge and Grace, 2007; Procaccini et al., 2011). Additionally, such behavioral abnormality can be rescued by restoring hippocampal GABAergic interneurons (Marissal et al., 2018) or by pharmacological or chemogenetic inhibition of hippocampal excitatory neurons (Maksimovic et al., 2014; Aitta-Aho et al., 2019). Collectively, these findings support a hypothesis in which psychosis is a consequence of hippocampal excitation/inhibition (E/I) imbalance.

In individual neurons, synaptic inputs are highly regulated to ensure proper excitatory or inhibitory activity across dendritic segments (Gao and Penzes, 2015). Numerous genes derived from linkage and association studies of psychiatric disorders encode proteins involved with synaptic processes (Kirov et al., 2012; Fromer et al., 2014). Among them are several genes that encode members of the 14-3-3 family of proteins which are particularly enriched at synapses (Bell et al., 2000; Jia et al., 2004; Middleton et al., 2005; Wong et al., 2005; Ikeda et al., 2008). Accumulating evidence reveals that 14-3-3 proteins are important modulators of synaptic transmission and plasticity (Zhang and Zhou, 2018), thus making them potential therapeutic targets. Transgenic mouse models with 14-3-3 deficiency exhibit synaptic, network activity, and behavioral alterations that correspond to core schizophrenia phenotypes (Ramshaw et al., 2013; Qiao et al., 2014; Foote et al., 2015; Jaehne et al., 2015; Xu et al., 2015; Jones et al., 2021). Most interestingly, recent work reveals that adeno-associated virus (AAV) mediated 14-3-3 isoform-independent inhibition specifically in the dHP CA1 (dCA1) pyramidal neurons induces psychomotor behavior in wild type (WT) mice provoked by novel environment (Graham et al., 2019). However, the circuitry mechanism underlying such hippocampal dysfunction-induced psychomotor behavior and how 14-3-3 deficiency in the dCA1 alters hippocampal E/I balance and disturbs downstream neural activities remain to be determined.

In this study, we demonstrate that 14-3-3 dysfunction in the dCA1 induces psychomotor behavior in mice *via* over-activation of the lateral septum (LS) neurons, which results in increased VTA DA neuronal activity. We also reveal that 14-3-3 inhibition-induced alterations in neuronal activity and behavior are likely due to an increased dCA1 neuronal activation, and provided evidence showing that direct chemogenetic activation of the dCA1-LS pathway is sufficient to induce locomotor hyperactivity in mice. Together, these findings demonstrate how the loss of function of one pivotal family of proteins in the hippocampus may contribute to a shift in E/I balance and induces psychotic-like behavioral abnormality in mice through dysregulation of the downstream pathway.

MATERIALS AND METHODS

Experimental Animals

Both male and female adult (3–6 months old) wildtype (C57BL/6J), DAT-cre [B6.SJL-Slc6a3tm1.1(cre)Bkmn/J, Jackson Laboratory], and CaMKIIa-cre [B6.Cg-Tg(Camk2a-cre)T29-1Stl/J, Jackson Laboratory] mice were included in this study. Mice were housed on a 12 h light/dark cycle and provided ad libitum access to water and food. Prior to stereotaxic surgical injection, mice were housed in groups (2–4 per cage). Littermates were randomly assigned to experimental groups or control groups. Following the surgical procedure, mice were subsequently single caged until all experimental procedures were finished. Mice were handled daily for 2 weeks prior to behavioral tests, which were conducted during the light cycle. All experiments were carried out in accordance with Florida State University's laboratory animal care and use guidelines and approved by the Florida State University Animal Care and Use Committee.

Viral Vectors

The AAV2/9-CaMKIIa-YFP-difopein (titer at 7.82×10^{12} v.g./ml), AAV2-CaMKIIa-tdTomato (titer at 4.42×10^{12} v.g./ml), and AAV2/9-CMV-DIO-EGFP (titer at 9.05×10^{12} v.g./ml) were constructed and produced by OBiO Technology (Shanghai) Corp., Ltd. Briefly, cDNA encoding YFP-difopein, tdTomato, or DIO-EGFP was subcloned into a rAAV vector. The viral vectors were then produced using the triple transfection method in HEK 293 cells and AAV titers were determined by real-time PCR. Control vector (AAV2-CaMKIIa-YFP, titer at 5.1×10^{12} v.g./ml) was purchased from the UNC viral core facility. For chemogenetic manipulations, AAV5-hSyn-hM4D(Gi)-mCherry (Addgene #50475, titer at 1.2×10^{13} v.g./ml), AAV5-hSyn-DIO-hM4D(Gi)-mCherry (Addgene #44362, titer at 8×10^{12} v.g./ml), AAV5-hSyn-mCherry (Addgene #114472, titer at 2.8×10^{13} v.g./ml), AAV5-hSyn-hM3D(Gq)-mCherry (Addgene #50474, titer at 1×10^{13} v.g./ml), AAV5-hSyn-DIO-hM3D(Gq)-mCherry (Addgene #44361, titer at 1×10^{13} v.g./ml), and AAVretro-hSyn-Cre-WPRE-hGH (Addgene #105553, titer at 2.1×10^{13} v.g./ml) were purchased from Addgene. Upon arrival, all viral vectors were aliquoted and stored at −80°C prior to stereotaxic injections.

Stereotaxic Viral Injections

Mice were anesthetized with intraperitoneal (i.p.) injections of a mixture of ketamine (100 mg/kg)/xylazine (10 mg/kg) and placed in a stereotaxic frame (David Kopf Instruments, Tujunga, CA). The animal's skull was exposed *via* a small incision on the scalp. Small burr holes were made directly above the viral injection sites unilaterally or bilaterally using a micro-precision drill. For micro-injections, Hamilton syringes (10 μl, 33-gauge)

loaded with AAV virus or tracer were slowly lowered into the target area according to the corresponding coordinates: dCA1 (AP: − 2.0 mm, ML: ± 1.5 mm, DV: − 1.1 mm from dura); LS (AP: + 0.6 mm, ML: ± 0.7 mm, DV: − 2.25 mm from dura with a 10° coronal rotation angle); VTA (AP: − 3.0 mm, ML: ± 0.5 mm, DV: − 4.25 mm from dura); NAc (AP: + 1.3 mm, ML: ± 0.8 mm, DV: − 4.3 mm from dura); MM (AP: − 2.9 mm, ML: ± 0.5 mm, DV: − 4.9 mm from dura). Virus or tracer (0.5–1 ul) was slowly injected at 75 nl/min. Injection needles were left in place for an additional 10 min to assure adequate viral delivery before slowly being withdrawn. The scalp incision was then closed and treated with topical neomycin. For postoperative care, ketoprofen (5 mg/kg in 0.05 ml saline) was used for pain relief immediately following surgery. Mice were allowed 2 weeks for expression of viral proteins and recovery from surgery before beginning behavioral testing.

Pharmacology

The stock solution of clozapine (1 mg/ml, TOCRIS) was prepared in 0.1 N HCl and diluted in saline. On the day of the experiment, 2 mg/kg clozapine in 0.2 ml saline was prepared for injections. Compound 21 dihydrochloride (C21) was purchased from Hello Bio. For hM4D(Gi)-mediated inhibition and hM3D(Gq)-mediated excitation, 1–2 mg/kg C21 in 0.2 ml saline was used. Diluted pharmacological agents (or saline as control) were intraperitoneally (i.p.) given to each testing subject 30 min prior to open field testing.

Open Field Testing

All mice were habituated in the behavioral room for a minimum of 30 min prior to beginning experimental sessions. To assess locomotive behavior, mice were placed into a square open field arena (Med Associates Open Field Arena, 43.2 cm × 43.2 cm × 30.5 cm, with IR photo-beam sensors) and the total distance traveled in 30 min was measured using Med Associates Activity Monitor software.

Immunofluorescence and Imaging

Mice were anesthetized with ketamine/xylazine and perfused with 0.1 M phosphate-buffered saline (PBS), followed by 4% paraformaldehyde (PFA) in 0.1 M PBS. Brains were extracted and post-fixed overnight at 4°C in 4% PFA before transferring to PBS solution. A vibratome (Leica Microsystems) was used for brain sectioning at 40 μm. Brain slices were collected and stored in PBS with 0.1% sodium azide. For immunohistochemistry, brain sections were blocked in a PBS solution (PBST) containing 10% goat serum and 0.7% Triton-X for 1 h at room temperature. The brain sections were then incubated overnight (two nights for c-Fos) at 4°C with primary antibodies. Then after three PBST washes, the brain sections were incubated with secondary antibodies at room temperature for 2 h (4 h for c-Fos). The sections were rinsed three times with PBST, followed by one PBS wash. If DAPI counterstaining was needed, brain sections were then incubated in PBS with 300 nM DAPI (Invitrogen, P3571) for 10 min before being mounted using an antifade mounting medium (VECTASHIELD). Keyence and Zeiss confocal microscopes were used for imaging.

Primary antibodies including rabbit anti-c-Fos (abcam, ab190289); mouse anti-TH (Millipore, MAB318); rabbit anti-Alexa Fluor 488 IgG (Invitrogen, Cat#A11094); mouse anti-GAD67 (Millipore, MAB5406); rabbit anti-GABA (Sigma-Aldrich, A2052); mouse anti-beta subunit Cholera Toxin (abcam, ab62429); mouse anti-cre recombinase (Millipore, MAB3120); and secondary antibodies including Alexa Fluor 647 donkey anti-rabbit IgG(H + L; Invitrogen, A31573); mouse IgG F(c) Antibody DyLight^{TM} 405 Conjugated (Rockland, Cat# 610-146-003); anti-rabbit IgG(H + L) FITC (SouthernBiotech, 4050-02); and Alexa Fluor 647 donkey anti-mouse IgG(H + L; Invitrogen, A31571) were used in this study.

Anterograde and Retrograde Tracing

For dual anterograde and retrograde tracing, 0.8 ul recombinant cholera toxin-b conjugated to Alexa Fluor 488 (CTB488, Invitrogen Cat#C34775) in PBS was unilaterally injected into the VTA of WT mice, followed by 0.5 ul AAV2-CaMKIIa-tdTomato (OBiO Technology) injected into the dCA1 ipsilateral to the CTB-injected VTA. For retrograde tracing from the LS, 0.5 ul CTB488 was unilaterally injected into the targeted LS region. Mice (n = 4 each tracing experiment) were perfused on day 14 following the surgery. Coronal brain slices (40 μm) were sectioned and immunohistochemistry against Alexa Fluor 488 IgG was performed to enhance CTB signals. LS sections containing CTB-labeled VTA-projecting cells were further co-stained with anti-GAD67 or anti-GABA for identification of cell type. Tracing results were examined under a Zeiss confocal microscope with 10×, 20×, and 60× objectives.

c-Fos Induction and Quantifications

To minimize unrelated c-Fos expression, all virally transduced mice were habituated in the behavioral room for at least 4 h prior to testing. For experiments aiming to assess c-Fos expression associated with difopein-induced locomotive hyperactivity, four groups of mice were used: difopein-OFT, YFP-OFT, difopein-handled only, and YFP-handled only. After habituation, difopein-OFT mice and YFP-OFT mice were put through 30-min OFT, returned to home cages, and then perfused 60 min following the end of OFT. Difopein- and YFP-handled only mice were briefly handled and perfused 90 min after returning to their home cages. Each mouse brain was sectioned into six sets of 40 μm coronal slices. For whole brain c-Fos analysis, one set of slices from each brain was used for immunohistochemistry against c-Fos (Alexa Fluor 647 donkey anti-mouse IgG(H + L) was used as a secondary antibody). A Keyence microscope (20× objective) was used to collect images for brain-wide c-Fos quantification in 28 brain nuclei selected based on three criteria: (1) c-Fos expression in the region was previously found to be associated with open field exposure (Badiani et al., 1998; Hale et al., 2008); (2) the region showed c-Fos activity in any of the four groups following OFT or handling; (3) the region was identified as having efferent projections to the VTA and/or receive input from the dHP (Strange et al., 2014; Beier et al., 2015). The regions selected were: nucleus accumbens core (NAcore), nucleus accumbens shell (lateral part, NAsh L), nucleus accumbens shell (medial part, NAsh M), cingulate cortex (Cg), secondary motor

cortex (M2), primary motor cortex (M1), agranular insular cortex (AI), claustrum (Cl), dorsal endopiriform nucleus (DEn), piriform cortex (Pir), lateral septum (rostral part, LSr), lateral septum (caudal, LSc), bed nucleus of the stria terminalis (BST), paraventricular thalamic nucleus (PVT), central amygdaloid nucleus (Ce), lateral amygdaloid nucleus (LA), basolateral amygdaloid nucleus (BLA), medial amygdaloid nucleus (Me), basomedial amygdaloid nucleus (BMA), lateral hypothalamus (LH), reticular thalamic nucleus (RT), dHP CA1 (dCA1), dHP CA3 (dCA3), dentate gyrus (DG), lateral entorhinal cortex (LEnt), ventral hippocampus CA1 (vCA1), subiculum (Sub), and mammillary body (MM). The number of c-Fos-ir cells in each image was programmatically counted using ImageJ.

For VTA cell-type specific c-Fos analysis, VTA-containing coronal sections from another set of slices were used. Brain slices were co-stained with primary antibodies against c-Fos and tyrosine hydroxylase, followed by secondary antibodies Alexa Fluor 647 donkey anti-mouse IgG(H + L) and 405 conjugated anti-mouse IgG. Fluorescent images were collected using a Zeiss confocal microscope. All images were taken under the same settings and processed identically to avoid artificial representations of data. Z-stack images of the VTA from four slices (200 μm apart, correspond roughly to Bregma − 3.1 mm, − 3.3 mm, − 3.5 mm, and − 3.7 mm in the mouse brain atlas) per animal were collected using the 20× objective, and neurons expressing c-Fos and/or TH were manually counted. TH-ir cells in the VTA were considered c-Fos-positive if the c-Fos signal clearly overlapped with the neuronal soma of the TH-ir cells. The sum of cells counted from four sections on one hemisphere of each mouse was used for statistical analysis.

For the experiment analyzing c-Fos expression in VTA-projecting LS cells, virally transduced mice were put through 30-min OFT 14 days after the surgery and then perfused 60 min following the end of the test. LS-containing sections from one set of slices were used for immunohistochemistry co-staining of c-Fos and CTB. Alexa Fluor 647 donkey anti-mouse IgG(H + L) and 405 conjugated anti-mouse IgG were used as secondary antibodies. Z-stack images of the LS from six slices (200 μm apart) per mouse were collected using Zeiss confocal with a 10× objective. Neurons expressing c-Fos and/or CTB were manually counted. CTB-ir cells in the LS were considered c-Fos-positive if the c-Fos signal clearly overlapped with neuronal soma of the CTB-ir cells. The total cell numbers counted from six sections on one hemisphere per mouse were used for statistical analysis.

Chemogenetic Manipulations

To validate the effect of C21-mediated chemogenetic activation or inhibition, saline or C21 was administered to hM3D- or hM4D-injected mice 30 min prior to OFT. Animals were then perfused 60 min after 30 min OFT. Brain sections containing hM3D or hM4D injection sites from one set of slices per brain were used for immunohistochemistry against c-Fos. Z-stack images were taken using a Zeiss confocal microscope with a 20× objective. Neurons expressing hM3D or hM4D were considered c-Fos-positive if the c-Fos signal clearly overlapped with neuronal soma of the mCherry-positive cells. The number of cells expressing mCherry and/or c-Fos were manually counted.

For experiments using hM4D, one set of virally transduced mice from each group was first put through 30-min OFT with i.p. injections of saline 30 min prior to the first trial. Two weeks later, these mice were given i.p. injections of C21 prior to the second trial. Mice were perfused 60 min after the end of the second trial for c-Fos analysis. To assess the effect of repeat testing, a separate set of virally transduced mice was given C21 administration prior to the first trial and was given saline injections prior to the second trial.

Statistical Analysis

Power analysis was performed to ensure the appropriately minimal number of mice is used in each experimental context. Our considerations are based on a significant level (alpha set at 0.05), power set at 80%, and effective size which was established through our published and preliminary studies. Following *post-hoc* histological confirmation of viral infections, only mice with accurate viral infections were included in data analysis. All data were analyzed using Prism 7.01 (GraphPad software). Statistical analyses were performed using two-tailed unpaired Student's t-tests, paired Student's t-tests, or two-way ANOVA when appropriate. When homogeneity of variance was violated, a Welch test was used as a correction. Values are reported as mean ± standard error of the mean (SEM). The cutoff value of significance was $P = 0.05$. Symbols used: $^{*}p < 0.05$; $^{**}p < 0.01$; $^{***}p < 0.001$; ns, not significant.

RESULTS

Locomotor Hyperactivity Induced by 14-3-3 Dysfunction in the dCA1 Is Attenuated by Clozapine Administration

Novelty-induced locomotor hyperactivity in rodents are thought to share the underlying neurobiology of psychosis due to their similar pharmacological responses to antipsychotics and psychostimulants (van den Buuse, 2010). Therefore, novel open field exposure is commonly used to evaluate psychosis-like behavior in rodents. We previously demonstrated that AAV-mediated 14-3-3 inhibition in the dCA1 alone induces locomotor hyperactivity (Graham et al., 2019). Here, we examined the effect of clozapine, a DA receptor-targeting antipsychotic drug, on attenuating this behavioral abnormality. 14-3-3 inhibition in the dCA1 subregion was achieved by utilizing a previously established AAV to drive regional expression of a YFP-fused isoform-independent dimeric fourteen-three-three peptide inhibitor (difopein) under CaMKIIa promotor (AAV-difopein; **Figure 1A**; Masters and Fu, 2001). Consistent with previous findings, the difopein-injected WT mice exhibited significantly increased novelty-induced locomotor activity during 30-min open field testing (OFT; **Figure 1B**). Interestingly, administration of clozapine at a non-sedative dose (2 mg/kg) was sufficient to normalize the locomotor activity of the difopein-injected mice (**Figure 1B**). Given the preferential, although not selective, effect of clozapine

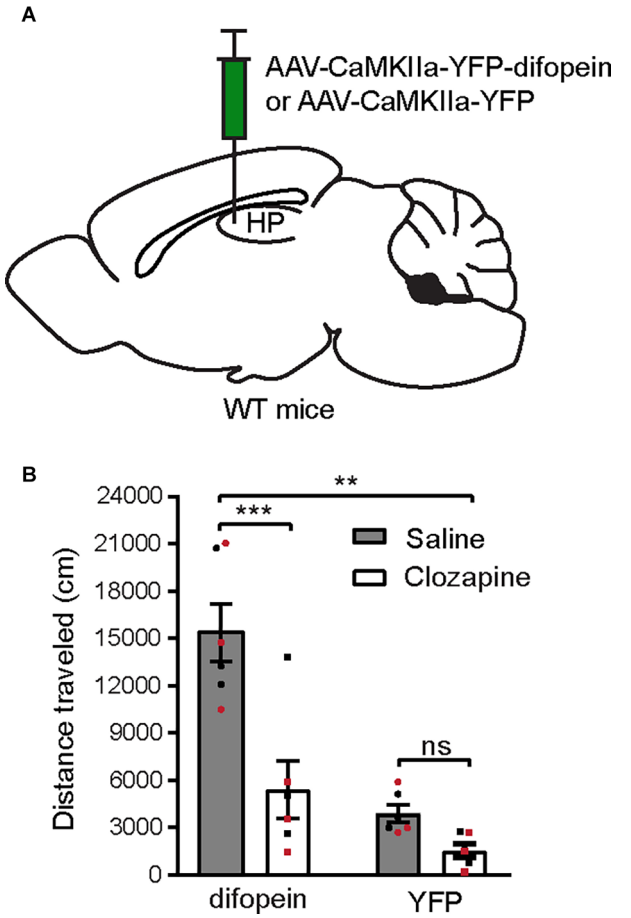

FIGURE 1 | Systemic clozapine administration attenuates locomotor hyperactivity induced by 14-3-3 dysfunction in the dCA1. **(A)** Schematic depiction illustrating viral transduction of the dHP CA1 of WT mice with AAV-CaMKIIa-YFP-difopein or AAV-CaMKIIa-YFP. **(B)** Novelty-induced locomotor activity (distance traveled) of difopein- or YFP-injected mice during OFT following saline or clozapine (2 mg/kg) administration [n = 6 (3 males and 3 females)/group; two-way ANOVA, Drug × Virus interaction $F_{(1,20)} = 8.214$, $^{**}p = 0.0096$, *post hoc* multiple Student's unpaired two-tailed t-tests; difopein, $^{***}p < 0.0001$; YFP, $p = 0.2239$]. All data are presented as mean ± SEM. Data points from male and female mice are shown as black and red symbols, respectively. ns, not significant.

on antagonizing DA transmission (Kapur and Seeman, 2001), these results suggest that a hyperactive DA system may underlie the locomotor hyperactivity induced by 14-3-3 inhibition in the dCA1.

14-3-3 Dysfunction in dCA1 Triggers Robust C-Fos Expression in VTA DA Neurons During OFT

Having established that difopein-induced locomotor hyperactivity is sensitive to clozapine administration, we then sought to directly evaluate whether DA neuronal activity was altered during such behavior. Specifically, we focused on DAergic activity in the VTA, given that a hyperactive mesolimbic DA pathway is thought to give rise to psychosis (Boekhoudt et al., 2016). We injected AAV-difopein or AAV-YFP into the dCA1 of WT mice (**Figure 2A**) and examined the expression of c-Fos protein in the VTA following OFT. This protocol induced significantly increased numbers of total c-Fos-immunoreactive (ir) cells in the VTA of both difopein- and YFP-injected mice compared with their handled-only controls (**Figures 2B,C**), which is consistent with a previous report (Bourgeois et al., 2012) and suggests that the OFT induced neuronal activation in the VTA. Furthermore, among the mice that were exposed to the open field arena, we found a significantly higher total number of c-Fos-ir cells in the VTA of difopein-injected mice (**Figure 2C**). This indicates that 14-3-3 inhibition in the dCA1 further increases VTA neuronal activation in OFT.

It is known that the VTA comprises DAergic, GABAergic, glutamatergic, and co-releasing neurons (Yoo et al., 2016; Kim et al., 2019). To specifically identify the activation of DA neurons in virus-injected mice, we performed dual immunohistochemistry against tyrosine hydroxylase (TH) and c-Fos on VTA-containing brain sections. A significantly higher number of double-labeled neurons was found in the VTA of difopein-injected mice compared to control, indicating increased activation of DA neurons induced by 14-3-3 inhibition in the dCA1 during OFT (**Figure 2D**). Interestingly, we did not observe any statistically significant differences in either total or TH co-labeled c-Fos-ir cell numbers between difopein- and YFP-injected groups that were handled only (**Figures 2C,D**). This might suggest that inhibition of 14-3-3 disrupts the function of dCA1 in processing novel environmental stimuli and thus results in over-activation of the VTA DA neurons during OFT.

Chemogenetic Inhibition of VTA DA Neurons Attenuates Difopein-Induced Locomotor Hyperactivity

Next, we directly tested whether over-activation of VTA DA neurons is necessary for 14-3-3 dysfunction-induced locomotor hyperactivity. We employed a chemogenetic DREADD (Designer Receptors Exclusively Activated by Designer Drugs) approach, which allows us to regulate neuronal activity with spatiotemporal precision. To selectively manipulate DA neurons, we injected an AAV expressing a Cre-recombinase-dependent inhibitory DREADD (AAV-hSyn-DIO-hM4D(Gi)-mCherry) bilaterally into the VTA of DAT-cre mice in addition to bilateral AAV-difopein injections into the dCA1 (**Figure 3A**). To circumvent potential off-target effects of clozapine-N-oxide on locomotion, we used an alternative DREADD agonist, Compound 21 (C21), for acute activation of designer receptors in this study (Manvich et al., 2018; Thompson et al., 2018). C21 administration (2 mg/kg) significantly reduced the number of c-Fos-expressing hM4D-positive neurons (**Figure 3B**), demonstrating an effective C21-mediated inactivation of DA neurons. Interestingly, we found that C21-mediated inhibition of VTA DA neurons is sufficient in attenuating locomotor hyperactivity in difopein-injected mice (**Figure 3C**), suggesting that DA activation is necessary for difopein-induced locomotor hyperactivity. Together, these findings demonstrate that activation of VTA DA neurons plays a significant role in the

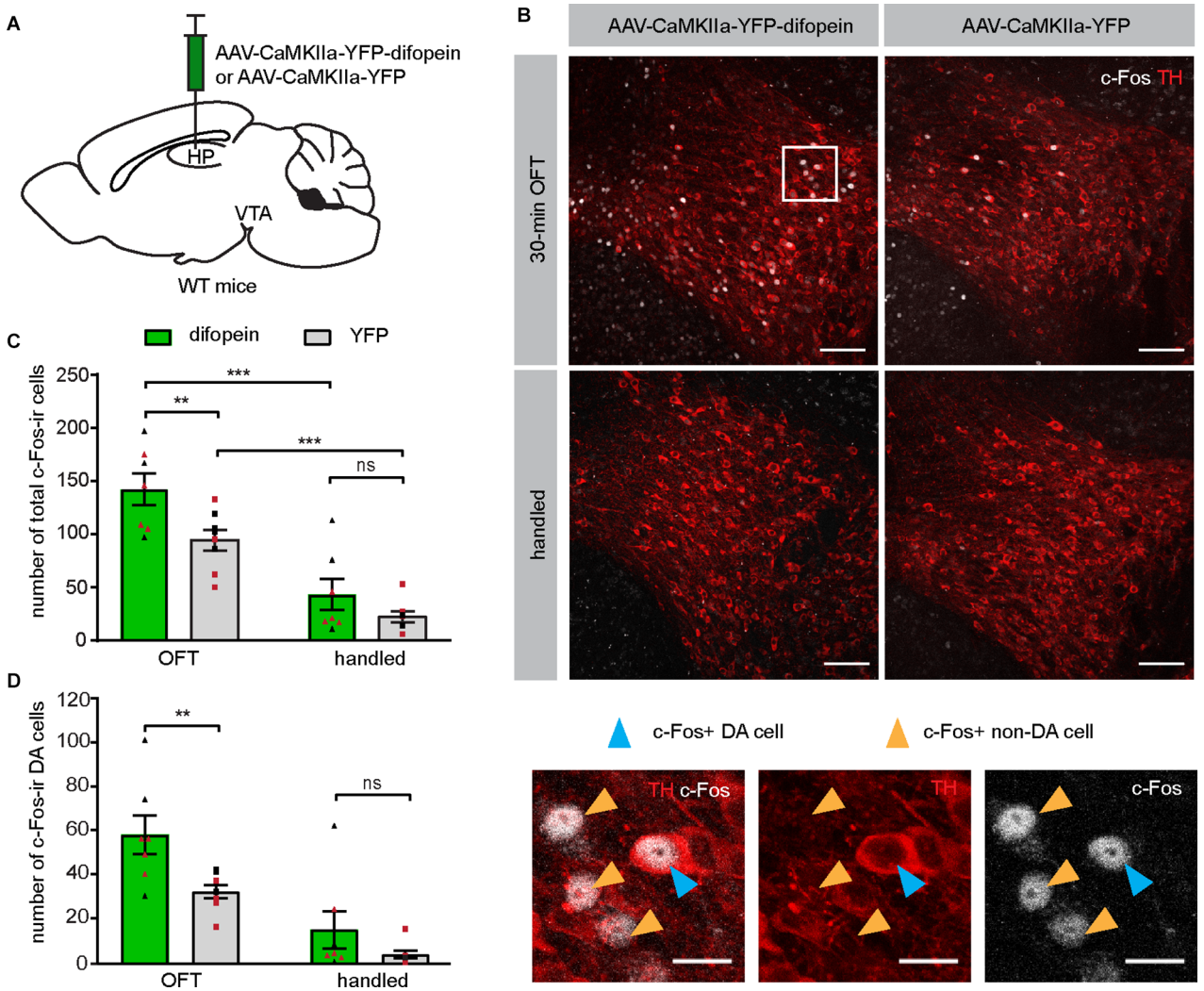

FIGURE 2 | Inhibition of 14-3-3 in the dCA1 increases the number of c-Fos-ir cells in the VTA during OFT. **(A)** Schematic depiction illustrating viral transduction of the dHP CA1 of WT mice with AAV-CaMKIIa-YFP-difopein or AAV-CaMKIIa-YFP. **(B)** Top, representative confocal images of c-Fos and TH co-staining revealing activation of neurons in the VTA of difopein- or YFP-injected mice following either 30-min OFT or gentle handling. Scale bar = 100 μm. Bottom, magnified representative image. Blue arrowheads point to examples of c-Fos and TH co-labeled cells (putative c-Fos-ir DA neurons). Orange arrowheads point to examples of c-Fos-ir only cells (putative c-Fos-ir non-DA neurons). Scale bar = 20 μm. **(C)** Total numbers of c-Fos-ir cells in the VTA of difopein- [n = 7 (3 males and 4 females)/group] or YFP-injected mice [n = 8 (4 males and 4 females)/group] following OFT or handling (multiple Student's unpaired two-tailed t-tests; difopein-OFT vs. YFP-OFT, $^{**}p = 0.0059$; difopein-handled vs. YFP-handled, $p = 0.2070$; difopein-OFT vs. difopein-handled, $^{***}p < 0.001$; YFP-OFT vs. YFP-handled, $^{***}p < 0.001$). **(D)** Numbers of c-Fos and TH co-labeled cells (putative c-Fos-ir DA neurons) in the VTA of difopein- or YFP-injected mice following OFT or handling (multiple Student's unpaired two-tailed t-tests; OFT, $^{**}p = 0.0049$; handled, $p = 0.1968$). All data are presented as mean ± SEM. Data points from male and female mice are shown as black and red symbols, respectively. ns, not significant.

locomotor hyperactivity induced by 14-3-3 inhibition in the dCA1.

14-3-3 Inhibition in the dCA1 Induces Robust C-Fos Expression in the LS, a Relay Between the dCA1 and VTA

As the dCA1 does not directly project to the VTA, we sought to identify the intermediary brain nuclei through which 14-3-3 dysfunction in the dCA1 indirectly modulates VTA activity during OFT. Previous work has established that OFT induces c-Fos expression in several brain regions (Hale et al., 2008; Bourgeois et al., 2012). As the difopein expression in the dCA1 induces locomotor hyperactivity in WT mice, the resulting c-Fos level alterations in specific brain nuclei likely reflect their involvement in the dCA1-VTA pathway. Therefore, we assessed the differences in c-Fos expression between difopein- and YFP-injected mice in response to OFT. Specifically, we examined 28 brain regions previously reported to be associated with either OFT or DA-associated hyperlocomotive behaviors

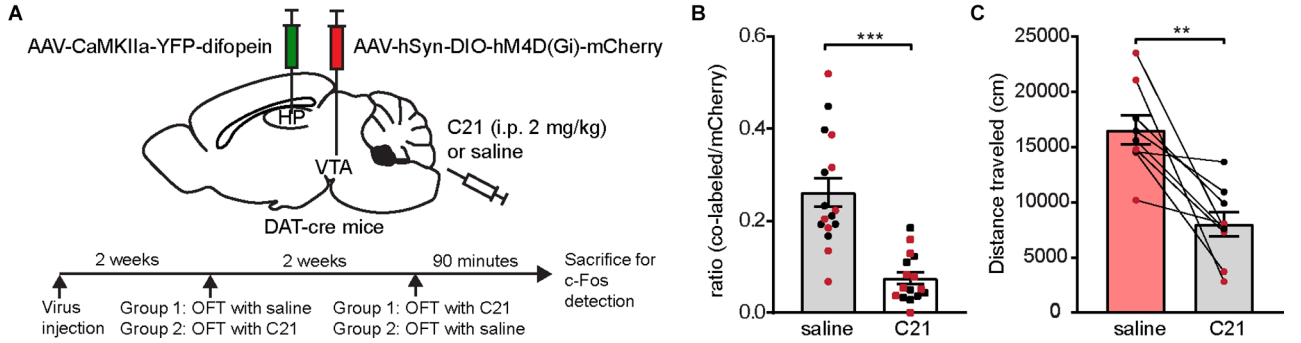

FIGURE 3 | Chemogenetic inhibition of VTA DA neurons attenuates locomotor hyperactivity induced by 14-3-3 inhibition in the dCA1. **(A)** Schematic depiction illustrating (top) DAT-cre mice transduced with AAV-CaMKIIa-YFP-difopein in the dHP CA1 and cre-dependent hM4D in the VTA, and (bottom) experimental timeline. **(B)** Ratio of c-Fos/hM4D co-labeled DA cells to total hM4D-expressing DA cells in the VTA following OFT with saline or C21 administration (n = 16 sections from 2 male and 2 female mice/treatment, Student's unpaired two-tailed t-test with Welch's correction, $^{***}p < 0.0001$), indicating an effective reduction of VTA DA neuronal activity using chemogenetic manipulation. **(C)** Distance traveled for virally transduced DAT-cre mice during OFT following either saline or C21 administration [n = 9 (4 males and 5 females), Student's paired two-tailed t-test, $^{**}p = 0.0021$]. All data are presented as mean ± SEM. Data points from male and female mice are shown as black and red symbols, respectively.

(Badiani et al., 1998; Hale et al., 2008; Strange et al., 2014; Beier et al., 2015; **Figures 4A,B**). Interestingly, we found that AAV-mediated difopein expression in the dCA1 results in robust c-Fos expression in the dCA1 (**Figure 4C** and **Supplementary Figure 1**), suggesting that 14-3-3 dysfunction may lead to over-excitation of the dCA1 neurons during OFT. Of note, significantly higher numbers of c-Fos-ir cells were also identified in the cingulate cortex (Cg), LS, bed nucleus of the stria terminalis (BST), lateral hypothalamus (LH), reticular thalamic nucleus (RT), and other subregions of the hippocampus in difopein-injected mice compared to control (**Figure 4C** and **Supplementary Figure 2**). Among these identified brain regions, difopein-expressing dCA1 efferent projections were particularly evident in the medial part of the caudal LS (LSc) and the dorsomedial part of the rostral LS (LSr; **Supplementary Figure 2**).

The LS is predominantly composed of GABAergic neurons and is involved in motivated behavior, addiction, anxiety, and affect by integrating multiple sensory inputs and adjusting behaviors in response to environmental stimuli (Sheehan et al., 2004; Luo et al., 2011; Jiang et al., 2018; Leroy et al., 2018). Additionally, several lines of evidence support the involvement of the LS in psychiatric disorders, while its precise role remains unclear (Sheehan et al., 2004). To verify the role of the LS in connecting the dCA1 and the VTA, we unilaterally injected an anterograde virus (AAV-CaMKIIa-tdTomato) into the dCA1 and a retrograde tracer (CTB488) into the ipsilateral VTA of WT mice (**Figure 4D**). We found that tdTomato-filled dCA1 axons innervate the medial parts of the LSc and the LSr (**Figure 4D**), which is identical to the projection patterns observed in the LS of difopein-injected mice (**Supplementary Figure 2**). CTB-labeled VTA-projecting cells were found in both the LSc and LSr, including the regions where dHP axons innervate (**Figure 4D**). Using immunohistochemistry against GAD67 or GABA, these VTA-projecting LS cells were identified to be GABAergic (**Figures 4E,F**). Finally, we injected CTB488 into the LS and observed retrogradely labeled cells in the dHP CA1, suggesting that the dCA1 makes monosynaptic connection with the LS (**Figure 4G**). Together, these results demonstrate that the LS is over-activated during difopein-induced locomotor hyperactivity and anatomically connected with both the dCA1 and the VTA.

14-3-3 Inhibition in dCA1 Increases the Number of C-Fos-Expressing VTA-Projecting LS Neurons Following Open Field Exposure

Having observed that difopein expression in the dCA1 leads to increased numbers of c-Fos-ir cells in the LS during locomotor hyperactivity, we next sought to determine whether the activities of the VTA-projecting LS neurons are altered as a result of 14-3-3 inhibition in the dCA1. In this experiment, AAV-difopein (or AAV-YFP as control) and CTB488 were bilaterally injected into the dCA1 and VTA of WT mice, respectively (**Figures 5A,B** and **Supplementary Figure 3**). In response to OFT, a significantly higher number of c-Fos-ir/CTB-ir co-labeled cells were found in the LS of difopein-injected mice compared to control (**Figures 5C–E**), indicating an increased activation of VTA-projecting LS neurons. As the LS is populated by GABAergic neurons (**Figures 4E,F**; Onténiente et al., 1987; Risold and Swanson, 1997), this result suggests that an increased activation of inhibitory projection from the LS to the VTA is associated with difopein-induced locomotor hyperactivity.

Chemogenetic Inhibition of the LS Attenuates Difopein-Induced Locomotor Hyperactivity and DA Neuron Over-Activation

We then asked whether activation of the LS is necessary for difopein-induce locomotor hyperactivity. To address this question, we bilaterally injected AAV-hSyn-hM4D(Gi)-mCherry (or AAV-hSyn-mCherry as control) into the LS of WT mice in addition to AAV-difopein (or AAV-YFP) into the dCA1

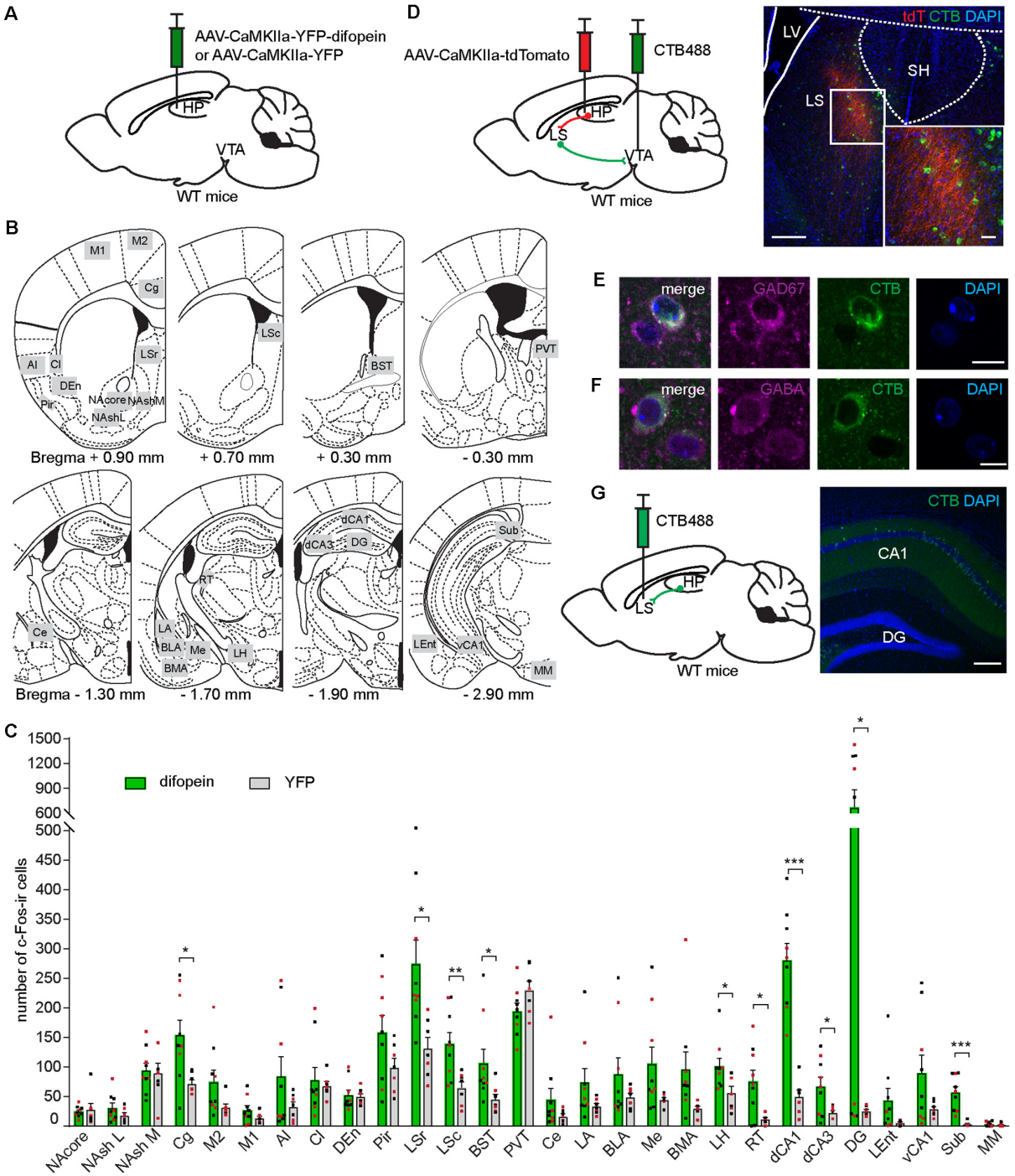

FIGURE 4 | Inhibition of 14-3-3 in the dCA1 increases c-Fos expression in the LS, an anatomical relay between the dCA1 and VTA. **(A)** Schematic depiction illustrating viral transduction of WT mice dHP CA1 with AAV-CaMKIIa-YFP-difopein or AAV-CaMKIIa-YFP. **(B)** Line drawings (adapted from Paxinos and Franklin, 2001) showing the 28 brain nuclei where c-Fos-ir cells were quantified. Number below each diagram indicates the distance from Bregma. **(C)** Numbers of c-Fos-ir cells in 28 brain nuclei of difopein- [n = 9 (5 males and 4 females)] or YFP-injected [n = 7 (4 males and 3 females)] mice following OFT (Student's unpaired two-tailed t-tests; Cg, $^{*}p$ = 0.0133; LSr, $^{*}p$ = 0.0102; LSc, $^{**}p$ = 0.0069; BST, $^{*}p$ = 0.0466; LH, $^{*}p$ = 0.0255; RT, $^{*}p$ = 0.0115; dCA1, $^{***}p < 0.0001$; dCA3, $^{*}p$ = 0.0286; DG, $^{*}p$ = 0.0189; Sub, $^{***}p$ = 0.0003). **(D)** Left, schematic illustration of dual anterograde and retrograde tracing strategy. Right, representative confocal images of CTB-labeled VTA-projecting cells (green) and dHP efferent projections (red) overlapping the LS. Scale bar = 200 μm (100 μm for zoom in image). **(E,F)** Representative confocal images of VTA-projecting CTB-labeled cells in the LS colocalized with GAD67-ir **(E)** or GABA-ir cells **(F)**. Scale bar = 10 μm. **(G)** Left, schematic illustration of retrograde tracer CTB488 unilaterally injected into the LS. Right, representative confocal image of CTB-labeled LS-projecting cells in the dCA1. Scale bar = 200 μm. All data are presented as mean ± SEM. Data points from male and female mice are shown as black and red symbols, respectively.

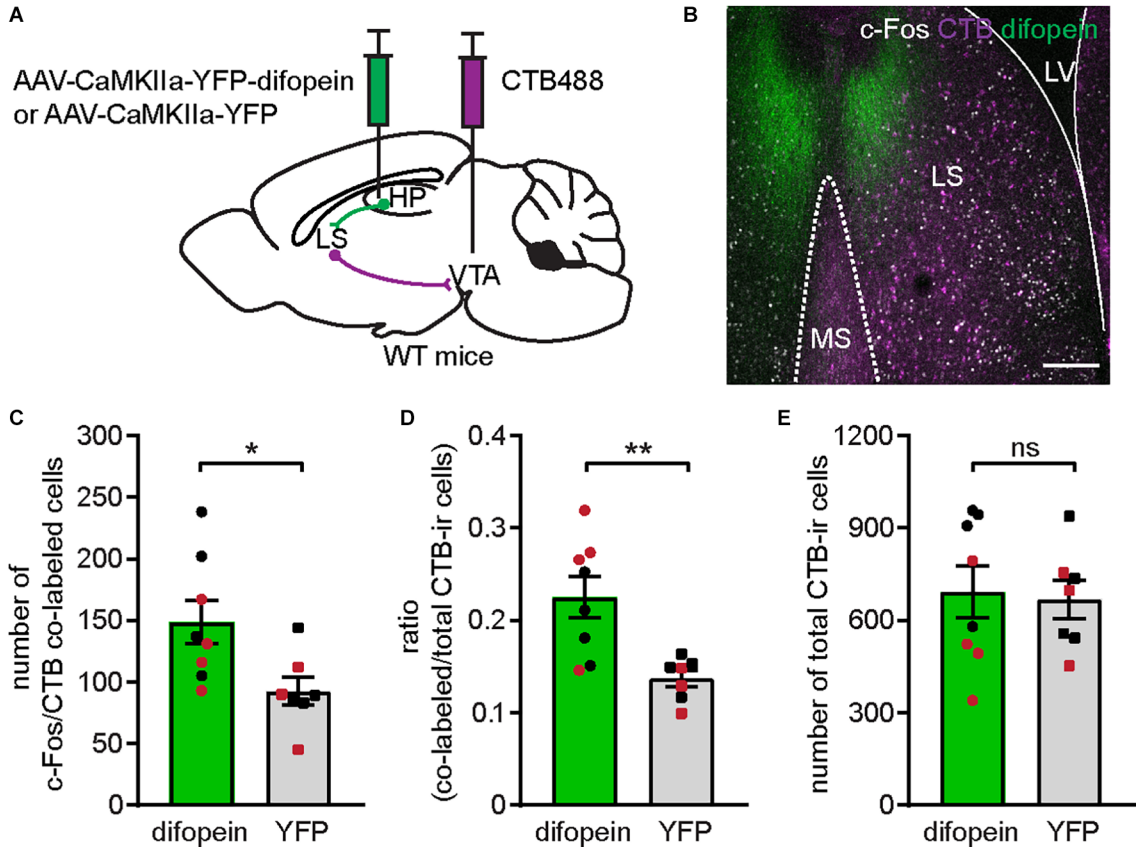

FIGURE 5 | Inhibition of 14-3-3 in the dCA1 activates VTA-projecting LS cells. **(A)** Schematic illustration of AAV-CaMKIIa-YFP-difopein (or AAV-CaMKIIa-YFP) and CTB488 bilaterally injected into the dHP CA1 and VTA of WT mice, respectively. **(B)** Representative confocal image of c-Fos-ir cells (white) and VTA-projecting CTB-ir cells (purple) in the LS of a difopein-injected mouse. Scale bar = 200 μm. **(C–E)** Comparison of the numbers of c-Fos/CTB co-labeled cells **(C)** (Student's unpaired two-tailed t-test, $^{*}p = 0.0237$); the ratio of c-Fos/CTB co-labeled cells to total CTB-ir cells **(D)** (Student's unpaired two-tailed t-test with Welch's correction, $^{**}p = 0.0049$); and the total number of CTB-ir cells **(E)** (Student's unpaired two-tailed t-test, $p = 0.8270$) in the LS of difopein-CTB [$n = 8$ (4 males and 4 females)] or YFP-CTB [$n = 7$ (4 males and 3 female)] injected mice following OFT, indicating an elevated LS-VTA projection associated with 14-3-3 inhibition in the dHP during OFT. All data are presented as mean ± SEM. Data points from male and female mice are shown as black and red symbols, respectively. ns, not significant.

(**Figures 6A–D** and **Supplementary Figure 4**). Administration of C21 (2 mg/kg) significantly lowered the ratio of c-Fos-ir hM4D(Gi)-expressing neurons to total hM4D(Gi)-expressing cells in the LS (**Figure 6E** and **Supplementary Figure 4**), indicating an effective suppression of LS neuronal activity. When assessed with an open field assay, we found that LS inhibition is sufficient to attenuate locomotor hyperactivity (**Figure 6F**). These results suggest that LS activation is necessary for locomotor hyperactivity induced by 14-3-3 inhibition in the dCA1.

To determine whether LS inhibition attenuates difopein-induced locomotor hyperactivity by modulating VTA DA neuronal activation, we analyzed the number of c-Fos-expressing cells in the VTA of C21 injected mice from each viral group following OFT. C21-induced LS inhibition significantly reduced the total number of c-Fos-ir cells in the VTA of difopein-hM4D mice compared to difopein-mCherry mice (**Figure 6G** and **Supplementary Figure 5**). Further cell-type-specific analysis showed that inhibition of the LS leads to a significantly lower number of c-Fos-ir DA neurons in difopein-hM4D mice compare with difopein-mCherry mice (**Figure 6H**). Collectively, these results indicate that LS activation is required for the increased activation of VTA DA neurons during locomotor hyperactivity induced by 14-3-3 inhibition in the dCA1.

Chemogenetic Activation of dCA1 Imitates Difopein-Induced Behavioral and Neuronal Activity Alterations

Having observed a robust c-Fos expression in dCA1 neurons during difopein-induced hyperlocomotive behavior (**Figure 4C** and **Supplementary Figure 1**), we hypothesized that 14-3-3 inhibition leads to increased neuronal activation in difopein-expressing dCA1 cells, which results in locomotor hyperactivity *via* the dCA1-LS-VTA pathway. If so, direct chemogenetic activation of the dCA1 should be sufficient to elicit the behavioral and molecular alterations seen in

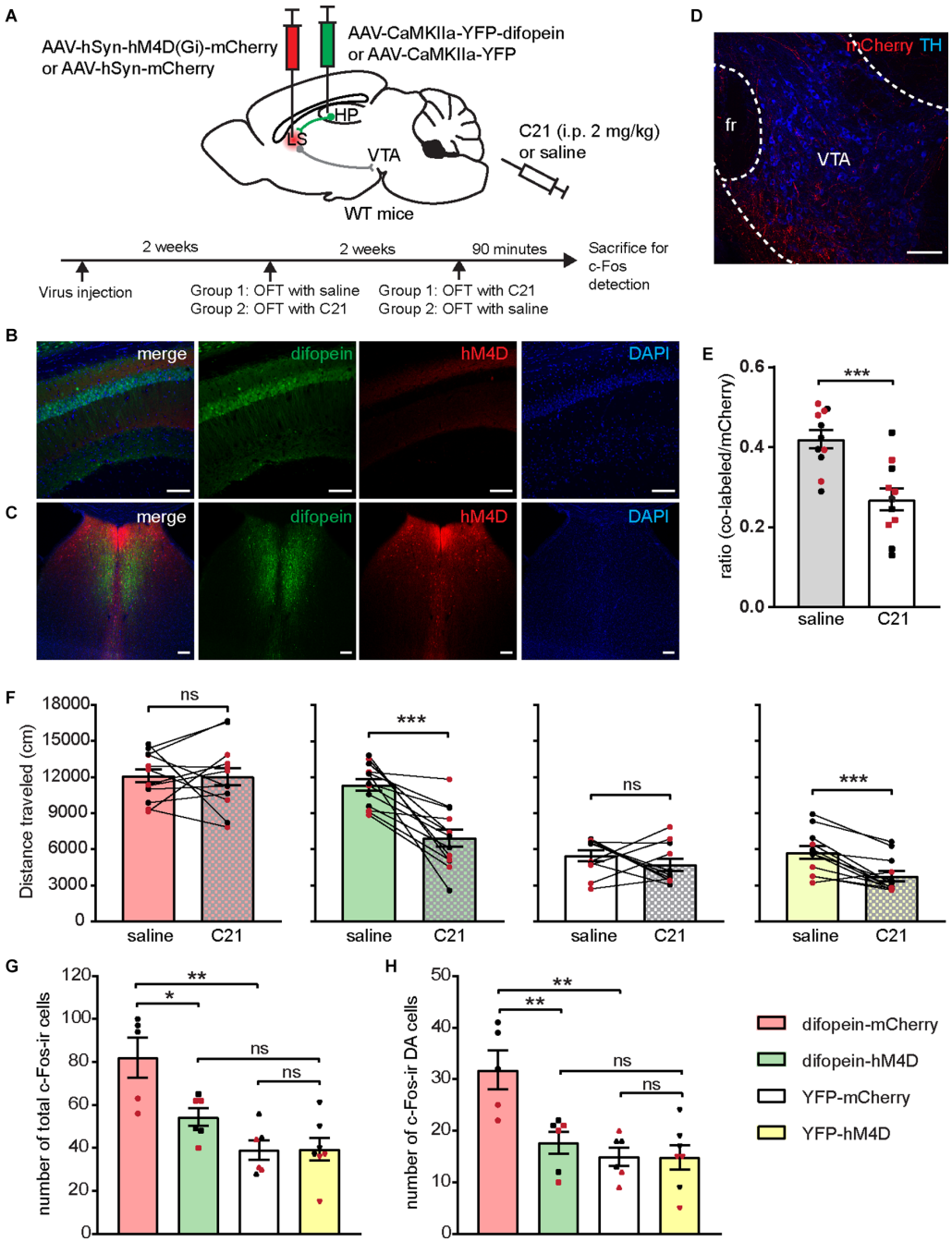

FIGURE 6 | Chemogenetic inhibition of the LS attenuates 14-3-3 inhibition induced locomotor hyperactivity and DA neuron over-activation. **(A)** Schematic illustration of viral transductions and experimental timeline. **(B–D)** Representative images of difopein and hM4D expression in the dCA1 **(B)** and the LS **(C)**, as well as efferent projections from mCherry-infected LS neurons in the VTA **(D)**. Scale bar = 100 μm. **(E)** Ratio of c-Fos/hM4D co-labeled cells to total hM4D-expressing cells in the LS during OFT following saline or C21 treatment (n = 11 sections from 2 male and 2 female mice/group, Student's unpaired two-tailed t-test, ***p = 0.0004), indicating an effective chemogenetic inhibition of LS neural activity. **(F)** Distance traveled of injected mice in OFT following either saline or C21 administration. Student's paired two-tailed t-test: difopein-mCherry [n = 12 (5 males and 7 females), p = 0.9711]; difopein-hM4D (n = 13 (7 males and 6 females), ***p = 0.0001); YFP-mCherry [n = 11 (6 males and 5 females), p = 0.3457]; and YFP-hM4D [n = 12 (6 males and 6 females), ***p = 0.0004]. **(G,H)** Number of total c-Fos-ir **(G)** and c-Fos-ir DA cells **(H)** in the VTA of injected mice during OFT following C21 administration: difopein-mCherry (n = 3 males and 2 females), difopein-hM4D (n = 3 males and 3 females), YFP-mCherry (n = 3 males and 3 females), and YFP-hM4D (n = 4 males and 3 females). Student's unpaired two-tailed t-tests. **(G)** difopein-mCherry vs. difopein-hM4D, *p = 0.0176; difopein-mCherry vs. YFP-mCherry, **p = 0.0017; difopein-hM4D vs. YFP-hM4D, p = 0.0544; YFP-mCherry vs. YFP-hM4D, p = 0.9532. **(H)** difopein-mCherry vs. difopein-hM4D, **p = 0.0075; difopein-mCherry vs. YFP-mCherry, **p = 0.0019; difopein-hM4D vs. YFP-hM4D, p = 0.4051; YFP-mCherry vs. YFP-hM4D, p = 0.9634. All data are presented as mean ± SEM. Data points from male and female mice are shown as black and red symbols, respectively. ns, not significant.

the difopein-injected mice. To selectively activate pyramidal neurons in the dCA1, we bilaterally injected AAV-hSyn-DIO-hM3D(Gq)-mCherry (or AAV-CMV-DIO-EGFP as control) into the dCA1 of CaMKIIa-cre mice (**Figure 7A**). Compared with saline administration, C21 (1 mg/kg) injection sufficiently induced robust c-Fos expression in hM3D-infected dCA1 pyramidal neurons (**Figure 7B**). With this approach, we assessed the locomotive activity of injected mice under saline or C21 administration, as well as c-Fos expression in the LS and the VTA following OFT with C21. We found that activation of the dCA1 significantly increased the locomotive activity of CaMKIIa-cre mice during OFT (**Figure 7C**). Furthermore, dCA1 activation induced significantly higher numbers of c-Fos-ir cells in both the LS (**Figure 7D**) and the VTA (**Figure 7E**). Specifically, we found an increased number of c-Fos-ir DA neurons in the VTA due to dCA1 activation (**Figure 7F**). Collectively, these results demonstrate that direct activation of the dCA1 is sufficient to reproduce behavioral as well as neuronal activity alterations in the dCA1-LS-VTA pathway which have been observed in mice with 14-3-3 inhibition in the dCA1. This suggests that 14-3-3 dysfunction might lead to over-activation of the affected pyramidal neurons, which in turn disrupt the neuronal activity within the downstream pathway.

Chemogenetic Activation of LS-Projecting dCA1 Neurons Induces Locomotor Hyperactivity and Increases Neuronal Activation in the LS and VTA

As dCA1 neurons project to several brain nuclei, we sought to determine whether activation of the dCA1-LS projection is sufficient to induce locomotor hyperactivity as well as neuronal activity alterations in the dCA1-LS-VTA pathway. To selectively activate dCA1-LS neurons, we bilaterally injected AAV-hSyn-DIO-hM3D(Gq)-mCherry (or AAV-CMV-DIO-EGFP as control) into the dCA1 of WT mice and a retrogradely propagating AAV encoding Cre-recombinase into the LS (**Figures 8A,B**). We found that activation of LS-projecting dCA1 neurons was sufficient to induce locomotor hyperactivity (**Figure 8C**), increased the number of c-Fos-ir cells in the LS (**Figure 8D**) and the VTA (**Figure 8E**), as well as increased the number of c-Fos-ir DA neurons in WT mice (**Figure 8F**). While the dCA1-LS pathway was specifically targeted to express hM3D, we found that LS-projecting dCA1 neurons also send collateral projections to the NAc and mammillary body (MM) to a lesser degree. As hippocampal bundles projecting to the NAc and MM pass through the LS, it is technically challenging to selectively activate dCA1 terminals in the LS without affecting the projections to other brain regions. Nonetheless, we investigated whether DREADD-mediated activation of NAc- or MM-projecting dCA1 neurons is sufficient to induce locomotor hyperactivity and found no significant changes in novelty-induced locomotor activity when either NAc- or MM-projecting dCA1 neurons were activated (**Supplementary Figure 6**). Considering that c-Fos expressions in either the NAc or MM were not different between difopein- and YFP-injected mice during OFT (**Figure 4C**), these results suggest that dCA1-LS projection is likely the primary pathway critical for psychomotor behavior induced by dCA1 hyperactivation.

Together, the results of this study support a model in which 14-3-3 loss of function results in over-activation of the affected dCA1 pyramidal neurons. Such hippocampal dysfunction leads to increased activation of LS GABAergic neurons. Escalating inhibitory input from the LS to the VTA enhances DA neuronal activation *via* disinhibition (Vega-Quiroga et al., 2018), which ultimately induces psychomotor behavior (**Figures 9A,B**).

DISCUSSION

In this study, we focused on identifying the neural circuitry mechanism underlying 14-3-3 dysfunction in the dCA1 induced psychosis-like behavior in mice. Several lines of evidence from imaging studies of schizophrenia patients found decreased hippocampal volume and enhanced cerebral blood flow in both anterior and posterior HP (vHP and dHP in rodent; Medoff et al., 2001; Schobel et al., 2009a; Talati et al., 2014; McHugo et al., 2019). A loss of parvalbumin-containing GABAergic interneurons in the HP has also been found both in postmortem schizophrenia patients and in several animal models of schizophrenia (Zhang and Reynolds, 2002; Lodge et al., 2009; Marissal et al., 2018). Collectively, these findings implicate a robust hippocampal hyperactivity as an endophenotype in schizophrenia. As the HP detects novelty/familiarity by comparing previous memories with current sensory input, a dysfunctional HP may result in the aberrant assignment of salience that causes psychosis (Lisman and Grace, 2005; Kätzel et al., 2020; Modinos et al., 2020). While the precise relationship between hippocampal hyperactivity and mesolimbic DA dysregulation remains to be established in humans, studies using rodent models have provided some supporting evidence. For example, excessive neuronal firing in the ventral hippocampus (vHP) is found to be necessary for amphetamine-induced locomotor hyperactivity and increased DA neuron population activity in a prenatal methylazoxymethanol acetate rodent model of schizophrenia (Lodge and Grace, 2007). Optogenetic activation of vHP CA1/subiculum (vSub) neurons is sufficient to induce hyperlocomotion and cognitive deficits in WT mice (Wolff et al., 2018). Here, we demonstrated that the dorsal portion of the HP also plays an important role in the pathophysiology of psychosis-like behavior in mice, which is supported by previous studies: (1) serotonergic lesion of the dHP, but not the vHP, normalizes psychostimulant-induced locomotion and sensorimotor gating (Kusljic and van den Buuse, 2004; Adams et al., 2009); (2) c-Fos expression in the dHP is increased during psychomotor behavior in GluA1 knockout mice (Procaccini et al., 2011); and (3) chemogenetic activation of parvalbumin-containing interneurons in the dCA1 is sufficient to restore WT-like physiology and behaviors in Lgdel/+ mouse model of schizophrenia (Marissal et al., 2018). To delineate the neural circuitries underlying hippocampal regulation of DA activities, elegant studies were carried

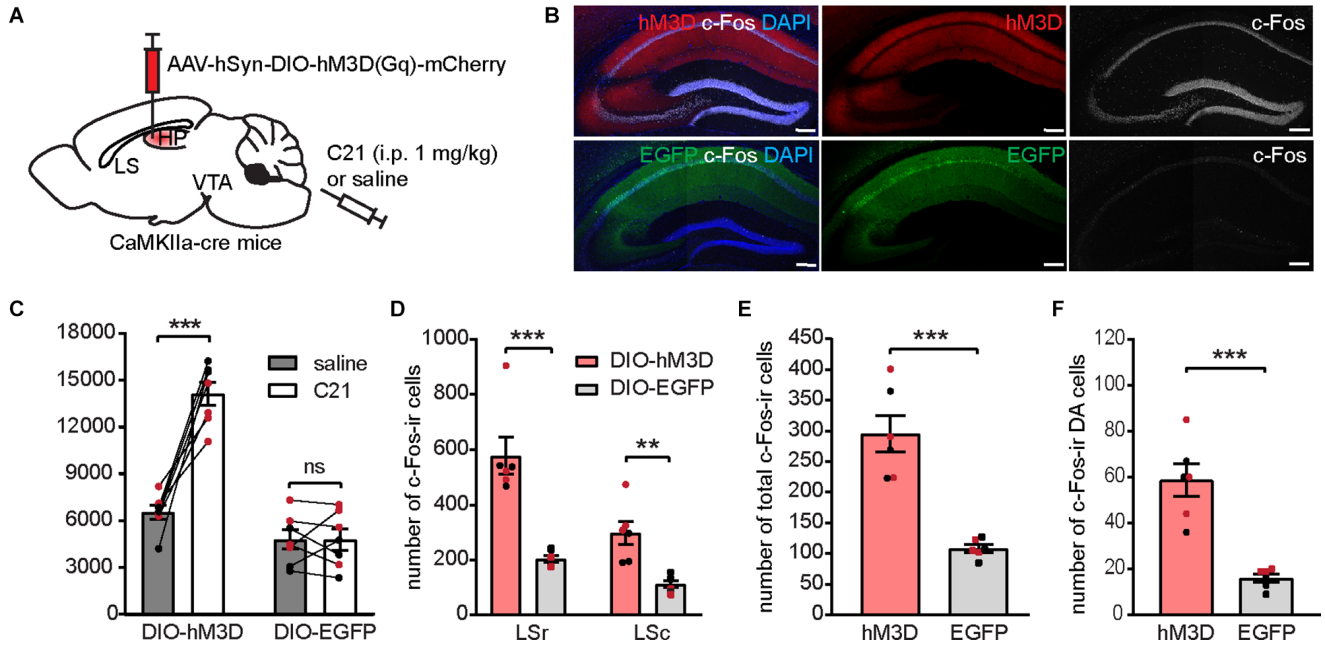

FIGURE 7 | Chemogenetic activation of the dCA1 induces locomotor hyperactivity and increases c-Fos expression in the LS and the VTA. **(A)** Schematic illustration of AAV-hSyn-DIO-hM3D(Gq)-mCherry bilaterally transduced into the dHP CA1 of CaMKIIa-cre mice. **(B)** Representative confocal images showing hM3D activation by C21 effectively elicited c-Fos-ir (white) in the injection site. Scale bar = 200 μm. **(C)** Distance traveled of virally transduced CaMKIIa-cre mice during OFT following either saline or C21 administration [n = 7 (3 males and 4 females)/group; Student's paired two-tailed t-tests; DIO-hM3D, ***p = 0.0003; DIO-EGFP, p = 0.9929]. **(D–F)** Number of total c-Fos-ir cells in the LS **(D)**, number of total c-Fos-ir cells in the VTA **(E)**, and number of c-Fos/TH co-labeled cells in the VTA **(F)** of virally transduced mice following C21 administration [n = 6 (3 males and 3 females)/group; **(D)**, multiple Student's unpaired two-tailed t-tests; LSr, ***$p < 0.0001$; LSc, **p = 0.004; **(E)**, Student's unpaired two-tailed t-tests, ***p = 0.0001; **(F)**, Student's unpaired two-tailed t-tests, ***p = 0.0002]. All data are presented as mean ± SEM. Data points from male and female mice are shown as black and red symbols, respectively. ns, not significant.

out illustrating a vSub/vCA1-nucleus accumbens-ventral pallidum-VTA pathway through which the vHP positively regulates VTA DA neuronal activities (Floresco et al., 2001; Lisman and Grace, 2005; Lodge and Grace, 2007, 2008, 2011). However, as dorsal and ventral portions of the HP have different anatomical connectivity and participate in distinct brain functions (Fanselow and Dong, 2010), it is possible that the dHP regulates the mesolimbic system *via* a distinct pathway. Furthermore, CA1 subfield abnormalities are especially highlighted in several human schizophrenia studies (Schobel et al., 2009b; Zierhut et al., 2013; Talati et al., 2014), yet the neural circuitry underlying dCA1's regulation of DAergic activity in psychotic behavior has not been previously established. While we do not rule out the involvement of other interconnecting brain nuclei such as NAc, our results highlight a dCA1-LS-VTA polysynaptic pathway through which molecular disturbance of an important family of proteins in the dCA1 leads to a shift in E/I regulation of DAergic activity triggering psychosis-like behavior.

Here, we found that regional 14-3-3 inhibition enhances c-Fos expression in the dCA1 during OFT (**Supplementary Figure 1**), indicating that the affected dCA1 neurons are abnormally activated during novel environmental exposure. Additionally, we provided, to our knowledge, the first evidence that chemogenetic activation of LS-projecting dCA1 pyramidal neurons is sufficient to induce locomotor hyperactivity *via* the dCA1-LS-VTA pathway. This indicates that 14-3-3 inhibition-induced disturbance in downstream neuronal activities may be due to an increased dCA1 activation. This is particularly interesting as 14-3-3 deficiency has also been implicated in schizophrenia. Linkage analysis reveals that Ywhah, which encodes 14-3-3η, is located within the established 22q12-13 candidate risk chromosomal region of schizophrenia (Toyooka et al., 1999), though it is by no means the only 14-3-3 isoform linked with this disorder. Genetic and post-mortem mRNA analyses have identified decreased expression of other 14-3-3 isoforms in multiple brain regions of schizophrenia patients (Middleton et al., 2005; Wong et al., 2005; Ikeda et al., 2008; Kido et al., 2014). Within the past two decades, several animal models of schizophrenia with 14-3-3 deficiency were established (Cheah et al., 2012; Foote et al., 2015) and provided valuable insight into the functions of 14-3-3 at postsynaptic site and how 14-3-3 deficiency affects synaptic activities. It was shown that 14-3-3 deficiency is associated with a decrease in levels of NMDA receptor subunits, a significant reduction of the NMDA receptor-mediated synaptic currents in CA1 pyramidal neurons which express the 14-3-3 inhibitor, as well as an impairment of long-term potentiation at hippocampal CA3-CA1 synapses (Qiao et al., 2014; Foote et al., 2015; Graham et al., 2019). Additionally, one study shows that 14-3-3 binding slows

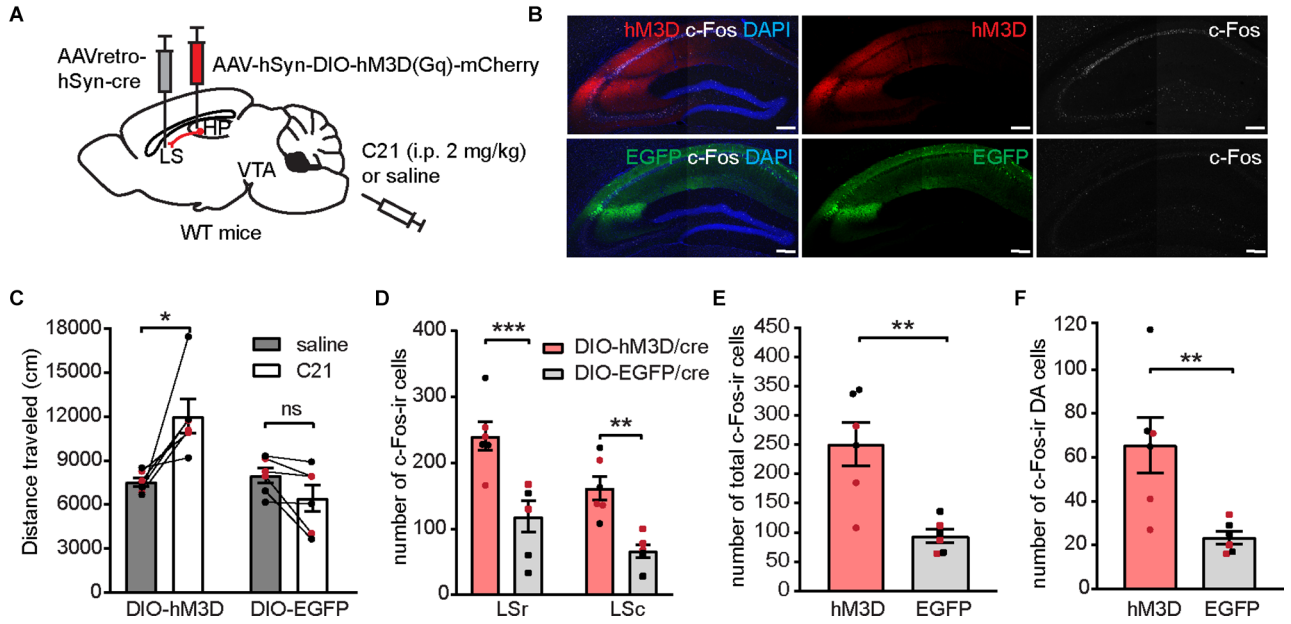

FIGURE 8 | Chemogenetic activation of the LS-projecting dCA1 neurons induces locomotor hyperactivity and increases c-Fos expression in the LS and the VTA. **(A)** Schematic depiction illustrating viral transduction of AAV-hSyn-DIO-hM3D(Gq)-mCherry in the dHP CA1 and AAVretro-cre in the LS. **(B)** Representative confocal images showing hM3D activation by C21 effectively elicited c-Fos-ir (white) in LS-projecting CA1 neurons. Scale bar = 200 μm. **(C)** Distance traveled of virally transduced WT mice during OFT following either saline or C21 administration [n = 6 (3 males and 3 females)/group; Student's paired two-tailed t-tests; DIO-hM3D/cre, $^{*}p$ = 0.0226; DIO-EGFP/cre, p = 0.6024]. **(D–F)** Number of total c-Fos-ir cells in the LS **(D)**, number of total c-Fos-ir cells in the VTA **(E)**, and number of c-Fos/TH co-labeled cells in the VTA **(F)** of virally transduced mice following C21 administration [n = 6 (3 males and 3 females)/group; **(D)**, multiple Student's unpaired two-tailed t-tests; LSr, $^{***}p < 0.0001$; LSc, $^{**}p$ = 0.0019; **(E)**, Student's unpaired two-tailed t-tests, $^{**}p$ = 0.0024; **(F)**, Student's unpaired two-tailed t-tests, $^{**}p$ = 0.0090]. All data are presented as mean ± SEM. Data points from male and female mice are shown as black and red symbols, respectively. ns, not significant.

desensitization kinetics of GluK2a-containing kainate receptor which mediates postsynaptic transmission, synaptic plasticity, and neuronal excitability (Sun et al., 2013). Moreover, 14-3-3 plays a significant role in synaptogenesis as 14-3-3 deficiency leads to a significant loss of the dendritic spine (Foote et al., 2015; Xu et al., 2015). However, it remains unclear what might be the molecular target of 14-3-3 that mediates dCA1 over-activation under 14-3-3 dysfunction. While we cannot determine solely with c-Fos expression whether 14-3-3 dysfunction-induced dCA1 activation is due to alterations in neuronal excitability, firing pattern, or receptor function, future studies using electrophysiology should help with future investigations of the precise mechanism. Nonetheless, given the critical roles 14-3-3 proteins play in synaptic transmission and plasticity, particularly in schizophrenia (Skoulakis and Davis, 1996; Broadie et al., 1997; Beguin et al., 2006; Li et al., 2006; Qiao et al., 2014; Chung et al., 2015), findings from this study should inspire novel therapeutic approaches for psychosis targeting 14-3-3-mediated neuronal processes. The LS receives strong glutamatergic input from the HP and is known to drive context-induced reinstatement *via* a dCA3-LS-VTA circuit (Luo et al., 2011), promote social aggression depending on dCA2 output (Leroy et al., 2018), and regulate feeding behaviors *via* vHP-LS pathways (Sweeney and Yang, 2015; Kosugi et al., 2021). Additionally, human studies have previously found abnormal septal structure and EEG activities in schizophrenia patients (Hanley et al., 1972; Heath and Walker, 1985), but the direct involvement of LS in psychosis-like behavior was previously undetermined. Here, we provide the following evidence that collectively supports a novel role of the LS in psychomotor behavior: (1) dCA1 dysfunction-induced locomotor hyperactivity and DA over-activation are associated with an over-activated LS as well as an elevated LS-VTA projection; (2) chemogenetic silencing of the LS is sufficient to attenuate both dCA1 dysfunction-induced locomotor hyperactivity and DA over-activation; (3) chemogenetic activation of dCA1-LS is sufficient to induce locomotor hyperactivity and DA over-activation. It is worth noting that while dCA1 projects predominantly to the dorsomedial part of the LS, other parts of the LS also contain c-Fos-ir cells induced by dCA1 dysfunction/activation. This might indicate the involvement of LS local interneurons that transmit hippocampal inputs within different subregions of the LS during locomotor hyperactivity, which will be investigated in future studies. Additionally, we showed that the LS positively regulates VTA DA neuronal activity, which is consistent with previous studies in which stimulation of the LS leads to activation of the DA neurons in the VTA by inhibiting local GABAergic activity (Luo et al., 2011; Vega-Quiroga et al., 2018). We presume that VTA GABAergic neurons play a similar role in the dCA1-LS-VTA pathway and will aim to elucidate such mechanisms in future studies.

In sum, our findings highlight a polysynaptic pathway through which 14-3-3 deficiency-induced dHP CA1 hyperactivation results in neural circuit abnormalities

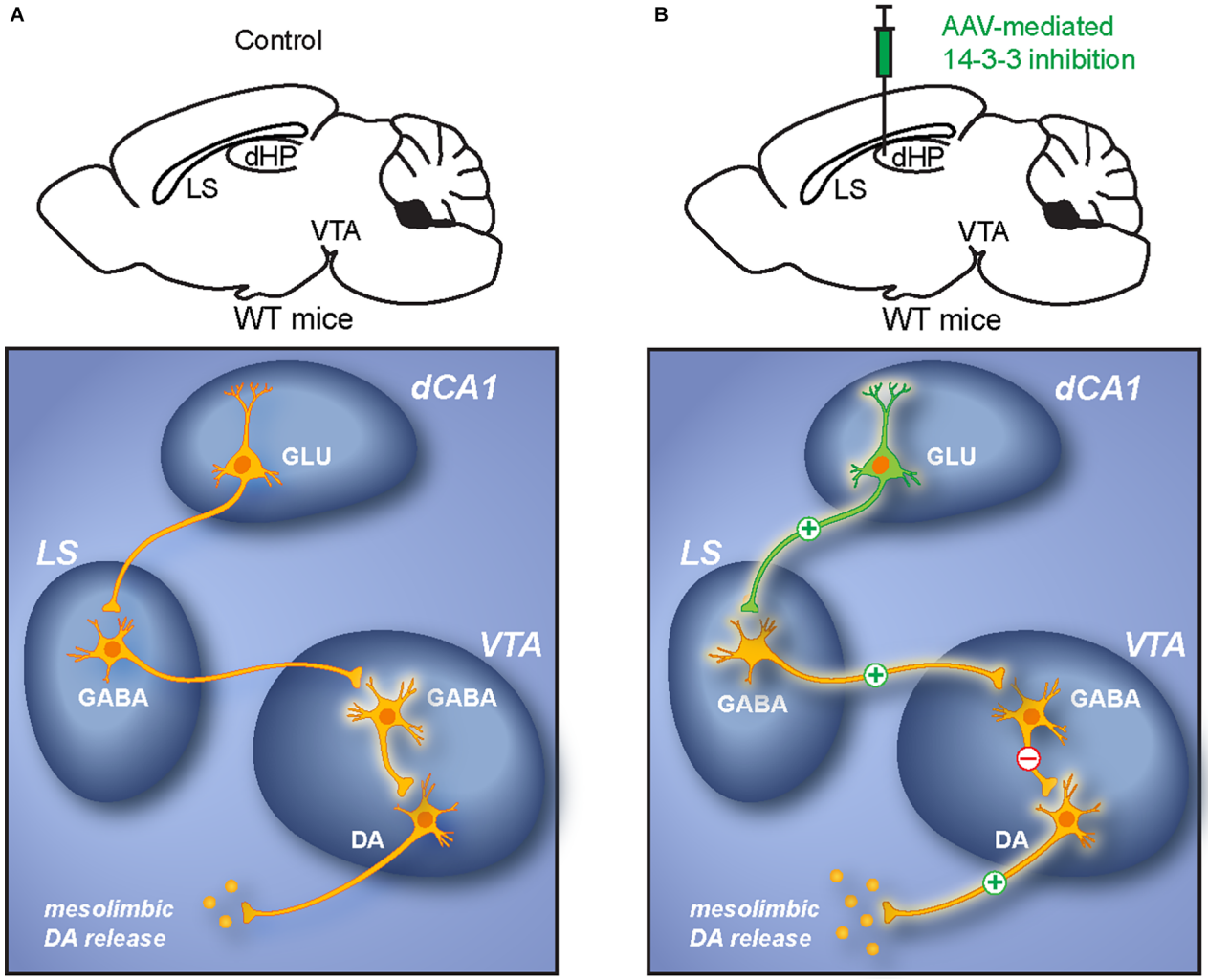

FIGURE 9 | Proposed dCA1-LS-VTA pathway underlying psychomotor behavior. **(A)** Schematic illustration of the dCA1-LS-VTA polysynaptic pathway in WT mice. **(B)** Schematic illustration of alterations in neuronal activity within the pathway due to dCA1 dysfunction. The model proposes that 14-3-3 inhibition results in increased activation of pyramidal neurons in the dCA1, which leads to enhanced glutamatergic output to the LS that excites VTA-projecting GABAergic LS neurons. DA neurons in the VTA are then disinhibited by the elevated GABAergic projections from the LS. As a result, increased activation of VTA DA neurons induces psychomotor behaviors.

that lead to pathological DA dysregulation associated with psychomotor behavior. These results address a potential mechanism of psychosis and provide valuable insights and potential targets for future therapeutic development.

DATA AVAILABILITY STATEMENT

The original contributions presented in the study are included in the article/**Supplementary Material**, further inquiries can be directed to the corresponding author.

ETHICS STATEMENT

The animal study was reviewed and approved by The Florida State University Animal Care and Use Committee.

AUTHOR CONTRIBUTIONS

JZ and YZ wrote the manuscript, conceived the project and designed the experiments. JZ performed all experiments, analyzed the data, and prepared the figures. YW assisted and supervised the maintenance of all mouse lines used in this study. MN assisted in genotyping and histology analysis. All authors contributed to the article and approved the submitted version.

FUNDING

This work was supported by the National Institutes of Health (award number R01 MH115188 to YZ).

ACKNOWLEDGMENTS

We thank Terra Bradley for her assistance with editing the manuscript and Charles Badland for his assistance with the figure creation. For the viral plasmids, we thank Dr. Karl Deisseroth (AAV2-CaMKIIa-EYFP and pAAV-hSyn-mCherry); Dr. Bryan Roth (pAAV-hSyn-hM4D(Gi)-mCherry, pAAV-hSyn-hM4D(Gq)-mCherry, pAAV-hSyn-DIO-hM3D(Gq)-mCherry, and pAAV-hSyn-DIO-hM3D(Gi)-mCherry); and Dr. James M. Wilson (pENN-AAV-hSyn-Cre-WPRE-hGH) for depositing their plasmids to the UNC vector core or Addgene.

SUPPLEMENTARY MATERIALS

The Supplementary Material for this article can be found online at: https://www.frontiersin.org/articles/10.3389/fnmol.2022.817227/full#supplementary-material.

REFERENCES

Abi-Dargham, A., van de Giessen, E., Slifstein, M., Kegeles, L. S., and Laruelle, M. (2009). Baseline and amphetamine-stimulated dopamine activity are related in drug-naïve schizophrenic subjects. *Biol. Psychiatry* 65, 1091–1093. doi: 10.1016/j.biopsych.2008.12.007

Adams, W., Ayton, S., and van den Buuse, M. (2009). Serotonergic lesions of the dorsal hippocampus differentially modulate locomotor hyperactivity induced by drugs of abuse in rats: implications for schizophrenia. *Psychopharmacology (Berl)* 206, 665–676. doi: 10.1007/s00213-009-1617-1

Aitta-Aho, T., Maksimovic, M., Dahl, K., Sprengel, R., and Korpi, E. R. (2019). Attenuation of novelty-induced hyperactivity of gria1-/- mice by cannabidiol and hippocampal inhibitory chemogenetics. *Front. Pharmacol.* 10:309. doi: 10.3389/fphar.2019.00309

Badiani, A., Oates, M. M., Day, H. E., Watson, S. J., Akil, H., and Robinson, T. E. (1998). Amphetamine-induced behavior, dopamine release and c-fos mRNA expression: modulation by environmental novelty. *J. Neurosci.* 18, 10579–10593. doi: 10.1523/JNEUROSCI.18-24-10579.1998

Beguin, P., Mahalakshmi, R., Nagashima, K., Cher, D., Ikeda, H., Yamada, Y., et al. (2006). Nuclear sequestration of beta-subunits by Rad and Rem is controlled by 14-3-3 and calmodulin and reveals a novel mechanism for Ca2+ channel regulation. *J. Mol. Biol.* 355, 34–46. doi: 10.1016/j.jmb.2005.10.013

Beier, K. T., Steinberg, E. E., DeLoach, K. E., Xie, S., Miyamichi, K., Schwarz, L., et al. (2015). Circuit architecture of VTA dopamine neurons revealed by systematic input-output mapping. *Cell* 162, 622–634. doi: 10.1016/j.cell.2015.07.015

Belforte, J. E., Zsiros, V., Sklar, E. R., Jiang, Z., Yu, G., Li, Y., et al. (2010). Postnatal NMDA receptor ablation in corticolimbic interneurons confers schizophrenia-like phenotypes. *Nat. Neurosci.* 13, 76–83. doi: 10.1038/nn.2447

Bell, R., Munro, J., Russ, C., Powell, J. F., Bruinvels, A., Kerwin, R. W., et al. (2000). Systematic screening of the 14-3-3 eta (η) chain gene for polymorphic variants and case-control analysis in schizophrenia. *Am. J. Med. Genet.* 96, 736–743. doi: 10.1002/1096-8628(20001204)96:6<736::AID-AJMG8>3.0.CO;2-2

Boekhoudt, L., Omrani, A., Luijendijk, M. C., Wolterink-Donselaar, I. G., Wijbrans, E. C., van der Plasse, G., et al. (2016). Chemogenetic activation of dopamine neurons in the ventral tegmental area, but not substantia nigra, induces hyperactivity in rats. *Eur. Neuropsychopharmacol.* 26, 1784–1793. doi: 10.1016/j.euroneuro.2016.09.003

Bourgeois, J. P., Meas-Yeadid, V., Lesourd, A. M., Faure, P., Pons, S., Maskos, U., et al. (2012). Modulation of the mouse prefrontal cortex activation by neuronal nicotinic receptors during novelty exploration but not by exploration of a familiar environment. *Cereb. Cortex* 22, 1007–1015. doi: 10.1093/cercor/bhr159

Broadie, K., Rushton, E., Skoulakis, E., and Davis, R. (1997). Leonardo, a Drosophila 14-3-3 protein involved in learning, regulates presynaptic function. *Neuron* 19, 391–402. doi: 10.1016/s0896-6273(00)80948-4

Cheah, P. S., Ramshaw, H. S., Thomas, P. Q., Toyo-Oka, K., Xu, X., Martin, S., et al. (2012). Neurodevelopmental and neuropsychiatric behaviour defects arise from 14-3-3ζ deficiency. *Mol. Psychiatry* 17, 451–466. doi: 10.1038/mp.2011.158

Chung, C., Wu, W., and Chen, B. (2015). Identification of novel 14-3-3 residues that are critical for isoform-specific interaction with GluN2C to regulate N-Methyl-D-aspartate (NMDA) receptor trafficking. *J. Biol. Chem.* 290, 23188–23200. doi: 10.1074/jbc.M115.648436

Dugré, J. R., Bitar, N., Dumais, A., and Potvin, S. (2019). Limbic hyperactivity in response to emotionally neutral stimuli in schizophrenia: a neuroimaging meta-analysis of the hypervigilant mind. *Am. J. Psychiatry* 176, 1021–1029. doi: 10.1176/appi.ajp.2019.19030247

Fanselow, M. S., and Dong, H. W. (2010). Are the dorsal and ventral hippocampus functionally distinct structures? *Neuron* 65, 7–19. doi: 10.1016/j.neuron.2009.11.031

Floresco, S. B., Todd, C. L., and Grace, A. A. (2001). Glutamatergic afferents from the hippocampus to the nucleus accumbens regulate activity of ventral tegmental area dopamine neurons. *J. Neurosci.* 21, 4915–4922. doi: 10.1523/JNEUROSCI.21-13-04915.2001

Foote, M., Qiao, H., Graham, K., Wu, Y., and Zhou, Y. (2015). Inhibition of 14-3-3 proteins leads to Schizophrenia-related behavioral phenotypes and synaptic defects in mice. *Biol. Psychiatry* 78, 386–395. doi: 10.1016/j.biopsych.2015.02.015

Fromer, M., Pocklington, A. J., Kavanagh, D. H., Williams, H. J., Dwyer, S., Gormley, P., et al. (2014). De novo mutations in schizophrenia implicate synaptic networks. *Nature* 506, 179–184. doi: 10.1038/nature12929

Gao, R., and Penzes, P. (2015). Common mechanisms of excitatory and inhibitory imbalance in schizophrenia and autism spectrum disorders. *Curr. Mol. Med.* 15, 146–167. doi: 10.2174/1566524015666150303003028

Gilani, A. I., Chohan, M. O., Inan, M., Schobel, S. A., Chaudhury, N. H., Paskewitz, S., et al. (2014). Interneuron precursor transplants in adult hippocampus reverse psychosis-relevant features in a mouse model of hippocampal disinhibition. *Proc. Natl. Acad. Sci. U S A* 111, 7450–7455. doi: 10.1073/pnas.1316488111

Graham, K., Zhang, J., Qiao, H., Wu, Y., and Zhou, Y. (2019). Region-specific inhibition of 14-3-3 proteins induces psychomotor behaviors in mice. *NPJ Schizophr.* 5:1. doi: 10.1038/s41537-018-0069-1

Hale, M. W., Hay-Schmidt, A., Mikkelsen, J. D., Poulsen, B., Shekhar, A., and Lowry, C. A. (2008). Exposure to an open-field arena increases c-Fos expression in a distributed anxiety-related system projecting to the basolateral amygdaloid complex. *Neuroscience* 155, 659–672. doi: 10.1016/j.neuroscience.2008.05.054

Hanley, J., Rickles, W. R., Crandall, P. H., and Walter, R. D. (1972). Automatic recognition of EEG correlates of behavior in a chronic schizophrenic patient. *Am. J. Psychiatry* 128, 1524–1528. doi: 10.1176/ajp.128.12.1524

Heath, R. G., and Walker, C. F. (1985). Correlation of deep and surface electroencephalograms with psychosis and hallucinations in schizophrenics: a report of two cases. *Biol. Psychiatry* 20, 669–674. doi: 10.1016/0006-3223(85)90102-7

Howes, O., McCutcheon, R., and Stone, J. (2015). Glutamate and dopamine in schizophrenia: an update for the 21st century. *J. Psychopharmacol.* 29, 97–115. doi: 10.1177/0269881114563634

Howes, O. D., and Nour, M. M. (2016). Dopamine and the aberrant salience hypothesis of schizophrenia. *World Psychiatry* 15, 3–4. doi: 10.1002/wps.20276

Ikeda, M., Hikita, T., Taya, S., Uraguchi-Asaki, J., Toyo-oka, K., Wynshaw-Boris, A., et al. (2008). Identification of YWHAE, a gene encoding 14-3-3 epsilon, as a possible susceptibility gene for schizophrenia. *Hum. Mol. Genet.* 17, 3212–3222. doi: 10.1093/hmg/ddn217

Jaehne, E., Ramshaw, H., Xu, X., Saleh, E., Clark, S., Schubert, K., et al. (2015). *In-vivo* administration of clozapine affects behaviour but does not reverse dendritic spine deficits in the 14-3-3 zeta KO mouse model of schizophrenia-like disorders. *Pharmacol. Biochem. Behav.* 138, 1–8. doi: 10.1016/j.pbb.2015.09.006

Jia, Y., Yu, X., Zhang, B., Yuan, Y., Xu, Q., and Shen, Y. (2004). An association study between polymorphisms in three genes of 14-3-3 (tyrosine 3-monooxygenase/tryptophan 5-monooxygenase activation protein) family and paranoid schizophrenia in northern Chinese population. *Eur. Psychiatry* 19, 377–379. doi: 10.1016/j.eurpsy.2004.07.006

Jiang, J. X., Liu, H., Huang, Z. Z., Cui, Y., Zhang, X. Q., Zhang, X. L., et al. (2018). The role of CA3-LS-VTA loop in the formation of conditioned place preference induced by context-associated reward memory for morphine. *Addict. Biol.* 23, 41–54. doi: 10.1111/adb.12468

Jones, Z. B., Zhang, J., Wu, Y., and Zhou, Y. (2021). Inhibition of 14-3-3 proteins alters neural oscillations in mice. *Front. Neural Circuits* 15:647856. doi: 10.3389/fncir.2021.647856

Kapur, S., and Seeman, P. (2001). Does fast dissociation from the dopamine d(2) receptor explain the action of atypical antipsychotics?: a new hypothesis. *Am. J. Psychiatry* 158, 360–369. doi: 10.1176/appi.ajp.158.3.360

Kätzel, D., Wolff, A. R., Bygrave, A. M., and Bannerman, D. M. (2020). Hippocampal hyperactivity as a druggable circuit-level origin of aberrant salience in Schizophrenia. *Front. Pharmacol.* 11:486811. doi: 10.3389/fphar.2020.486811

Kido, M., Nakamura, Y., Nemoto, K., Takahashi, T., Aleksic, B., Furuichi, A., et al. (2014). The polymorphism of YWHAE, a gene encoding 14-3-3 epsilon and brain morphology in schizophrenia: a voxel-based morphometric study. *PLoS One* 9:e103571. doi: 10.1371/journal.pone.0103571

Kim, H. J., Kim, M., Kang, B., Yun, S., Ryeo, S. E., Hwang, D., et al. (2019). Systematic analysis of expression signatures of neuronal subpopulations in the VTA. *Mol. Brain* 12:110. doi: 10.1186/s13041-019-0530-8

Kirov, G., Pocklington, A. J., Holmans, P., Ivanov, D., Ikeda, M., Ruderfer, D., et al. (2012). De novo CNV analysis implicates specific abnormalities of postsynaptic signalling complexes in the pathogenesis of schizophrenia. *Mol. Psychiatry* 17, 142–153. doi: 10.1038/mp.2011.154

Kosugi, K., Yoshida, K., Suzuki, T., Kobayashi, K., Mimura, M., and Tanaka, K. F. (2021). Activation of ventral CA1 hippocampal neurons projecting to the lateral septum during feeding. *Hippocampus* 31, 294–304. doi: 10.1002/hipo.23289

Kusljic, S., and van den Buuse, M. (2004). Functional dissociation between serotonergic pathways in dorsal and ventral hippocampus in psychotomimetic drug-induced locomotor hyperactivity and prepulse inhibition in rats. *Eur. J. Neurosci.* 20, 3424–3432. doi: 10.1111/j.1460-9568.2004.03804.x

Laruelle, M., Abi-Dargham, A., Gil, R., Kegeles, L., and Innis, R. (1999). Increased dopamine transmission in schizophrenia: relationship to illness phases. *Biol. Psychiatry* 46, 56–72. doi: 10.1016/s0006-3223(99)00067-0

Leroy, F., Park, J., Asok, A., Brann, D. H., Meira, T., Boyle, L. M., et al. (2018). A circuit from hippocampal CA2 to lateral septum disinhibits social aggression. *Nature* 564, 213–218. doi: 10.1038/s41586-018-0772-0

Li, Y., Wu, Y., and Zhou, Y. (2006). Modulation of inactivation properties of Ca(v)2.2 channels by 14-3-3 proteins. *Neuron* 51, 755–771. doi: 10.1016/j.neuron.2006.08.014

Lisman, J. E., and Grace, A. A. (2005). The hippocampal-VTA loop: controlling the entry of information into long-term memory. *Neuron* 46, 703–713. doi: 10.1016/j.neuron.2005.05.002

Lodge, D. J., Behrens, M. M., and Grace, A. A. (2009). A loss of parvalbumin-containing interneurons is associated with diminished oscillatory activity in an animal model of schizophrenia. *J. Neurosci.* 29, 2344–2354. doi: 10.1523/JNEUROSCI.5419-08.2009

Lodge, D. J., and Grace, A. A. (2007). Aberrant hippocampal activity underlies the dopamine dysregulation in an animal model of schizophrenia. *J. Neurosci.* 27, 11424–11430. doi: 10.1523/JNEUROSCI.2847-07.2007

Lodge, D. J., and Grace, A. A. (2008). Hippocampal dysfunction and disruption of dopamine system regulation in an animal model of schizophrenia. *Neurotox. Res.* 14, 97–104. doi: 10.1007/BF03033801

Lodge, D. J., and Grace, A. A. (2011). Hippocampal dysregulation of dopamine system function and the pathophysiology of schizophrenia. *Trends Pharmacol. Sci.* 32, 507–513. doi: 10.1016/j.tips.2011.05.001

Luo, A. H., Tahsili-Fahadan, P., Wise, R. A., Lupica, C. R., and Aston-Jones, G. (2011). Linking context with reward: a functional circuit from hippocampal CA3 to ventral tegmental area. *Science* 333, 353–357. doi: 10.1126/science.1204622

Maksimovic, M., Aitta-aho, T., and Korpi, E. R. (2014). Reversal of novelty-induced hippocampal c-Fos expression in GluA1 subunit-deficient mice by chronic treatment targeting glutamatergic transmission. *Eur. J. Pharmacol.* 745, 36–45. doi: 10.1016/j.ejphar.2014.10.005

Manvich, D. F., Webster, K. A., Foster, S. L., Farrell, M. S., Ritchie, J. C., Porter, J. H., et al. (2018). The DREADD agonist clozapine N-oxide (CNO) is reverse-metabolized to clozapine and produces clozapine-like interoceptive stimulus effects in rats and mice. *Sci. Rep.* 8:3840. doi: 10.1038/s41598-018-22116-z

Marissal, T., Salazar, R. F., Bertollini, C., Mutel, S., De Roo, M., Rodriguez, I., et al. (2018). Restoring wild-type-like CA1 network dynamics and behavior during adulthood in a mouse model of schizophrenia. *Nat. Neurosci.* 21, 1412–1420. doi: 10.1038/s41593-018-0225-y

Masters, S., and Fu, H. (2001). 14-3-3 proteins mediate an essential anti-apoptotic signal. *J. Biol. Chem.* 276, 45193–45200. doi: 10.1074/jbc.M105971200

McHugo, M., Talati, P., Armstrong, K., Vandekar, S. N., Blackford, J. U., Woodward, N. D., et al. (2019). Hyperactivity and reduced activation of anterior hippocampus in early psychosis. *Am. J. Psychiatry* 176, 1030–1038. doi: 10.1176/appi.ajp.2019.19020151

Medoff, D. R., Holcomb, H. H., Lahti, A. C., and Tamminga, C. A. (2001). Probing the human hippocampus using rCBF: contrasts in schizophrenia. *Hippocampus* 11, 543–550. doi: 10.1002/hipo.1070

Middleton, F. A., Peng, L., Lewis, D. A., Levitt, P., and Mirnics, K. (2005). Altered expression of 14-3-3 genes in the prefrontal cortex of subjects with schizophrenia. *Neuropsychopharmacology* 30, 974–983. doi: 10.1038/sj.npp.1300674

Modinos, G., Allen, P., Zugman, A., Dima, D., Azis, M., Samson, C., et al. (2020). Neural circuitry of novelty salience processing in psychosis risk: association with clinical outcome. *Schizophr. Bull.* 46, 670–679. doi: 10.1093/schbul/sbz089

Onténiente, B., Geffard, M., Campistron, G., and Calas, A. (1987). An ultrastructural study of GABA-immunoreactive neurons and terminals in the septum of the rat. *J. Neurosci.* 7, 48–54. doi: 10.1523/jneurosci.07-01-00048.1987

Paxinos, G., and Franklin, K. B. (2001). *The Mouse Brain in Stereotaxic Coordinates*. San Diego, CA: Elsevier Academic Press.

Procaccini, C., Aitta-aho, T., Jaako-Movits, K., Zharkovs.ky, A., Panhelainen, A., Sprengel, R., et al. (2011). Excessive novelty-induced c-Fos expression and altered neurogenesis in the hippocampus of GluA1 knockout mice. *Eur. J. Neurosci.* 33, 161–174. doi: 10.1111/j.1460-9568.2010.07485.x

Qiao, H., Foote, M., Graham, K., Wu, Y., and Zhou, Y. (2014). 14-3-3 proteins are required for hippocampal long-term potentiation and associative learning and memory. *J. Neurosci.* 34, 4801–4808. doi: 10.1523/JNEUROSCI.4393-13.2014

Ramshaw, H., Xu, X., Jaehne, E., McCarthy, P., Greenberg, Z., Saleh, E., et al. (2013). Locomotor hyperactivity in 14-3-3 zeta KO mice is associated with dopamine transporter dysfunction. *Transl. Psychiatry* 3:e327. doi: 10.1038/tp.2013.99

Risold, P. Y., and Swanson, L. W. (1997). Chemoarchitecture of the rat lateral septal nucleus. *Brain Res. Brain Res. Rev.* 24, 91–113. doi: 10.1016/s0165-0173(97)00008-8

Schobel, S. A., Kelly, M. A., Corcoran, C. M., Van Heertum, K., Seckinger, R., Goetz, R., et al. (2009a). Anterior hippocampal and orbitofrontal cortical structural brain abnormalities in association with cognitive deficits in schizophrenia. *Schizophr. Res.* 114, 110–118. doi: 10.1016/j.schres.2009.07.016

Schobel, S. A., Lewandowski, N. M., Corcoran, C. M., Moore, H., Brown, T., Malaspina, D., et al. (2009b). Differential targeting of the CA1 subfield of the hippocampal formation by schizophrenia and related psychotic disorders. *Arch. Gen. Psychiatry* 66, 938–946. doi: 10.1001/archgenpsychiatry.2009.115

Sheehan, T. P., Chambers, R. A., and Russell, D. S. (2004). Regulation of affect by the lateral septum: implications for neuropsychiatry. *Brain Res. Brain Res. Rev.* 46, 71–117. doi: 10.1016/j.brainresrev.2004.04.009

Skoulakis, E., and Davis, R. (1996). Olfactory learning deficits in mutants for leonardo, a Drosophila gene encoding a 14-3-3 protein. *Neuron* 17, 931–944. doi: 10.1016/s0896-6273(00)80224-x

Strange, B. A., Witter, M. P., Lein, E. S., and Moser, E. I. (2014). Functional organization of the hippocampal longitudinal axis. *Nat. Rev. Neurosci.* 15, 655–669. doi: 10.1038/nrn3785

Sun, C., Qiao, H., Zhou, Q., Wang, Y., Wu, Y., Zhou, Y., et al. (2013). Modulation of GluK2a subunit-containing kainate receptors by 14-3-3 proteins. *J. Biol. Chem.* 288, 24676–24690. doi: 10.1074/jbc.M113.462069

Sweeney, P., and Yang, Y. (2015). An excitatory ventral hippocampus to lateral septum circuit that suppresses feeding. *Nat. Commun.* 6:10188. doi: 10.1038/ncomms10188

Talati, P., Rane, S., Kose, S., Blackford, J. U., Gore, J., Donahue, M. J., et al. (2014). Increased hippocampal CA1 cerebral blood volume in schizophrenia. *Neuroimage Clin.* 5, 359–364. doi: 10.1016/j.nicl.2014.07.004

Thompson, K. J., Khajehali, E., Bradley, S. J., Navarrete, J. S., Huang, X. P., Slocum, S., et al. (2018). DREADD agonist 21 is an effective agonist for muscarinic-based DREADDs *in vitro* and *in vivo*. *ACS Pharmacol. Transl. Sci.* 1, 61–72. doi: 10.1021/acsptsci.8b00012

Toyooka, K., Muratake, T., Tanaka, T., Igarashi, S., Watanabe, H., Takeuchi, H., et al. (1999). 14-3-3 protein eta chain gene (YWHAH) polymorphism and its genetic association with schizophrenia. *Am. J. Med. Genet.* 88, 164–167.

van den Buuse, M. (2010). Modeling the positive symptoms of schizophrenia in genetically modified mice: pharmacology and methodology aspects. *Schizophr. Bull.* 36, 246–270. doi: 10.1093/schbul/sbp132

Vega-Quiroga, I., Yarur, H. E., and Gysling, K. (2018). Lateral septum stimulation disinhibits dopaminergic neurons in the antero-ventral region of the ventral tegmental area: Role of GABA-A alpha 1 receptors. *Neuropharmacology* 128, 76–85. doi: 10.1016/j.neuropharm.2017.09.034

Wolff, A. R., Bygrave, A. M., Sanderson, D. J., Boyden, E. S., Bannerman, D. M., Kullmann, D. M., et al. (2018). Optogenetic induction of the schizophrenia-related endophenotype of ventral hippocampal hyperactivity causes rodent correlates of positive and cognitive symptoms. *Sci. Rep.* 8:12871. doi: 10.1038/s41598-018-31163-5

Wong, A. H., Likhodi, O., Trakalo, J., Yusuf, M., Sinha, A., Pato, C. N., et al. (2005). Genetic and post-mortem mRNA analysis of the 14-3-3 genes that encode phosphoserine/threonine-binding regulatory proteins in schizophrenia and bipolar disorder. *Schizophr. Res.* 78, 137–146. doi: 10.1016/j.schres.2005.06.009

Xu, X., Jaehne, E. J., Greenberg, Z., McCarthy, P., Saleh, E., Parish, C. L., et al. (2015). 14-3-3ζ deficient mice in the BALB/c background display behavioural and anatomical defects associated with neurodevelopmental disorders. *Sci. Rep.* 5:12434. doi: 10.1038/srep12434

Yoo, J. H., Zell, V., Gutierrez-Reed, N., Wu, J., Ressler, R., Shenasa, M. A., et al. (2016). Ventral tegmental area glutamate neurons co-release GABA and promote positive reinforcement. *Nat. Commun.* 7:13697. doi: 10.1038/ncomms13697

Zhang, Z. J., and Reynolds, G. P. (2002). A selective decrease in the relative density of parvalbumin-immunoreactive neurons in the hippocampus in schizophrenia. *Schizophr. Res.* 55, 1–10. doi: 10.1016/s0920-9964(01)00188-8

Zhang, J., and Zhou, Y. (2018). 14-3-3 proteins in glutamatergic synapses. *Neural Plast.* 2018:8407609. doi: 10.1155/2018/8407609

Zierhut, K. C., Gra, R., Kaufmann, J., Steiner, J., Bogerts, B., and Schiltz, K. (2013). Hippocampal CA1 deformity is related to symptom severity and antipsychotic dosage in schizophrenia. *Brain* 136, 804–814. doi: 10.1093/brain/aws335

Conflict of Interest: The authors declare that the research was conducted in the absence of any commercial or financial relationships that could be construed as a potential conflict of interest.

Publisher's Note: All claims expressed in this article are solely those of the authors and do not necessarily represent those of their affiliated organizations, or those of the publisher, the editors and the reviewers. Any product that may be evaluated in this article, or claim that may be made by its manufacturer, is not guaranteed or endorsed by the publisher.

frontiers in Synaptic Neuroscience

ORIGINAL RESEARCH
published: 01 March 2022
doi: 10.3389/fnsyn.2022.840368

Hearing Loss Increases Inhibitory Effects of Prefrontal Cortex Stimulation on Sound Evoked Activity in Medial Geniculate Nucleus

*Chenae De Vis, Kristin M. Barry and Wilhelmina H. A. M. Mulders**

School of Human Sciences, The University of Western Australia, Crawley, WA, Australia

Sensory gating is the process whereby irrelevant sensory stimuli are inhibited on their way to higher cortical areas, allowing for focus on salient information. Sensory gating circuitry includes the thalamus as well as several cortical regions including the prefrontal cortex (PFC). Defective sensory gating has been implicated in a range of neurological disorders, including tinnitus, a phantom auditory perception strongly associated with cochlear trauma. Recently, we have shown in rats that functional connectivity between PFC and auditory thalamus, i.e., the medial geniculate nucleus (MGN), changes following cochlear trauma, showing an increased inhibitory effect from PFC activation on the spontaneous firing rate of MGN neurons. In this study, we further investigated this phenomenon using a guinea pig model, in order to demonstrate the validity of our finding beyond a single species and extend data to include data on sound evoked responses. Effects of PFC electrical stimulation on spontaneous and sound-evoked activity of single neurons in MGN were recorded in anaesthetised guinea pigs with normal hearing or hearing loss 2 weeks after acoustic trauma. No effect, inhibition and excitation were observed following PFC stimulation. The proportions of these effects were not different in animals with normal hearing and hearing loss but the magnitude of effect was. Indeed, hearing loss significantly increased the magnitude of inhibition for sound evoked responses, but not for spontaneous activity. The findings support previous observations that PFC can modulate MGN activity and that functional changes occur within this pathway after cochlear trauma. These data suggest hearing loss can alter sensory gating which may be a contributing factor toward tinnitus development.

Keywords: guinea pig, hearing loss, medial geniculate nucleus, prefrontal cortex, sensory gating, frontostriatal, electrophysiology

OPEN ACCESS

Edited by:
Michael Telias,
University of Rochester, United States

Reviewed by:
Akihisa Kimura,
Wakayama Medical University, Japan
Elouise Alexandra Koops,
Harvard Medical School, United States
Guang-Di Chen,
University at Buffalo, United States

***Correspondence:**
Wilhelmina H. A. M. Mulders
helmy.mulders@uwa.edu.au

Received: *21 December 2021*
Accepted: *08 February 2022*
Published: *01 March 2022*

Citation:
De Vis C, Barry KM and Mulders WHAM (2022) Hearing Loss Increases Inhibitory Effects of Prefrontal Cortex Stimulation on Sound Evoked Activity in Medial Geniculate Nucleus. Front. Synaptic Neurosci. 14:840368. doi: 10.3389/fnsyn.2022.840368

INTRODUCTION

Sensory gating is the process of inhibiting irrelevant neural stimuli from reaching higher cortical areas, allowing for attention to more relevant or salient sensory information (Cromwell and Atchley, 2015). Sensory gating requires activation of the frontoparietal attention network, which consists of several cortical regions including the prefrontal cortex (PFC) (Ptak, 2012), which is known to play an important role in a myriad of cognitive functions including attention, memory

and executive function (Jobson et al., 2021). Another critical component of sensory gating circuitry is the thalamus, the obligatory relay en route to cortex for all sensory input, but olfactory (Saalmann et al., 2012; Halassa and Kastner, 2017). In agreement, multiple pathways from PFC to thalamus have been shown to exist (Mathiasen et al., 2021; Rios-Florez et al., 2021).

Defective sensory gating has been implicated in a range of neurological disorders. For example, dysregulation of the inhibitory circuitry in thalamus as well as thalamocortical hyperconnectivity have been proposed to be involved in the sensory over-responsiveness that is observed in individuals diagnosed with autism spectrum disorders (Iidaka et al., 2019; Wood et al., 2021). Reduced sensory gating has also been reported in patients diagnosed with schizophrenia (Freedman et al., 2020) and anxiety disorders (Storozheva et al., 2021).

Hearing loss has been shown to lead to reduced sensory gating of auditory information (Campbell et al., 2020; Chen et al., 2021). This is in line with a MRI study showing reduced functional connectivity between auditory thalamus and multiple other brain regions, including parts of PFC, in individuals with hearing loss (Xu et al., 2019). Abnormal sensory gating has also been suggested to be involved in the development of tinnitus (Rauschecker et al., 2010, 2015; De Ridder et al., 2015; Sedley et al., 2019), a phantom auditory perception that is strongly associated with hearing loss and/or damage to the cochlea (Baguley et al., 2013). Indeed, human studies show that individuals with hearing impairment and tinnitus display decreased auditory sensory gating which correlates with their tinnitus severity (Campbell et al., 2019) and others show reduced grey matter in PFC of tinnitus patients (Leaver et al., 2011, 2012, 2016).

The PFC has no direct projections to the auditory thalamus, the medial geniculate nucleus (MGN), but has indirect, multi-synaptic projections involving the thalamic reticular nucleus (TRN) (Nakajima et al., 2019), which provides strong GABAergic input to the MGN (Pinault, 2004). In agreement, in our laboratory we have demonstrated functional connectivity between PFC and MGN in rats (Barry et al., 2017). Moreover, a recent elegant study from Nakajima and co-workers demonstrated that the PFC indeed modulates attentional filtering in MGN *via* inhibitory thalamic reticular networks (Nakajima et al., 2019).

Previously, we have demonstrated in a rat model that trauma to the cochlea results in altered connectivity between PFC and MGN (Barry et al., 2021) showing enhancement of inhibitory effects of PFC electrical stimulation on the spontaneous firing rates of MGN neurons. This observation demonstrates that damage to the auditory periphery can cause functional changes to the sensory gating circuitry. In the present study, we further investigated this phenomenon using a guinea pig model, in order to demonstrate the validity of our finding beyond a single species. Furthermore, we also recorded the effects of PFC electrical stimulation on sound-evoked responses in MGN, in addition to effects on spontaneous activity.

MATERIALS AND METHODS

Animals

Fifteen guinea pigs (Cavia porcellus, Hartley Tricolor) of either sex, weighing 200 to 300 g, were obtained from the University of Western Australia's Preclinical Facility (PCF). Guinea pigs were kept under controlled conditions and were provided with appropriate access to food, water and shelter throughout the duration of the experiment. They were divided into an experimental group (n = 5) which underwent an acoustic trauma procedure and a control group (n = 10) that received a sham procedure. Ethics regarding experimental procedures were approved by the Animal Ethics Committee of the University of Western Australia.

Recovery Experiment for Acoustic Trauma or Sham Procedure

Animals received a subcutaneous (s.c.) injection of atropine sulphate (0.05 mg/kg; 0.1 mL), followed by an intraperitoneal (i.p.) injection of Diazepam (Pamlin 5 mg/kg, 5 mg/mL diazepam). Then, guinea pigs received an intramuscular (i.m.) injection of Hypnorm (1 mL/kg; 0.315 mg/mL fentanyl citrate + 10 mg/mL fluanisone) to induce full surgical anaesthesia. Animals were shaved at the incision site and received a s.c. injection of Lignocaine (0.1 mL 1% solution). Once full depth of anaesthesia was obtained, animals were placed on a heating blanket in a soundproof room and mounted into hollow ear bars that allowed controlled acoustic stimuli to be delivered to the animal. The cochlea was exposed by a skin incision followed by a small opening in the bulla. An insulated silver wire recording electrode was positioned on the round window. Compound action potential (CAP) recordings were made to assess peripheral auditory thresholds between 4 and 24 kHz (2 kHz steps) (Johnstone et al., 1979). CAP recordings (32 averages per recording) were made in response to 10 ms tone bursts with repetition rate of 4/s.

When normal hearing was confirmed (Johnstone et al., 1979), a unilateral hearing loss was induced in the left ear in the experimental group by an acoustic trauma (continuous pure tone at 10 kHz and 124 dB SPL for 120 min). Plasticine was used to block the right ear. A half-inch condenser microphone driven in reverse was used as a speaker (Bruel and Kjaer, type 4134). A DIGI 96 soundcard connected to a digital/analog interface (ADI-9 DS, RME Intelligent Audio Solution, Haimhausen, Germany) and a custom-built software program (Neurosound MI Lloyd) was used to synthesise acoustic stimuli. This method of acoustic trauma is used routinely in our laboratory and causes a small, frequency restricted permanent hearing loss (Mulders and Robertson, 2009; Mulders et al., 2011). Sham animals received the same surgery and measurement of peripheral thresholds by CAP, but with no acoustic trauma. Animals received a top up of Hypnorm (one third of original dose) halfway the acoustic trauma. After the acoustic trauma, another CAP audiogram was recorded to determine the extent of immediate hearing loss, the incision

was sutured, and the animals recovered for 2 weeks before the final experiment.

Non-recovery Experiment for Thalamic Recordings With Prefrontal Cortex Stimulation

Two weeks after the recovery experiment, guinea pigs were administered a s.c. injection of atropine sulphate (0.05 mg/kg; 0.1 mL), followed by an i.p. injection of sodium pentobarbitone (30 mg/kg). Full surgical anaesthesia was then achieved by an i.m. injection of Hypnorm (initial dose 0.15 mL). Lignocaine (0.1 mL 1% solution) was injected s.c. at the incision site. Once full depth of anaesthesia was obtained, guinea pigs were placed on a heating blanket in the soundproof room. An electrocardiogram (ECG) was used to monitor the depth of anaesthesia throughout the experiment. Anaesthesia was maintained by half of the initial dose of sodium pentobarbitone every 2 h and a full dose of Hypnorm every hour. Guinea pigs were artificially ventilated by carbogen (95% oxygen and 5% carbon dioxide) through a tracheotomy. Animals were then positioned into hollow ear bars and as described in the recovery experiment (see section "Recovery Experiment for Acoustic Trauma or Sham Procedure"), a CAP audiogram was recorded from both the left and right ear to determine peripheral auditory thresholds.

Then the skull was exposed and using coordinates from a guinea pig atlas (Rapisarda and Bacchelli, 1977), position of the PFC and MGN were determined. A dental drill was used to perform two small craniotomies. A custom made (tungsten in glass) bipolar stimulating electrode was positioned in the PFC and a recording electrode [impedance < 1 MΩ at 1 kHz (Merrill and Ainsworth, 1972)] was lowered into the MGN. To minimise dehydration and limit movement of the brain, 5% agar in saline was used to cover the craniotomies. Ten minutes prior to recording, guinea pigs were administered an i.m. injection of Pancuronium Bromide (0.1 mL).

The stimulating electrode (Platinum-iridium, concentric bipolar electrode with a 2–3 μm tip, impedance 200 K, World Precision Instruments) was connected to an A-M Systems Isolated Pulse Stimulator (Model 2100). Neurosound software controlled the timing of electrical stimuli. Electrical stimulation was delivered as shock trains (50 ms duration) with a pulse duration of 0.5 ms and at a rate of 200 Hz. The intensity of the electrical current ranged from 100 μA to 1 mA. To increase the chance of observing an effect in the MGN, the current used to stimulate the PFC was initially applied at maximum (1 mA). The current was then decreased until threshold if the recording remained stable. Threshold was determined as the lowest possible current intensity that could elicit a response that was different to the neuron's firing pattern.

Single neurons in the MGN were identified using pure tone and broadband noise stimuli as a search stimulus. Noise stimuli were delivered to the left ear while the right ear was blocked with plasticine. A tungsten in a glass recording electrode was used to record single neuron activity in the MGN of the thalamus (Merrill and Ainsworth, 1972). Entry into the right (contralateral to noise stimulus) MGN was verified by the presence of a robust cluster response to broadband noise stimulus (50 ms duration, 1 ms rise and fall times, sample rate of 96 kHz) (Cook et al., 2021; Zimdahl et al., 2021). Electrophysiological recordings of single neuron activity were recorded in MGN in response to stimulation of the right (ipsilateral to MGN) PFC.

When a single neuron was isolated, characteristic frequency (CF) and acoustic threshold at CF were determined as described previously (Mulders et al., 2011; Barry et al., 2015, 2019). Spontaneous firing rates (SFRs) were measured for 10 sec. Peristimulus time histograms (75–100 stimulus presentations) were constructed at CF at 20 dB above threshold to determine neuronal response. Then histograms (500 ms samples; 50–100 sweeps) were collected to determine the effect of PFC stimulation as follows. Firstly, effects of PFC stimulation were investigated on spontaneous firing, followed by effects on sound evoked activity (at 20 dB above neuronal threshold). If an effect was observed, current was decreased in small steps (200–300 μA) until threshold was reached. For analysis, changes in firing rate were determined by comparing the total spike counts with and without electrical stimulation of PFC.

Once recordings were finished, animals received an overdose of Lethabarb (Sodium Pentobarbitone 325 mg/mL; 0.3 mL i.p injection). Guinea pigs were transcardially perfused by methods outlined by previous studies (Barry et al., 2015, 2017). Brain tissue was collected and stored overnight in 4% paraformaldehyde in 0.1 M phosphate buffer (PB), followed by cryoprotection in 30% sucrose in PB for another 24 h. Brains were cut on a freezing microtome-cryostat into 60 μm sections. Sections were mounted onto slides and allowed to dry overnight. Once dried, slides were stained with Toluidine Blue and coverslipped. A Nikon Eclipse 8oi was used to perform light microscopy. This procedure verified the position of stimulating and recording electrode tracks within the PFC and MGN.

Statistical Analysis

Multiple *t*-tests, corrected using Holm-Sidak method, were used to determine if sham or acoustic trauma had an effect on peripheral auditory thresholds and if hearing thresholds were different in the experimental and control group. A Mann-Whitney *U* Test was used to determine differences in spontaneous firing rates, characteristic frequencies (CF) and neural (acoustic) thresholds at CF between animals with normal hearing and hearing loss. To characterise the effect of PFC stimulation on single neuron MGN activity PSTHs without and with stimulation were compared using a paired *t*-test, with each time-bin as a separate variable. Proportions of neurons displaying no effect, inhibition or excitation were compared using a Chi-square analysis.

RESULTS

Compound Action Potential (CAP) Audiograms

The effects of acoustic trauma (AT) are shown in **Figure 1**. CAP thresholds in sham animals at the start of experiment were the

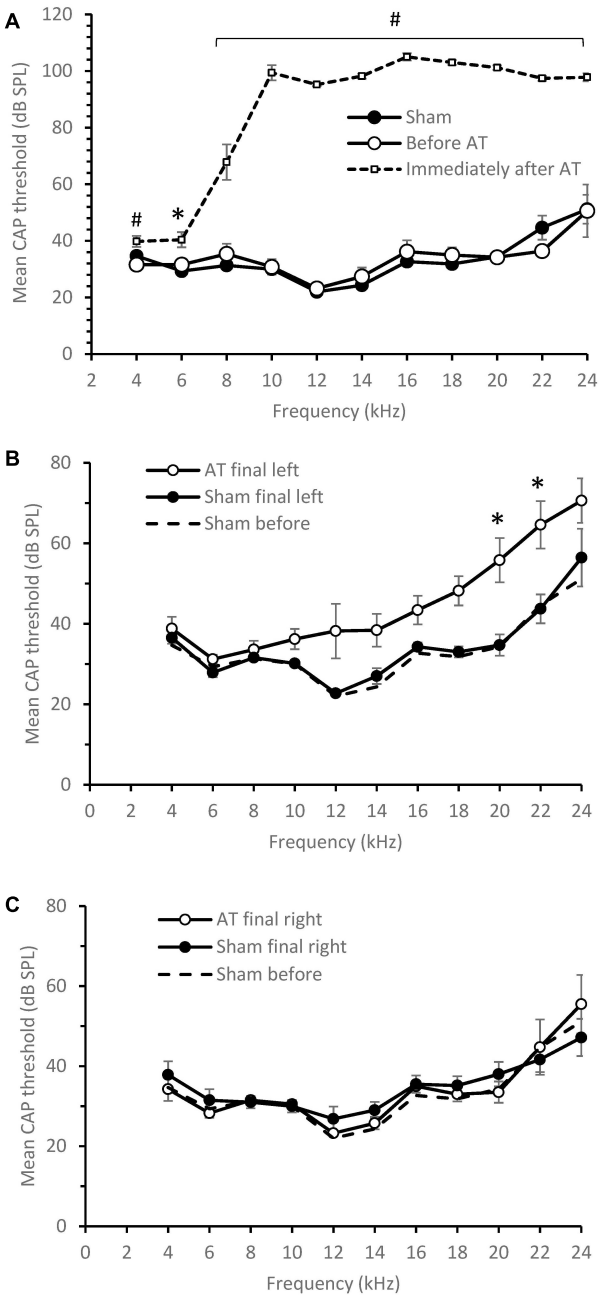

FIGURE 1 | CAP threshold audiograms. **(A)** Mean CAP threshold left ear vs. frequency at the time of initial surgery, Sham animals (n = 6), AT animals before and after AT (n = 5). Significance between Immediately after and before AT indicated. **(B)** Mean CAP threshold left ear vs. frequency at the time of final surgery, Sham animals (n = 6), AT animals (n = 5). **(C)** Mean CAP threshold right ear vs. frequency at the time of final surgery, Sham animals (n = 6), AT animals (n = 4). For comparison the sham audiogram at initial surgery also plotted as a dotted line in **(B,C)**. Data Mean ± SEM. *$p < 0.05$, #$p < 0.01$.

same as in the AT group before the AT (**Figure 1A**). Immediately after AT was finished a significant increase in CAP thresholds was observed at all frequencies with the largest increase seen at and above the AT frequency (**Figure 1A**; multiple t-tests, corrected using Holm-Sidak method) in line with our previous publications (Mulders and Robertson, 2013; Mulders et al., 2016; Cook et al., 2021). After 2 weeks of recovery, at the time of the final experiment, CAP thresholds had partially recovered but a difference remained between sham and AT animals (**Figure 1B**). CAP thresholds showed a significance increase only at 20 and 22 kHz ($p < 0.05$), with threshold at 12 kHz approaching significance ($p = 0.063$, multiple t-tests, corrected using Holm-Sidak method). Right ears (not exposed to AT or sham surgery) showed similar thresholds at the final experiment (**Figure 1C**) as measured during initial surgery in the left ears of either group, confirming the absence of an effect of the AT on the contralateral side. In **Figures 1B,C** the original left ear thresholds of shams are plotted as well to illustrate the stable thresholds in the sham group and the normal thresholds in the right ear at the final surgery.

Verification of Stimulating Electrode Position

Histology was used to verify the position of stimulating electrodes in all animals (**Figure 2** showing an example). Five animals from the AT group and seven animals from the sham group showed placement of the stimulation electrode in the PFC (Rapisarda and Bacchelli, 1977). Only these animals showed effects on MGN recordings and were therefore included in further analyses. Electrode placement was explored in some animals by changing the depth of the electrode. Stimulation at a depth of approximately 5 mm from the cortical surface, most likely reflecting placement in prelimbic cortex (Hennessy et al., 2018), yielded the largest and most consistent effects on MGN activity.

Medial Geniculate Nucleus (MGN) Neuronal Response Characteristics

Data were obtained from a total of 136 neurons with 68 neurons from control animals and 68 from AT animals. Characteristic frequency (CF) varied between 0.24 and 24.5 kHz (11.3 ± 0.8 kHz; mean ± SEM) in sham animals and between 0.6 and 19 kHz (8.1 ± 0.7 kHz; mean ± SEM) in AT animals. Mean CF was significantly different between the groups (unpaired t-test $p = 0.017$). It should be noted that CF could not be determined in seven neurons of the AT animals and four neurons of the sham animals though these neurons did show a response to noise. Mean SFRs were 0.66 ± 0.13 in AT animals (median 0.1) and 0.63 ± 0.15 in sham animals (median 0.1) and a Mann-Whitney showed no statistical difference ($p = 0.899$) between the groups.

Response type was based on a PSTH at CF 20 dB above threshold and could be determined in 57 of the neurons in AT animals and 61 of the neurons in sham animals. Examples of the PSTHs of the different response types are shown in **Figure 3**. Response types were in agreement with data described previous studies (Bordi and LeDoux, 1994; Barry et al., 2015, 2017). In both the sham and AT group, the majority of MGN neurons had an onset response to pure tone (46 neurons, 75.4% and 42 neurons, 73.7%, respectively), with a response latency ranging from 10 to 65 ms from the onset of the sound stimulus (**Figure 3A**). About a fifth of the neurons (12 neurons, 19.7% in sham group and 13

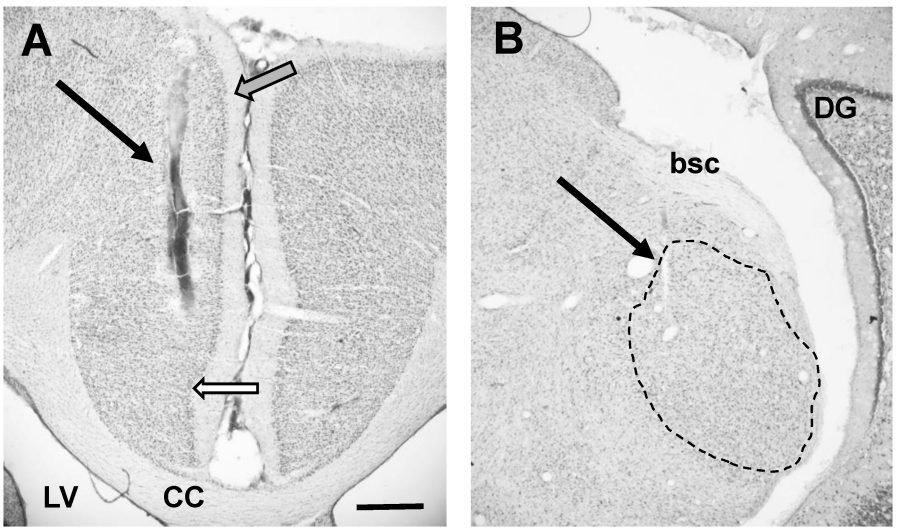

FIGURE 2 | (A) Photomicrograph showing placement of stimulating electrode in PFC (arrow). Note that this image does not show deepest point of electrode. White filled arrow points to tentative border infralimbic and cingulate cortex. Grey filled arrow points at tentative border between cingulate cortex and secondary motor cortex. Please note that delineations of the cortex are based on rat atlases (Paxinos and Watson, 2007; Swanson, 2018) since the guinea pig atlas (Rapisarda and Bacchelli, 1977) does not show detailed delineations. **(B)** Photomicrograph showing placement of recording electrode in MGN (arrow). Dotted line shows outline of MGN, based on rat atlas (Swanson, 2018). Individual subdivisions of the MGN not indicated. CC, corpus callosum; LV, lateral ventricle; DG, dentate gyrus; bsc, brachium of the superior colliculus. Scale bar for both images: 0.5 mm.

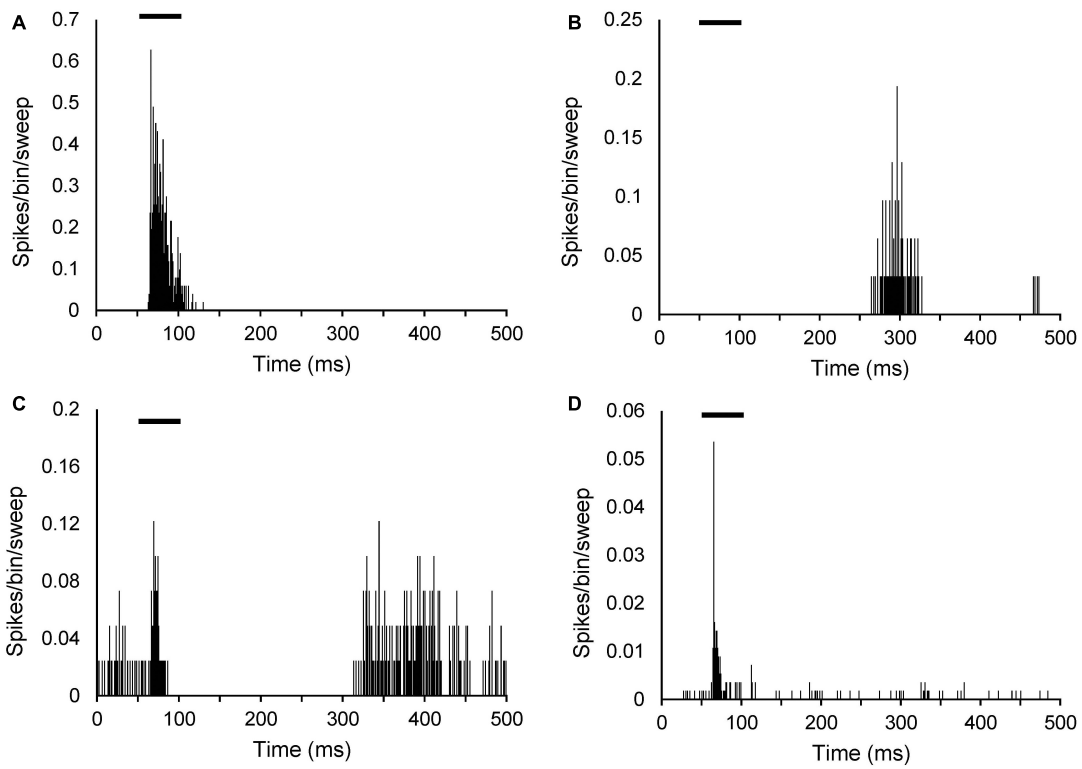

FIGURE 3 | Peristimulus time histograms (PSTHs) illustrating different sound evoked response types in MGN neurons. PSTHs show single neuron responses to a 50-ms pure tone at CF 20 dB above threshold. Spikes are shown as per bin width (bin width of 1 ms) per sweep (50 sweeps). **(A)** Onset neuron (CF: 6.5 kHz; threshold 43 dB SPL). **(B)** Off response neuron (CF: 619 Hz; threshold 66 dB SPL). **(C)** On and off response neuron (CF 16.3 kHz; threshold 77 dB SPL). **(D)** Sustained response neuron (CF 15.6 kHz; threshold 41 dB SPL). Black bars in each panel indicate timing and duration of the tone burst.

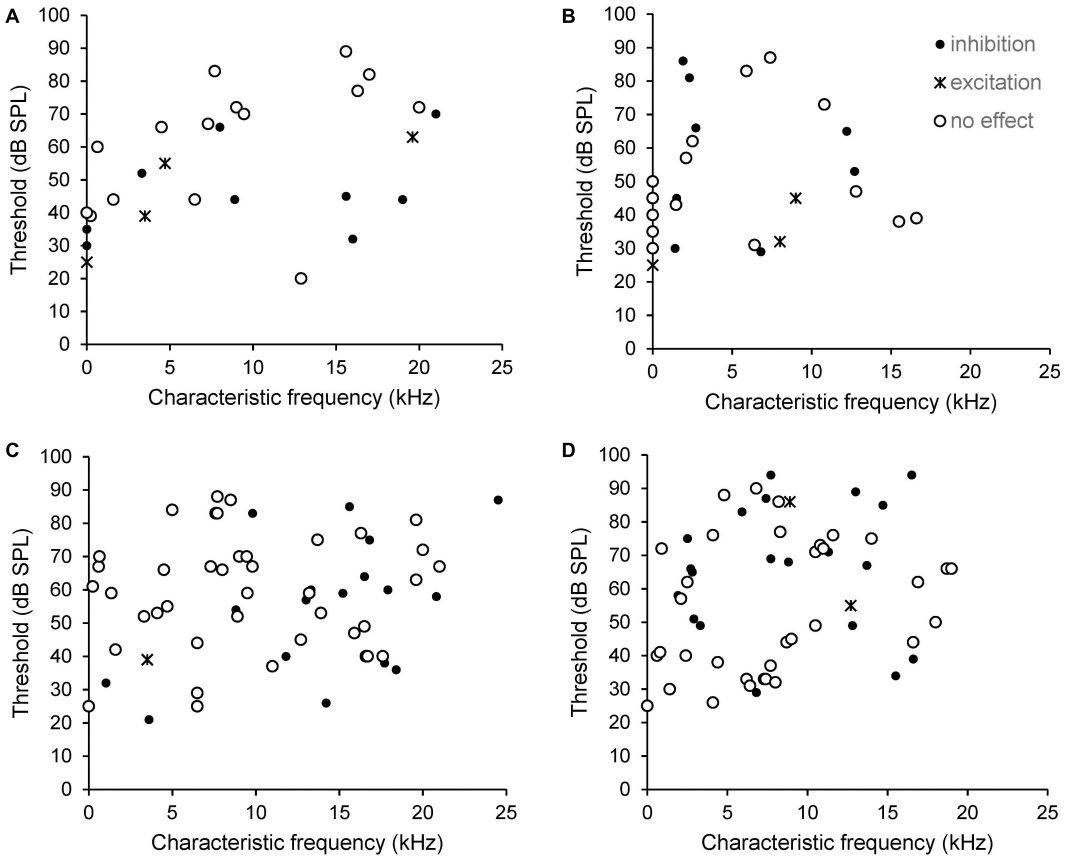

FIGURE 4 | Scatterplots showing the relationship between CF, threshold and type of effect from electrical stimulation of the PFC on SFR (**A**, sham and **B**, AT) and on sound evoked responses at CF 20 dB above threshold (**C**, sham and **D**, AT). Neurons that could not be tuned to a pure tone are shown arbitrarily with a CF of zero and an arbitrary threshold, so appear on the *Y*-axis. Black dots: neurons showing inhibition. Crosses: neurons showing excitation. Open circles: neurons showing no effect.

neurons, 22.8% in AT group) exhibited an on and off response (**Figure 3C**). An off response (firing related to offset of the tone burst) was observed in 1.6% (one neuron) of sham animals and 3.5% (two neurons) of AT animals (**Figure 3B**). The remainder of neurons exhibited a "sustained response" to pure tone (two neurons, 3.3% in sham animals, none in AT group) (**Figure 3D**). No difference was found in the proportion of response types between the sham and AT group [X2 (3, N = 118) = 2.422 p = 0.4895].

Effects of Prefrontal Cortex Stimulation

Since inhibitory effects cannot be ascertained in neurons with a zero or very low SFR when using extracellular recordings, potential effects on SFRs were only investigated in neurons with a SFR > 0.4 spikes/sec. This meant that effects of PFC stimulation on SFRs were assessed in 26 neurons in AT animals and 28 neurons in sham animals. Mean CF was 10.35 ± 1.36 kHz (mean ± SEM) in sham animals and 7.0 ± 1.17 kHz in AT animals and this difference was not statistically different (unpaired t-test p = 0.0711). Note that in four of the sham animals and five of the AT animals CF could not be determined. In AT animals, excitatory effects were seen in three neurons (12%), inhibitory effects in eight neurons (31%) and no effect in 15 neurons (58%) (Note percentages rounded, so not adding up to 100%). In sham animals, excitatory effects were seen in four neurons (14%), inhibitory effects in 9 (32%) and the remaining 15 neurons showed no effect (54%). These proportions in type of effect were not different between the AT and sham animals [X2 (2, N = 54) = 0.1278 p = 0.9381].

The effects of PFC stimulation were also assessed on sound evoked activity (at CF, 20 dB above threshold) in 57 neurons from AT animals and 59 neurons from sham animals. Mean CF was 10.82 ± 0.83 kHz (mean ± SEM) in sham animals and 8.43 ± 0.69 kHz in AT animals and this difference was statistically different (unpaired t-test p = 0.0291). In one neuron of both sham and AT animals CF could not be determined. In AT animals, excitatory effects were seen in two neurons (4%), inhibitory effects in 21 neurons (37%) and no effect in 34 neurons (60%). In sham animals, excitatory effects were observed in one neuron only (2%), 17 neurons showed inhibitory effects (29%) and the remaining 41 neurons showed no effect (69%). Chi-square analysis showed again no significant difference between the prevalence of effect types between the AT and sham animals [X2 (2, N = 116) = 1.374 p = 0.5032].

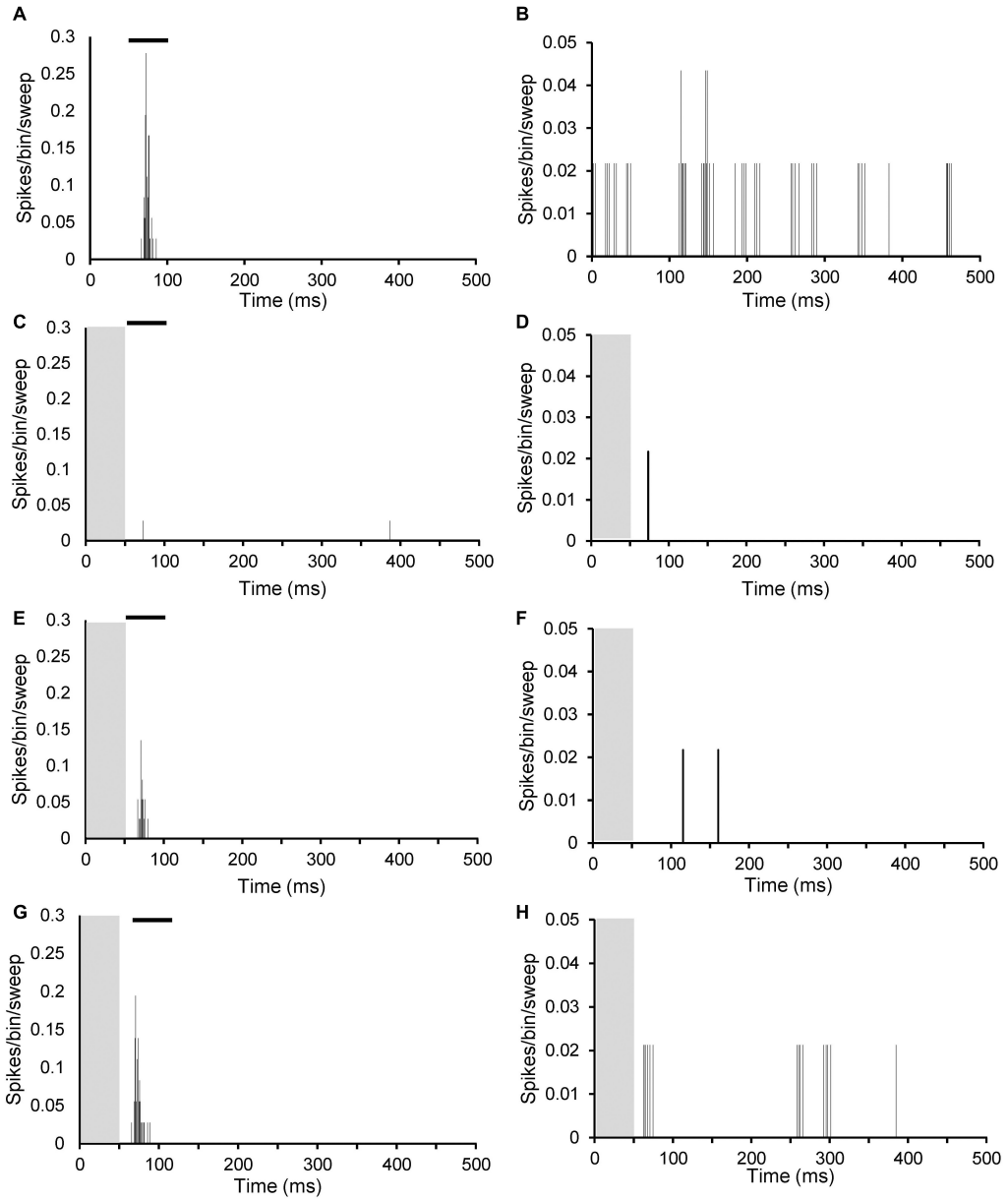

FIGURE 5 | Peristimulus time histograms (PSTHs) illustrating inhibitory effects of PFC electrical stimulation at different stimulation strengths on sound evoked response at CF 20 dB above threshold (left column; **A,C,E,G**) and on spontaneous firing (right column; **B,D,F,H**). **(A,B)** No stimulation; **(C,D)** 1 mA; **(E,F)** 0.7 mA; and **(G,H)** 0.4 mA. Both neurons from an AT animal. Neuron left column CF 2.5 kHz with threshold 74 dB SPL and SFR 0.1 spikes/sec. Neuron right column CF 1.9 kHz with threshold 86 dB SPL and SFR 2.1 spikes/sec. Grey column indicates electrical stimulation and black bar in **(A,C,E,G)** illustrates timing of tone burst.

Effects of PFC stimulation could be collected on both spontaneous and sound evoked activity from nine neurons in sham animals and 16 neurons in AT animals. From the nine neurons from sham animals, seven showed no effect on both spontaneous and sound evoked responses, one neuron showed excitatory effects on both and the remaining neuron inhibitory effects on both. From the 16 neurons from AT animals, five showed no effect on both responses and 4 neurons showed inhibitory effects on both. Four neurons showed an inhibitory effect on the sound evoked response without an effect on spontaneous firing, two neurons showed no effect on sound evoked responses but excitatory effects on spontaneous firing and the remaining neuron showed no effect on sound evoked responses but an inhibitory effect on spontaneous firing.

Although most neurons did not show an effect in response to PFC activation, it should be noted that they were located in the same tracks as neurons that displayed either inhibition or excitation. In addition, each animal included in the analysis showed some inhibitory or excitatory effects. It is therefore unlikely that the lack of effect was due to incorrect placement

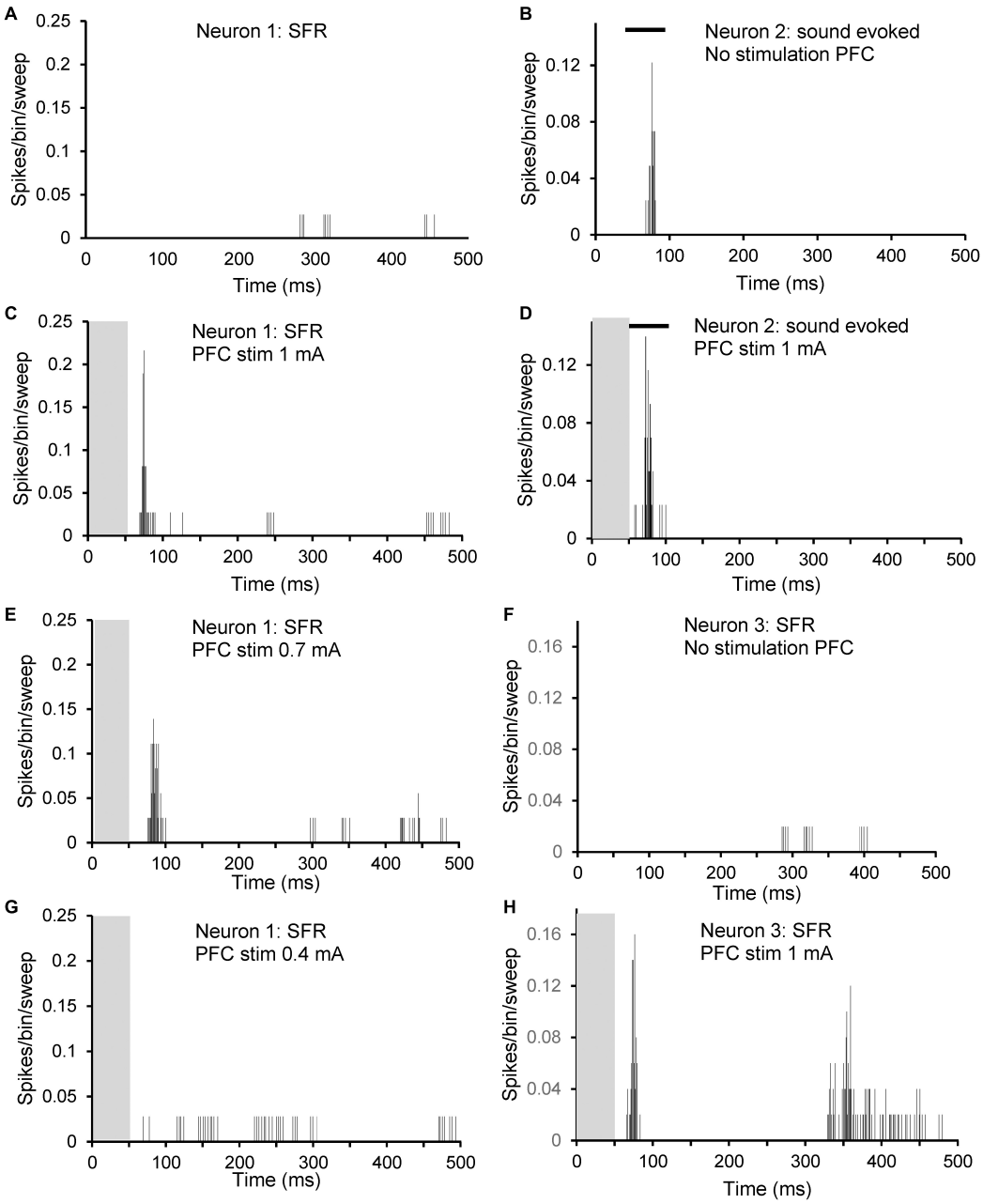

FIGURE 6 | Peristimulus time histograms (PSTHs) illustrating excitatory effects of PFC electrical stimulation at different stimulation strengths on three different neurons. Neuron 1: **(A,C,E,G)**: spontaneous firing of a neuron with CF 1.9 kHz, threshold at 86 dB SPL and with SFR 2.1 spikes/sec. **(A)** No stimulation; **(C)** 1 mA; **(E)** 0.7 mA; and **(G)** 0.4 mA. Neuron 2: **(B,D)**: sound evoked firing at CF at 20 dB over threshold of a neuron with CF 8.9 kHz, threshold 86 dB SPL and with SFR of 0.2 spikes/sec. **(B)** No stimulation; **(D)** 1 mA. Neuron 3: **(F,H)**: spontaneous firing of a neuron with CF 4.7 kHz, threshold at 55 dB SPL and with SFR 0.4 spikes/sec. **(F)** No stimulation; **(H)** 1 mA. Note that neuron 1 showed no effect of electrical stimulation on sound evoked activity. Grey column indicates electrical stimulation and black bar in **(B,D)** illustrates timing of tone burst.

of the stimulating electrode. Threshold of stimulation, the lowest possible current intensity that could elicit a response, was collected in 29 neurons from AT animals and 18 neurons from sham animals. Mean threshold was 740 ± 46 μA in AT animals and 711 ± 59 μA and these values were not significantly different (unpaired *t*-test, $p = 0.7221$).

The type of effect from PFC stimulation, excitatory, inhibitory or no effect, did not correlate with CF or thresholds. This is shown in **Figure 4**. Data from SFR measurements are shown in panels 4A (sham) and B (AT) whereas effects on sound evoked firing rates are shown in panels 4C (sham) and D (AT). Please note that in this figure neurons that could not be tuned to a pure tone are

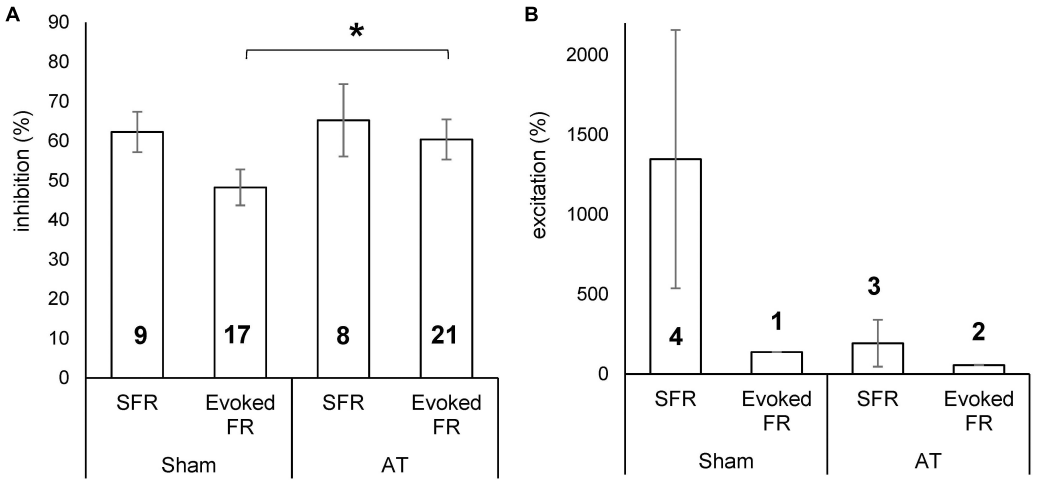

FIGURE 7 | Bar diagrams showing percentage inhibition **(A)** and percentage excitation **(B)** on spontaneous firing rate (SFR) and sound evoked FR in sham and AT animals. Data Mean ± SEM. *$p < 0.05$. Numbers in bars represent number of neurons in which effect was demonstrated.

shown arbitrarily with a CF of zero and an arbitrary threshold. Examples of inhibitory effects on sound evoked and spontaneous firing are shown in **Figure 5**. This figure also illustrates the effects of decreasing stimulation intensity. Examples of excitatory effects at different stimulation intensities are shown in **Figure 6**.

Effect Size

The magnitude of the effect from PFC stimulation was calculated as the percentage change from the PSTH of the unstimulated condition (spikes from 51 to 500 ms in PSTH to exclude contamination of stimulus artefact) and results are shown in **Figure 7**. The average inhibition in sham animals was 62 ± 5.1% (ranging from 41 to 83%) for SFRs and 48 ± 4.5% (ranging from 18 to 78%) for sound evoked responses. In AT animals the average inhibition for SFRs was 65 ± 9.2% (ranging from 35 to 100%) and for sound evoked responses 60 ± 5.1% (ranging from 24 to 100%) (**Figure 7A**). Excitatory effects on SFRs in sham animals ranged from 209 to 3740% (mean ± SEM, 1,348 ± 810). In the only neuron that showed an increase in sound evoked responses, the increase was 138%. In AT animals, excitatory effects on SFRs were seen in three neurons, ranging from 37 to 487% (193 ± 147%) and in two neurons in sound evoked response at 57 and 58% (**Figure 7B**). The magnitude of inhibition was significantly different between sham and AT animals with regards to the sound evoked response (unpaired *t*-test $p = 0.045$), but not for the SFRs. Due to the low numbers of neurons showing excitatory effects we did not run an analysis for statistical differences between groups.

To investigate the temporal pattern of effects of PFC stimulation, the average absolute magnitude of effect on SFRs and evoked FRs over time was calculated from the PSTHs (per bin) before and after PFC electrical stimulation for both sham and AT animals. Results are shown in **Figure 8**. The effects on SFRs are shown for sham (**Figure 8A**) and for AT animals (**Figure 8B**). In agreement with the findings above no apparent differences could be observed. The average effects on SFRs are dominated by the excitatory effects even though only few neurons showed an excitatory effect. This can be explained due to the general low SFRs, which means that even 100% inhibition is equivalent to only a small absolute change. The excitatory effects occurred within the first 50 ms after electrical stimulation had seized (grey column in graphs). The effects on sound evoked FRs are dominated by a large inhibitory effect in the first 50 ms after stimulation had stopped (**Figure 8C, shams** and **8D**, AT animals). The significant increased inhibitory effect on sound evoked FRs in AT animals compared to shams is clearly apparent when comparing **Figures 8C,D**.

DISCUSSION

This paper provides the first evidence for a functional effect of PFC activation on both spontaneous and sound evoked responses in MGN using a guinea pig model. Electrical stimulation of PFC resulted in inhibitory effects in about one third of the MGN neurons and excitatory effects in about 5% of neurons, with no effect on the remainder of neurons recorded. This result supports the notion that the PFC may be involved in the sensory gating of auditory information. In addition, the data show that the magnitude of the inhibitory effects on sound evoked responses increased in animals exposed to an acoustic trauma that resulted in a small permanent hearing loss. This result suggests that noise induced hearing loss may alter the sensory gating of auditory information.

The present results regarding effects on SFRs in control animals are in broad agreement with previous studies in rats (Barry et al., 2017, 2021). Electrical stimulation of PFC resulted in either no effect, excitation or inhibition of MGN neuronal activity. However, whereas in the present study more than half of the neurons showed no effect of PFC stimulation, in the studies of Barry et al. (2017, 2021) no effect was only seen in about 20% of neurons. It should be noted that neurons that did not exhibit

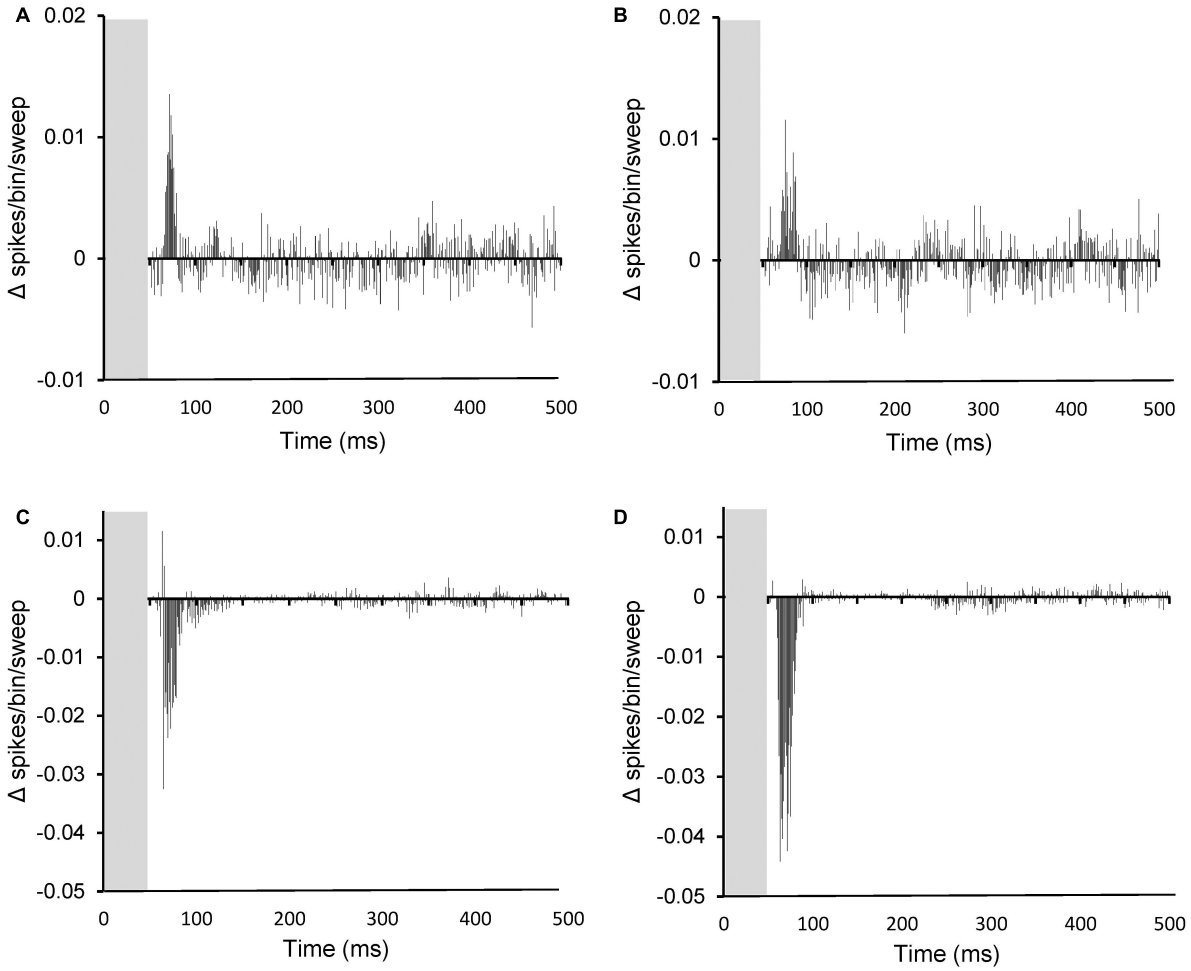

FIGURE 8 | Peristimulus time histograms (PSTHs) showing the summed difference between PSTHs (per bin) with and without PFC stimulation on spontaneous activity **(A,B)** and on sound evoked activity **(C,D)**. **(A,C)** data from sham animals and **(B,D)**, data from AT animals. Note the increased inhibition after AT on sound evoked responses (compare panel **C** and **D**). **(A)** Based on 11 PSTHs, **(B)** on 26 PSTHs, **(C)** on 58 PSTHs, and **(D)** on 57 PSTHs.

an effect were found in the same tracks as neurons that displayed either excitation or inhibition, which demonstrates that the lack of effect did not occur as a result of incorrect electrode placement or due to low levels of current intensity. Although it cannot be excluded that this represents a species difference, it is more likely due to the different methods used to classify the effects. Barry et al. (2017, 2019) used the criterion of >10% change in total number of spikes with and without stimulation to distinguish no effect from excitation or inhibition. In the present study, a paired *t*-test was used to compare between the histograms without and with stimulation. This analysis resulted in the smallest change being 35% on SFRs and 18% for sound evoked responses, which means that some smaller changes that were here classified as no effect, would have been incorporated as excitation or inhibition in the results of Barry et al. (2017, 2021), leading to a smaller proportion of neurons showing no effect in their data.

Similar to described in the rat (Barry et al., 2017, 2021), electrical stimulation of the prelimbic cortex resulted in the most pronounced and consistent results in MGN. Some of the functions associated with rodent prelimbic cortex, such as fear learning and attentional processes (Frysztak and Neafsey, 1991; Broersen and Uylings, 1999; Corcoran and Quirk, 2007) are in humans associated with activation of the ventromedial and dorsolateral PFC (Brown and Bowman, 2002; Uylings et al., 2003), suggesting some analogy between these structures in humans and rats. In addition, similar to rats and humans, the medial prefrontal cortex of the guinea pig has afferent and efferent connections with the mediodorsal nucleus of the thalamus (Markowitsch and Pritzel, 1981; Groenewegen, 1988; Uylings and van Eden, 1990).

The anatomical pathway by which PFC affects MGN activity is not yet fully elucidated. No evidence exists for a direct monosynaptic pathway and an indirect pathway *via* the thalamic reticular nucleus (TRN) is likely. The TRN, which provides predominantly GABA-ergic input to MGN (Yu et al., 2009a,b), receives indirect input from PFC (O'Donnell et al., 1997) and the

GABA-ergic input would explain the predominantly inhibitory effects observed. Alternatively, other indirect pathways exist, which could account for the effects observed, potentially involving nucleus accumbens (O'Donnell et al., 1997). Past studies have proposed a multisynaptic network involving the nucleus accumbens as it is interconnected with both the PFC and the TRN (Sesack et al., 1989; O'Donnell et al., 1997; Rauschecker et al., 2010). Additionally, it has also been found that the nucleus accumbens projects indirectly to the TRN *via* the ventral pallidum and the globus pallidus (O'Donnell et al., 1997). Multisynaptic pathways may also involve or feedback connections from auditory cortical areas (Zhang and Suga, 2000; Winer et al., 2001; He et al., 2002), which receive direct input from PFC (Barbas et al., 2005; Golubic et al., 2014, 2019; Medalla and Barbas, 2014; Winkowski et al., 2018). The fact that different pathways may exist between PFC and MGN may explain the divergent effects (excitatory vs. inhibitory) observed in MGN following PFC stimulation.

Our observation that an AT and subsequent hearing loss increased the magnitude of the inhibitory effects observed in MGN, is in broad agreement with the recent study of Barry et al. (2021) in rats. However, the former study described this AT induced change on the effect on SFRs whereas in the present study it was only observable in the sound evoked FRs. Barry et al. (2021) did not investigate effects on sound evoked FRs. The fact that no change in effect magnitude on SFRs was observed in the present study may be due to the fact that SFRs were low as compared to other studies (Barry et al., 2019; Cook et al., 2021), which impacts the ability to measure an inhibitory change. For sound evoked responses this is not an issue as the evoked responses were generally robust and indeed the change in effect magnitude was clearly visible and statistically significant. The reason for the lower than expected SFRs may be the sampling of neurons. In previous studies aimed at investigating the average SFRs without and with AT (Kalappa et al., 2014; Barry et al., 2019; Cook et al., 2021), the emphasis is generally on collecting data from as many neurons as possible, and only a limited number of data are collected from each neuron. In the present study, the time taken for each neuron to obtain all required information, was longer and hence resulted in less neurons to be able to be recorded. This also means the possibility cannot be excluded that the populations of neurons recorded from is different as compared to our previous study in guinea pig (Cook et al., 2021). Finally, it is also possible that the difference between Barry and colleagues' study in rat and our study in guinea pigs is due to intrinsic species differences.

Since the proportion of neurons showing inhibitory effects did not change after AT and subsequent hearing loss, this means it was the inhibitory effect on individual neurons that was increased. The inhibitory effect most likely involves GABA-ergic input from TRN (Yu et al., 2009a,b). The change observed may be due to either presynaptic or post-synaptic plasticity. Presynaptic GABA content and thereby GABAergic efficacy can be modified by alterations in the synthesis, transport, and degradation of GABA or related molecules (Roth and Draguhn, 2012). Post-synaptic changes may involve GABA receptor clustering (Marsden et al., 2007; Petrini et al., 2014), increasing the effect of GABA release on the post-synaptic MGN cell. This plasticity or synaptic scaling of the functional connection between PFC and MGN, may be driven by the hyperactivity that is induced by AT as described in a multitude of auditory structures including the MGN (Mulders and Robertson, 2009; Kalappa et al., 2014; Eggermont and Roberts, 2015; Wu et al., 2016; Cook et al., 2021).

As suggested by Barry et al. (2021) such a homeostatic mechanism, observed only 2 weeks after AT, may be an early compensatory effect to prevent the conscious perception of the hyperactivity that evolved due to AT. An increase in inhibitory effects from PFC activation, as observed in our study, is not in line with what has been suggested to occur in tinnitus development, which is thought to be due to a breakdown of inhibition (Rauschecker et al., 2010, 2015; De Ridder et al., 2011). So why do some individuals with hearing loss continue to develop tinnitus, and other do not (Baguley et al., 2013)? Is it possible that this compensatory mechanism fails in some individuals over time thereby allowing the hyperactivity to reach cortex and lead to a percept such as tinnitus? Populations with high levels of anxiety or post-traumatic stress disorder show higher prevalence of tinnitus (Hinton et al., 2006; Shargorodsky et al., 2010; Clifford et al., 2019). Anxiety is associated with both structural and functional changes in PFC (Hare and Duman, 2020), which may possibly affect the ability of the system to suppress tinnitus-like activity. In agreement with this notion, patients with panic disorder show reduced sensory gating as compared to healthy controls (Cheng et al., 2019). Further studies comparing the functionality of the PFC-MGN circuitry in animals with and without tinnitus are necessary to investigate the role of PFC in the development of tinnitus.

DATA AVAILABILITY STATEMENT

The raw data supporting the conclusions of this article will be made available by the authors, without undue reservation.

ETHICS STATEMENT

The animal study was reviewed and approved by the Animal Ethics Committee of the University of Western Australia.

AUTHOR CONTRIBUTIONS

WM and CD contributed to conception and design of the study. CD, WM, and KB performed the statistical analysis and wrote sections of the manuscript. CD wrote the first draft of the manuscript. All authors contributed to manuscript revision, read, and approved the submitted version.

FUNDING

This work was funded by contributions of the University of Western Australia.

REFERENCES

Baguley, D., Mcferran, D., and Hall, D. (2013). Tinnitus. *Lancet* 382, 1600–1607.

Barbas, H., Medalla, M., Alade, O., Suski, J., Zikopoulos, B., and Lera, P. (2005). Relationship of prefrontal connections to inhibitory systems in superior temporal areas in the rhesus monkey. *Cereb. Cortex* 15, 1356–1370. doi: 10.1093/cercor/bhi018

Barry, K. M., Paolini, A. G., Robertson, D., and Mulders, W. H. (2015). Modulation of medial geniculate nucleus neuronal activity by electrical stimulation of the nucleus accumbens. *Neuroscience* 308, 1–10. doi: 10.1016/j.neuroscience.2015.09.008

Barry, K. M., Robertson, D., and Mulders, W. (2017). Medial geniculate neurons show diverse effects in response to electrical stimulation of prefrontal cortex. *Hear. Res.* 353, 204–212. doi: 10.1016/j.heares.2017.07.002

Barry, K. M., Robertson, D., and Mulders, W. (2019). Changes in auditory thalamus neural firing patterns after acoustic trauma in rats. *Hear. Res.* 379, 89–97. doi: 10.1016/j.heares.2019.05.001

Barry, K. M., Robertson, D., and Mulders, W. (2021). Changes in Prefrontal Cortex-Thalamic Circuitry after Acoustic Trauma. *Biomedicines* 9:77. doi: 10.3390/biomedicines9010077

Bordi, F., and LeDoux, J. E. (1994). Response properties of single units in areas of rat auditory thalamus that project to the amygdala. II. Cells receiving convergent auditory and somatosensory inputs and cells antidromically activated by amygdala stimulation. *Exp. Brain Res.* 98, 275–286. doi: 10.1007/BF00228415

Broersen, L. M., and Uylings, H. B. (1999). Visual attention task performance in Wistar and Lister hooded rats: response inhibition deficits after medial prefrontal cortex lesions. *Neuroscience* 94, 47–57. doi: 10.1016/s0306-4522(99)00312-7

Brown, V. J., and Bowman, E. M. (2002). Rodent models of prefrontal cortical function. *Trends Neurosci.* 25, 340–343. doi: 10.1016/s0166-2236(02)02164-1

Campbell, J., Labrec, A., Bean, C., Nielsen, M., and So, W. (2019). Auditory Gating and Extended High-Frequency Thresholds in Normal-Hearing Adults With Minimal Tinnitus. *Am. J. Audiol.* 28, 209–224. doi: 10.1044/2019_AJA-TTR17-18-0036

Campbell, J., Nielsen, M., Bean, C., and Labrec, A. (2020). Auditory Gating in Hearing Loss. *J. Am. Acad. Audiol.* 31, 559–565. doi: 10.1055/s-0040-1709517

Chen, Y. X., Xu, X. R., Huang, S., Guan, R. R., Hou, X. Y., Sun, J. Q., et al. (2021). Auditory Sensory Gating in Children With Cochlear Implants: A P50-N100-P200 Study. *Front. Neurosci.* 15:768427. doi: 10.3389/fnins.2021.768427

Cheng, C. H., Chan, P. S., Hsu, S. C., and Liu, C. Y. (2019). Abnormal frontal generator during auditory sensory gating in panic disorder: an MEG study. *Psychiatry Res. Neuroimag.* 288, 60–66. doi: 10.1016/j.pscychresns.2019.04.006

Clifford, R. E., Baker, D., Risbrough, V. B., Huang, M., and Yurgil, K. A. (2019). Impact of TBI, PTSD, and Hearing Loss on Tinnitus Progression in a US Marine Cohort. *Mil. Med.* 184, 839–846. doi: 10.1093/milmed/usz016

Cook, J. A., Barry, K. M., Zimdahl, J. W., Leggett, K., and Mulders, W. (2021). Spontaneous firing patterns in the medial geniculate nucleus in a guinea pig model of tinnitus. *Hear. Res.* 403:108190. doi: 10.1016/j.heares.2021.108190

Corcoran, K. A., and Quirk, G. J. (2007). Activity in prelimbic cortex is necessary for the expression of learned, but not innate, fears. *J. Neurosci.* 27, 840–844. doi: 10.1523/JNEUROSCI.5327-06.2007

Cromwell, H. C., and Atchley, R. M. (2015). Influence of emotional states on inhibitory gating: animals models to clinical neurophysiology. *Behav. Brain Res.* 276, 67–75. doi: 10.1016/j.bbr.2014.05.028

De Ridder, D., Elgoyhen, A. B., Romo, R., and Langguth, B. (2011). Phantom percepts: tinnitus and pain as persisting aversive memory networks. *Proc. Natl. Acad. Sci. U.S.A.* 108, 8075–8080. doi: 10.1073/pnas.1018466108

De Ridder, D., Vanneste, S., Langguth, B., and Llinas, R. (2015). Thalamocortical Dysrhythmia: a Theoretical Update in Tinnitus. *Front. Neurol.* 6:124. doi: 10.3389/fneur.2015.00124

Eggermont, J. J., and Roberts, L. E. (2015). Tinnitus: animal models and findings in humans. *Cell Tissue Res.* 361, 311–336. doi: 10.1007/s00441-014-1992-8

Freedman, R., Olsen-Dufour, A. M., Olincy, A., and Consortium on the Genetics of Schizophrenia (2020). P50 inhibitory sensory gating in schizophrenia: analysis of recent studies. *Schizophr. Res.* 218, 93–98. doi: 10.1016/j.schres.2020.02.003

Frysztak, R. J., and Neafsey, E. J. (1991). The effect of medial frontal cortex lesions on respiration, "freezing," and ultrasonic vocalizations during conditioned emotional responses in rats. *Cereb. Cortex* 1, 418–425. doi: 10.1093/cercor/1.5.418

Golubic, S. J., Aine, C. J., Stephen, J. M., Adair, J. C., Knoefel, J. E., and Supek, S. (2014). Modulatory role of the prefrontal generator within the auditory M50 network. *Neuroimage* 92, 120–131. doi: 10.1016/j.neuroimage.2014.02.013

Golubic, S. J., Jurasic, M. J., Susac, A., Huonker, R., Gotz, T., and Haueisen, J. (2019). Attention modulates topology and dynamics of auditory sensory gating. *Hum. Brain Mapp.* 40, 2981–2994. doi: 10.1002/hbm.24573

Groenewegen, H. J. (1988). Organization of the afferent connections of the mediodorsal thalamic nucleus in the rat, related to the mediodorsal-prefrontal topography. *Neuroscience* 24, 379–431. doi: 10.1016/0306-4522(88)90339-9

Halassa, M. M., and Kastner, S. (2017). Thalamic functions in distributed cognitive control. *Nat. Neurosci.* 20, 1669–1679. doi: 10.1038/s41593-017-0020-1

Hare, B. D., and Duman, R. S. (2020). Prefrontal cortex circuits in depression and anxiety: contribution of discrete neuronal populations and target regions. *Mol. Psychiatry* 25, 2742–2758. doi: 10.1038/s41380-020-0685-9

He, J., Yu, Y. Q., Xiong, Y., Hashikawa, T., and Chan, Y. S. (2002). Modulatory effect of cortical activation on the lemniscal auditory thalamus of the Guinea pig. *J. Neurophysiol.* 88, 1040–1050. doi: 10.1152/jn.2002.88.2.1040

Hennessy, M. B., Watanasriyakul, W. T., Price, B. C., Bertke, A. S., and Schiml, P. A. (2018). Adult males buffer the cortisol response of young guinea pigs: changes with age, mediation by behavior, and comparison with prefrontal activity. *Horm. Behav.* 98, 165–172. doi: 10.1016/j.yhbeh.2017.12.017

Hinton, D. E., Chhean, D., Pich, V., Hofmann, S. G., and Barlow, D. H. (2006). Tinnitus among Cambodian refugees: relationship to PTSD severity. *J. Trauma Stress* 19, 541–546. doi: 10.1002/jts.20138

Iidaka, T., Kogata, T., Mano, Y., and Komeda, H. (2019). Thalamocortical Hyperconnectivity and Amygdala-Cortical Hypoconnectivity in Male Patients With Autism Spectrum Disorder. *Front. Psychiatry* 10:252. doi: 10.3389/fpsyt.2019.00252

Jobson, D. D., Hase, Y., Clarkson, A. N., and Kalaria, R. N. (2021). The role of the medial prefrontal cortex in cognition, ageing and dementia. *Brain Commun.* 3:fcab125. doi: 10.1093/braincomms/fcab125

Johnstone, J. R., Alder, V. A., Johnstone, B. M., Robertson, D., and Yates, G. K. (1979). Cochlear action potential threshold and single unit thresholds. *J. Acoust. Soc. Am.* 65, 254–257. doi: 10.1121/1.382244

Kalappa, B. I., Brozoski, T. J., Turner, J. G., and Caspary, D. M. (2014). Single unit hyperactivity and bursting in the auditory thalamus of awake rats directly correlates with behavioural evidence of tinnitus. *J. Physiol.* 592, 5065–5078. doi: 10.1113/jphysiol.2014.278572

Leaver, A. M., Renier, L., Chevillet, M. A., Morgan, S., Kim, H. J., and Rauschecker, J. P. (2011). Dysregulation of limbic and auditory networks in tinnitus. *Neuron* 69, 33–43. doi: 10.1016/j.neuron.2010.12.002

Leaver, A. M., Seydell-Greenwald, A., and Rauschecker, J. P. (2016). Auditory-limbic interactions in chronic tinnitus: challenges for neuroimaging research. *Hear. Res.* 334, 49–57. doi: 10.1016/j.heares.2015.08.005

Leaver, A. M., Seydell-Greenwald, A., Turesky, T. K., Morgan, S., Kim, H. J., and Rauschecker, J. P. (2012). Cortico-limbic morphology separates tinnitus from tinnitus distress. *Front. Syst. Neurosci.* 6:21. doi: 10.3389/fnsys.2012.00021

Markowitsch, H. J., and Pritzel, M. (1981). Prefrontal cortex of the guinea pig (Cavia porcellus) defined as cortical projection area of the thalamic mediodorsal nucleus. *Brain Behav. Evol.* 18, 80–95. doi: 10.1159/000121778

Marsden, K. C., Beattie, J. B., Friedenthal, J., and Carroll, R. C. (2007). NMDA receptor activation potentiates inhibitory transmission through GABA receptor-associated protein-dependent exocytosis of GABA(A) receptors. *J. Neurosci.* 27, 14326–14337. doi: 10.1523/JNEUROSCI.4433-07.2007

Mathiasen, M. L., Nelson, A. J. D., Amin, E., O'mara, S. M., and Aggleton, J. P. (2021). A Direct Comparison of Afferents to the Rat Anterior Thalamic Nuclei and Nucleus Reuniens: overlapping But Different. *eNeuro* 8:ENEURO.0103-20.2021. doi: 10.1523/ENEURO.0103-20.2021

Medalla, M., and Barbas, H. (2014). Specialized prefrontal "auditory fields": organization of primate prefrontal-temporal pathways. *Front. Neurosci.* 8:77. doi: 10.3389/fnins.2014.00077

Merrill, E. G., and Ainsworth, A. (1972). Glass-coated platinum-plated tungsten microelectrodes. *Med. Biol. Eng.* 10, 662–672. doi: 10.1007/BF02476084

Mulders, W. H., Ding, D., Salvi, R., and Robertson, D. (2011). Relationship between auditory thresholds, central spontaneous activity, and hair cell loss after acoustic trauma. *J. Comp. Neurol.* 519, 2637–2647. doi: 10.1002/cne.22644

Mulders, W. H., and Robertson, D. (2009). Hyperactivity in the auditory midbrain after acoustic trauma: dependence on cochlear activity. *Neuroscience* 164, 733–746. doi: 10.1016/j.neuroscience.2009.08.036

Mulders, W. H., and Robertson, D. (2013). Development of hyperactivity after acoustic trauma in the guinea pig inferior colliculus. *Hear. Res.* 298, 104–108. doi: 10.1016/j.heares.2012.12.008

Mulders, W. H. A. M., Vooys, V., Makowiecki, K., Tang, A., and Rodger, J. (2016). The effects of repetitive transcranial magnetic stimulation in an animal model of tinnitus. *Sci. Rep.* 6:38234. doi: 10.1038/srep38234

Nakajima, M., Schmitt, L. I., and Halassa, M. M. (2019). Prefrontal Cortex Regulates Sensory Filtering through a Basal Ganglia-to-Thalamus Pathway. *Neuron* 103:e410. doi: 10.1016/j.neuron.2019.05.026

O'Donnell, P., Lavin, A., Enquist, L. W., Grace, A. A., and Card, J. P. (1997). Interconnected parallel circuits between rat nucleus accumbens and thalamus revealed by retrograde transynaptic transport of pseudorabies virus. *J. Neurosci.* 17, 2143–2167. doi: 10.1523/JNEUROSCI.17-06-02143.1997

Paxinos, G., and Watson, C. (2007). *The Rat Brain in Stereotaxic Coordinates*. Amsterdam: Elsevier.

Petrini, E. M., Ravasenga, T., Hausrat, T. J., Iurilli, G., Olcese, U., Racine, V., et al. (2014). Synaptic recruitment of gephyrin regulates surface GABAA receptor dynamics for the expression of inhibitory LTP. *Nat. Commun.* 5:3921. doi: 10.1038/ncomms4921

Pinault, D. (2004). The thalamic reticular nucleus: structure, function and concept. *Brain Res. Rev.* 46, 1–31. doi: 10.1016/j.brainresrev.2004.04.008

Ptak, R. (2012). The frontoparietal attention network of the human brain: action, saliency, and a priority map of the environment. *Neuroscientist* 18, 502–515. doi: 10.1177/1073858411409051

Rapisarda, C., and Bacchelli, B. (1977). The brain of the guinea pig in stereotaxic coordinates. *Arch. Sci. Biol.* 61, 1–37. doi: 10.1007/978-1-4419-8372-5_1

Rauschecker, J. P., Leaver, A. M., and Muhlau, M. (2010). Tuning out the noise: limbic-auditory interactions in tinnitus. *Neuron* 66, 819–826. doi: 10.1016/j.neuron.2010.04.032

Rauschecker, J. P., May, E. S., Maudoux, A., and Ploner, M. (2015). Frontostriatal Gating of Tinnitus and Chronic Pain. *Trends Cogn. Sci.* 19, 567–578. doi: 10.1016/j.tics.2015.08.002

Rios-Florez, J. A., Lima, R. R. M., Morais, P., De Medeiros, H. H. A., Cavalcante, J. S., and Junior, E. S. N. (2021). Medial prefrontal cortex (A32 and A25) projections in the common marmoset: a subcortical anterograde study. *Sci. Rep.* 11:14565. doi: 10.1038/s41598-021-93819-z

Roth, F. C., and Draguhn, A. (2012). GABA metabolism and transport: effects on synaptic efficacy. *Neural Plast* 2012:805830. doi: 10.1155/2012/805830

Saalmann, Y. B., Pinsk, M. A., Wang, L., Li, X., and Kastner, S. (2012). The pulvinar regulates information transmission between cortical areas based on attention demands. *Science* 337, 753–756. doi: 10.1126/science.1223082

Sedley, W., Alter, K., Gander, P. E., Berger, J., and Griffiths, T. D. (2019). Exposing Pathological Sensory Predictions in Tinnitus Using Auditory Intensity Deviant Evoked Responses. *J. Neurosci.* 39, 10096–10103. doi: 10.1523/JNEUROSCI.1308-19.2019

Sesack, S. R., Deutch, A. Y., Roth, R. H., and Bunney, B. S. (1989). Topographical organization of the efferent projections of the medial prefrontal cortex in the rat: an anterograde tract-tracing study with Phaseolus vulgaris leucoagglutinin. *J. Comp. Neurol.* 290, 213–242. doi: 10.1002/cne.902900205

Shargorodsky, J., Curhan, G. C., and Farwell, W. R. (2010). Prevalence and characteristics of tinnitus among US adults. *Am. J. Med.* 123, 711–718. doi: 10.1016/j.amjmed.2010.02.015

Storozheva, Z. I., Akhapkin, R. V., Bolotina, O. V., Korendrukhina, A., Novototsky-Vlasov, V. Y., Shcherbakova, I. V., et al. (2021). Sensorimotor and sensory gating in depression, anxiety, and their comorbidity. *World J. Biol. Psychiatry* 22, 183–193. doi: 10.1080/15622975.2020.1770859

Swanson, L. W. (2018). Brain maps 4.0-Structure of the rat brain: an open access atlas with global nervous system nomenclature ontology and flatmaps. *J. Comp. Neurol.* 526, 935–943. doi: 10.1002/cne.24381

Uylings, H. B., Groenewegen, H. J., and Kolb, B. (2003). Do rats have a prefrontal cortex? *Behav. Brain Res.* 146, 3–17.

Uylings, H. B., and van Eden, C. G. (1990). Qualitative and quantitative comparison of the prefrontal cortex in rat and in primates, including humans. *Prog. Brain Res.* 85, 31–62.

Winer, J. A., Diehl, J. J., and Larue, D. T. (2001). Projections of auditory cortex to the medial geniculate body of the cat. *J. Comp. Neurol.* 430, 27–55.

Winkowski, D. E., Nagode, D. A., Donaldson, K. J., Yin, P., Shamma, S. A., Fritz, J. B., et al. (2018). Orbitofrontal Cortex Neurons Respond to Sound and Activate Primary Auditory Cortex Neurons. *Cereb. Cortex* 28, 868–879. doi: 10.1093/cercor/bhw409

Wood, E. T., Cummings, K. K., Jung, J., Patterson, G., Okada, N., Guo, J., et al. (2021). Sensory over-responsivity is related to GABAergic inhibition in thalamocortical circuits. *Transl. Psychiatry* 11:39. doi: 10.1038/s41398-020-01154-0

Wu, C., Martel, D. T., and Shore, S. E. (2016). Increased Synchrony and Bursting of Dorsal Cochlear Nucleus Fusiform Cells Correlate with Tinnitus. *J. Neurosci.* 36, 2068–2073. doi: 10.1523/JNEUROSCI.3960-15.2016

Xu, X. M., Jiao, Y., Tang, T. Y., Zhang, J., Lu, C. Q., Salvi, R., et al. (2019). Sensorineural hearing loss and cognitive impairments: contributions of thalamus using multiparametric MRI. *J. Magn. Reson. Imag.* 50, 787–797. doi: 10.1002/jmri.26665

Yu, X. J., Xu, X. X., Chen, X., He, S., and He, J. (2009a). Slow recovery from excitation of thalamic reticular nucleus neurons. *J. Neurophysiol.* 101, 980–987. doi: 10.1152/jn.91130.2008

Yu, X. J., Xu, X. X., He, S., and He, J. (2009b). Change detection by thalamic reticular neurons. *Nat. Neurosci.* 12, 1165–1170. doi: 10.1038/nn.2373

Zhang, Y., and Suga, N. (2000). Modulation of responses and frequency tuning of thalamic and collicular neurons by cortical activation in mustached bats. *J. Neurophysiol.* 84, 325–333. doi: 10.1152/jn.2000.84.1.325

Zimdahl, J. W., Thomas, H., Bolland, S. J., Leggett, K., Barry, K. M., Rodger, J., et al. (2021). Excitatory Repetitive Transcranial Magnetic Stimulation Over Prefrontal Cortex in a Guinea Pig Model Ameliorates Tinnitus. *Front. Neurosci.* 15:693935. doi: 10.3389/fnins.2021.693935

Conflict of Interest: The authors declare that the research was conducted in the absence of any commercial or financial relationships that could be construed as a potential conflict of interest.

Publisher's Note: All claims expressed in this article are solely those of the authors and do not necessarily represent those of their affiliated organizations, or those of the publisher, the editors and the reviewers. Any product that may be evaluated in this article, or claim that may be made by its manufacturer, is not guaranteed or endorsed by the publisher.

frontiers | Frontiers in Molecular Neuroscience

REVIEW
published: 29 April 2022
doi: 10.3389/fnmol.2022.826679

Paradoxical Hyperexcitability in Disorders of Neurodevelopment

*Michelle W. Antoine**

Section on Neural Circuits, National Institute on Alcohol Abuse and Alcoholism, National Institutes of Health, Bethesda, MD, United States

Autism Spectrum Disorder (ASD), Rett syndrome (RTT) and Angelman Syndrome (AS) are neurodevelopmental disorders (NDDs) that share several clinical characteristics, including displays of repetitive movements, developmental delays, language deficits, intellectual disability, and increased susceptibility to epilepsy. While several reviews address the biological basis of non-seizure-related ASD phenotypes, here, I highlight some shared biological mechanisms that may contribute to increased seizure susceptibility. I focus on genetic studies identifying the anatomical origin of the seizure phenotype in loss-of-function, monogenic, mouse models of these NDDs, combined with insights gained from complementary studies quantifying levels of synaptic excitation and inhibition. Epilepsy is characterized by a sudden, abnormal increase in synchronous activity within neuronal networks, that is posited to arise from excess excitation, largely driven by reduced synaptic inhibition. Primarily for this reason, elevated network excitability is proposed to underlie the causal basis for the ASD, RTT, and AS phenotypes. Although, mouse models of these disorders replicate aspects of the human condition, i.e., hyperexcitability discharges or seizures on cortical electroencephalograms, measures at the synaptic level often reveal deficits in excitatory synaptic transmission, rather than too much excitation. Resolving this apparent paradox has direct implications regarding expected outcomes of manipulating GABAergic tone. In particular, in NDDs associated with seizures, cortical circuits can display reduced, rather than normal or increased levels of synaptic excitation, and therefore suggested treatments aimed at increasing inhibition could further promote hypoactivity instead of normality. In this review, I highlight shared mechanisms across animal models for ASD, RTT, and AS with reduced synaptic excitation that nevertheless promote hyperexcitability in cortical circuits.

Keywords: seizures, autism, excitation, Rett, Angelman

OPEN ACCESS

Edited by:
Michael Telias,
University of Rochester, United States

Reviewed by:
Moran Rubinstein,
Tel Aviv University, Israel
Matthew Weston,
University of Vermont, United States

***Correspondence:**
Michelle W. Antoine
michelle.antoine@nih.gov

Specialty section:
This article was submitted to Brain Disease Mechanisms, a section of the journal Frontiers in Molecular Neuroscience

Received: *01 December 2021*
Accepted: *14 March 2022*
Published: *29 April 2022*

Citation:
Antoine MW (2022) Paradoxical Hyperexcitability in Disorders of Neurodevelopment. Front. Mol. Neurosci. 15:826679. doi: 10.3389/fnmol.2022.826679

INTRODUCTION

Rett syndrome (RTT) is an X-linked disorder that in ∼95% of cases is caused by mutations in the gene encoding the transcription factor Methyl-CpG-binding protein 2 (*MECP2*) (Amir et al., 1999). RTT occurs almost exclusively in females and is characterized by

largely normal development for the initial 6-18 months after birth, followed by regression of previously acquired speech and motor skills (Guy et al., 2001). Epileptic seizures of various types (for example: tonic-clonic, absence, myoclonic, tonic) occur in 60-80% of Rett syndrome patients (Operto et al., 2019). Typically, seizure onset initiates between 2 and 3 years of age, with seizure severity often increasing until 7-12 years of age (Glaze et al., 2010).

Like Rett Syndrome, Angelman Syndrome (AS) is a rare neurodevelopmental disorder that affects ∼1/10,000 to 1/20,000 individuals, and is characterized by developmental delay, intellectual disability, increased susceptibility to seizures, impaired language development, and movement or balance dysfunction (Kishino et al., 1997; Matsuura et al., 1997; Williams, 2005). Approximately, 5-15% of AS cases are attributed to reduced or absent maternal expression on chromosome 15q of the gene *UBE3A*, which encodes the E6-AP ubiquitin ligase, an enzyme that links ubiquitin to specific proteins thereby targeting them for degradation within the cell proteasome (Huibregtse et al., 1993; Horsthemke and Wagstaff, 2008). These pathogenic point mutations in UBE3A are more common in familial rather than sporadic patients and though several seizure types occur, atypical absence seizures and myoclonic seizures are the more common forms.

Autism spectrum disorder shares aspects with both RTT and AS. Of the three disorders, ASD is the most common, currently affecting 1 in 54 eight-year-old children in the United States (Knopf, 2020). Unlike, RTT and AS, hundreds of genes have been identified that increase susceptibility to developing ASD. Of these genes, loss-of-function mutations in *SCN2A*, which encodes the $Na_v1.2$ voltage-gated sodium channel pore-forming alpha II subunit, has one of the strongest genetic associations with ASD susceptibility (Satterstrom et al., 2020). Functionally, $Na_v1.2$ is involved in the initiation and propagation of action potentials in immature neurons throughout the central nervous system (Catterall, 2017) and appears essential for spiking in a subpopulation of immature oligodendrocytes (Gould and Kim, 2021). The development of patients with SCN2A mutations and ASD is mostly typical until 6-months of age, after which motor and verbal delays manifest, and between 18 months to 4 years of age, one-third of these cases will display seizures or milder and/or later-onset epilepsies (Wolff et al., 2017; Sanders et al., 2018). Here, we focus on mechanisms that may help drive these milder and/or later-onset epilepsies.

Loss-of-function mutations in *MECP2*, *UBE3A*, and *SCN2A* yield a shared neurodevelopmental disorder phenotype that strongly features abnormal electroencephalograms (EEGs) and increased susceptibility to seizures. It is often theorized that this increased association with epilepsy reflects a shared biological mechanism. Typically, this mechanism is proposed to involve excess synaptic excitation that is largely driven by too little inhibition at the synaptic and circuit levels (Rubenstein and Merzenich, 2003). To date, several molecular and physiology-based studies in mouse models carrying loss-of-function mutations in either *Mecp2*, *Ube3A* or *Scn2a* have demonstrated key aspects of the human phenotype, i.e. the occurrence of either hyperexcitability discharges or seizure activity on cortical electroencephalograms (Born et al., 2017; Ogiwara et al., 2018; Wither et al., 2018). Unexpectedly, measures at the synaptic level also revealed a shared phenotype for deficient, rather than excess, excitatory synaptic transmission (Dani et al., 2005; Wood and Shepherd, 2010; Wallace et al., 2012; Banerjee et al., 2016; Spratt et al., 2019). In the ensuing sections of this review, guided first by Cre/Lox genetic studies that identify the causal cell source(s) of the seizure or hyperexcitability phenotype, and second by parallel studies in these mice that quantify synaptic excitation and inhibition levels, I propose that shared mechanisms account for hyperexcitability discharges or seizure activity in ASD, RTT and AS despite impaired excitatory synaptic transmission.

A Shared Cortical Locus for Absence Seizure Susceptibility in *Mecp2* and *Scn2a* Haploinsufficiency

In the human condition, a key diagnostic criterion for absence epilepsy is the display of spike-and-wave discharges (SWDs) on cortical electroencephalograms (EEGs) (Terlau et al., 2020). SWDs are defined by a characteristic electroencephalographic pattern consisting of a sharp, negative spike followed by a slow wave. Unlike other seizure phenotypes, absence seizures typically lack overt displays of convulsions. Instead, during seizures, EEGs may indicate bilaterally synchronized 3–4 Hz SWDs while electromyography (EMG) measures show brief periods of behavior arrest (Panayiotopoulos, 2001; Blumenfeld, 2005; Idro et al., 2008). Mice with a heterozygous deletion of *Scn2a* (*Scn2a*$^{+/-}$) recapitulate the human phenotype of "absence-like" seizures (Ogiwara et al., 2018). Electrocorticogram (ECoG)-EMG recordings in *Scn2a*$^{+/-}$ mice at 10-27 weeks of age reveal occurrences of synchronous, bilateral, cortical SWDs during behavioral quiescence. As *Scn2a* haploinsufficiency reduces the $Na_v1.2$ current by half, the projected result is reduced neuronal excitability, but surprisingly seizure activity is observed.

Dissection of the cell types underlying this seizure phenotype with Cre-lox genetics revealed critical contributions of $Na_v1.2$ haploinsufficiency in neurons that are excitatory rather than inhibitory. In this experiment, *Emx1*$^{Cre/+}$;*Scn2a* $^{fx/+}$ mice were generated from a cross between *Emx1*-Cre mice (Gorski et al., 2002) and the *Scn2a* floxed allele (Ogiwara et al., 2018), and showed reduced expression of *Scn2a* in dorsal-telencephalic derivatives (e.g., neocortical and hippocampal excitatory neurons). ECoG-EMG recordings in 6–8 week-old *Emx1*$^{Cre/+}$;*Scn2a* $^{fx/+}$ mice showed "absence-like" seizures featuring SWDs with EMG suppression. Like the human condition, administration of the anticonvulsant ethosuximide suppressed seizures (Ogiwara et al., 2018). In contrast, this "absence-like" seizure phenotype was not observed when using the vesicular GABA transporter Cre mouse line (Vgat-Cre) to reduce $Na_v1.2$ expression specifically in interneurons (Ogiwara et al., 2018; Miyamoto et al., 2019). Thus, a loss of *Scn2a* from GABAergic cell types may not be a primary cause underlying SWDs.

Finer resolution cell-type dissection of the seizure phenotype showed that SWDs can be generated in mice with a reduction of *Scn2a* in cortical layer (L)5 pyramidal neurons (i.e., *Trpc4*$^{Cre/+}$;*Scn2a* $^{fx/fx}$ mice) but not in *Ntsr*$^{Cre/+}$;*Scn2a* $^{fx/fx}$ mice, where *Scn2a* expression is reduced in cortical L6 neurons (Miyamoto et al., 2019). These findings in mice support studies conducted in rat models of absence epilepsy, which suggest that the deep layers of the somatosensory cortex may act as the initiation site of SWDs (Blumenfeld, 2005; Pinault and O'Brien, 2005; Lüttjohann and van Luijtelaar, 2015; Depaulis and Charpier, 2018; McCafferty et al., 2018). Thus, the pathological origins of "absence-like" seizures in rats may be similar to the mouse ASD condition.

Whole-cell current clamp recordings in adult L5b PYR neurons deficient in *Scn2a*, due to AAV-EF1a-Cre-mCherry virus-mediated recombination of the floxed allele (Scn2a$^{fx/fx}$), indicated that cell excitability was elevated. Namely, the number of action potentials increased in response to somatic depolarizing current injections, input resistance increased, action potential (AP) repolarization speed decreased, and the afterhyperpolarization (AHP) during spike trains was more depolarized, when compared to wild type (Scn2a$^{fx/+}$ or Scn2a$^{fx/fx}$) neurons in the contralateral uninfected hemisphere of the medial prefrontal cortex (mPFC) (Spratt et al., 2021). Compartmental modeling revealed two interesting findings. The first and main finding was that complete deletion of $Na_v1.2$ promoted an exponential rather than linear shift in the relationship between the Na_v and K-channel current during an AP (Spratt et al., 2021). This effect can potentially increase overall L5 excitability because repolarization in neurons is incomplete between APs, so threshold attainment and AP generation can occur more rapidly. The second finding was that increased input resistance can shift the onset of the Firing/Current (F/I) curve left, which can theoretically increase the number of APs generated at current onset. Intriguingly, during this current onset period, *Scn2a* deficient neurons regularly produce high-frequency bursts (Spratt et al., 2021).

Besides L5b PYR excitatory neurons, *Scn2a* is expressed in somatostatin-positive (SSt^+) and vasoactive intestinal peptide-positive (VIP^+) interneurons, as well as in unmyelinated axons of GABAergic medium spiny neurons (MSNs) (Li et al., 2014; Miyazaki et al., 2014; Yamagata et al., 2017). It is currently unclear whether excitability is similarly altered in SSt^+ and VIP^+ interneurons under conditions where *Scn2a* is severely reduced or absent. However, another recent study, using a mixed striatal MSN population, linked drastically reduced *Scn2a* levels to an increase in intrinsic excitability. Patch-clamp recordings in brain slices from an $Na_v1.2$ hypomorph mouse (Scn2a$^{gt/gt}$) (Eaton et al., 2021) with 25-30% of the wild-type protein level, revealed enhanced neuronal excitability in striatal MSNs (i.e., an increased number of action potentials/spikes generated in response to depolarizing current injections, reduced rheobase, a mildly elevated fast after-hyperpolarization, and increased input resistance) (Zhang et al., 2021). *Ex vivo* recordings in adult MSNs, with sparse rescue of the severe Nav1.2 deficiency via viral transduction, showed that these alterations to intrinsic excitability were largely cell autonomous and likely driven by the downstream effects of a reduction in the total potassium current (Zhang et al., 2021). Spratt et al. (2021) did not observe changes in potassium channel function in L5 cortical neurons. Nevertheless, both studies identified largely cell autonomous changes in input resistance and AHP hyperpolarization that may contribute to epilepsy in cases of severe *Scn2a* deficiency, even though seizure activity was not reported specifically for Scn2a$^{gt/gt}$ mice (Eaton et al., 2021; Zhang et al., 2021). Studies on human neurons also show evidence of paradoxical hyperexcitability. Induced pluripotent stem cell derived *SCN2A*$^{-/-}$ neurons when compared with isogenic controls display an increased number of spikes on multielectrode arrays and impaired excitatory synapse formation and function (Brown et al., 2021). Key observations from mouse studies were also replicated with human neurons, including increased input resistance, reduced AP height, and reduction in the somatic component of the rising phase of the AP. However, unlike in mice, only a minor increase in the number of APs generated at current onset was observed (Brown et al., 2021). Excitatory neurons derived from an ASD patient heterozygous for the R607* truncating mutation in *SCN2A* also showed reduced excitatory synapse function. Future studies incorporating measures of synaptically-evoked spiking and excitatory currents (which are reduced in *Scn2a* haploinsufficiency and presumably in more severe *Scn2a* deficiencies), will help to confirm the predicted effects of physiological changes on seizure-related behaviors.

Similar to *Scn2a*$^{+/-}$ mice, adult female mice heterozygous for a null mutation in *Mecp2* (*Mecp2*$^{+/-}$) exhibit the cardinal hallmarks of "absence-like" seizures, i.e., the occurrence of brief ($\leq$ 2 s) spontaneous cortical epileptiform discharges with frequencies of 6-8 Hz in the somatosensory cortex during acute behavioral arrest with sensitivity to ethosuximide (Wither et al., 2018). Here too, Cre-lox genetics was used to dissect potential causal roles of *Mecp2* loss in excitatory and GABAergic neurons in the seizure phenotype. Mice in which calcium-calmodulin-dependent protein kinase II (CaMKII)-Cre (Chen et al., 2001) was used to delete *Mecp2* (Chen et al., 2001) selectively in forebrain excitatory neurons during early postnatal development reproduce RTT associated features such as increased anxiety, impaired motor coordination, and social deficits (Gemelli et al., 2006). However, the effects on seizures were not reported.

Like the *Scn2a* mutant condition, deleting the floxed *Mecp2* allele from excitatory neurons and glia in the neocortex and hippocampus using the *Emx1-Cre* mice (*Emx1*$^{Cre/+}$; *Mecp2* $^{fx/y}$) results in detection of absence seizures during EEG recordings between 6-8 weeks of age (Zhang et al., 2014). Although, the authors attributed the phenotype to *Mecp2* reduction in neurons rather than glia, intriguingly, *Mecp2* is expressed in astrocytes throughout the brain. Indeed, it has been proposed that while neurons may initiate several symptoms of RETT syndrome, loss of *Mecp2* in astrocytes may strongly affect disease progression (Lioy et al., 2011). Loss of MECP2 from astrocytes, using the floxed *Mecp2* allele (Chen et al., 2001) and the *hGFAPcreT2* mouse line (Hirrlinger et al., 2006) results in a smaller body

size, clasped hindlimb posture and irregular breathing (Lioy et al., 2011). Notably, as the *hGFAPcreT2* mouse line does not recombine very well in the cortex and the substantia nigra, this phenotype could be potentially more severe upon additional loss of *Mecp2* expression from these brain regions (Lioy et al., 2011). However, the authors buttress their premise that altered neuronal physiology mediated the "absence-like" seizure phenotype by showing that although the intrinsic excitability, resting potential, input resistance and spike threshold of L5 pyramidal neurons in the cortex is normal, mild depolarizations in the membrane potential (i.e., from −59 mV to −53 mV) produced significantly more spikes in the *Emx1*$^{Cre/+}$;*Mecp2* $^{fx/y}$ mice than in controls due to reduced inhibitory tone (Zhang et al., 2014). As we will discuss in the next section of the review, this reduction in inhibitory tone may arise from the combined effects of reductions in inhibitory inputs onto postsynaptic excitatory PYR neurons and cell autonomous changes in astrocytes that diminish synaptic GABA levels. Nevertheless, hyperactivity of cortical L5 pyramidal neurons may be a central mechanism that drives seizures when either *Scn2a* or *Mecp2* gene expression is absent or reduced.

Dual Roles for Reduced Inhibition in Seizure Susceptibility and Spiking Stability

Absence seizures in *Scn2a* or *Mecp2* cortical mouse models have been linked to hyperactivity of cortical L5 pyramidal (PYR) neurons (Zhang et al., 2014; Ogiwara et al., 2018; Miyamoto et al., 2019). However, the mechanism underlying hyperexcitation warrants further dissection. Studies on *Emx1*$^{Cre/+}$;*Mecp2* $^{fx/y}$ mice proposed a model whereby MECP2 loss in cortical PYR neurons causes a reduction of GABAergic transmission, driving hyperactivity (Zhang et al., 2014). Whole-cell patch-clamp recording in L5 PYR neurons in both the mPFC and somatosensory cortex of acute brain slices from *Emx1*$^{Cre/+}$;*Mecp2* $^{fx/y}$ mice at P17–P20 showed that although the amplitude and the kinetics of spontaneous IPSCs (sIPSCs) and miniature(m) IPSCs were unchanged, the frequency of both parameters were reduced (Zhang et al., 2014). In mutant neurons, measures of evoked monosynaptic IPSCs (i.e., recorded in the presence of DNQX and kynurenic acid) at P18-P20 showed stable IPSC thresholds but significantly reduced peak IPSC amplitudes when compared to control neurons. Notably, this reduction in inhibition is long-lasting and remained as mice aged to 6–7 weeks (Zhang et al., 2014). Comparable changes in immunofluorescent staining of puncta for the vesicular GABA transporter (VGAT, a marker for GABAergic synaptic terminals) in L5 PYR neurons from *Emx1*$^{Cre/+}$;*Mecp2* $^{fx/y}$ mice were also observed, with a 42% reduction in puncta at P18-P19 and a 37% reduction at 7–8 weeks of age. In L2/3 PYR somatosensory cortical neurons, sIPSC frequency reduced by 57% in mutant neurons, and sIPSC amplitude decreased by 20%. Interestingly, these observed reductions in synaptic inhibitory currents were not replicated when *Mecp2* was deleted from forebrain GABAergic neurons using the *Dlx5/6-Cre* mice (Zhang et al., 2014). Overall, these results show that the loss of *Mecp2* in PYR cortical neurons causes a reduction in GABAergic transmission onto postsynaptic excitatory neurons.

Remarkably, an identical phenotype of a reduction in GABAergic transmission onto postsynaptic CA1 excitatory PYR neurons was observed after PYR-specific deletion of the ASD-related gene, tuberous sclerosis complex 1 (*Tsc1*) (Bateup et al., 2013). The authors also suggested that such reductions in inhibition could alone drive Tsc1-related hyperexcitability at the network level to result in seizures. However, an alternative explanation exists. Namely, that these changes in inhibition are compensatory, rather than being a primary defect that directly drives seizure activity. It was previously shown that a primary deficit in either excitatory synaptic input or intrinsic excitability in excitatory neurons can induce a decrease in inhibitory inputs onto these neurons to balance the levels of synaptic excitation and inhibition (Xue et al., 2014; He et al., 2018). In this activity-dependent phenomenon, decreases in synaptic excitation are matched by greater reductions in synaptic inhibition levels to preserve the magnitude of cell depolarization and maintain spiking stability (Antoine et al., 2019). **Figure 1**, adapted from Antoine et al. (2019), illustrates results of a simulation examining the effect of differently scaled excitatory (Gex) and inhibitory (Gin) conductance combinations on the peak change in the membrane potential (Vm) in postsynaptic cortical PYR neurons. Indicated in **Figure 1** is the black "PSP stability contour" line illustrating the postsynaptic Gex and Gin conductance combinations that maintain a wild type-sized PSP peak. Notably, Gin changes primarily reflect the alterations to parvalbumin- positive (PV^+) interneuron mediated inhibition onto postsynaptic cortical PYR neurons. In regions where the contour rests above the blue diagonal or unity line, when Gex decreases, Gin must decrease more than Gex to maintain a normal PSP peak.

Thus, it is possible that the observed reduction in GABAergic transmission onto postsynaptic excitatory neurons in *Tsc1* and/or *Mecp1* reflects a change that compensates for either diminished excitatory drive or intrinsic excitability in PYR neurons, rather than to directly drive seizure activity. In line with this alternative interpretation, current clamp recordings from *Tsc1*-deficient CA1 PYR excitatory neurons revealed that mutant neurons are significantly less excitable than control neurons: exhibiting reduced action potential firing in response to a wide-range of depolarizing current injections, increased action potential threshold, decreased membrane resistance and increased capacitance (Bateup et al., 2013). Furthermore, in response to increasing stimulus intensities, no significant difference in either the amplitude of excitatory postsynaptic potentials (EPSPs) or firing frequencies were observed. Thus, these cell autonomous reductions in GABAergic transmission onto postsynaptic excitatory neurons may not be sufficient to drive circuit hyperexcitability when they co-occur with either diminished excitatory input or reduced intrinsic excitability in PYR neurons. In line with this conclusion, *Tsc1* mutations that promote increases in PYR intrinsic excitability co-occurs with hyperexcitability (Abs et al., 2013; Koene et al., 2021).

Multiple studies reveal a cell autonomous reduction in excitatory drive or activity in cortical and hippocampal PYR

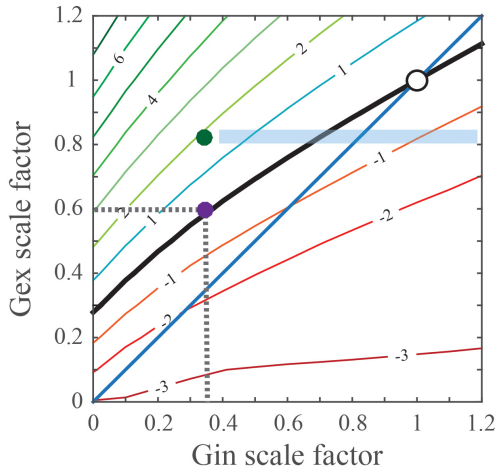

FIGURE 1 | Predicted changes in excitatory and inhibitory conductances that maintain a normal/wild type-sized PSP. Simulation calculates the effect of differentially scaled excitatory (Gex) and inhibitory (Gin) conductance combinations on the peak change in the membrane potential (Vm) of postsynaptic cortical PYR neurons. Points on the black 'PSP stability contour' line comprise the postsynaptic Gex and Gin conductance combinations that maintain a wild type-sized PSP. For example, the purple dot (•) on the contour line indicates that inhibition was reduced by 65%, which is indicated as 0.35 on the x-axis, whereas excitation was reduced by 40% and is indicated as 0.6 on the y-axis. The blue diagonal or unity line indicates numerically equal changes in Gex and Gin conductances. For regions where the contour rests above the diagonal, when Gex decreases, Gin must decrease more than Gex to maintain a normal-sized PSP. Compensatory changes in Gin can potentially be imperfect, maintaining balance in one brain region but not another. The green dot (•) illustrates a hypothetical case where Gex is reduced but features of hyperexcitability are present, i.e., PSPs are 2 mVs larger. For this case, the blue shaded rectangular area predicts that pharmacological treatments selectively increase synaptic GABA, may induce circuit hypoexcitability as Gin levels near normal.

neurons with *Mecp2* deficiency (Chao et al., 2007; Blackman et al., 2012; Qiu et al., 2012; Meng et al., 2016). To determine the functional role of *Mecp2* in PYR glutamatergic neurons, Meng and colleagues used the vesicular glutamate transporter 2-Cre mice (Vglut2$^{Cre/+}$, Vong et al., 2011) to delete the conditional *Mecp2* allele (Guy et al., 2001) from excitatory neurons throughout the brain. Whole-cell patch-clamp recordings from cortical L5 PYR neurons in the somatosensory cortex of mutant 6- to 8-week-old mice showed reduced spontaneous action potential firing (Meng et al., 2016). Measurements of postsynaptic currents (PSCs) showed a drop in both spontaneous excitatory postsynaptic currents (sEPSCs) and miniature excitatory postsynaptic currents (mEPSCs) compared to controls. Consistent with the idea that PYR neurons cell autonomously decrease inhibitory inputs to compensate for reduced levels of excitation, reductions in spontaneous inhibitory postsynaptic currents (sIPSCs) were also observed. In an otherwise *Mecp2* null mouse containing no MECP2 protein throughout the brain and body, restoration of *Mecp2* only in Vglut2^{Cre} excitatory neurons normalized spontaneous action potential firing and mEPSCs to control levels (Meng et al., 2016).

C57BL/6J mice that are heterozygous for *Ube3a*, where the deficient allele is inherited by the mother (m) rather than the father (p) (*Ube3a*$^{m-/p+}$), serve as a mouse model for Angelman Syndrome (AS) (Jiang et al., 1998; Wallace et al., 2012). Electrophysiology studies on these mice by Wallace and colleagues, provided evidence that preferential decreases in inhibitory inputs that co-occur with decreases in excitatory input or PYR activity may not be sufficient to induce a seizure phenotype. Whole-cell patch-clamp recordings from neocortical slices in L2/3 pyramidal (PYR) neurons of the visual cortex in WT and *Ube3a*$^{m-/p+}$ mice at postnatal day (P) 80, showed no genotypic difference in the amplitude of either miniature (m)EPSCs or mIPSCs (Wallace et al., 2012). However, decreases in the frequency of both mEPSCs and mIPSCs were observed, with a preferential 50% reduction in spontaneous inhibitory synaptic activity and a 28% decrease in excitatory synaptic activity (Wallace et al., 2012). Interestingly, when mIPSC recordings are performed at an earlier age during the critical period for ocular dominance plasticity, both the amplitude and the frequency of mIPSCs in these P21–P28 mice appear normal. Consistent with inhibitory changes serving a compensatory role, excitatory deficits are observed during the critical period prior to observed changes in inhibition. Furthermore, synaptic deficits may be limited to the excitatory neurons, as neither the amplitude nor the frequency of miniature EPSCs or mIPSCs onto fast-spiking inhibitory interneurons was affected. Analogous to the data of the mIPSC recordings, reductions in L4-evoked inhibitory postsynaptic currents on L2/3 PYR neurons (eIPSCs) were also observed at P80 but not at P25 (Wallace et al., 2012). Despite decreases in both excitatory and inhibitory synaptic activity, spontaneous network activity and baseline firing rates were not altered by the loss of *Ube3a* expression. Likewise, recordings of spontaneous local network activity in L2/3 regular spiking (RS) putative pyramidal neurons of the visual cortex during presentation of a gray screen, showed that neither average spontaneous firing rates nor UP state frequency and duration were significantly different between wild type and mutant mice (Wallace et al., 2017).

Overall, these results show that the loss of *Mecp2*, *Tsc1,* and *Ube3a* in postsynaptic excitatory cortical neurons can induce preferential reductions in inhibition that may have a compensatory role that is aimed at stabilizing synaptic activity, rather than the deficiencies in inhibition directly driving seizures. Thus, these alterations in inhibition alone may not be sufficient to cause seizures. What additional factors might be required? Despite employing Cre-lox approaches to delete *Mecp2* from glutamatergic excitatory neurons in both *Emx1*$^{Cre/+}$;*Mecp2*$^{fx/y}$ and Vglut2$^{Cre/+}$;*Mecp2*$^{fx/y}$ mutants, both mice exhibit different levels of seizure severity. Video-EEG recordings at 10-weeks of age showed that ∼37.5% of Vglut2$^{Cre/+}$;*Mecp2*$^{fx/y}$ mice displayed SWDs at a frequency of 3.3 ± 2.1 episodes/hour and with an episode duration of 4.1 ± 0.4 s (Meng et al., 2016). In contrast 100% of *Emx1*$^{Cre/+}$;*Mecp2*$^{fx/y}$ mutant mice, displayed spike-and-wave discharges at a frequency of 36 ± 7 episodes/hour and episode duration of 1.3 ± 0.1 s (Zhang et al., 2014).

At least two differences may account for the variance in seizure severity. Firstly, in addition to glutamatergic excitatory

neurons, *Emx1*$^{Cre/+}$ deletes *Mecp2* in astrocytes. In fact, cell-specific deletion of *Mecp2* in astrocytes significantly reduces ambient GABA levels in the extracellular space and decreases tonic inhibition through increases in GAT3 GABA transporter expression (Dong et al., 2020).

Therefore, the loss of *Mecp2* in astrocytes could exacerbate reductions in synaptic inhibition beyond the point needed to compensate for the initial decline in synaptic excitation. In support of non-glutamatergic *Mecp2*-deficient cell types contributing to seizure phenotypes in *Mecp2* null mice, restoration of *Mecp2* in Vglut2^{Cre} excitatory neurons only slightly reduces seizure incidence by ∼12.5%.

Secondly, the *Emx1*^{Cre} and the Vglut2^{Cre} drivers recombine in some non-overlapping brain regions at different developmental timepoints and at different recombination efficiencies. For example, unlike *Vglut2*$^{Cre/+}$;*Mecp2* $^{fx/y}$ mice, *Mecp2* is not deleted in the thalamus or cerebellum of *Emx1*$^{Cre/+}$;*Mecp2* $^{fx/y}$ mice. Therefore, it is possible that the loss of *Mecp2* from these additional brain areas in the *Vglut2*$^{Cre/+}$;*Mecp2* $^{fx/y}$ mice contributed to effects that help mitigate circuit hyperexcitability. Alternatively, *Emx1*^{Cre} recombines in cells at early stages of the cortical PYR cell lineage, whereas *Vglut2*^{Cre} recombines in essentially mature PYR neurons. Thus, it is possible that *Mecp2* plays a role in PYR neuron maturation as well as activity. Regardless of the genetic explanations for the differing severities in the *Emx1*^{Cre} and *Vglut2*^{Cre} driven phenotypes, differences in the extent to which PYR excitatory drive or activity is reduced may have contributed to the pointedly increased seizure severity in the *Emx1*$^{Cre/+}$;*Mecp2* $^{fx/y}$ mutant mice. In the next section, we will explore the effects of ASD gene deletion in inhibitory neurons on circuit hyperexcitability and seizure susceptibility.

Contributions of Reductions in Inhibition Due to the Dysfunction of Inhibitory Neurons to Circuit Hyperexcitability and Seizure Susceptibility

Two independent studies showed that seizures or epileptiform activity are not produced in mice where a forebrain-specific GABAergic Cre (i.e., *Dlx5/6-Cre*; Monory et al., 2006) was used to delete *Mecp2* from inhibitory neurons (Chao et al., 2010; Zhang et al., 2014). The *Dlx5* and *Dlx6* promoter is expected to drive Cre expression in GABAergic interneurons (including parvalbumin-positive (PV$^+$), somatostatin-positive (SSt$^+$+), and vasoactive intestinal peptide-positive (VIP$^+$) interneurons) throughout the cerebral cortex, striatum, and hypothalamus (De Lombares et al., 2019). However, additional Cre-lox studies to elucidate the cause of the seizures showed that the loss of *Mecp2* from SSt$^+$ interneurons throughout the brain via SSt$^{Cre/+}$ mice (Taniguchi et al., 2011) resulted in spontaneous seizures but with a substantially delayed onset (Ito-Ishida et al., 2015). Hence, *Mecp2* loss from interneurons that are not located in the forebrain may be needed exclusively, or perhaps required in combination with *Mecp2* loss from forebrain interneurons to drive hyperexcitability or the seizure phenotype. At 15-weeks of age, almost 10% of *SSt*$^{Cre/+}$;*Mecp2*$^{-/y}$ mice developed spontaneous epileptic seizures and by 45-weeks of age 50% percent of these mice developed spontaneous epileptic seizures (Ito-Ishida et al., 2015). Generalized tonic clonic seizures were also observed in *SSt*$^{Cre/+}$;*Mecp2*$^{-/y}$ mice during routine handling (Ito-Ishida et al., 2015). As these seizure phenotypes were not observed upon deletion of *Mecp2* from forebrain SSt$^+$ interneurons alone, these results suggest that SSt$^+$ neurons in the midbrain and/or hindbrain may play a particularly salient role in seizure generation. In contrast, the loss of *Mecp2* from parvalbumin positive (PV$^+$) interneurons, using a Pvalb-2A-Cre driver (Madisen et al., 2010), did not produce seizures (Ito-Ishida et al., 2015). The lack of a phenotype was highly unexpected, especially given that fast-spiking PV$^+$ neurons provide a major source of inhibition that regulates pyramidal cell output (Atallah et al., 2012; Kepecs and Fishell, 2014). More importantly, PV$^+$ neurons, rather than SSt$^+$ neurons, play a dominant role in maintaining the excitatory/inhibitory balance in the cortex (Xue et al., 2014; Ito-Ishida et al., 2015).

More widespread deletion of *Mecp2* from all GABAergic and glycinergic neurons, using the Viaat-Cre mouse line, further outlines a subtler role for the cell autonomous loss of *Mecp2* from interneurons in driving seizures. Interestingly, deletion of *Mecp2* expression using Viaat-Cre produces frequent hyperexcitability discharges but no seizures (Chao et al., 2010). Immunohistochemical and electrophysiological analyses reveal subtle disruptions of GABAergic neuronal function, namely reduced mRNA transcript levels for the genes encoding enzymes involved in the conversion of glutamate to GABA (*Gad1* and *Gad2*), reduced GABA immunoreactivity, and reduced mIPSCs amplitude and charge (Chao et al., 2010). *Mecp2* re-expression in Viaat-Cre expressing neurons in the *Mecp2* null normalized mRNA levels of Gad1 and Gad2 but the reduction in mEPSC amplitude remained (Ure et al., 2016). Furthermore, the incidence of non-seizure hyperexcitability discharges and seizures were dramatically reduced (Ure et al., 2016). Collectively, these data suggest that loss of *Mecp2* from multiple cell types (i.e., glutamatergic neurons, astrocytes, and interneurons) reduce inhibition levels to a range that may drive seizures at early postnatal developmental stages, but restoration of *Mecp2* in inhibitory neurons may be sufficient to elevate inhibition above the seizure induction threshold.

A recent contrasting report is worth discussing. This study, in which the same floxed *Mecp2* allele (Guy et al., 2001) as above was purportedly recombined with Cre lines targeting interneurons, namely *Dlx5/6-Cre* mice (Monory et al., 2006), SSt^{Cre} mice (Taniguchi et al., 2011), *Pvalb*^{Cre} mice (Hippenmeyer et al., 2005) and *Vip*^{Cre} mice (Taniguchi et al., 2011), detected seizure activity in each conditional *Mecp2* mutant line (Mossner et al., 2020). Seizures manifest in 100% of *Mecp2*$^{-/y}$, 100% of *Dlx5/6-Cre;Mecp2* $^{fx/y}$, 52.9% of SSt$^{Cre/+}$;Mecp2$^{-/y}$, 35.0% of PV$^{Cre/+}$;Mecp2$^{-/y}$, and 37.5% of *VIP*$^{Cre/+}$;*Mecp2* $^{fx/y}$ mutants. Seizures were also detected in *Mecp2*$^{fx/y}$ controls. However, as described above, previous studies failed to detect either hyperexcitability discharges or seizures in *Dlx5/6-Cre;Mecp2* $^{fx/y}$ mice even at 39-weeks of age (Ito-Ishida et al., 2015). It should be noted that Dlx5/6-Cre produces maternal germline recombination for several alleles (Luo et al., 2020), providing a possible explanation for

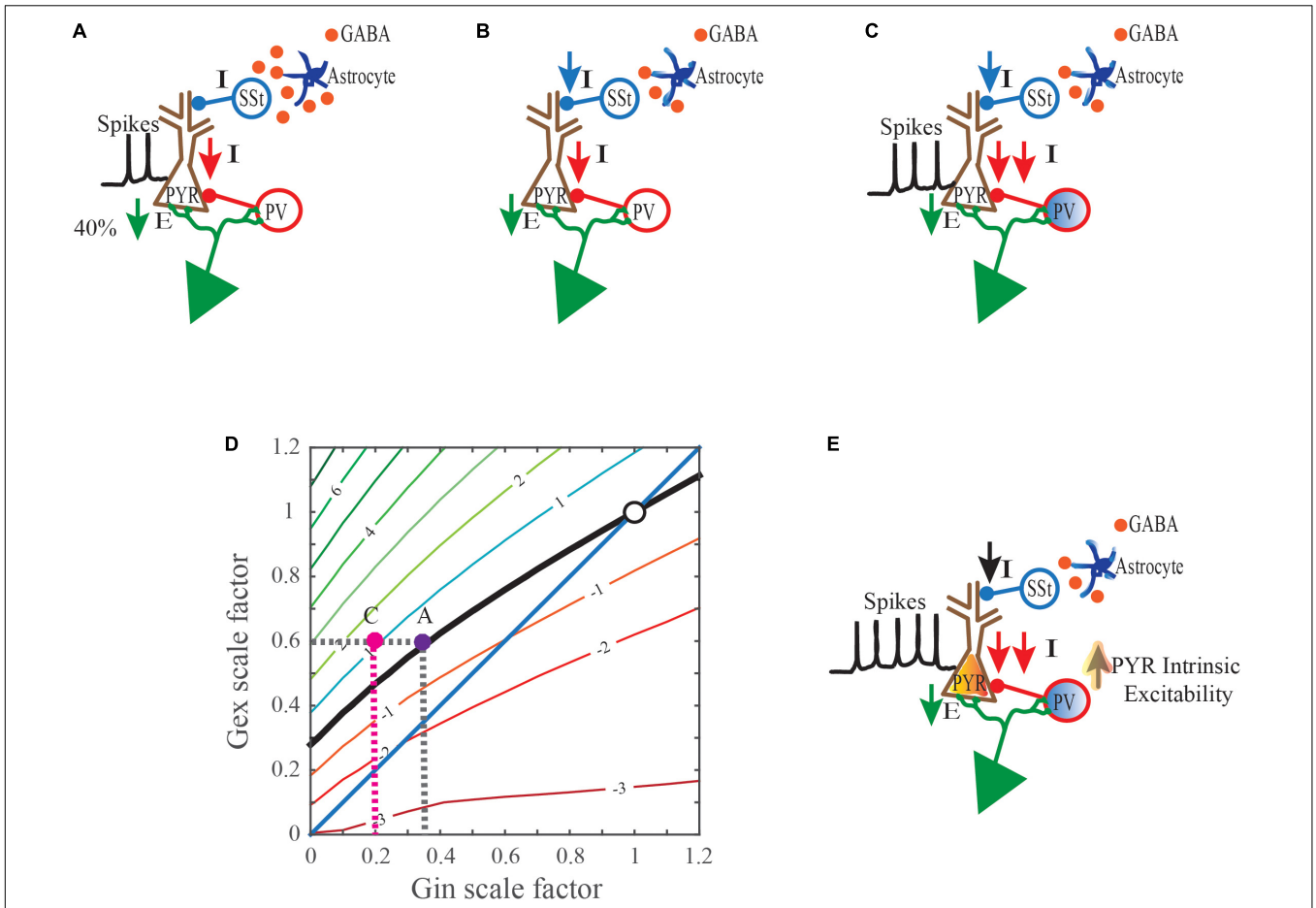

FIGURE 2 | Collective mechanisms that may drive hyperexcitability when synaptic excitation levels are reduced. **(A)** A gene mutation that is linked to a neurodevelopmental disorder (NDD) induces cell autonomous changes in glutamatergic PYR neurons that reduce their excitatory postsynaptic input (E). This primary defect in the PYR neurons triggers cell autonomous decreases in inhibitory postsynaptic inputs (I). **(B)** The same NDD-linked gene mutation also induces cell autonomous changes in astrocytes that may reduce ambient GABA levels in the extracellular space. Reduced GABA levels may consequently lessen inhibitory output in select subsets of interneurons. In this example, somatostatin-positive (SSt^{+}) neuron-mediated inhibition is reduced. **(C)** This NDD-linked gene mutation can also induce cell autonomous changes in parvalbumin-positive (PV+) interneurons which impair their inhibitory output. Moreover, these inefficiencies are perhaps exacerbated during incidences of strong or sustained inputs, as the ability of PV neurons to scale-up their responses is compromised. **(D)** In response to the 40% reduction in excitatory postsynaptic input from **(A)**, even less inhibition is now provided due to the combined effects of cell autonomous changes in astrocytes and PV+ interneurons. i.e. in C (• pink dot) an 80% drop, instead of the expected 65% that would typically occur in **(A)** (• purple dot). The net effect is PSPs that are 1mV larger than normal and increased depolarization levels (• pink dot). **(E)** Events in **(D)** help drive an increase in the intrinsic excitability of PYR neurons.

100% expressivity of seizures in not only the *Mecp2*$^{-/y}$ null, but also the *Dlx5/6-Cre; Mecp2* $^{fx/y}$ mice in Mossner et al. (2020). Contributions from strain background may also play a role in modifying the phenotype. Despite this potential caveat, this study demonstrated that single-unit recordings from putative regular-spiking cortical excitatory PYR neurons in awake mice, have 3 fold-larger firing rates in *Dlx5/6-Cre;Mecp2* $^{fx/y}$, *VIP*$^{Cre/+}$;*Mecp2* $^{fx/y}$ and SSt$^{Cre/+}$; Mecp2$^{-/y}$ mice (Mossner et al., 2020).

Interestingly, studies on the *Ube3a*$^{m-/p+}$ heterozygotes on the C57BL/6J strain background provide evidence that genetic alterations in interneurons that reduce their activity, can alter the intrinsic properties of excitatory PYR neurons to increase their excitability (Wallace et al., 2017). Continuous video EEG recording (24 hours a day for 5 days) for spontaneous seizure activity showed a significant increase in the amplitude and frequency of spontaneous polyspike activity in the somatosensory cortex (146 ± 54.64 events/day in *Ube3a*$^{m-/p+}$ mice compared to 1.04 ± 0.20 events/day in control mice) (Born et al., 2017). However, similar to the Viaat-Cre; *Mecp2* $^{fx/y}$ mice, despite this increase in abnormal epileptiform activity, no spontaneous seizures were recorded in the *Ube3a*$^{m-/p+}$ mice. Equally, seizures induced by exposure to a 140 dB aversive auditory stimulus were not observed and seizures induced via kainic acid administration bore similar latencies in the wildtype and *Ube3a*$^{m-/p+}$ mutants (Born et al., 2017). *In vivo* whole cell recordings of L2/3 PYR neurons to dissect the hyperexcitability phenotype, showed that *Ube3a* mutant mice exhibited mildly increased spiking

activity following current injection compared with control mice. This increase in the intrinsic excitability of L2/3 PYR neurons in the visual cortex was attributed to an increase in membrane resistance as no differences occurred between groups in resting membrane potential. *In vitro* experiments replicated the finding; showing a modest increase in intrinsic excitability of L2/3 PYR neurons in *Ube3a*$^{m-/p+}$ mice compared to wildtype (Wallace et al., 2012).

To address whether the increased intrinsic excitability in L2/3 PYR neurons was cell autonomous or arose as a compensatory result to a reduction in inhibitory synaptic activity, Wallace and colleagues used the Gad2-Cre line (Taniguchi et al., 2011) to conditionally reinstate *Ube3a* expression in all GABAergic neurons of Ube3a$^{STOP/p+}$ mice. This Cre-mediated gene re-expression is facilitated by the removal of a STOP cassette inserted between exons 3 and 4 of *Ube3a* (Silva-Santos et al., 2015). Reinstatement of *Ube3a* restored intrinsic excitability to control levels and thus illustrated that increased intrinsic excitability in PYR neurons can be induced solely from *Ube3a* loss in interneurons.

CONCLUSION

Altogether, the studies discussed here implicate L5 of the visual, somatosensory, and prefrontal cortex as potential loci for further study into the mechanisms mediating seizure activity in ASD, RTT, and AS. Cortical L5 neurons integrate inputs from many sources (including L2/3 cortex) and output to both cortical and subcortical structures to mediate functions such as perception and movement. Future studies are required to further connect physiological abnormalities in L5 PYR neurons and their input and output sources to the generation of absence seizure-like activity (Miyamoto et al., 2019). While it is tempting to explain the cause of seizures solely in terms of deficits in inhibition, as illustrated in **Figure 2**, the overall source of the reduction can be quite complex. Some aspect of the total reduction in inhibition levels may compensate for reductions in either excitatory synaptic input or intrinsic excitability in glutamatergic PYR neurons. If left unchecked, circuits can become hypoactive. Decreases in inhibition that are mediated by cell autonomous effects in interneurons can prove more deleterious as they can enhance losses in inhibition and induce alterations to increase intrinsic excitability in glutamatergic PYR neurons. Other cell types such as astrocytes may also act to reduce inhibition levels. Studies of mice with seizure phenotypes where gene function is restored to one or more cell-types (e.g. interneurons, glia, excitatory PYR neurons) in an otherwise null background could significantly aid in our efforts to identify the most crucial cell-types for targeted therapies. Additional insights into the acute and long-term consequences of gene deficiencies on behavior and brain physiology are also needed to ensure that cell type targeted pharmacologic or genetic therapies do not disrupt compensatory mechanisms and worsen the severity of symptoms.

AUTHOR CONTRIBUTIONS

The author confirms being the sole contributor of this work and has approved it for publication.

FUNDING

This work was supported by the ZIAAA000440 award from the NIAAA/National Institutes of Health, K22NS105922, NINDS/NIH.

REFERENCES

Abs, E., Goorden, S. M. I., Schreiber, J., Overwater, I. E., Hoogeveen-Westerveld, M., Bruinsma, C. F., et al. (2013). TORC1-dependent epilepsy caused by acute biallelicTsc1deletion in adult mice. *Ann. Neurol.* 74, 569–579. doi: 10.1002/ana.23943

Amir, R. E., van den Veyver, I. B., Wan, M., Tran, C. Q., Francke, U., and Zoghbi, H. Y. (1999). Rett syndrome is caused by mutations in X-linked MECP2, encoding methyl-CpG-binding protein 2. *Nat. Genet.* 23, 185–188. doi: 10.1038/13810

Antoine, M. W., Langberg, T., Schnepel, P., and Feldman, D. E. (2019). Increased excitation-inhibition ratio stabilizes synapse and circuit excitability in four autism mouse models. *Neuron* 101, 648–661.e4. doi: 10.1016/j.neuron.2018.12.026

Atallah, B. V., Bruns, W., Carandini, M., and Scanziani, M. (2012). Parvalbumin-expressing interneurons linearly transform cortical responses to visual stimuli. *Neuron* 73, 159–170. doi: 10.1016/j.neuron.2011.12.013

Banerjee, A., Rikhye, R. V., Breton-Provencher, V., Tang, X., Li, C., Li, K., et al. (2016). Jointly reduced inhibition and excitation underlies circuit-wide changes in cortical processing in Rett syndrome. *Proc. Natl. Acad. Sci. U.S.A.* 113, E7287–E7296. doi: 10.1073/pnas.1615330113

Bateup, H. S., Johnson, C. A., Denefrio, C. L., Saulnier, J. L., Kornacker, K., and Sabatini, B. L. (2013). Excitatory/inhibitory synaptic imbalance leads to hippocampal hyperexcitability in mouse models of tuberous sclerosis. *Neuron* 78, 510–522. doi: 10.1016/j.neuron.2013.03.017

Blackman, M. P., Djukic, B., Nelson, S. B., and Turrigiano, G. G. A. (2012). Critical and cell-autonomous role for MeCP2 in synaptic scaling up. *J. Neurosci.* 32, 13529–13536. doi: 10.1523/jneurosci.3077-12.2012

Blumenfeld, H. (2005). Cellular and network mechanisms of spike-wave seizures. *Epilepsia* 46, 21–33. doi: 10.1111/j.1528-1167.2005.00311.x

Born, H. A., Dao, A. T., Levine, A. T., Lee, W. L., Mehta, N. M., Mehra, S., et al. (2017). Strain-dependence of the angelman syndrome phenotypes in Ube3a maternal deficiency mice. *Sci. Rep.* 7:8451. doi: 10.1038/s41598-017-08825-x

Brown, C. O., Uy, J., Murtaza, N., Rosa, E., Alfonso, A., Xing, S., et al. (2021). Disruption of the autism-associated gene SCN2A alters synaptic development and neuronal signaling in patient iPSC-glutamatergic neurons. *bioRxiv* [Preprint] doi: 10.1101/2021.09.14.460368

Catterall, W. A. (2017). Forty years of sodium channels: structure, function, pharmacology, and epilepsy. *Neurochem. Res.* 42, 2495–2504. doi: 10.1007/s11064-017-2314-9

Chao, H. T., Chen, H., Samaco, R. C., Xue, M., Chahrour, M., Yoo, J., et al. (2010). Dysfunction in GABA signalling mediates autism-like stereotypies and Rett syndrome phenotypes. *Nature* 468, 263–269. doi: 10.1038/nature09582

Chao, H.-T., Zoghbi, H. Y., and Rosenmund, C. (2007). MeCP2 controls excitatory synaptic strength by regulating glutamatergic synapse number. *Neuron* 56, 58–65. doi: 10.1016/j.neuron.2007.08.018

Chen, R. Z., Akbarian, S., Tudor, M., and Jaenisch, R. (2001). Deficiency of methyl-CpG binding protein-2 in CNS neurons results in a Rett-like phenotype in mice. *Nat. Genet.* 27, 327–331. doi: 10.1038/85906

Dani, V. S., Chang, Q., Maffei, A., Turrigiano, G. G., Jaenisch, R., and Nelson, S. B. (2005). Reduced cortical activity due to a shift in the balance between excitation and inhibition in a mouse model of Rett syndrome. *Proc. Natl. Acad. Sci. U.S.A.* 102, 12560–12565. doi: 10.1073/pnas.0506071102

De Lombares, C., Heude, E., Alfama, G., Fontaine, A., Hassouna, R., Vernochet, C., et al. (2019). Dlx5 and Dlx6 expression in GABAergic neurons controls behavior, metabolism, healthy aging and lifespan. *Aging* 11, 6638–6656. doi: 10.18632/aging.102141

Depaulis, A., and Charpier, S. (2018). Pathophysiology of absence epilepsy: insights from genetic models. *Neurosci. Lett.* 667, 53–65. doi: 10.1016/j.neulet.2017.02.035

Dong, Q., Kim, J., Nguyen, L., Bu, Q., and Chang, Q. (2020). An astrocytic influence on impaired tonic inhibition in hippocampal CA1 pyramidal neurons in a mouse model of Rett syndrome. *J. Neurosci.* 40, 6250–6261. doi: 10.1523/jneurosci.3042-19.2020

Eaton, M., Zhang, J., Ma, Z., Park, A. C., Lietzke, E., Romero, C. M., et al. (2021). Generation and basic characterization of a gene-trap knockout mouse model of Scn2a with a substantial reduction of voltage-gated sodium channel Nav1.2 expression. *Genes Brain Behav.* 20:e12725. doi: 10.1111/gbb.12725

Gemelli, T., Berton, O., Nelson, E. D., Perrotti, L. I., Jaenisch, R., and Monteggia, L. M. (2006). Postnatal loss of Methyl-CpG binding protein 2 in the forebrain is sufficient to mediate behavioral aspects of Rett syndrome in mice. *Biol. Psychiatry* 59, 468–476. doi: 10.1016/j.biopsych.2005.07.025

Glaze, D. G., Percy, A. K., Skinner, S., Motil, K. J., Neul, J. L., Barrish, J. O., et al. (2010). Epilepsy and the natural history of Rett syndrome. *Neurology* 74, 909–912. doi: 10.1212/wnl.0b013e3181d6b852

Gorski, J. A., Talley, T., Qiu, M., Puelles, L., Rubenstein, J. L. R., and Jones, K. R. (2002). Cortical excitatory neurons and glia, but not GABAergic neurons, are produced in the Emx1-expressing lineage. *J. Neurosci.* 22, 6309–6314. doi: 10.1523/jneurosci.22-15-06309.2002

Gould, E., and Kim, J. H. (2021). SCN2A contributes to oligodendroglia excitability and development in the mammalian brain. *Cell Rep.* 36:109653. doi: 10.1016/j.celrep.2021.109653

Guy, J., Hendrich, B., Holmes, M., Martin, J. E., and Bird, A. (2001). A mouse Mecp2-null mutation causes neurological symptoms that mimic Rett syndrome. *Nat. Genet.* 27, 322–326. doi: 10.1038/85899

He, H., Shen, W., Zheng, L., Guo, X., and Cline, H. T. (2018). Excitatory synaptic dysfunction cell-autonomously decreases inhibitory inputs and disrupts structural and functional plasticity. *Nat. Commun.* 9:2893. doi: 10.1038/s41467-018-05125-4

Hippenmeyer, S., Vrieseling, E., Sigrist, M., Portmann, T., Laengle, C., Ladle, D. R., et al. (2005). A developmental switch in the response of DRG neurons to ETS transcription factor signaling. *PLoS Biol.* 3:e159. doi: 10.1371/journal.pbio.0030159

Hirrlinger, P. G., Scheller, A., Braun, C., Hirrlinger, J., and Kirchhoff, F. (2006). Temporal control of gene recombination in astrocytes by transgenic expression of the tamoxifen-inducible DNA recombinase variant CreERT2. *Glia* 54, 11–20. doi: 10.1002/glia.20342

Horsthemke, B., and Wagstaff, J. (2008). Mechanisms of imprinting of the prader-willi/angelman region. *Am. J. Med. Genet. A* 146A, 2041–2052. doi: 10.1002/ajmg.a.32364

Huibregtse, J. M., Scheffner, M., and Howley, P. M. (1993). Cloning and expression of the cDNA for E6-AP, a protein that mediates the interaction of the human papillomavirus E6 oncoprotein with p53. *Mol. Cell. Biol.* 13, 775–784. doi: 10.1128/mcb.13.2.775

Idro, R., Gwer, S., Kahindi, M., Gatakaa, H., Kazungu, T., Ndiritu, M., et al. (2008). The incidence, aetiology and outcome of acute seizures in children admitted to a rural Kenyan district hospital. *BMC Pediatr.* 8:5. doi: 10.1186/1471-2431-8-5

Ito-Ishida, A., Ure, K., Chen, H., Swann, J. W., and Zoghbi, H. Y. (2015). Loss of MeCP2 in parvalbumin-and somatostatin-expressing neurons in mice leads to distinct Rett syndrome-like phenotypes. *Neuron* 88, 651–658. doi: 10.1016/j.neuron.2015.10.029

Jiang, Y., Armstrong, D., Albrecht, U., Atkins, C. M., Noebels, J. L., Eichele, G., et al. (1998). Mutation of the angelman ubiquitin ligase in mice causes increased cytoplasmic p53 and deficits of contextual learning and long-term potentiation. *Neuron* 21, 799–811. doi: 10.1016/s0896-6273(00)80596-6

Kepecs, A., and Fishell, G. (2014). Interneuron cell types are fit to function. *Nature* 505, 318–326. doi: 10.1038/nature12983

Kishino, T., Lalande, M., and Wagstaff, J. (1997). UBE3A/E6-AP mutations cause Angelman syndrome. *Nat. Genet.* 15, 70–73. doi: 10.1038/ng0197-70

Knopf, A. (2020). Autism prevalence increases from 1 in 60 to 1 in 54: CDC. *Brown Univ. Child Adolesc. Psychopharmacol. Update* 22, 6–7. doi: 10.1002/cpu.30499

Koene, L. M., Niggl, E., Wallaard, I., Proietti-Onori, M., Rotaru, D. C., and Elgersma, Y. (2021). Identifying the temporal electrophysiological and molecular changes that contribute to TSC-associated epileptogenesis. *JCI Insight* 6:e150120. doi: 10.1172/jci.insight.150120

Li, T., Tian, C., Scalmani, P., Frassoni, C., Mantegazza, M., Wang, Y., et al. (2014). Action potential initiation in neocortical inhibitory interneurons. *PLoS Biology* 12:e1001944. doi: 10.1371/journal.pbio.1001944

Lioy, D. T., Garg, S. K., Monaghan, C. E., Raber, J., Foust, K. D., Kaspar, B. K., et al. (2011). A role for glia in the progression of Rett's syndrome. *Nature* 475, 497–500. doi: 10.1038/nature10214

Luo, L., Ambrozkiewicz, M. C., Benseler, F., Chen, C., Dumontier, E., Falkner, S., et al. (2020). Optimizing nervous system-specific gene targeting with cre driver lines: prevalence of germline recombination and influencing factors. *Neuron* 106, 37–65.

Lüttjohann, A., and van Luijtelaar, G. (2015). Dynamics of networks during absence seizure's on- and offset in rodents and man. *Front. Physiol.* 6:16. doi: 10.3389/fphys.2015.00016

Madisen, L., Zwingman, T. A., Sunkin, S. M., Oh, S. W., Zariwala, H. A., Gu, H., et al. (2010). A robust and high-throughput Cre reporting and characterization system for the whole mouse brain. *Nat. Neurosci.* 13, 133–140. doi: 10.1038/nn.2467

Matsuura, T., Sutcliffe, J. S., Fang, P., Galjaard, R.-J., Jiang, Y., Benton, C. S., et al. (1997). De novo truncating mutations in E6-AP ubiquitin-protein ligase gene (UBE3A) in Angelman syndrome. *Nat. Genet.* 15, 74–77. doi: 10.1038/ng0197-74

McCafferty, C., David, F., Venzi, M., Lőrincz, M. L., Delicata, F., Atherton, Z., et al. (2018). Cortical drive and thalamic feed-forward inhibition control thalamic output synchrony during absence seizures. *Nat. Neurosci.* 21, 744–756. doi: 10.1038/s41593-018-0130-4

Meng, X., Wang, W., Lu, H., He, L. J., Chen, W., Chao, E., et al. (2016). Manipulations of MeCP2 in glutamatergic neurons highlight their contributions to Rett and other neurological disorders. *Elife* 5:e14199. doi: 10.7554/eLife.14199

Miyamoto, H., Tatsukawa, T., Shimohata, A., Yamagata, T., Suzuki, T., Amano, K., et al. (2019). Impaired cortico-striatal excitatory transmission triggers epilepsy. *Nat. Commun.* 10:1917. doi: 10.1038/s41467-019-09954-9

Miyazaki, H., Oyama, F., Inoue, R., Aosaki, T., Abe, T., Kiyonari, H., et al. (2014). Singular localization of sodium channel β4 subunit in unmyelinated fibres and its role in the striatum. *Nat. Commun.* 5:5525. doi: 10.1038/ncomms6525

Monory, K., Massa, F., Egertová, M., Eder, M., Blaudzun, H., Westenbroek, R., et al. (2006). The endocannabinoid system controls key epileptogenic circuits in the hippocampus. *Neuron* 51, 455–466. doi: 10.1016/j.neuron.2006.07.006

Mossner, J., Batista-Brito, R., Pant, R., and Cardin, J. (2020). Developmental loss of MeCP2 from VIP interneurons impairs cortical function and behavior. *Elife* 9:e55639. doi: 10.7554/elife.55639

Ogiwara, I., Miyamoto, H., Tatsukawa, T., Yamagata, T., Nakayama, T., Atapour, N., et al. (2018). Nav1.2 haplodeficiency in excitatory neurons causes absence-like seizures in mice. *Commun. Biol.* 1:96. doi: 10.1038/s42003-018-0099-2

Operto, F., Mazza, R., Pastorino, G., Verrotti, A., and Coppola, G. (2019). Epilepsy and genetic in Rett syndrome: a review. *Brain Behav.* 9:e01250.

Panayiotopoulos, C. P. (2001). Treatment of typical absence seizures and related epileptic syndromes. *Paediatr. Drugs* 3, 379–403. doi: 10.2165/00128072-200103050-00006

Pinault, D., and O'Brien, T. J. (2005). Cellular and network mechanisms of genetically-determined absence seizures. *Thalamus Relat. Syst.* 3, 181–203. doi: 10.1017/S1472928807000209

Qiu, Z., Sylwestrak, E. L., Lieberman, D. N., Zhang, Y., Liu, X.-Y., and Ghosh, A. (2012). The Rett syndrome protein MeCP2 regulates synaptic scaling. *J. Neurosci.* 32, 989–994. doi: 10.1523/JNEUROSCI.0175-11.2012

Rubenstein, J. L. R., and Merzenich, M. M. (2003). Model of autism: increased ratio of excitation/inhibition in key neural systems. *Genes Brain Behav.* 2, 255–267. doi: 10.1034/j.1601-183x.2003.00037.x

Sanders, S., Campbell, A., Cottrell, J., Moller, R., Wagner, F., Auldridge, A., et al. (2018). Progress in understanding and treating SCN2A-mediated disorders. *Trends Neurosci.* 41, 442–456. doi: 10.1016/j.tins.2018.03.011

Satterstrom, F. K., Kosmicki, J. A., Wang, J., Breen, M. S., de Rubeis, S., An, J. Y., et al. (2020). Large-scale exome sequencing study implicates both developmental and functional changes in the neurobiology of autism. *Cell* 180, 568–584.e23. doi: 10.1016/j.cell.2019.12.036

Silva-Santos, S., van Woerden, G. M., Bruinsma, C. F., Mientjes, E., Jolfaei, M. A., Distel, B., et al. (2015). Ube3a reinstatement identifies distinct developmental windows in a murine Angelman syndrome model. *J. Clin. Invest.* 125, 2069–2076. doi: 10.1172/jci80554

Spratt, P. W., Ben-Shalom, R., Keeshen, C. M., Burke, K. J., Clarkson, R. L., Sanders, S. J., et al. (2019). The autism-associated gene Scn2a contributes to dendritic excitability and synaptic function in the prefrontal cortex. *Neuron* 103, 673–685.e5. doi: 10.1016/j.neuron.2019.05.037

Spratt, P. W. E., Alexander, R. P. D., Ben-Shalom, R., Sahagun, A., Kyoung, H., Keeshen, C. M., et al. (2021). Paradoxical hyperexcitability from NaV1.2 sodium channel loss in neocortical pyramidal cells. *Cell Rep.* 36:109483. doi: 10.1016/j.celrep.2021.109483

Taniguchi, H., He, M., Wu, P., Kim, S., Paik, R., Sugino, K., et al. (2011). A resource of Cre driver lines for genetic targeting of GABAergic neurons in cerebral cortex. *Neuron* 71, 995–1013. doi: 10.1016/j.neuron.2011.12.010

Terlau, J., Yang, J., Khastkhodaei, Z., Seidenbecher, T., Luhmann, H. J., Pape, H., et al. (2020). Spike-wave discharges in absence epilepsy: segregation of electrographic components reveals distinct pathways of seizure activity. *J. Physiol.* 598, 2397–2414. doi: 10.1113/jp279483

Ure, K., Lu, H., Wang, W., Ito-Ishida, A., Wu, Z., He, L., et al. (2016). Restoration of Mecp2 expression in GABAergic neurons is sufficient to rescue multiple disease features in a mouse model of Rett syndrome. *Elife* 5:e14198. doi: 10.7554/eLife.14198

Vong, L., Ye, C., Yang, Z., Choi, B., Chua, S., and Lowell, B. B. (2011). Leptin action on GABAergic neurons prevents obesity and reduces inhibitory tone to POMC neurons. *Neuron* 71, 142–154. doi: 10.1016/j.neuron.2011.05.028

Wallace, M., van Woerden, G., Elgersma, Y., Smith, S., and Philpot, B. (2017). Ube3a loss increases excitability and blunts orientation tuning in the visual cortex of Angelman syndrome model mice. *J. Neurophysiol.* 118, 634–646. doi: 10.1152/jn.00618.2016

Wallace, M. L., Burette, A. C., Weinberg, R. J., and Philpot, B. D. (2012). Maternal loss of Ube3a produces an excitatory/inhibitory imbalance through neuron type specific synaptic defects. *Neuron* 74, 793–800. doi: 10.1016/j.neuron.2012.07.013

Williams, C. A. (2005). Neurological aspects of the Angelman syndrome. *Brain Dev.* 27, 88–94. doi: 10.1016/j.braindev.2003.09.014

Wither, R. G., Colic, S., Bardakjian, B. L., Snead, O. C., Zhang, L., and Eubanks, J. H. (2018). Electrographic and pharmacological characterization of a progressive epilepsy phenotype in female MeCP2-deficient mice. *Epilepsy Res.* 140, 177–183. doi: 10.1016/j.eplepsyres.2018.01.015

Wolff, M., Johannesen, K. M., Hedrich, U. B. S., Masnada, S., Rubboli, G., Gardella, E., et al. (2017). Genetic and phenotypic heterogeneity suggest therapeutic implications in SCN2A-related disorders. *Brain* 140, 1316–1336. doi: 10.1093/brain/awx054

Wood, L., and Shepherd, G. M. (2010). Synaptic circuit abnormalities of motor-frontal layer 2/3 pyramidal neurons in a mutant mouse model of Rett syndrome. *Neurobiol. Dis.* 38, 281–287. doi: 10.1016/j.nbd.2010.01.018

Xue, M., Atallah, B. V., and Scanziani, M. (2014). Equalizing excitation–inhibition ratios across visual cortical neurons. *Nature* 511, 596–600. doi: 10.1038/nature13321

Yamagata, T., Ogiwara, I., Mazaki, E., Yanagawa, Y., and Yamakawa, K. (2017). Nav1.2 is expressed in caudal ganglionic eminence-derived disinhibitory interneurons: mutually exclusive distributions of Nav1.1 and Nav1.2. *Biochem. Biophys. Res. Commun.* 491, 1070–1076. doi: 10.1016/j.bbrc.2017.08.013

Zhang, J., Chen, X., Eaton, M., Wu, J., Ma, Z., Lai, S., et al. (2021). Severe deficiency of the voltage-gated sodium channel NaV1.2 elevates neuronal excitability in adult mice. *Cell Rep.* 36:109495. doi: 10.1016/j.celrep.2021.109495

Zhang, W., Peterson, M., Beyer, B., Frankel, W. N., and Zhang, Z. (2014). Loss of MeCP2 from forebrain excitatory neurons leads to cortical hyperexcitation and seizures. *J. Neurosci.* 34, 2754–2763. doi: 10.1523/jneurosci.4900-12.2014

Conflict of Interest: The author declares that the research was conducted in the absence of any commercial or financial relationships that could be construed as a potential conflict of interest.

Publisher's Note: All claims expressed in this article are solely those of the authors and do not necessarily represent those of their affiliated organizations, or those of the publisher, the editors and the reviewers. Any product that may be evaluated in this article, or claim that may be made by its manufacturer, is not guaranteed or endorsed by the publisher.

frontiers | Frontiers in Synaptic Neuroscience

ORIGINAL RESEARCH
published: 24 May 2022
doi: 10.3389/fnsyn.2022.826601

Dentate Granule Cells Are Hyperexcitable in the TgF344-AD Rat Model of Alzheimer's Disease

*Lindsey A. Smith†, Anthoni M. Goodman† and Lori L. McMahon**

Cell, Developmental, and Integrative Biology, University of Alabama at Birmingham, Birmingham, AL, United States

The dentate gyrus is both a critical gatekeeper for hippocampal signal processing and one of the first brain regions to become dysfunctional in Alzheimer's disease (AD). Accordingly, the appropriate balance of excitation and inhibition through the dentate is a compelling target for mechanistic investigation and therapeutic intervention in early AD. Previously, we reported an increased long-term potentiation (LTP) magnitude at medial perforant path-dentate granule cell (MPP-DGC) synapses in slices from both male and acutely ovariectomized female TgF344-AD rats compared with wild type (Wt) as early as 6 months of age that is accompanied by an increase in steady-state postsynaptic depolarization during the high-frequency stimulation used to induce plasticity. Subsequently, we found that heightened function of β-adrenergic receptors (β-ARs) drives the increase in the LTP magnitude, but the increase in steady-state depolarization was only partially due to β-AR activation. As we previously reported no detectable difference in spine density or presynaptic release probability, we entertained the possibility that DGCs themselves might have modified passive or active membrane properties, which may contribute to the significant increase in charge transfer during high-frequency stimulation. Using brain slice electrophysiology from 6-month-old female rats acutely ovariectomized to eliminate variability due to fluctuating plasma estradiol, we found significant changes in passive membrane properties and active membrane properties leading to increased DGC excitability in TgF344-AD rats. Specifically, TgF344-AD DGCs have an increased input resistance and decreased rheobase, decreased sag, and increased action potential (AP) spike accommodation. Importantly, we found that for the same amount of depolarizing current injection, DGCs from TgF344-AD compared with Wt rats have a larger magnitude voltage response, which was accompanied by a decreased delay to fire the first action potential, indicating TgF344-AD DGCs membranes are more excitable. Taken together, DGCs in TgF344-AD rats are more excitable, which likely contributes to the heightened depolarization during high-frequency synaptic activation.

Keywords: dentate granule cell, hyperexcitability, TgF344-AD rat, Alzheimer's disease, dentate

OPEN ACCESS

Edited by:
Michael Telias,
University of Rochester, United States

Reviewed by:
J. Josh Lawrence,
Texas Tech University Health Sciences Center, United States
Paul S. Garcia,
Columbia University, United States

***Correspondence:**
Lori L. McMahon
mcmahonl@musc.edu

†These authors have contributed equally to this work

Received: *01 December 2021*
Accepted: *05 April 2022*
Published: *24 May 2022*

Citation:
Smith LA, Goodman AM and McMahon LL (2022) Dentate Granule Cells Are Hyperexcitable in the TgF344-AD Rat Model of Alzheimer's Disease.
Front. Synaptic Neurosci. 14:826601.
doi: 10.3389/fnsyn.2022.826601

INTRODUCTION

Increased neuronal activity is directly linked to the production, secretion, and regional deposition of Aβ (Wei et al., 2010; Yamamoto et al., 2015) and tau (Wu et al., 2016; Vogel et al., 2020). While the locus coeruleus (LC) is now known to be the first site of pathological tau accumulation (Braak et al., 2011), cortical regions associated with high metabolic activity, such as the default mode network, including the entorhinal cortex and hippocampus, are early targets of network abnormalities in Alzheimer's disease (AD) (Reiman et al., 2012; Vogel et al., 2020). Functional imaging studies reveal hyperactivity in the hippocampus during mild cognitive impairment (Dickerson et al., 2004) and even in preclinical AD (Quiroz et al., 2010; Reiman et al., 2012). While decreased synaptic inhibition is commonly observed in AD mouse models (Rocher et al., 2008; Verret et al., 2012; Hazra et al., 2013), compensatory remodeling of inhibitory circuits is thought to result from early aberrant excitation (Palop and Mucke, 2016). In support, APP23×PS45 mice have increased activity of hippocampal CA1 pyramidal neurons prior to plaque formation (Busche and Konnerth, 2016). Additionally, increased intrinsic excitability from mature dentate granule cells (DGCs) is reported in Tg2576 AD mice (Hazra et al., 2013; Nenov et al., 2015).

We previously reported increased postsynaptic depolarization during long-term potentiation (LTP)-inducing high frequency stimulation and enhanced LTP magnitude at medial performant path synapses onto dentate gyrus granule cells (MPP-DGCs) in 6-month-old TgF344-AD rats (Smith and McMahon, 2018; Goodman et al., 2021), a rodent model that more fully recapitulates AD-like pathology in an age-dependent manner (Cohen et al., 2013; Do Carmo and Cuello, 2013; Tsai et al., 2014; Joo et al., 2017; Rorabaugh et al., 2017; Bazzigaluppi et al., 2018; Muñoz-Moreno et al., 2018; Pentkowski et al., 2018; Smith and McMahon, 2018; Voorhees et al., 2018). Specifically, the spatiotemporal spread of synaptic dysfunction in the hippocampus begins in the dentate gyrus (DG) prior to area CA1 in both male and female TgF344-AD rats. At 6 months of age, amyloid plaques are first detected in the hippocampus, and tau tangles are absent, but gliosis is significant (Cohen et al., 2013). In addition, we recently reported a significant loss of noradrenergic (NA) fibers in the hippocampus beginning at 6 months (Goodman et al., 2021) when accumulation of hyperphosphorylated tau (pTau) is present in the LC (Rorabaugh et al., 2017), the origin of hippocampal NA innervation (Loy and Moore, 1979). Furthermore, concurrent with the degeneration of the hippocampal NA input, we observed heightened function of β-adrenergic receptors (β-ARs) at MPP-DGC synapses that were responsible for the enhanced LTP magnitude at 6 months in TgF344-AD rats (Goodman et al., 2021). Importantly, while the β-AR antagonist propranolol prevented the heightened LTP magnitude in TgF344-AD rats, it did not completely abolish the increase in steady-state depolarization during the high-frequency stimulation used to induce LTP (Goodman et al., 2021), suggesting that another mechanism is contributing to the increased postsynaptic depolarization.

Since our previous work detected no differences in spine density or presynaptic release probability (Smith and McMahon, 2018), we considered that heightened intrinsic excitability of DGCs could contribute to the increase in steady-state depolarization at MPP-DGC synapses in TgF344-AD rats during high-frequency stimulation (Smith and McMahon, 2018; Goodman et al., 2021). Thus, we measured passive and active membrane properties using whole-cell current clamp recordings in acute hippocampal slices from female rats to determine if DGCs are hyperexcitable in TgF344-AD rats compared with those of wild type (Wt). While increased excitability in the dentate has been reported in transgenic mice with the same human transgenes (Hazra et al., 2013; Nenov et al., 2015), it is not known whether this functional change also occurs in DGCs in the novel TgF344-AD rat model that more faithfully recapitulates human AD (Cohen et al., 2013; Rorabaugh et al., 2017). Demonstrating that dentate hyperexcitability is a common feature in early disease pathogenesis in both mouse and rat transgenic AD models strengthens the concept that hyperexcitability could be a biomarker for progressing pathology. In this study, we reported decreased rheobase, increased voltage response, increased probability of firing an action potential (AP), decreased sag voltage, and greater spike accommodation in 6-month DGCs in TgF344-AD rats compared with those of Wt. Together, these data show that TgF344-AD DGCs are hyperexcitable, and this gain of function may contribute to the enhanced depolarization during tetanus used to induce LTP we observed at 6 months of age (Smith and McMahon, 2018; Goodman et al., 2021).

METHODS

Animals

All breeding and experimental procedures were approved by the University of Alabama at Birmingham Institutional Animal Care and Use Committee and follow the guidelines outlined by the National Institutes of Health. TgF344-AD males harboring the amyloid precursor protein Swedish (APP_{swe}) and delta exon 9 mutant human presenilin-1 ($PS1_{\Delta E9}$) transgenes were bred to Wt F344 females (Envigo, Indianapolis, IN), as carried out previously in our lab (Smith and McMahon, 2018). Rats were maintained under standard laboratory conditions (12 h light/dark cycle, lights off at 14:00 h, 22°C, 50% humidity, food (Harlan 2916; Teklad Diets, Madison, WI) and water *ad libitum*). Animals were housed using standard rat cages [7 in. (height) × 144 in^2 (floor)]. Female TgF344-AD and Wt littermates were aged to 6–8 months for these experiments. Transgene incorporation was verified by polymerase chain reaction (PCR) as described previously (Smith and McMahon, 2018).

Surgery

Fluctuations in ovarian hormones, particularly 17 estradiol, during the estrus cycle elicit significant effects on hippocampal dendritic spine density, N-methyl-D-aspartate receptor (NMDAR)/α-amino-3-hydroxy-5-methyl-4-isoxazolepropionic acid receptor (AMPAR) ratio, synaptic plasticity, and learning

and memory (Woolley and McEwen, 1993; Woolley, 1998; Smith and McMahon, 2005, 2006; Hajszan et al., 2007; Smith et al., 2010; Vedder et al., 2013). Therefore, to eliminate this variable that could confound results, all rats underwent ovariectomy. Briefly, TgF344-AD and Wt littermate female rats were bilaterally ovariectomized (OVX) under 2.5% isoflurane in 100% oxygen, using aseptic conditions. A 10–14 day minimum postoperative interval was used prior to the experimentation, which allows for the depletion of endogenous ovarian hormones as previously published (Smith and McMahon, 2005, 2006; Smith et al., 2010). Importantly, the LTP magnitude at CA3–CA1 synapses in OVX rats 10–14 days post OVX is not different from ovary intact cycling rats at diestrus (when plasma E2 is lowest in ovary intact cycling rats) (Smith et al., 2009). This confirms that 10–14 days of E2 deprivation and the OVX surgery do not negatively affect synaptic function.

Hippocampal Slice Preparation

Animals were deeply anesthetized *via* inhalation anesthesia using isoflurane, rapidly decapitated, and brains removed. Coronal slices (400 μm) from the dorsal hippocampus were prepared using a Leica VT 1000A vibratome (Leica Microsystems Inc, Buffalo Grove, IL). To preserve neuronal health and limit excitotoxicity, slices were sectioned in low Na^+ and sucrose-substituted ice-cold artificial cerebrospinal fluid (aCSF) containing [in mM: NaCl 85; KCl 2.5; $MgSO_4$ 4; $CaCl_2$ 0.5; NaH_2PO_4 1.25; $NaHCO_3$ 25; glucose 25; sucrose 75 (saturated with 95% O_2, 5%CO_2, pH 7.4)]. Slices were held at room temperature for 1 h in (4-(2-hydroxyethyl)-1-piperazineethanesulfonic acid) (HEPES)-buffered artificial cerebrospinal fluid (aCSF) [in mM: 92.0 NaCl, 2.5 KCl, 2.0 $MgSO_4$, 2.0 $CaCl_2$, 1.25 NaH_2PO_4, 30 $NaHCO_3$, 25 glucose, 5 L-ascorbic acid (saturated with 95% O_2, 5%CO_2, pH 7.4)] before transfer to the submersion chamber for recordings. HEPES-modified storing ringer was used to reduce cell swelling and slice damage and robustly improves slice health for path clamp recordings in aged animals (Ting et al., 2014). Following the 1 h recovery, slices were transferred to a submersion chamber and continuously perfused (∼2–3 ml/min) with standard artificial cerebrospinal fluid (aCSF) [in mM: 119.0 NaCl, 2.5 KCl, 1.3 $MgSO_4$, 2.5 $CaCl_2$, 1.0 NaH_2PO_4, 26.0 $NaHCO_3$, 11.0 Glucose (saturated with 95% O_2, 5%CO_2, pH 7.4)] held at 26–28°C.

Whole-Cell Current Clamp

Whole-cell patch clamp recordings were performed from DGCs in the ectal limb (i.e., upper blade). Somas of DGCs were blind patched using borosilicate glass pipettes (3–6 MΩ) filled with intracellular solution containing (in mM) 120 K-gluconate, 0.6 (ethylene glycol-bis(β-aminoethyl ether)-N,N,N′,N′-tetraacetic acid) (EGTA), 5.0 $MgCl_2$, 2.0 ATP, 0.3 GTP, 20.0 HEPES, 270–280 mOsm, pH 7.2 adjusted with KOH. To assess intrinsic excitability, somatic current injections were performed in the presence of glutamatergic antagonists, (2R)-amino-5-phosphonovaleric acid (APV, 100 μM), Ro 25-6981 [0.5 μM], and 6,7-dinitroquinoxaline-2,3-dione (DNQX, 10 μM), and the GABAergic antagonist Picrotoxin (100 μM), to block synaptic transmission. Nifedipine [10 μM] was also used to block $Ca_{V1.1-4}$, which contributes to heightened β-AR function in TgF344-AD rats (Goodman et al., 2021). After achieving the whole-cell configuration, cells were voltage clamped at −70 mV for 3–5 min, and the amplifier was then switched to the current clamp. Hyperpolarizing and depolarizing square wave current injections, 800 ms duration at 100 pA increments, were elicited serially from −400 to +900 pA, repeated 3 times, with a 3–5 min rest period between each current injection round and trials averaged within a single cell. Series resistance was monitored at the beginning and the end of each trial, and cells were excluded if there was a ≥20% change. The resting membrane potential (RMP) was obtained at the initial starting potential in the 100 ms prior to the start of the current injection. To avoid contamination by hyperpolarization-activated cation currents (I_h or "sag"), which were evident in the first 3 hyperpolarizing current steps (−400 pA, −300 pA, and −200 pA), input resistance (R_I) was measured at the −100 pA hyperpolarizing current step. Rheobase was measured as the minimum current required to evoke one or more APs during an 800 ms depolarizing current step from RMP; voltage "sag" potential was measured as the difference between the maximum negative peak at −400 pA and when the voltage reaches steady state (i.e., final 160 ms). Membrane time constant, (time for mV to reach 67% of steady state) was calculated at hyperpolarizing steps. The AP number was calculated at each depolarizing current step, and the AP threshold was measured from the first AP fired. AP accommodation was calculated as the instantaneous frequency at each spike interval. AP waveform properties including AP amplitude, half-width, after hyperpolarization (AHP), and rise and decay times were measured. The AP amplitude and AHP were measured relative to the threshold, and half-width was measured at 50% max amplitude. Instantaneous frequency of firing was measured as the frequency between two consecutive spikes and was plotted against spike interval number. This allows for the measurement of burst like firing as well as accommodation. AP interval number was highly variable among cells making interpretation of accommodation at later spike interval numbers difficult. Therefore, to reduce this variability and to ensure similar health of recorded neurons included in the dataset, only cells that spiked more than 5 times at +100 pA were included in the dataset. Delay to the first AP was measured as the time it took from the start of current injection to the peak amplitude of the first AP. Signals were collected using an Axopatch 200B amplifier (Molecular Devices, Sunnyvale, CA). Recordings were low-pass-filtered at 5 kHz, gain 5×, and sampled at 10 kHz using a Digidata 1440A (Molecular Devices, LLC, San Jose, CA) and stored on a computer equipped with pClamp10 (Molecular Devices, LLC, Sunnyvale, CA).

Data Analysis

All data were acquired using the electrophysiology data acquisition software pClamp10 (Molecular Devices, LLC, Sunnyvale, CA.) and analyzed using Origin 2016 (OriginLab), Graphpad Prism 7 (GraphPad Software, Inc.), and SPSS 22 (IBM Corp.). *N* (number) is reported as the number of cells recorded from at least 5 animals per genotype with several data sets from 7 rats per genotype (see figure legends). The experimenter was blind to genotype during the experimental procedure and data

collection, with genotype only revealed at the final analysis. Results reported at mean ± SEM with significance set at $p < 0.05$ (*) determined by unpaired Student's *t*-test assuming (with Welch's correction for unequal variance) or Mann–Whitney *U*-test for non-parametric data. Outliers were determined with a Grubb's test (GraphPad Software, Inc.), and significant outliers were removed.

RESULTS

Excitability Is Increased in Dentate Granule Cells From TgF344-AD Rats

Increased DGC excitability has been reported in other transgenic rodent models of AD (Hazra et al., 2013; Nenov et al., 2015; Kim et al., 2021). We recently reported increased steady-state postsynaptic depolarization of DGCs during high-frequency stimulation and heightened LTP magnitude at MPP-DGC synapses in 6-month-old TgF344-AD rats (Smith and McMahon, 2018; Goodman et al., 2021). The increased steady-state depolarization is partially driven by heightened activity of β-ARs at MPP-DGC synapses, as a β-AR antagonist does not completely eliminate the increased depolarization (Goodman et al., 2021). Therefore, we sought to determine if heightened intrinsic excitability could also be occurring and tested this using whole-cell current clamp recordings of DGC neurons. Intrinsic excitability was isolated from synaptic transmission using the AMPAR antagonist DNQX (10 μM), NMDAR antagonist d,l-APV (100 μM), and the GABAergic antagonist picrotoxin (100 μM). Voltage-gated calcium channels $Ca_{V1.1-4}$ were blocked with nifedipine (10 μM) to eliminate any contribution from the heightened β-AR function in TgF344-AD rats (Goodman et al., 2021) (**Figure 1A**). Incremental hyperpolarizing and depolarizing current steps of 100 pA, 800 ms in duration, were used to assess passive and active membrane properties (for experimental protocol, refer to **Figure 1B**). RMP was measured immediately after obtaining the whole-cell configuration in the absence of a current injection (I = 0). Although the average RMP recorded from DGCs in TgF344-AD rats was not significantly different from that measured in Wt littermates [**Figure 1C**; $t_{(28.73)} = 1.69$, $p = 0.10$], Wt DGCs were over 4-fold more likely to rest below −80 mV than their TgF344-AD counterparts (Wt: 7/22 [31.81%] vs. Tg: 1/13 [0.077%]). R_I was calculated from the steady-state hyperpolarization generated at −100 pA (in which sag current is undetectable). Input resistance in TgF344-AD DGCs was significantly higher than that measured in Wt littermates [**Figure 1D**; Tg (*Mdn* = 168.1), Wt (*Mdn* = 133.8), $U = 69.0$, $p = 0.011$]. Together, these data demonstrate modified passive membrane properties in DGCs from TgF344-AD rats.

DGCs Fire at Lower Depolarizing Current Injections in TgF344 Rats

Fast voltage-gated and slow persistent Na^+ currents dictate active membrane properties, and alterations in both types of Na^+ currents have been implicated in AD (Verret et al., 2012; Corbett et al., 2013). To determine if active membrane properties are modified in TgF344-AD rats, we measured AP threshold, rheobase, AP number, and their rise and decay times. Incremental 100 pA depolarizing current steps reliably elicited APs in DGCs from both TgF344-AD rats and Wt littermates (**Figure 1**). We did not detect a difference in AP threshold between genotypes when measured from baseline [**Figure 1F**; $t_{(33)} = 1.11$, $p = 0.27$] nor when AP threshold was normalized to the cell's RMP [$t_{(33)} = 0.65$, $p = 0.52$] (**Figure 1G**). Interestingly, the rheobase, or the minimum depolarizing current needed to generate an AP, was significantly lower in TgF344-AD rats compared with that in Wt DGCs [**Figure 1E**; $t_{(32.27)} = 2.542$, $p = 0.016$]. This reduced depolarizing current to generate an AP in TgF344-AD rat DGCs is congruent with the increased input resistance in TgF344-AD DGCs (**Figure 1D**). A decrease in rheobase could lead to an increase in AP number, which was evaluated next at each of the depolarizing current steps. While there was no difference in AP number at current step values higher than 200 pA, TgF344-AD rat DGCs fired more APs at 100 pA [**Figure 1H**; $t_{(25)} = 2.26$, $p = 0.033$]. The greater number of APs at this low current step suggests an enhanced sensitivity to fire following weak stimulation.

To further investigate initial firing properties, we reasoned that in addition to firing more APs at the minimal depolarizing step as mentioned above, they should also fire more reliably at this minimal depolarizing current injection than Wt DGCs. Indeed, we found that at a depolarizing current injection of +100 pA, the probability of successful AP generation is greater in DGCs from TgF344-AD compared with that in Wt rats, with "0" denoting failure to fire at least one AP and "1" indicating successful AP generation (**Figures 2A,B**), although no significant difference in the rise time (τ) of the membrane potential resulting from the 100 pA current injection [$t_{(35)} = 0.017$, $p = 0.986$] was detected. In fact, we found that DGCs in TgF344-AD rats were almost 2-fold more likely to fire an AP than DGCs from Wt rats at the smallest depolarizing current injection (**Figure 2C**). Consistent with this observation, the voltage response during the first depolarizing current step (+100 pA) in TgF344-AD DGCs is significantly increased [**Figure 2D**; $t_{(31.27)} = 3.146$, $p = 0.004$], and the delay to fire the first AP was significantly reduced [**Figures 2E,F**; Tg (*Mdn* = 0.15), Wt (*Mdn* = 0.23), $U = 9.0$, $p = 0.016$]. Together, these data show that for the same amount of excitable input, TgF344-AD DGCs fire more consistently and experience a greater steady-state membrane depolarization compared to Wt. This finding is consistent with our previous observations of greater steady-state depolarization as early as 6 months in extracellular dendritic field potential recordings in TgF344-AD dentate following a high-frequency depolarization used to induce LTP (Smith and McMahon, 2018; Goodman et al., 2021).

Action Potential Kinetics Do Not Account for Increased Excitability in TgF344-AD DGCs

To assess whether changes in rheobase and the increased depolarizing voltage response (**Figures 1E**, **2D**) impact the AP kinetics, we quantified several properties of the AP waveform

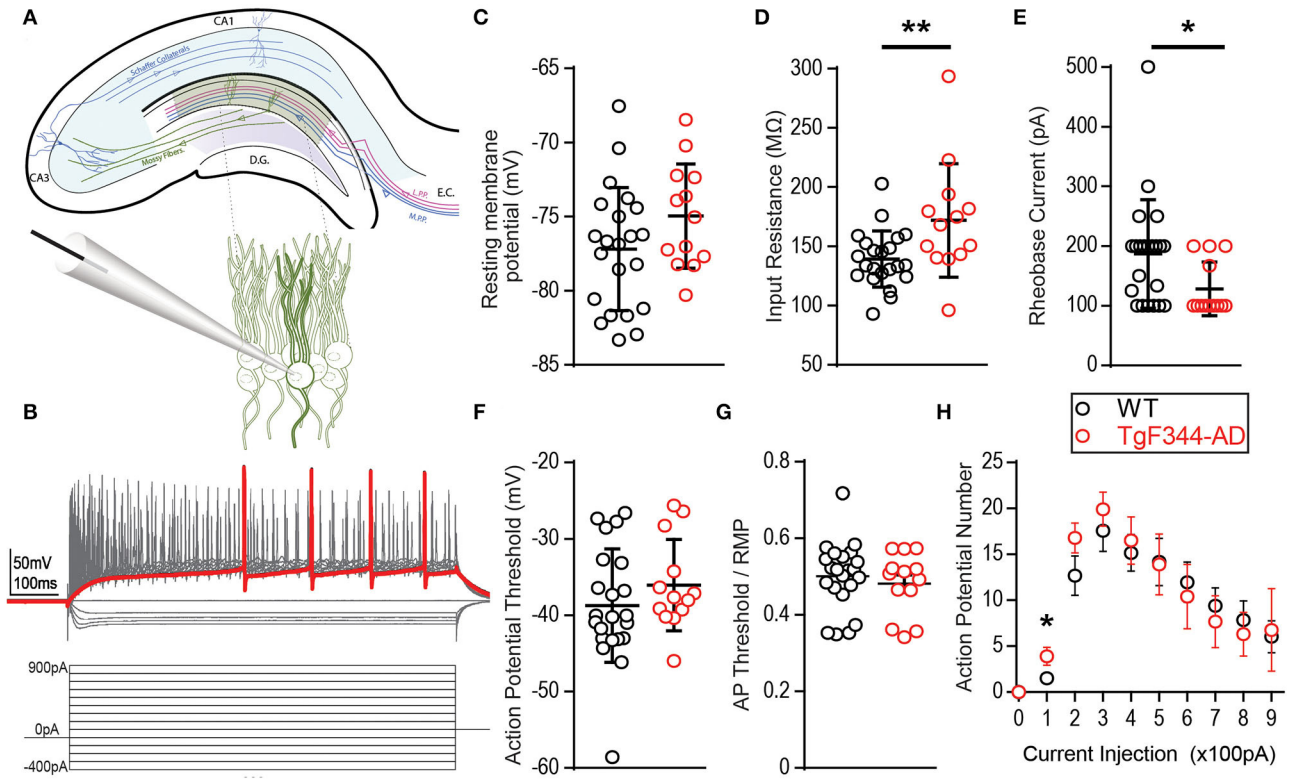

FIGURE 1 | Membrane properties are altered in TgF344-AD dentate granule cells (DGCs). **(A)** Schematic of the trisynaptic circuit in a coronal slice from rat hippocampus (top) with expanded recording setup (bottom). **(B)** Illustration of the experimental protocol: 14 serial 100 pA hyperpolarizing to depolarizing current steps at 800 ms duration from −400 pA to +900 pA. The red trace represents the first depolarizing current step to fire and action potential. **(C)** Mean resting membrane potential is not different between wild type (Wt) (black, 22 cells/8 animals) and TgF344-AD female rats (red, 13 cells/6 animals; $p > 0.05$, but a higher fraction in Wt has values below −80 mV). **(D)** Input resistance is significantly decreased in TgF344-AD DGCs (Wt $n = 22$ cells/8 animals; Tg, $n = 13$ cells/6 animals; $^{**}p \leq 0.01$). Data represent mean ± SEM. Significance is determined using the unpaired *t*-test. **(E)** The first depolarizing current step to elicit and action potential, Rheobase (pA), is significantly decreased in TgF344 compared with Wt ($^{*}p < 0.05$). **(F)** Action potential threshold is not different between genotypes ($p > 0.05$). **(G)** When AP threshold is normalized to RMP, there remains no difference between genotype ($p > 0.05$). **(H)** AP number was enhanced for TgF344-AD rat DGCs at 100 pA current injection ($p < 0.05$) but not at higher current injections. For all panels, Wt, $n = 22$ cells/8 animals; Tg, $n = 13$ cells/6 animals). Data represent mean ± SEM. Significance is determined using the unpaired Student's *t*-test.

to include amplitude, rise and decay times, half-width, and the amplitude of AHP (**Figure 3A**). We chose to quantify kinetics of the first AP fired at rheobase, to prevent modification of AP waveform due to inactivation of Na^+ and K^+ channels, as well as activation of currents at hyperpolarized potentials. The first AP waveform was averaged from all cells recorded in each group (Wt = black, Tg = red) (**Figure 3B**). AP amplitude $t_{(16.52)} = 0.915$, $p = 0.374$ (**Figure 3C**), half-width $t_{(17.31)} = 1.123$, $p = 0.277$ (**Figure 3D**), and AHP amplitude $t_{(22.80)} = 0.615$, $p = 0.272$ (**Figure 3E**) were not significantly different between genotypes. AP rise time and decay were also not different [rise: ($t_{(28)} = 0.704$, $p = 0.487$; decay $t_{(25)} = 0.220$, $p = 0.828$]. Together, these data suggest that voltage-gated Na^+ and K^+ channels that mediate membrane depolarization and repolarization are not functionally altered at this early pathological stage in TgF344-AD rats.

Sag-Mediated Current Is Decreased in TgF344-AD DGCs

Hyperpolarization activates hyperpolarization-activated-cyclic-nucleotide gated currents, I_h (HCN channels), which mediate excitability and rhythmic firing in neurons. DGCs typically contain less I_h current, although patients with severe epilepsy have increased HCN channel expression confined to the dentate (Poolos et al., 2002; Bender et al., 2005; Poolos and Johnston, 2012), likely a compensatory mechanism in response to overexcitation since HCN channels typically decrease excitability. To determine if decreased HCN channel function could explain the increased excitability observed at this early stage, we additionally measured the "sag," a voltage signature of HCN channels (**Figure 4A**). At −400 pA, DGCs in TgF344-AD rats did not show a significant decrease in sag amplitude [**Figure 4B**; $t_{(21.43)} = 1.181$, $p = 0.25$], but we noted an enhanced voltage response in DGCs from TgF344-AD rats at the −400 pA current injection used to measure sag [**Figure 4C**; $t_{(18.44)} = 2.27$, $p = 0.04$], which is consistent with the observation that R_I is increased in TgF344-AD rats. We detected no change in the membrane time constant in response to hyperpolarizing pulses [(−400 pA) $t_{(34)} = 0.445$, $p = 0.659$; (−300 pA) $t_{(34)} = 0.966$, $p = 0.341$; (−200 pA) $t_{(34)} = 1.191\ 48$, $p = 0.242$; (−100 pA) $t_{(34)} = 0.0998$, $p = 0.424$]. To compensate for the enhanced R_I, sag amplitude

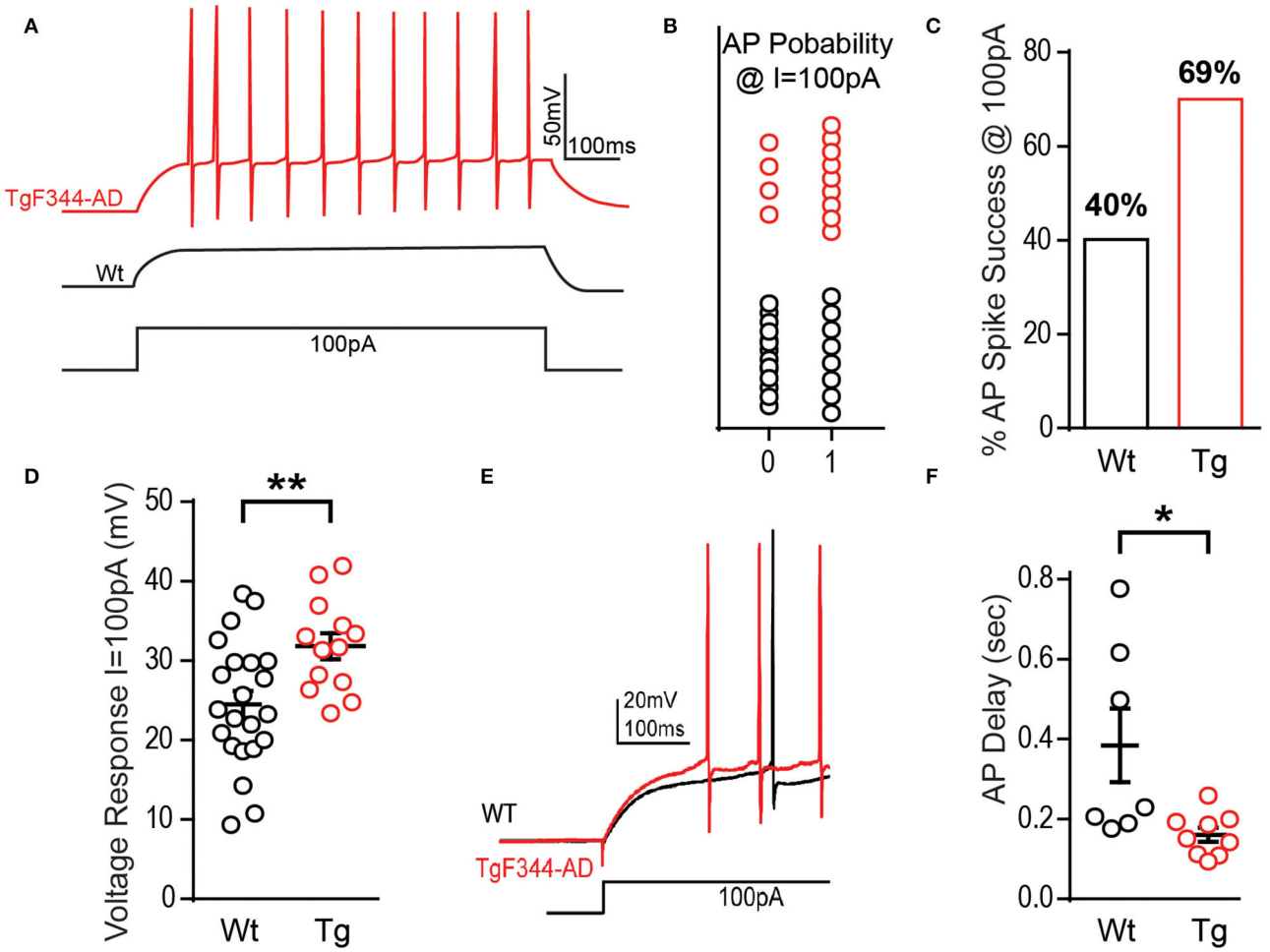

FIGURE 2 | TgF344-AD rats have a lower excitation threshold and fire sooner. **(A)** Example traces from a DGC recorded from a TgF344-AD and Wt littermate to illustrate that +100 pA depolarizing step can elicit action potentials more readily in TgF344-AD rats vs. Wt DGCs. **(B)** The probability of firing an action potential at +100 pA (0 = did not fire an AP, 1 = fired at least one AP) is greater in TgF344-AD DGCs (Wt 9/22 cells fired, Tg 9/13 cells fired). **(C)** DGCs from Wt rats discharged at +100 pA 40.9% of the time compared with a 69.2% success rate observed in TgF344-AD rats. **(D)** Regardless of whether the cell discharged or not, TgF344-AD DGC membranes have a greater voltage change (mV) compared with Wt during the first at +100 pA (Wt, $n = 22$ cells/8 animals; Tg, $n = 13$ cells/6 animals; $^{**}p < 0.01$). **(E)** Representative traces of the delay to fire the first action potential (Wt = black, Tg = red). **(F)** TgF344-AD DGCs had a decreased delay to fire during the first depolarizing current step at +100 pA (Wt $n = 7$ cells/5 animals, Tg $n = 9$ cells/6 animals; $^{*}p < 0.05$). Data represent mean ± SEM. Significance is determined using the unpaired Student's *t*-test.

was normalized to the hyperpolarized voltage response, which resulted in a significant decrease in the sag amplitude in DGCs from TgF344-AD rats [**Figure 4D**; $t_{(29.94)} = 2.09$, $p = 0.045$]. When taken together, the reduced sag/voltage response may indicate that I_h current mediated by HCN channels is impaired in DGCs of TgF344-AD rats.

TgF344-AD DGCs Have Increased Initial Spike Frequency and Greater Accommodation

During prolonged depolarization, neurons undergo spike frequency accommodation, where a reduction in the AP frequency occurs over time (Madison and Nicoll, 1984) and is mediated by gradual activation and recruitment of K^+ channel currents. Enhanced excitability of DGCs in TgF344-AD rats may be a result of increased input resistance and reduced rheobase, yet there is no increase in the AP number above 100 pA current injection suggesting that accommodation may clamp AP number at higher currents. At the first depolarizing step, +100 pA (**Figure 5A**), differences in instantaneous firing frequency are not interpretable since overall spike number is low and several cells fail to spike. To address this, we assessed accommodation at +200 pA (**Figure 5B**) when 92% of cells fire an AP as revealed in Brown et al. (2011). We found that DGCs in TgF344-AD rats begin with a mean instantaneous firing frequency of 76.15 ± 6.33 Hz and accommodate to 20.52 ± 2.07 Hz by 17 spike intervals (**Figure 5B**, red). In contrast, Wt

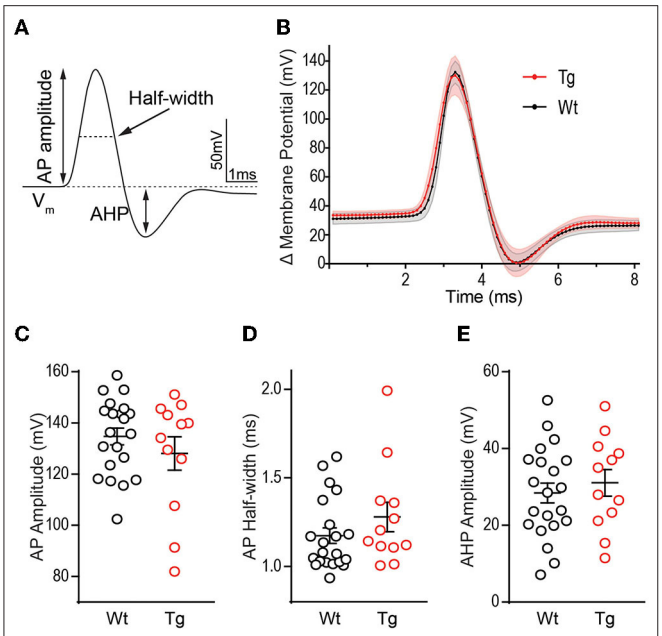

FIGURE 3 | Action potential waveform properties are not different between TgF344-AD and wild-type (Wt) DGCs. **(A)** Schematic of measurements derived from a typical action potential waveform, including, AP amplitude, half-width, and after hyperpolarization (AHP). **(B)** Averages of the first action potential fired at rheobase in each genotype (error bars represent scanning electron microscope (SEM)). **(C)** Action potential height (mV), **(D)** action potential half-width (ms), and **(E)** AHP amplitude (mV) in DGCs from 6 month TgF344-AD and Wt female rats are not different. For all panels, Wt, $n = 22$ cells/8 animals, Tg, $n = 13$ cells/6 animals, $p > 0.05$. Data represent mean ± SEM. Significance is determined using the unpaired Student's *t*-test.

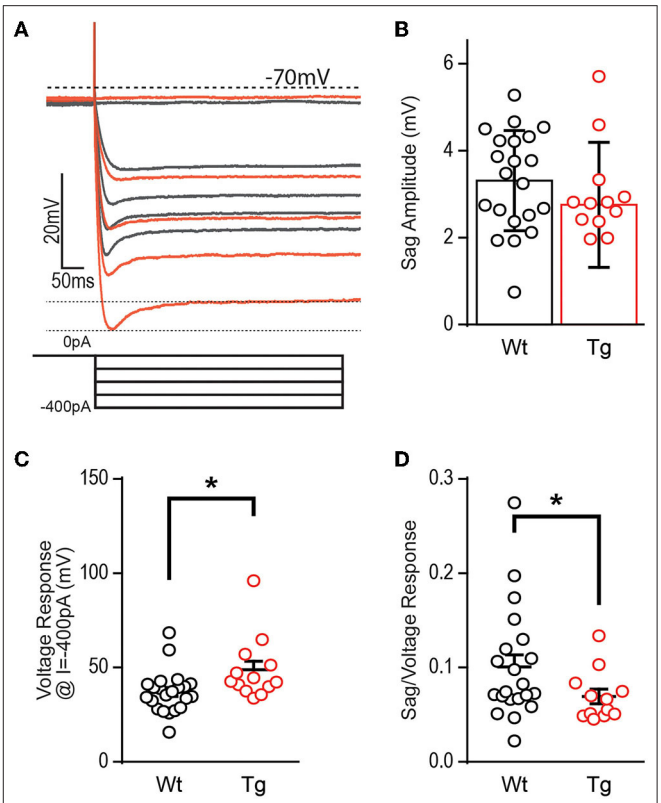

FIGURE 4 | Voltage sag potential is decreased in TgF344-AD DGCs. **(A)** Example trace of "sag" current measurements taken at −400 pA current injection. **(B)** The raw amplitude of the sag current is not different between TgF344-AD and Wt littermate DGCs (Wt, $n = 21$ cells/8 animals; Tg, $n = 12$ cells/6 animals; $p > 0.05$). **(C)** The voltage response at −400 pA is greater in TgF344-AD rats (Wt, $n = 22$ cells/8 animals; Tg, $n = 13$ cells/6 animals; $^*p < 0.05$). **(D)** When sag amplitude is normalized to voltage response a significant deficit in TgF344-AD DGC sag is unmasked (Wt, $n = 21$ cells/8 animals; Tg, $n = 12$ cells/6 animals; $^*p < 0.05$). Data represent mean ± SEM. Significance is determined using the unpaired Student's *t*-test.

DGCs have a lower initial spike frequency (59.05 ± 9.85 Hz) and accommodate to 31.42 ± 3.71 Hz by steady state (**Figure 5B**, black). The initial instantaneous firing frequency is not different between TgF344-AD DGCs and Wt (**Figure 5B**; $p > 0.05$). The second and third intervals, however, suggest a greater instantaneous firing frequency for TgF344-AD DGCs compared with their Wt littermates [$t_{(22.70)} = 2.032$, $p = 0.054$; $t_{(22.68)} = 2.275$, $p = 0.032$, respectively]. When the final 5 spike intervals (15–20) are collapsed (**Figure 5B**, dashed box), the TgF344-AD rat DGCs have a significantly reduced instantaneous frequency [$t_{(9.66)} = 11.08$, $^{****}p < 0.0001$], indicating a greater accommodation. Together, these data suggest TgF344-AD DGCs accommodate to a greater degree than Wt, but that the accommodation mechanism is slower to engage. To further validate this finding, a larger depolarizing step (+300 pA) was also used to measure accommodation with similar results as in Brown et al. (2011) (**Figure 5C**). The first spike interval is significantly shorter for TgF344-AD rat DGCs [$t_{(23.54)} = 2.906$, $p = 0.008$) but quickly becomes comparable to Wt at the second and third interval [$t_{(29.93)} = 1.758$, $p = 0.089$; $t_{(26.31)} = 0.677$, $p = 0.504$, respectively] (**Figure 5C**). When the final 7 spike intervals (19–25) are collapsed (**Figure 5C**, inset), the TgF344-AD rat DGCs have a significantly reduced instantaneous frequency [$t_{(11.98)} = 20.13$, $^{****}p < 0.0001$], again indicating a heightened accommodation. These findings are consistent with the interpretation that the lack of change in total AP number at a given depolarizing current step is a consequence of a simultaneous increase in instantaneous AP frequency and a greater frequency accommodation in DGCs of TgF344-AD rats.

DISCUSSION

Hyperexcitability in hippocampal circuits is reported in many mouse models of AD (Palop et al., 2007; Roberson et al., 2007; Rocher et al., 2008; Verret et al., 2012; Hazra et al., 2013; Šiškov et al., 2014; Nenov et al., 2015). However, in transgenic rat models of AD, there is a lack of information regarding intrinsic excitability, especially in the DG. In this study, we explored whether intrinsic excitability is altered in the novel TgF344-AD rat model, as it might contribute to synaptic changes such as the increased steady-state depolarization during high-frequency tetanus and the enhanced LTP magnitude we previously reported

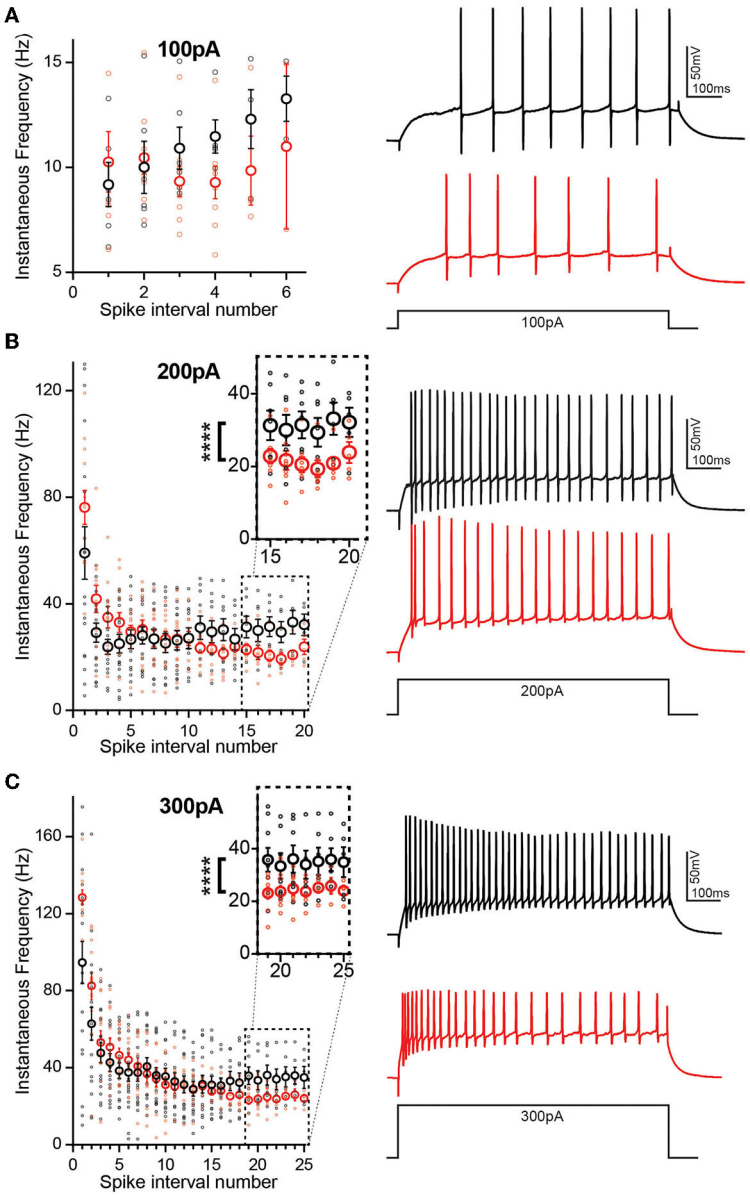

FIGURE 5 | Initial spike frequency and spike accommodation are greater in TgF344-AD DGCs. **(A)** (left) Graph of instantaneous firing frequency (Hz) between action potentials (spike intervals) at 100 pA to include TgF344-AD (red) and Wt (black) DGCs that successfully fired an action potential at +100 pA current injection. (Right) example traces. **(B)** (Left) graph of instantaneous firing frequency (Hz) between action potentials (spike intervals) at 200 pA showing both increased initial spike frequency and greater accommodation (inset) ($p < 0.0001$). (Right) example traces. (Wt, $n = 7$ cells/5 animals; Tg, $n = 5$ cells/5 animals) **(C)** (left) Graph of instantaneous firing frequency (Hz) between action potentials (spike intervals) at 300 pA showing both increased initial spike frequency and greater accommodation (inset) ($p < 0.0001$). (Right) example traces. (****$p < 0.0001$ Wt, $n = 7$ cells/5 animals; Tg, $n = 7$ cells/5 animals). Data represent mean ± SEM. Significance is determined using the unpaired *t*-test with Welch's correction.

in TgF344-AD rats (Smith and McMahon, 2018; Goodman et al., 2021), which more faithfully recapitulates human AD pathology than other transgenic rodent models (Cohen et al., 2013; Do Carmo and Cuello, 2013; Rorabaugh et al., 2017).

Passive and active membrane properties of neurons determine RMP, which can be altered by the presence of soluble Aβ (Fernandez-Perez et al., 2016). We did not detect a genotype difference in RMP of DGCs but did find that DGCs in TgF344-AD rats had both a greater likelihood of resting above −80 mV and an elevated R_I (**Figures 1C,D**). A depolarizing shift in RMP has been reported in cortical and CA1 pyramidal cells in various transgenic tau-expressing or AD mouse lines (Minkeviciene et al., 2009; Verret et al., 2012). K^+ leak and G-protein coupled inwardly rectifying K^+ (GIRK) channels play a major role

in determining RMP (Lüscher and Slesinger, 2010), and their membrane expression could be directly linked to measures of R_I. Future studies should explore whether changes in these channels underlie the increased R_I or even the increased likelihood of a depolarized RMP in the DGCs of TgF344-AD rats.

The enhanced input resistance is further evidenced by the heightened voltage response to both depolarizing and hyperpolarizing currents (**Figures 1C**, **2D**, respectively). Furthermore, the current required to produce APs in TgF344-AD rats is reduced (**Figure 1E**). Upon closer inspection, the minimal depolarizing current injection used to elicit APs (+100 pA) showed both a significant enhancement in the probability of AP firing, and a decreased delay to fire in DGCs from TgF344-AD rats DGCs (**Figure 3**). It remains unclear whether these changes are due to altered ion channel expression or function.

K^+ channels function to dampen membrane excitability and impaired K^+ channel expression and function is implicated as a mechanism for hyperexcitability in AD models (Scala et al., 2015). Specifically, K^+ channel dysfunction should reduce the AP width and AHP magnitude (Tamagnini et al., 2015). However, we did not detect a decrease in AP width during the falling phase (**Figure 4D**), suggesting delayed rectifying K^+ channels, are intact at this age. The AHP shape is mediated by Ca^{2+}-activated K^+ channels such as the large conductance BK-type channels and the small conductance SK-type channels (Andrade et al., 2012). Unsurprisingly, we did not observe a difference in AHP amplitude in TgF344-AD rats (**Figure 3E**), suggesting decreased BK and/or SK-type mediated currents likely do not underlie the changes we see. Alternatively, increased intrinsic excitability can be linked to enhanced LTP by an A-type K^+ channel-mediated increase in back-propagating APs resulting from enhanced dendritic excitability and Ca^{2+} influx (Frick et al., 2004).

Membrane repolarization is mediated in large part by I_A, which dampens excitatory postsynaptic potentials (EPSPs), raises the threshold for AP initiation, and suppresses back-propagating APs (Hoffman et al., 1997). Activation of I_A clamps the membrane below threshold thereby determining the delay to the first AP spike (Storm, 1990). We calculated the time to first spike in DGCs from TgF344-AD rats and Wt littermates and revealed a decreased delay to fire an AP in TgF344-AD rats (**Figure 2E**), suggesting the effect of I_A on dampening excitability may be compromised. While our somatic recordings did not reveal a difference in AHP, whether the threshold for local dendritic I_A current is altered or if a downregulation of K^+ current is responsible for the increased excitability is not known. An elegant study by Kim et al. (2021) in Tg2576 mice shows that decreased expression of Kv4.1 causes DGC hyperexcitability that is associated with impaired pattern recognition. It is possible that loss of Kv4.1 is also occurring in TgF344-AD DG that is leading to increased excitability.

Voltage-gated Na^+ channels (VGNaCs) are responsible for the initiation of APs and tightly control AP threshold. Decreased VGNaCs have been previously observed in AD mouse models (Verret et al., 2012; Corbett et al., 2013). Specifically, the VGNaC, $Na_{V1.1}$, is decreased in glutamatergic and GABAergic neurons in Tg-AD mouse models leading to increased hyperexcitability, likely through enhanced E/I ratio (Verret et al., 2012; Corbett et al., 2013). We found AP threshold is not different between TgF344-AD and Wt (**Figures 1F,G**). Furthermore, changes to VGNaC should produce changes to AP amplitude or half-width, yet we did not detect a difference in either measure (**Figures 3C,D**). Together, these data suggest VGNaC function on DGCs is intact in TgF344-AD rats at 6–8 months, yet whether these channels are decreased on interneurons that innervate DGCs remains to be investigated (Palop et al., 2007; Verret et al., 2012). Unlike the rapidly activating/inactivating VGNaC, persistent Na (I_{NaP}) currents do not inactivate, lasting for hundreds of milliseconds with the ability to influence rheobase. These I_{NaP} can augment cell excitability with an additive effect to other depolarizing currents experienced by the cell, can reduce rheobase, and have been implicated in epileptic firing. Our data show a significant decrease in rheobase (**Figure 1E**), which may indicate a change in I_{NaP}.

Hyperpolarization-activated currents can mediate DGC excitability and HCN channel function is impaired in Tg-mouse models of AD (Kaczorowski et al., 2011). While the raw amplitude of the sag current was not different, we found enhanced hyperpolarized shift in the voltage response in TgF344-AD rat DGCs (**Figure 4C**). Importantly, when the sag amplitude is normalized to voltage response, a deficit in sag response is unmasked, suggesting that for the same amount of membrane hyperpolarization, fewer HCN channels are activated (**Figure 4D**). These data support that decreased HCN channel function could mediate the DGC hyperexcitability we reported in TgF344-AD rats at 6 months.

Interestingly, while the overall number of APs was not different between genotypes, both the initial AP frequency and spike accommodation were elevated in TgF344-AD DGCs, suggesting the dynamics of AP firing frequency is also altered in TgF344-AD rats. The AP number was highly variable among cells in each group, and therefore, cells that did not meet a minimum spike number (5 spikes at 100 pA, or 17 spikes at 200 pA and above) were excluded for accommodation analysis. Interestingly, when these low-fidelity cells were entered into the analysis, the difference in initial firing frequency was abolished, regardless of spike number, and therefore we cannot rule out the possibility that we were recording from two populations of mature dentate granule cells (Nenov et al., 2015). In fact, variability in the spike number among cells even within the same group indicates there may be multiple populations of mature DGCs from which we are recording (Nenov et al., 2015). While we did not directly measure DGC bursting activity, enhanced instantaneous frequency within the bursting range of 3–8 APs in the TgF344-AD rat may enhance the propagation of signals through the dentate or functionally rearrange feedforward inhibition (Neubrandt et al., 2018). This may be especially true of signals, which otherwise would not evoke a DGC AP due to their increased R_I. Changes in initial firing frequency and spike rate accommodation support a role for altered Na^+ and K^+ channel function in DGCs during short or extended depolarization, and therefore, future studies should aim to determine their functional role in this AD model.

CONCLUSION

Excitation inhibition imbalance is an early feature of pathology in the hippocampus of patients with preclinical AD, and this imbalance has been recapitulated in several rodent models of AD-like pathology. We previously reported increased steady-state depolarization and LTP magnitude in TgF344-AD DG at 6 months. While the enhanced LTP was dependent on heightened β-AR function, this enhanced function was not sufficient to account for the heightened SSD (Smith and McMahon, 2018; Goodman et al., 2021). In this study, we used whole-cell current clamp recordings to show that intrinsic excitability is increased in DGCs from TgF344-AD rats, and this provides one mechanistic explanation for heightened excitability in response to high-frequency synaptic activation, which likely contributes to early increase in LTP magnitude.

DATA AVAILABILITY STATEMENT

The raw data supporting the conclusions of this article will be made available by the authors, without undue reservation.

ETHICS STATEMENT

The animal study was reviewed and approved by University of Alabama at Birmingham Institutional Animal Care and Use Committee.

AUTHOR CONTRIBUTIONS

LS and LM designed the study. LS, AG, and LM wrote the manuscript. LS performed the electrophysiological experiments. LS and AG conducted data analysis, statistical tests, and created figures. AG completed the final data analysis and revised the text and figures. All authors contributed to the article and approved the submitted version.

FUNDING

This work was funded by grants of NIA R01 AG066489 and NIA R21 AG053067 to LM, F31 AG054087 to LS, and T32-NS-061788 in support of AG.

REFERENCES

Andrade, R., Foehring, R. C., and Tzingounis, A. V. (2012). The calcium-activated slow AHP: cutting through the Gordian knot. *Front. Cell. Neurosci.* 6, 47. doi: 10.3389/fncel.2012.00047

Bazzigaluppi, P., Beckett, T. L., Koletar, M. M., Lai, A. Y., Joo, I. L., Brown, M. E., et al. (2018). Early-stage attenuation of phase-amplitude coupling in the hippocampus and medial prefrontal cortex in a transgenic rat model of Alzheimer's disease. *J. Neurochem.* 144, 669–679. doi: 10.1111/jnc.14136

Bender, R. A., Galindo, R., Mameli, M., Gonzalez-Vega, R., Valenzuela, C. F., and Baram, T. Z. (2005). Synchronized network activity in developing rat hippocampus involves regional hyperpolarization-activated cyclic nucleotide-gated (HCN) channel function. *Eur. J. Neurosci.* 22, 2669–2674. doi: 10.1111/j.1460-9568.2005.04407.x

Braak, H., Thal, D. R., Ghebremedhin, E., and Del Tredici, K. (2011). Stages of the pathologic process in Alzheimer disease: age categories from 1 to 100 years. *J. Neuropathol. Exp. Neurol.* 70, 960–969. doi: 10.1097/NEN.0b013e318232a379

Brown, J. T., Chin, J., Leiser, S. C., Pangalos, M. N., and Randall, A. D. (2011). Altered intrinsic neuronal excitability and reduced Na+ currents in a mouse model of Alzheimer's disease. *Neurobiol. Aging* 32, 2109.e1–14. doi: 10.1016/j.neurobiolaging.2011.05.025

Busche, M. A., and Konnerth, A. (2016). Impairments of neural circuit function in Alzheimer's disease. *Philos. Trans. R. Soc. Lond. B Biol. Sci.* 371, 20150429. doi: 10.1098/rstb.2015.0429

Cohen, R. M., Rezai-Zadeh, K., Weitz, T. M., Rentsendorj, A., Gate, D., Spivak, I., et al. (2013). A transgenic Alzheimer rat with plaques, tau pathology, behavioral impairment, oligomeric aβ, and frank neuronal loss. *J. Neurosci.* 33, 6245–6256. doi: 10.1523/JNEUROSCI.3672-12.2013

Corbett, B. F., Leiser, S. C., Ling, H.-P., Nagy, R., Breysse, N., Zhang, X., et al. (2013). Sodium channel cleavage is associated with aberrant neuronal activity and cognitive deficits in a mouse model of Alzheimer's disease. *J. Neurosci.* 33, 7020–7026. doi: 10.1523/JNEUROSCI.2325-12.2013

Dickerson, B. C., Salat, D. H., Bates, J. F., Atiya, M., Killiany, R. J., Greve, D. N., et al. (2004). Medial temporal lobe function and structure in mild cognitive impairment. *Ann. Neurol.* 56, 27–35. doi: 10.1002/ana.20163

Do Carmo, S., and Cuello, A. C. (2013). Modeling Alzheimer's disease in transgenic rats. *Mol. Neurodegener.* 8, 37. doi: 10.1186/1750-1326-8-37

Fernandez-Perez, E. J., Peters, C., and Aguayo, L. G. (2016). Membrane damage induced by amyloid beta and a potential link with neuroinflammation. *Curr. Pharm. Des.* 22, 1295–1304. doi: 10.2174/1381612822101603041117 02

Frick, A., Magee, J., and Johnston, D. (2004). LTP is accompanied by an enhanced local excitability of pyramidal neuron dendrites. *Nat. Neurosci.* 7, 126–135. doi: 10.1038/nn1178

Goodman, A. M., Langner, B. M., Jackson, N., Alex, C., and McMahon, L. L. (2021). Heightened hippocampal β-adrenergic receptor function drives synaptic potentiation and supports learning and memory in the TgF344-AD rat model during prodromal Alzheimer's disease. *J. Neurosci.* 41, 5747–5761. doi: 10.1523/JNEUROSCI.0119-21.2021

Hajszan, T., MacLusky, N. J., Johansen, J. A., Jordan, C. L., and Leranth, C. (2007). Effects of androgens and estradiol on spine synapse formation in the prefrontal cortex of normal and testicular feminization mutant male rats. *Endocrinology.* 148, 1963–1967. doi: 10.1210/en.2006-1626

Hazra, A., Gu, F., Aulakh, A., Berridge, C., Eriksen, J. L., and Ziburkus, J. (2013). Inhibitory neuron and hippocampal circuit dysfunction in an aged mouse model of Alzheimer's disease. *PLoS ONE* 8, e64318. doi: 10.1371/journal.pone.0064318

Hoffman, D. A., Magee, J. C., Colbert, C. M., and Johnston, D. (1997). K+ channel regulation of signal propagation in dendrites of hippocampal pyramidal neurons. *Nature* 387, 869–875. doi: 10.1038/43119

Joo, I. L., Lai, A. Y., Bazzigaluppi, P., Koletar, M. M., Dorr, A., Brown, M. E., et al. (2017). Early neurovascular dysfunction in a transgenic rat model of Alzheimer's disease. *Sci. Rep.* 7, 46427. doi: 10.1038/srep46427

Kaczorowski, C. C., Sametsky, E., Shah, S., Vassar, R., and Disterhoft, J. F. (2011). Mechanisms underlying basal and learning-related intrinsic excitability in a mouse model of Alzheimer's disease. *Neurobiol. Aging* 32, 1452–1465. doi: 10.1016/j.neurobiolaging.2009.09.003

Kim, K.-R., Kim, Y., Jeong, H.-J., Kang, J.-S., Lee, S. H., Kim, Y., et al. (2021). Impaired pattern separation in Tg2576 mice is associated with hyperexcitable dentate gyrus caused by Kv4.1 downregulation. *Mol. Brain* 14, 62. doi: 10.1186/s13041-021-00774-x

Loy, R., and Moore, R. Y. (1979). Ontogeny of the noradrenergic innervation of the rat hippocampal formation. *Anat. Embryol.* 157, 243–253. doi: 10.1007/BF00304992

Lüscher, C., and Slesinger, P. A. (2010). Emerging roles for G protein-gated inwardly rectifying potassium (GIRK) channels in health and disease. *Nat. Rev. Neurosci.* 11, 301–315. doi: 10.1038/nrn2834

Madison, D. V., and Nicoll, R. A. (1984). Control of the repetitive discharge of rat CA 1 pyramidal neurones *in vitro*. *J. Physiol.* 354, 319–331. doi: 10.1113/jphysiol.1984.sp015378

Minkeviciene, R., Rheims, S., Dobszay, M. B., Zilberter, M., Hartikainen, J., Fülöp, L., et al. (2009). Amyloid beta-induced neuronal hyperexcitability triggers progressive epilepsy. *J. Neurosci.* 29, 3453–3462. doi: 10.1523/JNEUROSCI.5215-08.2009

Muñoz-Moreno, E., Tudela, R., López-Gil, X., and Soria, G. (2018). Early brain connectivity alterations and cognitive impairment in a rat model of Alzheimer's disease. *Alzheimers Res. Ther.* 10, 16. doi: 10.1186/s13195-018-0346-2

Nenov, M. N., Tempia, F., Denner, L., Dineley, K. T., and Laezza, F. (2015). Impaired firing properties of dentate granule neurons in an Alzheimer's disease animal model are rescued by PPARγ agonism. *J. Neurophysiol.* 113, 1712–1726. doi: 10.1152/jn.00419.2014

Neubrandt, M., Oláh, V. J., Brunner, J., Marosi, E. L., Soltesz, I., and Szabadics, J. (2018). Single bursts of individual granule cells functionally rearrange feedforward inhibition. *J. Neurosci.* 38, 1711–1724. doi: 10.1523/JNEUROSCI.1595-17.2018

Palop, J. J., Chin, J., Roberson, E. D., Wang, J., Thwin, M. T., Bien-Ly, N., et al. (2007). Aberrant excitatory neuronal activity and compensatory remodeling of inhibitory hippocampal circuits in mouse models of Alzheimer's disease. *Neuron* 55, 697–711. doi: 10.1016/j.neuron.2007.07.025

Palop, J. J., and Mucke, L. (2016). Network abnormalities and interneuron dysfunction in Alzheimer disease. *Nat. Rev. Neurosci.* 17, 777–792. doi: 10.1038/nrn.2016.141

Pentkowski, N. S., Berkowitz, L. E., Thompson, S. M., Drake, E. N., Olguin, C. R., and Clark, B. J. (2018). Anxiety-like behavior as an early endophenotype in the TgF344-AD rat model of Alzheimer's disease. *Neurobiol. Aging* 61, 169–176. doi: 10.1016/j.neurobiolaging.2017.09.024

Poolos, N. P., and Johnston, D. (2012). Dendritic ion channelopathy in acquired epilepsy. *Epilepsia* 53(Suppl. 9), 32–40. doi: 10.1111/epi.12033

Poolos, N. P., Migliore, M., and Johnston, D. (2002). Pharmacological upregulation of h-channels reduces the excitability of pyramidal neuron dendrites. *Nat. Neurosci.* 5, 767–774. doi: 10.1038/nn891

Quiroz, Y. T., Budson, A. E., Celone, K., Ruiz, A., Newmark, R., Castrillón, G., et al. (2010). Hippocampal hyperactivation in presymptomatic familial Alzheimer's disease. *Ann. Neurol.* 68, 865–875. doi: 10.1002/ana.22105

Reiman, E. M., Quiroz, Y. T., Fleisher, A. S., Chen, K., Velez-Pardo, C., Jimenez-Del-Rio, M., et al. (2012). Brain imaging and fluid biomarker analysis in young adults at genetic risk for autosomal dominant Alzheimer's disease in the presenilin 1 E280A kindred: a case-control study. *Lancet Neurol.* 11, 1048–1056. doi: 10.1016/S1474-4422(12)70228-4

Roberson, E. D., Scearce-Levie, K., Palop, J. J., Yan, F., Cheng, I. H., Wu, T., et al. (2007). Reducing endogenous tau ameliorates amyloid beta-induced deficits in an Alzheimer's disease mouse model. *Science* 316, 750–754. doi: 10.1126/science.1141736

Rocher, A. B., Kinson, M. S., and Luebke, J. I. (2008). Significant structural but not physiological changes in cortical neurons of 12-month-old Tg2576 mice. *Neurobiol. Dis.* 32, 309–318. doi: 10.1016/j.nbd.2008.07.014

Rorabaugh, J. M., Chalermpalanupap, T., Botz-Zapp, C. A., Fu, V. M., Lembeck, N. A., Cohen, R. M., et al. (2017). Chemogenetic locus coeruleus activation restores reversal learning in a rat model of Alzheimer's disease. *Brain* 140, 3023–3038. doi: 10.1093/brain/awx232

Scala, F., Fusco, S., Ripoli, C., Piacentini, R., Li Puma, D. D., Spinelli, M., et al. (2015). Intraneuronal Aβ accumulation induces hippocampal neuron hyperexcitability through A-type K(+) current inhibition mediated by activation of caspases and GSK-3. *Neurobiol. Aging* 36, 886–900. doi: 10.1016/j.neurobiolaging.2014.10.034

Šišková, Z., Justus, D., Kaneko, H., Friedrichs, D., Henneberg, N., Beutel, T., et al. (2014). Dendritic structural degeneration is functionally linked to cellular hyperexcitability in a mouse model of Alzheimer's disease. *Neuron* 84, 1023–1033. doi: 10.1016/j.neuron.2014.10.024

Smith, C. C., and McMahon, L. L. (2005). Estrogen-induced increase in the magnitude of long-term potentiation occurs only when the ratio of NMDA transmission to AMPA transmission is increased. *J. Neurosci.* 25, 7780–7791. doi: 10.1523/JNEUROSCI.0762-05.2005

Smith, C. C., and McMahon, L. L. (2006). Estradiol-induced increase in the magnitude of long-term potentiation is prevented by blocking NR2B-containing receptors. *J. Neurosci.* 26, 8517–8522. doi: 10.1523/JNEUROSCI.5279-05.2006

Smith, C. C., Vedder, L. C., and McMahon, L. L. (2009). Estradiol and the relationship between dendritic spines, NR2B containing NMDA receptors, and the magnitude of long-term potentiation at hippocampal CA3-CA1 synapses. *Psychoneuroendocrinology* 34(Suppl. 1), S130–S142. doi: 10.1016/j.psyneuen.2009.06.003

Smith, C. C., Vedder, L. C., Nelson, A. R., Bredemann, T. M., and McMahon, L. L. (2010). Duration of estrogen deprivation, not chronological age, prevents estrogen's ability to enhance hippocampal synaptic physiology. *Proc. Natl. Acad. Sci. U.S.A.* 107, 19543–19548. doi: 10.1073/pnas.1009307107

Smith, L. A., and McMahon, L. L. (2018). Deficits in synaptic function occur at medial perforant path-dentate granule cell synapses prior to Schaffer collateral-CA1 pyramidal cell synapses in the novel TgF344-Alzheimer's Disease Rat Model. *Neurobiol. Dis.* 110, 166–179. doi: 10.1016/j.nbd.2017.11.014

Storm, J. F. (1990). Potassium currents in hippocampal pyramidal cells. *Prog. Brain Res.* 83, 161–187. doi: 10.1016/S0079-6123(08)61248-0

Tamagnini, F., Novelia, J., Kerrigan, T. L., Brown, J. T., Tsaneva-Atanasova, K., and Randall, A. D. (2015). Altered intrinsic excitability of hippocampal CA1 pyramidal neurons in aged PDAPP mice. *Front. Cell. Neurosci.* 9, 372. doi: 10.3389/fncel.2015.00372

Ting, J. T., Daigle, T. L., Chen, Q., and Feng, G. (2014). Acute brain slice methods for adult and aging animals: application of targeted patch clamp analysis and optogenetics. *Methods Mol. Biol.* 1183, 221–242. doi: 10.1007/978-1-4939-1096-0_14

Tsai, Y., Lu, B., Ljubimov, A. V., Girman, S., Ross-Cisneros, F. N., Sadun, A. A., et al. (2014). Ocular changes in TgF344-AD rat model of Alzheimer's disease. *Invest. Ophthalmol. Vis. Sci.* 55, 523–534. doi: 10.1167/iovs.13-12888

Vedder, L. C., Smith, C. C., Flannigan, A. E., and McMahon, L. L. (2013). Estradiol-induced increase in novel object recognition requires hippocampal NR2B-containing NMDA receptors. *Hippocampus* 23, 108–115. doi: 10.1002/hipo.22068

Verret, L., Mann, E. O., Hang, G. B., Barth, A. M. I., Cobos, I., Ho, K., et al. (2012). Inhibitory interneuron deficit links altered network activity and cognitive dysfunction in Alzheimer model. *Cell* 149, 708–721. doi: 10.1016/j.cell.2012.02.046

Vogel, J. W., Iturria-Medina, Y., Strandberg, O. T., Smith, R., Levitis, E., Evans, A. C., et al. (2020). Spread of pathological tau proteins through communicating neurons in human Alzheimer's disease. *Nat. Commun.* 11, 2612. doi: 10.1038/s41467-020-15701-2

Voorhees, J. R., Remy, M. T., Cintrón-Pérez, C. J., El Rassi, E., Khan, M. Z., Dutca, L. M., et al. (2018). (-)-P7C3-S243 protects a rat model of Alzheimer's disease from neuropsychiatric deficits and neurodegeneration without altering amyloid deposition or reactive glia. *Biol. Psychiatry* 84, 488–498. doi: 10.1016/j.biopsych.2017.10.023

Wei, W., Nguyen, L. N., Kessels, H. W., Hagiwara, H., Sisodia, S., and Malinow, R. (2010). Amyloid beta from axons and dendrites reduces local spine number and plasticity. *Nat. Neurosci.* 13, 190–196. doi: 10.1038/nn.2476

Woolley, C. S. (1998). Estrogen-mediated structural and functional synaptic plasticity in the female rat hippocampus. *Horm. Behav.* 34, 140–148. doi: 10.1006/hbeh.1998.1466

Woolley, C. S., and McEwen, B. S. (1993). Roles of estradiol and progesterone in regulation of hippocampal dendritic spine density during the estrous cycle in the rat. *J. Comp. Neurol.* 336, 293–306. doi: 10.1002/cne.903360210

Wu, J. W., Hussaini, S. A., Bastille, I. M., Rodriguez, G. A., Mrejeru, A., Rilett, K., et al. (2016). Neuronal activity enhances tau propagation and tau pathology *in vivo*. *Nat. Neurosci.* 19, 1085–1092. doi: 10.1038/nn.4328

Yamamoto, K., Tanei, Z.-I., Hashimoto, T., Wakabayashi, T., Okuno, H., Naka, Y., et al. (2015). Chronic optogenetic activation augments aβ

pathology in a mouse model of Alzheimer disease. *Cell Rep.* 11, 859–865. doi: 10.1016/j.celrep.2015.04.017

Conflict of Interest: The authors declare that the research was conducted in the absence of any commercial or financial relationships that could be construed as a potential conflict of interest.

Publisher's Note: All claims expressed in this article are solely those of the authors and do not necessarily represent those of their affiliated organizations, or those of the publisher, the editors and the reviewers. Any product that may be evaluated in this article, or claim that may be made by its manufacturer, is not guaranteed or endorsed by the publisher.

Advantages of publishing in Frontiers

OPEN ACCESS
Articles are free to read for greatest visibility and readership

FAST PUBLICATION
Around 90 days from submission to decision

HIGH QUALITY PEER-REVIEW
Rigorous, collaborative, and constructive peer-review

TRANSPARENT PEER-REVIEW
Editors and reviewers acknowledged by name on published articles

Frontiers
Avenue du Tribunal-Fédéral 34
1005 Lausanne | Switzerland

Visit us: www.frontiersin.org
Contact us: frontiersin.org/about/contact

REPRODUCIBILITY OF RESEARCH
Support open data and methods to enhance research reproducibility

DIGITAL PUBLISHING
Articles designed for optimal readership across devices

FOLLOW US
@frontiersin

IMPACT METRICS
Advanced article metrics track visibility across digital media

EXTENSIVE PROMOTION
Marketing and promotion of impactful research

LOOP RESEARCH NETWORK
Our network increases your article's readership